

Investigation of Nanostructured Conducting Polymers and Graphene/Polyaniline Nanocomposite Based Thin Films for Hydrogen Gas Sensing

A thesis submitted in fulfilment of the requirements for the degree of
Doctor of Philosophy

Laith Al-Mashat

BSc. (Electrical Engineering / Electronics & Communications)
University of Technology, Baghdad, Iraq

**School of Electrical and Computer Engineering
Science, Engineering and Health Portfolio
RMIT University, Melbourne, Australia**

December 2012

Declaration

I certify that except where due acknowledgement has been made, the work is that of the author alone; the work has not been submitted previously, in whole or in part, to qualify for any other academic award; the content of the thesis is the result of work which has been carried out since the official commencement date of the approved research program; any editorial work, paid or unpaid, carried out by a third party is acknowledged; and, ethics procedures and guidelines have been followed.

Laith Al-Mashat

4 / 12 / 2012

Contents

List of Tables.....	vi
List of Figures.....	vii
Acknowledgements	xii
Abstract	xiv
List of Author's Publications	xvi
Refereed Journal Papers.....	xvi
Conference Proceedings	xvii
Chapter 1 Introduction.....	1
1.1 Motivation	1
1.1.1 Hydrogen Gas Properties and Applications.....	1
1.1.2 Gas Sensors	4
1.1.2.1 Gas Sensing Films.....	4
Metals.....	4
Metal Oxides	5
Carbon Nanotubes and Graphene	5
Conducting Polymers.....	6
1.1.2.2 Transduction Platforms.....	7
1.2 Objectives	9
1.3 Outcomes and Author's Achievements	9
1.4 Thesis Organization	10
Chapter 2 Literature Review.....	12
2.1 Introduction to Conducting Polymers.....	12
2.2 Growth Methods of Nanostructured Conducting Polymers.....	15
2.2.1 Syntheses Based on Templates	16
2.2.2 Template-free Syntheses	17
Electropolymerization.....	18
Chemical Polymerization.....	19
2.3 Gas Sensors Based on Conducting Polymers.....	20
2.3.1 Polythiophene	20
2.3.2 Polypyrrole.....	23
2.3.3 Polyaniline	28

2.4	Gas Sensors Based on Composites of Conducting Polymers and Organic or Inorganic Materials.....	31
2.4.1	Graphene/Polyaniline Nanocomposite	33
2.5	Summary.....	35
Chapter 3	Theoretical Background on Conductometric and SAW Gas Sensors	36
3.1	Variable Range Hopping Model	36
3.2	Modeling of Conductometric Gas Sensors Based on Conducting Polymers.....	38
3.2.1	Gas Diffusion Model	38
3.2.2	Gas Sensor Conductance Model	43
3.3	Theory of SAW Gas Sensors	47
3.3.1	Mass Sensitivity	49
3.3.2	Elastic and Viscoelastic Sensitivities.....	50
3.3.3	Conductometric Sensitivity	51
3.4	Summary.....	53
Chapter 4	Transducers Microfabrication	55
4.1	Introduction to IDT's Microfabrication	55
4.2	Preparation of Photolithographic Masks	57
4.3	Substrate Cleaning.....	58
4.4	Metal Thin Film Deposition	58
4.5	Photolithography	59
4.6	Chemical Etching.....	60
4.7	Wafer Dicing	60
4.8	ZnO Sputtering on SAW Transducers.....	61
4.9	Gold Wire Bonding	62
4.10	Transducers Testing.....	63
4.11	Summary.....	63
Chapter 5	Synthesis and Deposition of Nanostructured Materials	64
5.1	Polymerization Concept.....	65
5.2	Deposition Techniques.....	67
5.3	Polythiophene Nanostructures.....	68
	Electropolymerization.....	69
	Chemical Polymerization.....	71
5.4	Polypyrrole Nanostructures	72
	Electropolymerization.....	72
	Chemical Polymerization.....	73
5.5	Nanoporous Polyaniline.....	73

5.6	Derivatives of Polyaniline	74
5.7	Graphene/Polyaniline Nanocomposite	74
5.8	Summary.....	76
Chapter 6	Characterization of Nanostructured Materials	77
6.1	Characterization Techniques	77
6.1.1	Scanning Electron Microscopy (SEM)	78
6.1.2	Transmission Electron Microscopy (TEM).....	78
6.1.3	Ultraviolet-visible (UV-vis) Spectroscopy	79
6.1.4	Fourier Transform Infrared (FT-IR) Spectroscopy	79
6.1.5	Raman Spectroscopy.....	80
6.1.6	X-Ray Photoelectron Spectroscopy (XPS).....	81
6.2	Charaterization Results of Polythiophene Nanostructures.....	81
6.2.1	Electropolymerized Polythiophene Nanostructures	81
	The Effect of Electrolyte's Anion Type	82
	Electropolymerization with Different Electrolyte's Concentrations....	86
	Electropolymerization with Different Applied Potentials.....	91
	The Effect of Electropolymerization Time.....	94
6.2.2	Chemically Synthesized Polythiophene Nanofibers	98
6.3	Charaterization Results of Polypyrrole Nanostructures	99
6.3.1	Electropolymerized Polypyrrole Nanowires.....	99
6.3.2	Chemically Synthesized Polypyrrole Nanofibers.....	104
6.4	Charaterization Results of Nanostructured Polyaniline and its Alkyl-Substituted Derivatives	106
6.4.1	Nanoporous Polyaniline.....	106
6.4.2	Polyanisidine Nanofibers.....	107
6.4.3	Polyethylaniline Nanofibers.....	109
6.5	Charaterization Results of Graphene/Polyaniline Nanocomposite.....	110
6.6	Summary.....	116
Chapter 7	Gas Sensing Results and Discussions	120
7.1	Gas Sensing System Configuration.....	121
7.2	Gas Sensors with Nanostructured Polythiophene Sensitive Films.....	122
7.2.1	Conductometric Gas Sensors Based on Electropolymerized Polythiophene Nanostructures.....	123
	The Effect of Electrolyte's Anion Type	123
	The Effect of Different Electrolyte's Concentrations	126
	The Effect of Electropolymerization's Potential	128

The Effect of Nanostructured Film's Thickness.....	130
7.2.2 Layered SAW Gas Sensor with Chemically Synthesized Polythiophene Nanofibers Sensitive Film.....	133
7.2.3 Gas Sensing Mechanism for Polythiophene.....	135
7.3 Gas Sensors Based on Polypyrrole Nanostructures.....	136
7.3.1 Conductometric Gas Sensors.....	136
Conductometric Gas Sensors Based on Electropolymerized Polypyrrole Nanowires	136
Conductometric Gas Sensor Based on Chemically Synthesized Polypyrrole Nanofibers	138
7.3.2 Layered SAW Gas Sensor Based on Polypyrrole Nanofibers	142
7.3.3 Gas Sensing Mechanism for Polypyrrole	145
7.4 Layered SAW Gas Sensors Based on Nanostructured Polyaniline and its Alkyl-Substituted Derivatives	145
7.4.1 Layered SAW Gas Sensor Based on Nanoporous Polyaniline.....	146
7.4.2 Layered SAW Gas Sensor Based on Polyanisidine Nanofibers.....	148
7.4.3 Layered SAW Gas Sensor Based on Polyethylaniline Nanofibers	150
7.4.4 Gas Sensing Mechanism for Polyaniline and its Alkyl-Substituted Derivatives	152
7.5 Graphene/Polyaniline Nanocomposite Based Gas Sensor	153
7.6 Summary.....	156
Chapter 8 Conclusions and Future Work.....	161
8.1 Conclusions.....	163
8.1.1 Characterization of Nanomaterials.....	163
Nanostructured Polythiophene.....	163
Nanostructured Polypyrrole	165
Nanostructured Polyaniline and its Alkyl-Substituted Derivatives..	165
Graphene/Polyaniline Nanocomposite.....	166
8.1.2 Electrical Characterization of Conductometric Gas Sensors.....	166
Nanostructured Polythiophene Based Gas Sensors.....	166
Nanostructured Polypyrrole Based Gas Sensors	168
Graphene/Polyaniline Nanocomposite Based Gas sensor	168
8.1.3 Electrical Characterization of Layered SAW Gas Sensors	169
Polythiophene Nanofibers/ZnO/36° YX LiTaO ₃ SAW Gas Sensor	169
Polypyrrole Nanofibers/ZnO/36° YX LiTaO ₃ SAW Gas Sensor.....	169
Nanoporous Polyaniline/ZnO/36° YX LiTaO ₃ SAW Gas Sensor	169

	Polyaniline Nanofibers/ZnO/36° YX LiTaO ₃ SAW Gas Sensor	169
	Polyethylaniline Nanofibers/ZnO/36° YX LiTaO ₃ SAW Gas Sensor..	170
8.2	Future Work	170
	Bibliography.....	172

List of Tables

Table 1.1. Safety related properties of hydrogen gas and methane gas [2, 3].....	2
Table 2.1. Structures and conductivities of some conjugated polymers [51].....	13
Table 3.1. Electrical response of localized electrons in systems of different dimensionality [204].	37
Table 3.2. The analytical expressions for the adsorbed gas concentration and sites occupancy during adsorption; adopted from ref: [207].....	41
Table 3.3. The adsorbed gas concentration and sites occupancy analytical expressions during desorption; adopted from ref: [207].....	42
Table 5.1. Deposition time versus film thickness of electrochemically deposited nanostructured polythiophene films.....	71
Table 6.1. Elemental composition of the nanostructured polythiophene.	95
Table 7.1. Response time and recovery time of the graphene/PANI, PANI nanofibers and graphene based gas sensors towards 1% of H ₂ gas.	155

List of Figures

Figure 1.1. Schematic of a conductometric transducer.....	8
Figure 1.2. Schematic of a SAW transducer.....	8
Figure 2.1. Polarons and bipolarons in polypyrrole [53].....	14
Figure 2.2. Gas adsorption in a bulk film (left) and in a nanostructured film (right), adapted from [63].....	16
Figure 2.3. Doping and dedoping of polyaniline [144].	28
Figure 3.1. Schematic diagram of a gas sensor with semi-infinite electrodes; reproduced from ref.: [206].....	39
Figure 3.2. (A) Schematic diagram of the resistive network [209] (B) Possible node connections [210].....	44
Figure 3.3. Schematic diagram of a gas sensor with finite coplanar electrodes; reproduced from ref.: [206].	46
Figure 3.4. Layered SAW sensor oscillator circuit configuration.	53
Figure 4.1. Microfabrication steps for the IDTs of conductometric and SAW transducers.	56
Figure 4.2. Conductometric transducers mask and the overall device layout.	57
Figure 4.3. Microfabricated and diced silicon/SiO ₂ wafer with 50 μm IDTs.	61
Figure 4.4. A microfabricated 36° YX LiTaO ₃ substrate with sputtered ZnO thin film...61	
Figure 5.1. Polymerization steps of a heterocyclic monomer [59].	66
Figure 5.2. Gas sensors based on chemically synthesized nanostructured conducting polymers: (A) Layered SAW sensor, (B) Conductometric sensor.....	67
Figure 5.3. (A) A sensor based on nanostructured polythiophene deposited by two-electrodes cell, (B) A sensor based on polypyrrole nanowires deposited by a three-electrodes cell.	68
Figure 6.1. Polythiophene electropolymerization currents utilizing 1.2 mM FeCl ₃ and 0.5 M LiClO ₄ electrolytes.....	83
Figure 6.2. SEM images of electropolymerized polythiophene nanostructures using: (A) 0.5 M LiClO ₄ solution, (B) 1.2 mM FeCl ₃ solution.	84
Figure 6.3. Magnified SEM image of polythiophene electropolymerized utilizing 1.2 mM FeCl ₃ solution.....	84

Figure 6.4. The effect of utilizing FeCl_3 concentration higher than 1.8 mM.....	86
Figure 6.5. Electropolymerization currents during polythiophene deposition with different FeCl_3 solution concentrations.....	86
Figure 6.6. SEM images of electropolymerized polythiophene at FeCl_3 solution concentrations of: (A) 0.6 mM, (B) 0.9 mM, (C) 1.2 mM, (D) 1.5 mM, (E) 1.8 mM.....	87
Figure 6.7. SEM image of polythiophene nanofiber segment obtained through electropolymerization with 1.8 mM FeCl_3 electrolyte.....	89
Figure 6.8. UV-vis spectra of polythiophene nanostructured films deposited with different electrolyte's concentrations.....	90
Figure 6.9. Electropolymerization currents recorded during polythiophene deposition with different deposition potentials.	91
Figure 6.10. SEM images of electropolymerized polythiophene at deposition potentials of: (A) 0.65 V, (B) 0.7 V, (C) 0.75 V, (D) 0.8 V, (E) 0.85 V.....	92
Figure 6.11. UV-vis spectra of polythiophene nanostructured films electropolymerized with different applied potentials.	94
Figure 6.12. SEM images for the nanostructured polythiophene film electropolymerized with 1.2 mM FeCl_3 solution, 0.75 V of applied potential and 20 minutes of deposition time, (A) low magnification, (B) high magnification.	95
Figure 6.13. XPS spectrum of the synthesized nanostructured polythiophene.	96
Figure 6.14. S(2p) core level deconvolution for polythiophene.	96
Figure 6.15. Cl(2p) core level deconvolution for electropolymerized nanostructured polythiophene.....	97
Figure 6.16. SEM image of the chemically synthesized polythiophene nanofibers.	98
Figure 6.17. FT-IR spectrum of chemically synthesized polythiophene nanofibers.	99
Figure 6.18. High magnification SEM images of PPY sensitive films for: (A) Sensor A (13 mC), (B) Sensor B (55 mC), (C) Sensor C (90 mC) and (D) Magnified SEM image of the PPY nanowires on Sensor C.	100
Figure 6.19. An SEM image showing a 65° tilted view for the deposited PPY nanowires on a conductometric transducer.	101
Figure 6.20. SEM images showing the formation of PPY nanowires bridges between the gold fingers of conductometric IDT.....	102
Figure 6.21. XPS spectrum of electropolymerized PPY nanowires.	102
Figure 6.22. Deconvolution of C(1s) core level for electropolymerized PPY.....	103
Figure 6.23. N(1s) core level deconvolution of electropolymerized PPY.....	103
Figure 6.24. Deconvolution of O(1s) core level for electropolymerized PPY.....	104

Figure 6.25. (A) SEM images of PPY nanofibers with high magnification image in the inset, (B) TEM image of PPY nanofibers.....	105
Figure 6.26. FT-IR spectrum of PPY nanofibers.....	105
Figure 6.27. SEM image of the deposited nanoporous PANI film.....	106
Figure 6.28. UV-vis spectra of doped and dedoped nanoporous PANI films.....	107
Figure 6.29. SEM image of polyanisidine nanofibers.....	108
Figure 6.30. UV-vis spectrum for polyanisidine.....	108
Figure 6.31. SEM images of polyethylaniline nanofibers.....	109
Figure 6.32. UV-vis spectrum of polyethylaniline.....	109
Figure 6.33. SEM images of graphene/PANI nanocomposite: (A) top view, (B) tilted view (45°).....	110
Figure 6.34. TEM image of graphene/PANI nanocomposite.....	111
Figure 6.35. Raman spectra of: (A) graphene/PANI nanocomposite, (B) PANI and (C) graphene; the 2D band in the Raman spectrum of graphene/PANI nanocomposite is analyzed in the inset.....	112
Figure 6.36. Peak deconvolution of the C(1s) XPS core level for the graphene/PANI nanocomposite.....	114
Figure 6.37. Peak deconvolution of the O(1s) XPS core level for the graphene/PANI nanocomposite.....	115
Figure 6.38. Peak deconvolution of the N(1s) XPS core level for the graphene/PANI nanocomposite.....	115
Figure 7.1. Schematic illustrating the gas sensors' testing system (the gray double-sided arrows represent data cables).....	121
Figure 7.2. Dynamic responses of gas sensors: (A) Sensor (A) based on ClO_4^- doped polythiophene, (B) Sensor (B) based on Cl^- doped polythiophene.....	124
Figure 7.3. Responses of sensor (A) with ClO_4^- doped polythiophene and sensor (B) with Cl^- doped polythiophene.....	125
Figure 7.4. Dynamic responses of gas sensors based on polythiophene electropolymerized utilizing $FeCl_3$ concentrations of: (A) 0.6 mM, (B) 0.9 mM, (C) 1.5 mM, (D) 1.8 mM.....	127
Figure 7.5. Responses of gas sensors based on polythiophene nanostructures electropolymerized with different concentrations of $FeCl_3$	128
Figure 7.6. Dynamic responses of gas sensors based on polythiophene electropolymerized with the anodic potentials of: (A) 0.65 V, (B) 0.7 V, (C) 0.8 V, (D) 0.85 V.....	129
Figure 7.7. Responses of gas sensors based on polythiophene electropolymerized with the different anodic potentials.....	130

Figure 7.8. Responses of gas sensors based on nanostructured polythiophene films with different thicknesses.	131
Figure 7.9. Dynamic response of the gas sensor based on 200 nm thick polythiophene film.	131
Figure 7.10. Dynamic response of the gas sensor based on 1.5 μm thick nanostructured polythiophene film.	132
Figure 7.11. SEM images of the gas sensors based on the electropolymerized polythiophene nanostructures deposited for: (A) 20 minutes (1.5 μm thick film), (B) 60 minutes (10 μm thick film).	133
Figure 7.12. Frequency response of the layered SAW gas sensor with polythiophene nanofibers sensitive film.	133
Figure 7.13. The dynamic response of the layered SAW gas sensor with polythiophene nanofibers sensitive film.	134
Figure 7.14. Frequency deviations of the polythiophene nanofibers based SAW gas sensor during hydrogen gas exposure.	134
Figure 7.15. Scheme illustrating the proposed hydrogen gas sensing mechanism; reproduced for polythiophene from ref.: [286].	135
Figure 7.16. The responses of the hydrogen gas sensors based on electropolymerized ClO_4^- -doped polypyrrole nanowires.	137
Figure 7.17. The performance of an H_2 gas sensor based on polypyrrole nanowires with and without CO gas interference.	138
Figure 7.18. Dynamic response of the conductometric H_2 gas sensor based on Cl^- -doped PPY nanofibers.	139
Figure 7.19. Room temperature response of the Cl^- -doped PPY nanofibers based conductometric H_2 gas sensor.	139
Figure 7.20. The effect of elevating the operating temperature on the polypyrrole nanofibers based conductometric sensor's resistance under synthetic air only (no hydrogen gas).	140
Figure 7.21. The steady-state response of the polypyrrole nanofibers based conductometric gas sensor at different operating temperatures.	141
Figure 7.22. The polypyrrole nanofibers based conductometric gas sensor's response as a function of temperature increase during the exposure to 0.25%, 0.5% and 1% of hydrogen gas.	141
Figure 7.23. Frequency response of the layered SAW gas sensor with polypyrrole nanofibers sensitive film.	142

Figure 7.24. The dynamic reponse of the layered SAW gas sensor with polypyrrole nanofibers sensitive film towards hydrogen gas.	143
Figure 7.25. Frequency deviations of the polypyrrole nanofibers based SAW gas sensor during hydrogen gas exposure.	143
Figure 7.26. The polypyrrole nanofibers based layered SAW gas sensor's response towards 2.1 ppm of NO ₂ gas diluted in synthetic air.	144
Figure 7.27. Scheme showing the redox reaction for polypyrrole [59].	145
Figure 7.28. Frequency response of the layered SAW gas sensor based on nanoporous polyaniline.	146
Figure 7.29. The dynamic reponse of the layered SAW gas sensor based on nanoporous polyaniline.	146
Figure 7.30. Frequency deviations of the nanoporous polyaniline based SAW gas sensor during the exposure to hydrogen gas at room temperature.	147
Figure 7.31. Frequency response of the layered SAW gas sensor based on polyanisidine nanofibers.	148
Figure 7.32. The dynamic reponse of the layered SAW gas sensor based on polyanisidine nanofibers.	149
Figure 7.33. Frequency shifts of the SAW gas sensor based on polyanisidine nanofibers during the interaction with hydrogen gas.	149
Figure 7.34. The frequency response of the polyethylaniline nanofibers/ZnO/36°YX LiTaO ₃ SAW gas sensor.	150
Figure 7.35. The dynamic reponse of the layered SAW gas sensor based on polyethylaniline nanofibers.	151
Figure 7.36. Frequency shifts of the layered SAW gas sensor based on polyethylaniline nanofibers during the interaction with hydrogen gas.	151
Figure 7.37. Scheme illustrating the proposed hydrogen gas sensing mechanism for polyaniline and its alkyl-substituted derivatives [64].	152
Figure 7.38. The dynamic responses of the conductometric H ₂ gas sensors with sensitive layers of: (A) graphene/PANI, (B) PANI nanofibers and (C) graphene.	153
Figure 7.39. Responses of the conductometric H ₂ gas sensors with sensitive layers of: (A) graphene/PANI, (B) PANI nanofibers and (C) graphene.	154

Acknowledgements

FIRST of all, I would like to deeply thank the creator of the universe and mankind, the most merciful Allah, for inspiring me to pursue this research and for helping me to overcome the hurdles that I faced along the way. Then, I wish to express my sincere gratitude and appreciation to RMIT University for giving me the opportunity to conduct the PhD research presented in this thesis, granting me the RMIT PhD Scholarship that covered my living expenses during the program and awarding me with the prestigious 2012 Vice-Chancellor's Higher Degree by Research Publication Excellence Award. In particular, I am especially grateful to my senior supervisor, Professor Wojtek Wlodarski, and my second supervisor, Associate Professor Kourosh Kalantar-zadeh, for their supervision and continuous encouragement throughout the program.

I would like to thank my colleagues Dr. Rashidah Arsat, Dr. Mahnaz Shafiei, Dr. Micheal Breedon, Dr. Mohd. Hanif Yaacob, Dr. Chen Zhang, Dr. Abu Z. Sadek, Mr. Aminuddin Ahmad Kayani, and Mr. Mahyar Nasabi for providing a friendly environment while conducting my research. A great deal of appreciation goes to the technical staff of the Microelectronics and Materials Technology Centre (MMTC) at RMIT University Mr. Yuxun Cao, Mr. Paul Jones and Ms. Chin-Ping Wu for their assistance in microfabrication, measurements and general technical advice. Also, I wish to extend my gratitude to the research administrative officers of the School of Electrical and Computer Engineering at RMIT University Ms Karen Hewitt and Ms Laurie Clinton for their excellent support and understanding.

Many thanks go to Associate Professor Johan du Plessis and Dr. Samuel Ippolito from the School of Applied Sciences in RMIT University. A special big thank you goes to the technical staff of the RMIT Microscopy and Microanalysis Facility, Mr. Phil Francis and all the duty microscopists, who provided fantastic training and extended access hours to electron microscopes and other advanced material's characterization equipment. Also, I would like to express my gratitude to the staff of the School of Graduate Research for their workshops that were helpful throughout the entire PhD candidature.

During my research program, I had the magnificent opportunity to conduct collaborative endeavor with international and local universities. In that perspective, I would like express my sincere gratitude and appreciation to Professor Richard B. Kaner from

University of California, Los Angeles and his former students Dr. Henry D. Tran and Dr. Robert W. Kojima. Also, I would like to thank Professor Koo Shin of Sejong University in Korea and his team. Additionally, I wish to forward a special thank you to Dr. Catherine Debiemme-Chouvy and Mr. Stephan Borensztajn of Pierre and Marie Curie University in France. Locally, I would like to extend my appreciation to Professor Gordon G. Wallace of University of Wollongong and his team. Also, I wish to send many thanks to Associate Professor Dan Li from Monash University and his team.

The support of a loving and caring family gave me a lot of strength and determination to complete this project. Especially, I would like to thank my loving wife Ms Nibras Awaja from the bottom of my heart. Her remarkable love, patience, understanding and continuous encouragement kept me going during the time of my study. Whenever I was feeling down, she was always there to put me back on track towards completion. Also, I would like to thank her for the valuable feedback that she provided during the preparation of this thesis. I acknowledge that I can not find enough words to describe my gratitude for her substantial role in realizing my research accomplishments. I wish to take this opportunity to say thank you to my sons Yousif and Ayser for their love, support and understanding.

Extended family members were also very supportive. I would like to thank my brother Dr. Dheya Al-Mashat (MD) and my sister Ms Reem Al-Mashat. Additionally, I wish to thank my father in law Mr. Saheb Awaja and my mother in law Ms Fakhriyya Saleh. Also, I would like to thank my brothers in law Dr. Firas Awaja and Dr. Mohannad Awaja. I wish to thank my sister in law Ms Eynas Awaja and her husband Mr. Mohammed Ali Kazim. Finally, I wish to take this opportunity to pay tribute to the memory of my father Mr. Mohammed Al-Mashat and my mother Mrs. Fawzia Al-Mashat. Despite that they passed away before the commencement of this research, their encouragement to me to pursue academic achievements remains a constant internal stimulation.

Laith Al-Mashat

Abstract

THIS dissertation reports the development of novel conductometric and layered Surface Acoustic Wave (SAW) hydrogen gas sensors based on nanostructured conducting polymers and graphene/polyaniline nanocomposite. Due to the high surface to volume ratios of the gas sensitive films based on nanostructured materials, they permit deep and rapid penetration of target gas molecules. Template-free electropolymerization and/or chemical polymerization methods were employed during the synthesis of the nanostructured polythiophene, polypyrrole, polyaniline, polyanisidine, polyethylaniline and graphene/polyaniline nanocomposite which were investigated for their hydrogen gas sensing characteristics herein. The nanostructured gas sensitive films' physical and chemical properties were studied using scanning electron microscopy (SEM), transmission electron microscopy (TEM), Fourier transform infrared spectroscopy (FT-IR), Raman spectroscopy, Ultraviolet-visible spectroscopy (UV-Vis), and X-ray photoemission spectroscopy (XPS). A programmable gas calibration and data acquisition system was utilized to measure the sensors' responses towards hydrogen gas with different concentrations of at room temperature.

A comparative study on the performance of conductometric hydrogen gas sensors based on electropolymerized polythiophene nanostructured films was conducted for the first time in this thesis according to the best of the author's knowledge. Polythiophene gas sensitive films featuring nanofibers with diameters of 10-40 nm were successfully electrodeposited on conductometric transducers. Electropolymerization parameters such as counterion's type, the concentration of the electrolyte, the electropolymerization potential and the deposition time were shown by the author of this thesis to affect the morphology of the gas sensitive film and ultimately its response towards hydrogen gas.

For the first time, to the best knowledge of this dissertation's author, electropolymerized polypyrrole nanowires with diameters of 40-90 nm and chemically polymerized polypyrrole nanofibers of 18 nm in diameter were employed for hydrogen gas sensing in this PhD project. The effect of polypyrrole's counterion type on the resultant gas sensor electrical characteristics was investigated herein. Via a comprehensive investigation, it was found that chemically synthesized chloride-doped polypyrrole nanofibers to be more sensitive to hydrogen gas than the perchlorate-doped electropolymerized polypyrrole

nanowires due to the smaller molecular size of the incorporated counterion into the polymer matrix.

Novel layered SAW gas sensors based on polythiophene nanofibers, polypyrrole nanofibers, nanoporous polyaniline, polyanisidine nanofibers and polyethylaniline nanofibers were developed and tested at room temperature. The highest response was observed for the polyanisidine nanofibers/ZnO/36° YX LiTaO₃ SAW gas sensor with a 294 kHz frequency shift from the center frequency upon exposure to hydrogen gas with the concentration of 1% in ambient air. Morphological analysis of the deposited polyanisidine nanofibers based thin film revealed that the nanofibers, ~55 nm in diameter, were not densely packed that allows deep and efficient penetration of target gas molecules into the sensitive film and makes gas sensing possible over the entire length of a nanofiber into a mesh.

To the best knowledge of the author of this dissertation, the first ever reported hydrogen gas sensor based on graphene/polyaniline nanocomposite was developed and characterized for the first time in this PhD program. This sensor outperformed hydrogen gas sensors based on polyaniline nanofibers at room temperature. After analyzing the nanocomposite's characterization results, the author of this thesis suggested that the observed high response is attributed to the graphene/polyaniline nanocomposite's high surface area compared to that of the pure polyaniline nanofibers due to the growth of polyaniline nanofibers in the order of 25-50 nm in diameter on the graphene nanosheets' surfaces.

In conclusion, the outcomes of this PhD research contributed significantly to the development of nanostructured gas sensitive films. It is obvious that for hydrogen-based transport and energy generation systems, hydrogen gas sensors play a major role in preventing catastrophic consequences associated with hydrogen explosions. All the developed room temperature hydrogen gas sensors based on nanostructured conducting polymers and graphene/polyaniline nanocomposite herein were capable of sensing hydrogen gas with concentrations as low as 0.06%. As such, these gas sensors can certainly serve as prototypes for future commercialization purposes.

List of Author's Publications

Refereed Journal Papers

1. **L. Al-Mashat**, C. Debieemme-Chouvy, S. Borensztajn and W. Wlodarski, "Electropolymerized polypyrrole nanowires for hydrogen gas sensing", *The Journal of Physical Chemistry C*, vol. 116, pp. 13388-13394, 2012.
2. **L. Al-Mashat**, D. S. Ahn, S. H. Han, W. G. Hong, K. Shin, C. S. Yoon, K. Kalantar-zadeh and W. Wlodarski, "Layered surface acoustic wave hydrogen sensor with nanoporous polyaniline as the active layer", *Sensor Letters*, vol. 9, pp. 73-76, 2011.
3. K. Shin, **L. Al-Mashat**, J. S. Song, S. H. Han, D. S. Ahn, B. Y. Yoo, K. Kalantar-zadeh and W. Wlodarski, "Polyaniline/MWCNT nanocomposite based hydrogen sensor operating at room temperature", *Sensor Letters*, vol. 9, pp. 69-72, 2011.
4. K. Shin, **L. Al-Mashat**, D. Ahn, S. Han and W. Wlodarski, "A room temperature conductometric hydrogen sensor with polyaniline/WO₃ nanocomposite", *Sensor Letters*, vol. 9, pp. 77-81, 2011.
5. **L. Al-Mashat**, K. Shin, K. Kalantar-zadeh, J. D. Plessis, S. H. Han, R. W. Kojima, R. B. Kaner, D. Li, X. Gou, S. J. Ippolito and W. Wlodarski, "Graphene/Polyaniline nanocomposite for hydrogen sensing", *The Journal of Physical Chemistry C*, vol. 114, pp. 16168-16173, 2010.
6. M. B. Rahmani, S. H. Keshmiri, J. Yu, A. Z. Sadek, **L. Al-Mashat**, A. Moafi, K. Latham, Y. X. Li, W. Wlodarski and K. Kalantar-zadeh, "Gas sensing properties of thermally evaporated lamellar MoO₃", *Sensors and Actuators B: Chemical*, vol. 145, pp. 13-19, 2010.
7. **L. Al-Mashat**, H. D. Tran, W. Wlodarski, R. B. Kaner and K. Kalantar-zadeh, "Polypyrrole nanofiber surface acoustic wave gas sensors", *Sensors and Actuators B: Chemical*, vol. 134, pp. 826-831, 2008.
8. **L. Al-Mashat**, H. D. Tran, W. Wlodarski, R. B. Kaner and K. Kalantar-Zadeh, "Conductometric hydrogen gas sensor based on polypyrrole nanofibers", *IEEE Sensors Journal*, vol. 8, pp. 365-370, 2008.

Conference Proceedings

1. **L. Al-Mashat**, H.D. Tran, R.B. Kaner and W. Wlodarski, "Room temperature layered surface acoustic wave hydrogen gas sensor based on polymethylaniline nanofibers", *Proceedings of the 9th Asian Conference on Chemical Sensors*, pp. 38, Taipei, Taiwan, 14-17 November 2011. (poster presentation)
2. C. Debiemme-Chouvy, **L. Al-Mashat**, S. J. Ippolito, K. Kalantar-zadeh and W. Wlodarski, "Conductometric hydrogen gas sensor based on electrochemically deposited polypyrrole nanowires", *Proceedings of the 9th Spring Meeting of the International Society of Electrochemistry*, pp. 178, Turku, Finland, 8-11 May 2011. (poster presentation)
3. K. Shin, **L. Al-Mashat**, S. H. Han, K. Kalantar-zadeh and W. Wlodarski, "Graphene/Polythiophene nanocomposite based hydrogen sensor," *Proceedings of the 5th Asia-Pacific Conference on Transducers and Micro-Nano Technology*, pp. 120, Perth, Australia, 6-9 July 2010. (poster presentation)
4. R. W. Kojima, V. Strong, M. J. Allen, K. Kalantar-zadeh, **L. Al-Mashat**, W. Wlodarski and R. B. Kaner, "Nanostructured conducting polymer and graphene composite chemical sensors", *Proceedings of the 13th International Meeting on Chemical Sensors*, pp. 259, Perth, Australia, 11-14 July 2010. (oral presentation)
5. R. Arsat, X. He, **L. Al-Mashat**, M. Shafiei, W. Wlodarski and K. Kalantar-zadeh "Highly ordered dedoped polyaniline nanofibers based 36° YX LiTaO₃ surface acoustic wave H₂ gas sensor", *Proceedings of the 8th Asian Conference on Chemical Sensors*, pp. 115, Daegu, Korea, 11-14 November 2009. (poster presentation)
6. **L. Al-Mashat**, W. Hong, K. Shin, K. Kalantar-zadeh and W. Wlodarski, "Hydrogen sensors based on chemically synthesized polythiophene nanofibers – a study of the dopant effect on the gas sensing properties", *Proceedings of the 8th Asian Conference on Chemical Sensors*, pp. 127, Daegu, Korea, 11-14 November 2009. (poster presentation)
7. **L. Al-Mashat**, J. S. Song, K. Shin, B. Y. Yoo, K. Kalantar-zadeh and W. Wlodarski, "Polyaniline/MWCNT nanocomposite based hydrogen sensor operating at room temperature", *Proceedings of the 8th Asian Conference on Chemical Sensors*, pp. 128, Daegu, Korea, 11-14 November 2009. (poster presentation)
8. **L. Al-Mashat**, K. Shin, W. G. Hong, D. S. Ahn, C. S. Yoon, K. Kalantar-zadeh and W. Wlodarski, "Layered surface acoustic wave hydrogen sensor with

- nanoporous polyaniline as the active layer", *Proceedings of the 8th Asian Conference on Chemical Sensors*, pp. 129, Daegu, Korea, 11-14 November 2009. (poster presentation)
9. **L. Al-Mashat**, K. Shin, K. Kalantar-zadeh and W. Wlodarski, "A room temperature conductometric hydrogen sensor with polyaniline/WO₃ composite nanofibers", *Proceedings of the 8th Asian Conference on Chemical Sensors*, pp. 130, Daegu, Korea, 11-14 November 2009. (poster presentation)
 10. **L. Al-Mashat**, R. B. Kaner, H. D. Tran, K. Kalantar-zadeh and W. Wlodarski, "Layered surface acoustic wave hydrogen sensor based on polyethylaniline nanofibers", *Proceedings of the Eurosensors XXIII Conference in Elsevier's Procedia Chemistry*, vol. 1, pp. 220-223, Lausanne, Switzerland, 6-9 September 2009. (poster presentation)
 11. **L. Al-Mashat**, H. D. Tran, R. B. Kaner, R. Arsat, K. Kalantar-Zadeh and W. Wlodarski, "A hydrogen gas sensor fabricated from polythiophene nanofibers deposited on a 36° YX LiTaO₃ layered surface acoustic wave transducer", *Smart Structures, Devices, and Systems IV; Proceedings of SPIE*, vol. 7268, pp. 72680M-8, Melbourne, Australia, 9-12 December 2008. (oral presentation)
 12. **L. Al-Mashat**, H. D. Tran, R. B. Kaner, K. Kalantar-zadeh, Y. Li and W. Wlodarski, "A room temperature hydrogen sensor based on polythiophene nanofibers", *Proceedings of the Eurosensors XXII Conference*, pp. 1108-1111, Dresden, Germany, 7-10 September 2008. (poster presentation)
 13. **L. Al-Mashat**, H. D. Tran, W. Wlodarski, R. B. Kaner and K. Kalantar-zadeh, "Polypyrrole nanofibers as the sensing element of a conductometric hydrogen gas sensor", *Proceedings of Symposium A2 of the International Conference on Nanoscience and Nanotechnology (ICONN)*, pp. 23-24, Melbourne, Australia, 25-29 February 2008. (oral presentation)
 14. **L. Al-Mashat**, H. Tran, R. B. Kaner, W. Wlodarski, A. Z. Sadek and K. Kalantar-zadeh, "Polypyrrole nanofibers gas sensor based on 36° YX LiTaO₃ layered surface acoustic wave transducer" *Proceedings of the 7th East Asian Conference on Chemical Sensors*, pp. 70, Singapore, 3-5 December 2007. (poster presentation)
 15. **L. Al-Mashat**, H. D. Tran, W. Wlodarski, R. B. Kaner and K. Kalantar-zadeh, "Hydrogen gas sensor fabricated from polyanisidine nanofibers deposited on 36° YX LiTaO₃ layered surface acoustic wave transducer", *BioMEMS and Nanotechnology III; Proceedings of SPIE*, vol. 6799 pp. 67991B-8, Canberra, Australia, 5-7 December 2007. (poster presentation)

Chapter 1

Introduction

THE aim of the present chapter is to provide an introductory material on the research work conducted by the author. The motivation and the objectives behind the research presented in this PhD thesis are detailed in sections 1.1 and 1.2 respectively. While in sections 1.3 and 1.4, the research outcomes and the thesis organization are discussed.

1.1 Motivation

There is an increasing world wide effort to sustain our planet through minimizing the emission of toxic gases associated with the industrial and domestic everyday life activities. As a part of this endeavor, the replacement of fossil hydrocarbon fuels with environmentally friendly energy sources has been sought over the years. Hydrogen is considered as an alternative energy source which is becoming favorable in a rising number of applications. In order to explore the motivation for the research presented in this thesis, hydrogen gas properties, applications, and sensors are discussed in the subsequent subsections.

1.1.1 Hydrogen Gas Properties and Applications

Hydrogen is a colorless, odorless, tasteless and highly flammable gas [1]. Combustion of hydrogen in air results in no carbon emission, which is the main feature of using hydrogen as a fuel. When hydrogen is utilized as an energy carrier, its properties

become of utter importance for safety reasons. Hydrogen gas is usually considered to be more dangerous than other flammable gases such as methane, which is the main constituent of natural gas used for household appliances. Table 1.1 provides a comparison between safety related properties of hydrogen gas and methane gas.

Table 1.1. Safety related properties of hydrogen gas and methane gas [2, 3].

Property	Hydrogen	Methane
Limits of flammability in air, vol.%	4.0–75.0	5.3–15.0
Detonation limit in air, vol.%	18.3–59.0	6.3–13.5
Maximum energy for ignition in air, mJ	0.02	0.29
Auto-ignition temperature, K (°C)	858 (585)	813 (540)
Flame temperature, K (°C)	2318 (2045)	2148 (1875)
Flame velocity, m/s	1.85	0.38
Diffusion coefficient in NTP air, cm ² /s*	0.61	0.16
Molecular weight	2.016	16.043
Boiling Point, K (°C)	~20 (–253)	~112 (–161)

* NTP (normal temperature and pressure): 293 K (20 °C) and 1 atm

From the data presented in Table 1.1, the following safety related issues can be outlined:

- *Flammability and Detonation Limits.* Hydrogen burns with a lower concentration in air than methane, which is an economical feature but it highlights the importance of the early detection of any hydrogen gas leak. Hydrogen has a much wider flammability range than methane, which makes it very useful when a large amount of combustion energy is needed such as space applications. The detonation limit represents the range of concentrations by which a fuel/air mixture is considered explosive, which is much wider in the case of hydrogen compared with that of methane.
- *Ignition.* Much lower energy is needed to ignite hydrogen (0.02 mJ) than that for methane (0.29 mJ), which underlines the risks associated with hydrogen powered systems. However for its credit, hydrogen gas would self-ignite at a higher temperature than that of the methane gas.
- *Flame Temperature and Velocity.* A hydrogen flame is hotter and propagates much faster than a methane flame according to the data presented in Table 1.1.

Hydrogen flames are nearly invisible in daylight but their visibility is improved by the presence of humidity and/or impurities in the air [2].

- *Diffusion and Molecular Weight.* Hydrogen has a higher diffusion coefficient than methane. As a result hydrogen gas diffuses in air more rapidly than methane due to its low molecular weight compared to that of methane. From safety perspectives, this hydrogen property is considered favorable.
- *Boiling Point.* The extremely low boiling point of hydrogen ($-253\text{ }^{\circ}\text{C}$) is considered a safety aspect when liquid hydrogen is used as a fuel. If a leak occurs, liquid hydrogen transforms into gas phase instantly and diffuses in air rapidly in contrast to a gasoline spill that evaporates slowly [4].

Hydrogen in its molecular form is relatively inactive [1]. However when the hydrogen molecule is dissociated, the hydrogen atom becomes a powerful reducing agent. It can reduce metal salts such as nitrates, nitrites, and cyanides in order to extract free metals. Atomic hydrogen also reacts with a number of elements to yield hydrides such as NH_3 , NaH , KH , and PH_3 [3].

There is a growing number of hydrogen gas applications in domestic and industrial areas from being a clean source of energy to a process gas for many industries [5, 6]. Some of these applications are listed below:

- *Aerospace.* Hydrogen has been used as a rocket fuel for years. The rocket engines consume about 500,000 gallons of liquid hydrogen in every rocket launch.
- *Automobile Industry.* Some hydrogen fueled vehicles utilize fuel cells to create electricity through an electrochemical reaction between hydrogen and oxygen gases. While in another emerging technology, Internal Combustion Engines (ICE), hydrogen gas is combusted internally in a similar way to gasoline combustion in conventional vehicles [7].
- *Metal Production Industry.* Hydrogen gas is employed to provide a protective atmosphere in high-temperature operations such as manufacturing of stainless steel. It is also used to support plasma welding and cutting operations.
- *Pharmaceuticals Industry.* Hydrogen is a process gas in the production of vitamins A and C, surfactants, and cosmetics.
- *Food Industry.* Hydrogen gas is used to hydrogenate liquid oils (such as soybean, fish, cottonseed and corn), converting them to semisolid materials such as shortenings, margarine and peanut butter.
- *Chemical Processing.* A well known industrial application of hydrogen gas is a process gas in the manufacturing of ammonia and methanol. Also hydrogen gas

is utilized to hydrogenate non-edible oils for the production of soaps, insulation, plastics, ointments and other specialty chemicals.

- *Petroleum Industry.* Hydrogen gas is used to enhance the performance of petroleum products by removing organic sulfur from the crude oil. It is also employed to reformulate process exhaust gases in order for refiners to meet the Clean Air Act requirements.

For every application, gas sensors play a major role in protecting lives and properties through early detection of any hydrogen gas leak. In the next subsection, an introduction to the constantly developing field of gas sensors is presented.

1.1.2 Gas Sensors

The science and technology of gas sensors is an active multi-disciplinary research area. A gas sensor can be defined as a device that produces a meaningful output signal related to the concentration of a target gas [8]. Generally, a gas sensor consists of two combined physical parts known as the sensitive layer and the transducer. The sensitive layer is the chemically active part that changes its properties such as conductivity and/or mass due to the interaction with target gas molecules [9]. These changes in the sensitive layer are transformed into a measurable output signal by the transducer. Further discussions on both of the gas sensitive films and the transducers are provided in the upcoming subsections.

1.1.2.1 Gas Sensing Films

There is a vast number of sensitive materials reported in literature that can be deposited in the form of thin films. It is beyond the scope of this dissertation to detail every material useful for gas sensing, since many materials are specifically engineered to selectively sense certain type of target gases. However, a description of the main groups of sensing materials is provided in this section.

Metals

In the case of hydrogen gas, it is well known that the hydrogen molecules dissociate spontaneously upon the interaction of hydrogen gas with group VIII transition metals such as palladium and its alloys [10, 11]. However, palladium is more common as a sensitive layer due to its special expansion property upon exposure to hydrogen gas. Several palladium alloys have been investigated for hydrogen gas sensing, for example, Pd/Ni [12-14], Pd/Ag [15], and Pd/Mg [16] in order to improve the sensitivity and reduce

the overall cost of the sensors. Hydrogen adsorption in palladium consists of a two step process. In the first step, hydrogen molecules are dissociated into atoms on the palladium surface. While in the second step, hydrogen atoms diffuse into the palladium lattice which results in an expansion in the palladium lattice and a phase transition from the α phase (conductive metallic phase) to the β phase (less conductive phase) [17]. When the hydrogen gas is removed from the sensing film's environment, hydrogen atoms travel to the surface and recombine to form free hydrogen molecules causing a recovery in the sensing film resistance. However, palladium based gas sensors suffer from poor performance under anaerobic conditions since oxygen is essential in reversing the phase transition associated with hydrogen adsorption [18]. Also, palladium based gas sensitive films are susceptible to chemical poisoning by species like sulfide [18].

Metal Oxides

Gas sensors based on metal oxides thin films have been extensively reported in literature. Hydrogen gas sensors based on thin films of ZnO, TiO₂, SnO₂, NiO, Nb₂O₅, In₂O₃, and Co₃O₄ have been previously reported [19]. In another work, a lamellar MoO₃ was investigated for hydrogen gas sensing [20]. During the interaction between metal oxides and hydrogen gas at elevated temperatures, it is possible that the dissociation of hydrogen molecules followed by the adsorption of hydrogen atoms into the lattice of the metal oxide takes place [21, 22]. Also at high temperatures, the chemisorption of oxygen from the ambient into the metal oxide's lattice is possible [23]. Therefore, water molecules can be formed associated with the release of electrons resulting in an increase in the sensing film conductivity [22, 24]. The operational drawbacks of the metal oxides based sensors are their operation at elevated temperatures and poor selectivity [19, 25]. Their high operating temperatures at around (300–500°C) can decrease the sensors lifetime. Furthermore the elevated temperature operation causes high power consumption.

Carbon Nanotubes and Graphene

The discovery of carbon nanotubes (CNTs) in 1991 opened a new era in materials science and nanotechnology [26]. CNT may be conceptually viewed as a graphite sheet that is rolled into a nanoscale tube to form a single walled carbon nanotube (SWNT), or a multiwalled carbon nanotube (MWNT) with additional graphene coaxial tubes around the SWNT core. Due to the distortion of the electron clouds of CNTs from a uniform distribution in graphite to asymmetric distribution around cylindrical nanotubes, a rich

π electron conjugation forms outside the CNTs, making them electrochemically active [27]. Hence their conductivity can change reversibly during the interaction with oxidizing and reducing gases [28-30].

Graphene is a 2-D sheet of carbon atoms bonded through sp^2 hybridization [31]. Graphene nanosheets have very large surface area, which make them preferable for gas sensing application. Gas sensors based on graphene for NO_2 , NH_3 , CO, and H_2 gases have been developed [32, 33]. According to a density functional theory (DFT) study, hydrogen is physisorbed on the center of the carbon hexagon forming the graphene sheet [34]. By incorporating graphene into a nanocomposite a highly sensitive hydrogen gas sensor was developed by the author of this dissertation for the first time, to the best of the author's knowledge, and will be discussed in great detail in the upcoming chapters.

Conducting Polymers

Conducting polymers alternatively referred to as conjugated polymers received a large number of theoretical and experimental studies in the past three decades. Due to their chemical versatility, researchers around the globe were motivated to investigate their applications in many areas including batteries [35], light emitting diodes [36], biological and gas sensors [37-40]. Their conductivity is based on charge carriers transport throughout the polymer's backbone and hopping between neighboring polymer chains [41]. This particular class of organic matter can undergo an insulator to metal transition or vice versa during the interaction with an acidic or alkaline substance [42]. Therefore, conducting polymers can serve as gas sensitive materials due to the variation in their conductivities during the interaction with target gases. The key features of gas sensors based on conducting polymers are listed below:

- The sensors have fast adsorption and desorption of target gas molecules at ambient temperature [39, 43].
- The sensors feature low power consumption since they can operate at room temperature [43].
- Sensing film properties can be specifically engineered during the polymer synthesis through adding functional groups to the polymer matrix [38, 44].
- Simplicity of transducer fabrication since only one-sided photolithography is needed due to the elimination of the heating element that is usually fabricated at the backside of the transducer, making the overall gas sensor cost effective and viable for commercialization purposes.

In the past few years, a great deal of research has been devoted for developing nanotechnology-enabled sensors [9]. Nanostructured conducting polymers thin films are

favorable over their conventional counterparts for gas sensing application for the following reasons [45]:

- As the degree of the polymer's structural order increases, the behavior of the polymer during the interaction with the target gas becomes more predictable and reproducible.
- The nanostructured thin film has a high surface to volume ratio and hence a large interfacial area for the adsorption of gas molecules. Also due to its high porosity, the gas molecules can penetrate deep into the nanostructured sensitive layer leading to a higher sensitivity compared to that of its bulk counterpart.
- By synthesizing nanocomposites of conducting polymers with organic or inorganic inclusions, the physical and chemical properties of the resulting material can be tailored to enhance the gas sensor's static and dynamic characteristics.

The development of gas sensors based on nanostructured conducting polymers is a relatively new promising area of exploration [45]. Hence, the author of this dissertation was motivated to launch a thorough investigation in order to synthesize, deposit and characterize novel nanostructured conducting polymers and graphene/polyaniline nanocomposite for hydrogen gas sensing application.

1.1.2.2 Transduction Platforms

A transducer can be defined as a device that converts one form of energy to another [9]. There are many kinds of transduction platforms that transform the physiochemical changes occurring in the sensitive films into measurable output signals. To name few of them, there are conductometric, Surface Acoustic Wave (SAW), optical fiber, Schottky diode and Field Effect Transistor (FET). The author of this dissertation has made an informed decision to choose the conductometric and SAW transduction platforms for their compatibility with the deposition techniques of the synthesized nanostructured conducting polymers and graphene/polyaniline nanocomposite.

A conductometric transducer usually contains two sets of conductive electrodes patterned on an insulating substrate such as quartz or alumina (Al_2O_3) as shown in Figure 1.1. In the case of a successful transducer fabrication process, the resistance between the output wires is infinite. After the deposition of the gas sensitive film, the resistance of the gas sensor becomes a measurable value. Monitoring the changes in resistance during the interaction with a target gas provides an accurate account of the variations in the conductivity of the sensitive film accordingly. Conductometric

transducers are largely used in the field of gas sensors for their simple design and fabrication that allows their production in bulk for comprehensive investigation [19].

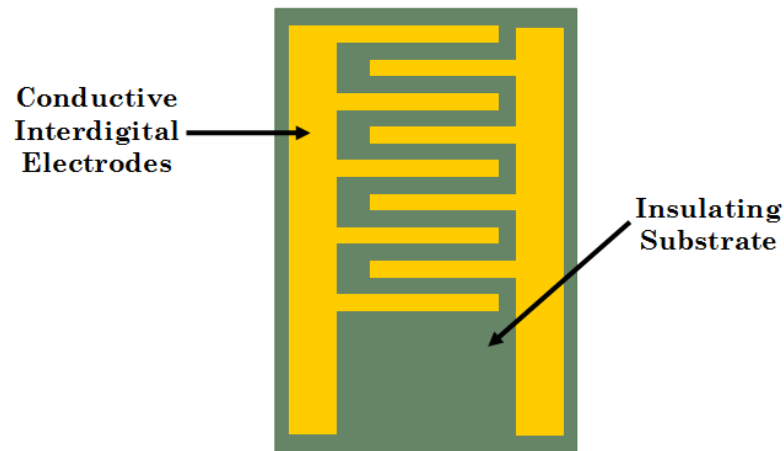


Figure 1.1. Schematic of a conductometric transducer.

A SAW transducer consists of a piezoelectric substrate such as lithium tantalate (LiTaO_3), quartz or lithium niobate (LiNbO_3) with a conductive pair of input and output interdigital transducers (IDTs) patterned on its surface as shown in Figure 1.2. For best performance, the IDT period is chosen to match the wavelength of the propagating surface acoustic wave. SAW gas sensors are highly sensitive to the surface perturbations along the wave propagation path caused by the changes in the deposited sensitive thin film's conductivity or mass during the interaction with target gases [32].

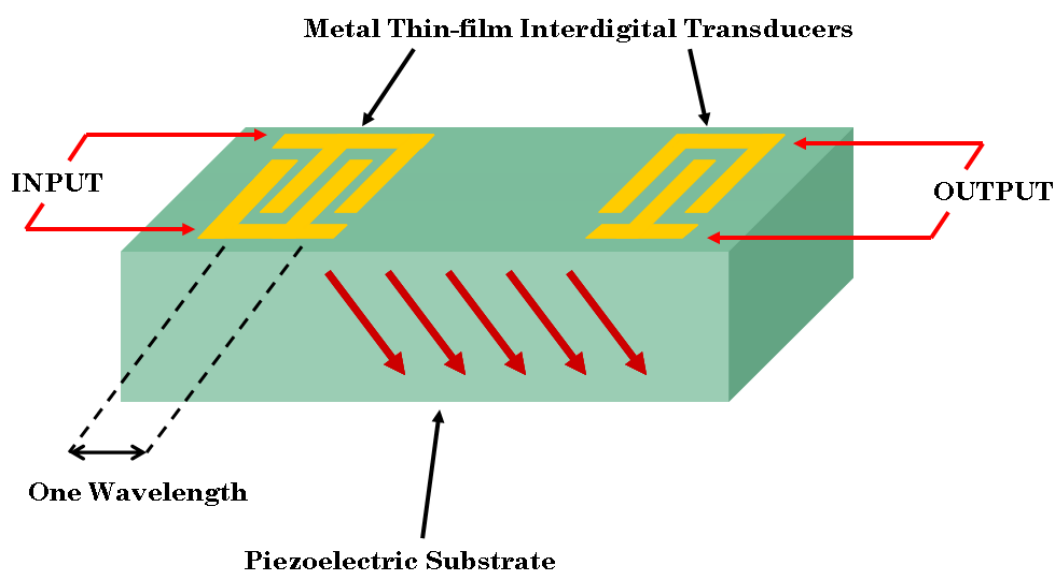


Figure 1.2. Schematic of a SAW transducer.

1.2 Objectives

The main purpose of the research program presented in this PhD dissertation is to develop and evaluate the performance of novel conductometric and layered SAW gas sensors based on nanostructured conducting polymers and graphene/polyaniline nanocomposite. It is understood that gas sensors based on nanostructured conducting polymers can outperform those based on their conventional counterparts in terms of sensitivity. This suggestion is supported by literature that is critically reviewed by the author of this thesis in Chapter 2. During the PhD research presented herein, the following objectives were sought to be met under the umbrella of investigating novel nanostructures of conducting polymers and their nanocomposites for gas sensing applications:

- Developing synthesis route for novel conducting polymer nanostructures suitable for gas sensing applications.
- Investigation of the developed nanostructured gas sensitive films' physical and chemical properties utilizing scanning electron microscopy (SEM), transmission electron microscopy (TEM), Fourier transform infrared spectroscopy (FT-IR), Raman spectroscopy, Ultraviolet-visible spectroscopy (UV-Vis), and X-ray photoemission spectroscopy (XPS).
- Development of gas sensors through microfabrication of conductometric and layered SAW transducers as well as nanostructured materials' syntheses and deposition.
- Investigation of the developed novel gas sensors' electrical characteristics towards different concentrations of hydrogen gas.

1.3 Outcomes and Author's Achievements

The research presented in this PhD thesis had many novel outcomes as outlined below:

- A comparative study on conductometric hydrogen gas sensors based on electropolymerized polythiophene nanostructures was conducted for the first time in this dissertation according to the best knowledge of the author of this thesis.
- Novel polythiophene nanofibers/ZnO/36° YX LiTaO₃ SAW gas sensor was developed and tested.
- Conductometric hydrogen gas sensors based on electropolymerized polypyrrole nanowires and chemically synthesized polypyrrole nanofibers were developed

and tested for the first time, to the best knowledge of the author of this dissertation.

- Novel polypyrrole nanofibers/ZnO/36° YX LiTaO₃ SAW gas sensor was developed and tested.
- Novel nanoporous polyaniline/ZnO/36° YX LiTaO₃ SAW gas sensor was developed and tested.
- Polyanisidine nanofibers/ZnO/36° YX LiTaO₃ SAW gas sensor was developed and tested for the first time in this dissertation, to the best knowledge of the author of this thesis.
- Novel polyethylaniline nanofibers/ZnO/36° YX LiTaO₃ SAW gas sensor was developed and tested.
- For the first time, to the best of the author's knowledge, graphene/polyaniline nanocomposite based conductometric hydrogen gas sensor was developed and investigated.

A number of refereed journal articles and conference proceedings have been published by the author of this PhD dissertation based on the aforementioned research outcomes. Some of the author's journal articles received a large number of citations. Consequently, the author of this thesis won the prestigious RMIT University's 2012 Vice-Chancellor's Higher Degree by Research Publication Excellence Award. Due to the author's publication record, he has been recognized by publishers in the field and became a reviewer for the following refereed journals:

- ACS Nano, published by American Chemical Society.
- Polymer International, published by Wiley.
- Sensors and Actuators A: Physical, published by Elsevier.
- Sensors, published by MDPI.

1.4 Thesis Organization

In organizing the following chapters of this thesis, the author attempted to provide a logical sequence of information from critically reviewing the current status of knowledge to the testing of the developed sensors. A brief description of the upcoming chapters is provided below:

- **Chapter 2:** In this chapter, a critical review of literature on the synthetic methods for nanostructured conducting polymers and the reported gas sensors based on them is provided.
- **Chapter 3:** A theoretical background on the conductometric and layered SAW gas sensors is given in this chapter.

- **Chapter 4:** The fabrication steps of the conductometric and layered SAW transducers are detailed in this chapter.
- **Chapter 5:** The syntheses and deposition of the nanostructured conducting polymers and graphene/polyaniline nanocomposite are detailed in this chapter.
- **Chapter 6:** The nanomaterials' characterization results are analyzed by the author of this thesis in this chapter.
- **Chapter 7:** In this chapter, the gas sensing results of all the developed sensors are analyzed by the author of this dissertation in conjunction with the characterization results presented in chapter 6. Also the author discusses the gas sensing mechanisms of the developed gas sensors in this chapter.
- **Chapter 8:** Conclusions and suggested future work are discussed in this chapter.

Chapter 2

Literature Review

SINCE the discovery of conducting polymers (CPs) in mid-1970s, they received an increasing attention from researchers around the world. The growing contribution of CPs to the development of science and technology has been globally recognized by the awarding of the prestigious Nobel Prize for chemistry in the year 2000 to the discoverers of CPs: Alan MacDiarmid, Alan Heeger and Hideki Shirakawa.

The aim of this chapter is to provide a critical review of literature on the synthetic methods of nanostructured CPs and the reported gas sensors based on them. Section 2.1 will give an introduction to CPs. Section 2.2 will review the synthesis methods for nanostructured CPs including the template-free method employed throughout this dissertation. A review of published reports on conductometric and surface acoustic wave (SAW) gas sensors based on CPs will be presented in section 2.3. Also, gas sensors based on composite materials reported in literature will be reviewed in section 2.4. Finally, this chapter will be summarized in the section 2.5.

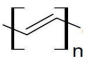
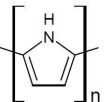
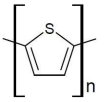
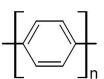
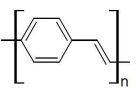
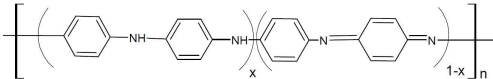
2.1 Introduction to Conducting Polymers

Conducting polymers are considered as organic semiconductors. Depending on the synthetic conditions, their electrical and optical properties can be comparable to that of metals and semiconductors. Hence CPs are attractive for many applications such as light emitting diodes (LED) [46, 47], field-effect transistors (FET) [48], solar cells [49], and electroluminescent devices due to their conductivity dependent color [50].

Polymers in general consist of chains of large number of repeated monomer units. A CP is a polymer that has a π -conjugated electronic structure. The π -electrons are usually

delocalized along the polymer chain, which are responsible for making CPs conductive. Table 2.1 displays the structures and electronic properties of some CPs. The polymers' conjugated structure can be observed through the alternating single and double bonds in the aromatic rings or via conjugated segments coupled with heteroatoms (e.g. N, S) providing a continuous overlapping p -orbitals along the polymers' backbones [51].

Table 2.1. Structures and conductivities of some conjugated polymers [51].

Polymer	Structure	$\pi - \pi^*$ Gap (eV)	Conductivity (S/cm)
Polyacetylene		1.5	$10^3 - 1.7 \times 10^5$
Polypyrrole		3.1	$10^2 - 7.5 \times 10^3$
Polythiophene		2	$10 - 10^3$
Poly(p-phenylene)		3	$10^2 - 10^3$
Poly(p-phenylene vinylene)		2.5	$3 - 5 \times 10^3$
Polyaniline		3.2	30 - 200

For many years, the band theory has been implemented to describe the electrical properties of materials [52]. The materials with small band gap energies (E_g) are considered conductors and those with large E_g are regarded as insulators. CPs are sp^2 hybridized π -electron materials. Therefore, the bonding and anti-bonding of the π -electrons generates energy bands similar to the valence and conduction bands in other class of materials. At room temperature and atmospheric pressure, the π -band (valence) is fully occupied and the π^* -band (conduction) is empty.

Similar to inorganic semiconductors, the CPs band structure allows π - π^* electronic excitation as well as removal or addition of electrons [53]. Adding or removing electrons from the conjugated backbone of a polymer is called doping. A cation-rich CP is called p-doped and an anion-rich CP is referred to as n-doped. It produces a localized electronic state within the π - π^* gap that causes chain deformation around the injected charge. Hence the added charge is not a free electron or hole, but rather trapped within the polymer chain deformation and referred to as polaron or bipolaron depending on the

level of doping. A polaron is a radical cation that is partially delocalized over several monomer units such as a polymer segment. While a bipolaron is a doubly charged spinless bound state of two holes. A schematic representation of polarons and bipolarons in the chains of polypyrrole is shown in Figure 2.1. The formation of polarons and bipolarons allows charge transport in polymer chains. Due to the delocalization of charge carriers along the polymer chain, the electronic transport occurs mainly through hopping.

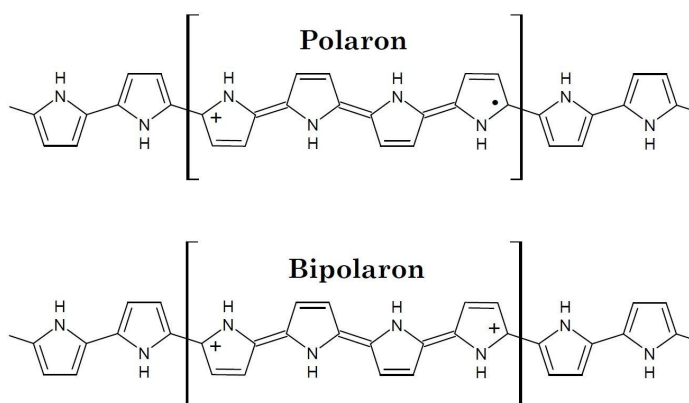


Figure 2.1. Polarons and bipolarons in polypyrrole [53].

CPs doping also involves the inclusion or repulsion of counter-ions, which are the dopant ions in order to maintain charge neutrality. Since every monomer unit is regarded as a potential redox site, CPs can be doped with high density of charge carriers. CPs doping can be achieved by chemical or electrochemical means [53]. The opposite process to doping is dedoping, which is achieved by reversing the redox reaction using the same means of doping that was implemented initially. So every CP has a conductivity range between the dedoped and the doped states as shown in Table 2.1.

Hence the CPs' conjugated π bonds can undergo changes under the influence of chemical species adsorbed onto their surfaces due to a redox or acid-base type interaction between the polymer and the adsorbed chemical species. This particular feature makes CPs interesting materials for the development of gas sensors and biosensors since the CPs' redox reactions are fast and occur at room temperature.

It is evident from Table 2.1 that CPs have narrow band-gaps, which is the reason behind their ease of oxidation and reduction without heating or cooling. However polyacetylene is too reactive because of its low band-gap energy of 1.5 eV. It is extremely sensitive to oxygen in air or in water regardless of whether it is p-doped or n-doped and it can permanently lose its electro-activity under certain experimental conditions [54-58]. Hence the author of this dissertation made an informed decision on developing gas

sensors based on polythiophene, polypyrrole and polyaniline for their stability in air because of their higher band-gap energies compared to that of polyacetylene.

In general CPs can be prepared through either chemical polymerization or electropolymerization [59]. The chemical polymerization is made through mixing a monomer with a strong chemical oxidant such as ammonium peroxydisulfate (APS), ferric ions, permanganate or bichromate anions, or hydrogen peroxide in a polar solvent. These oxidants are capable of generating cation radicals from the monomer units. When the polymerization continues, the cation radicals link with the remaining monomer units to produce oligomers and subsequently insoluble polymers suspended or precipitated into the solution [60]. This technique is suitable for producing bulk quantities of a polymer. The polymer solution can be drop-casted or airbrushed on various substrates. However, it is difficult to obtain a uniform distribution of polymer chains over the surface [39]. On the other hand, electropolymerization allows a controllable polymer deposition on a conductive substrate connected to the working electrode of two or three electrodes electrochemical cell. The polymer film thickness can be controlled by varying the total charge passing between the electrodes [40]. Despite the prerequisite for the working electrode to be conducting, the polymer can still be deposited on the insulating gaps between the conductive fingers in patterned interdigital transducers (IDT) [61]. Many gas sensors have been developed by employing this technique, which will be reviewed in section 2.3.

2.2 Growth Methods of Nanostructured Conducting Polymers

Nanostructured materials are currently receiving a great deal of attention from scientists around the world in order to investigate their unique properties and to develop devices with molecular level interactions. Nanostructures are generally classified according to their dimensionality. For instance, nanoparticles are considered as zero-dimensional, (nanofibers, nanowires and nanorods) as one-dimensional, and (nanoplatelets and nanosheets) as two-dimensional nanostructures [62]. One of the applications that favors the use of nanomaterials is gas sensors for their porosity and high surface-to-volume ratio [9]. For instance, the sensitivities of the gas sensors based on polyaniline nanofibers were higher by several orders of magnitude than those based on bulk polyaniline towards HCl vapor and hydrogen gas [63, 64]. These observations were attributed to a larger penetration of gas molecules into a nanostructured film compared to the bulk one. Hence a nanostructured CP has more adsorption sites

compared to the bulk form which has adsorption sites that are confined to the surface of the sensing film as illustrated in Figure 2.2.

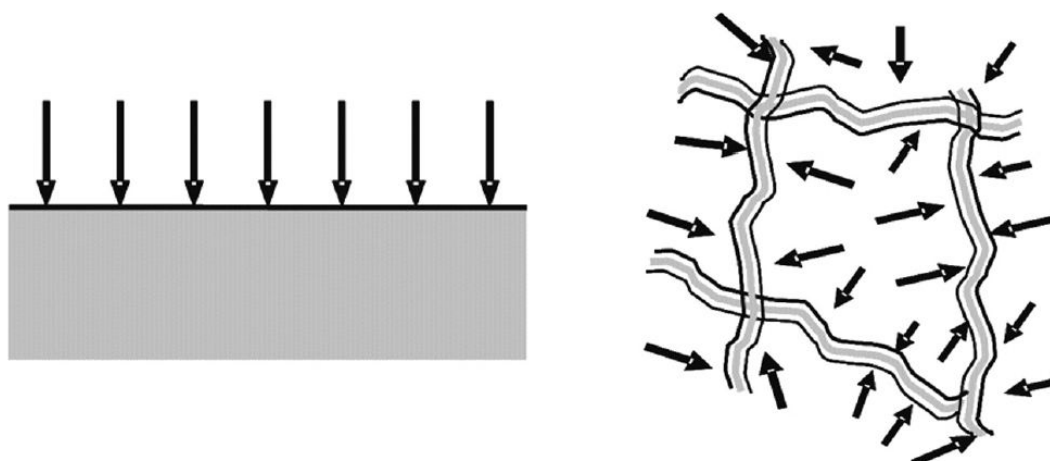


Figure 2.2. Gas adsorption in a bulk film (left) and in a nanostructured film (right), adapted from [63].

Numerous techniques have been developed to synthesize nanostructured CPs, which are reviewed extensively elsewhere [65-68]. The vast majority of these techniques are based on tailoring either the chemical polymerization or the electropolymerization to promote the growth of nanostructured CPs. According to the terminology used by scientists in the field of nanotechnology, they are categorized as “bottom-up” growth [68]. Generally there are two methods for synthesizing nanostructured CPs. The first method is based on employing nanosized templates to direct the polymer growth. The second method is template-free and relies entirely on controlling the polymer growth during the polymerization. Apart from the chemical approach, there is a physical approach to prepare nanostructured CPs, e.g. through mechanical stretching and electrospinning [69, 70]. It would be cumbersome to comprehensively review these approaches in this dissertation. However a concise discussion can be useful in order to support the author’s choice of the synthesis method employed herein for gas sensors development.

2.2.1 Syntheses Based on Templates

Template synthesis is one of the earliest methods adopted by scientists to develop nanostructured CPs. A variety of templates can be used for this purpose. They are usually classified as hard or soft templates. For instance, the anodic aluminum oxide (AAO) membrane, track-etched polycarbonate and channels of zeolites are members of the hard template group. While the surfactant, liquid crystalline polymer, and cyclodextrin are part of the soft template group [66]. For both cases the template has to be removed in order to obtain the nanostructured polymer.

Using the hard templates to produce nanostructured CPs was pioneered by Martin [71]. This technique is a stepwise process. At the beginning the template is deposited onto the substrate. Subsequently the monomer solution is poured into the pores of the template. Then the monomer is polymerized through chemical or electrochemical reactions. Afterwards the substrate is immersed into an acidic solution or an organic solvent, depending on the type of the hard template used, to dissolve the template and release the polymer. Martin reported the ability to control the morphology of the electropolymerized polypyrrole, polyaniline and poly(3-methylthiophene) through this method [71]. Nanotubes were obtained after depositing for a short period of time. However when the reaction was left to continue for a little bit longer, the polymer started to fill the hollow structure resulting in nanofibrillar morphology. The use of hard templates in the synthesis of nanostructured CPs has been extensively reviewed by Jackowska et al. [72].

CPs synthesis by soft templates is based on the formation of micelles from surfactants that self-assemble at a certain concentration of the solution in a process known as microemulsion polymerization [68, 73]. Performing a chemical polymerization within the micellar structure leads to the confinement of CP growth into zero-dimensional, one-dimensional, or two-dimensional nanostructures. However it is rather difficult to control the micelle formation during the microemulsion polymerization in the first place [66]. Several factors cause the kinetically and thermodynamically unstable polymerization such as Ostwald ripening, the collision of monomer droplets leading to secondary growth, as well as the depletion of monomer units [74, 75].

2.2.2 Template-free Syntheses

In the past few years, an increasing number of studies have been published on synthesizing nanostructured CPs without the use of any template in the process. The principle behind this method is simple. CPs are inherently semi-rigid rod-like polymers, which tend to grow linearly [68]. Therefore, it is possible to benefit from this anisotropy to promote the growth of nanoscale structures through the careful selection of synthetic conditions.

In the development of CPs based chemical sensors, the template-free method is preferable for the following reasons:

1. Removing the hard templates requires immersing the deposited film into harsh chemicals such as hydrofluoric acid (HF) and leaving it over night [76]. HF is a strong acid that etches titanium, which is used in this thesis as a support material for the gold IDTs of the SAW transducers.

2. Utilizing template-free synthesis prevents any thin film contamination that may occur because of the imperfect removal of the soft or hard templates.
3. CPs are active anion or cation exchangers with their surrounding medium. Hence post-synthetic chemical treatments to remove the templates can alter the conductivities of CPs and consequently affecting their chemical sensing performance.
4. Removal of a hard template supporting CP nanotubes or nanorods with diameters below 100 nm has caused the collapse of the oriented nanostructures and merging them into stacks of micron sized structures [77-80].

Template-free synthesis of nanostructured CPs can be achieved electrochemically or chemically. Novel hydrogen gas sensors based on CPs synthesized through both procedures were developed by the author and will be discussed in the subsequent chapters. In the upcoming subsections, the author will survey these techniques.

Electropolymerization

It is well established that controllable deposition of CPs colloids can be achieved by tailoring the various electropolymerization parameters such as deposition time, chemicals' concentrations, and the solvent volume [81]. Tang et al. reported a pulse potentiostatic technique for the electrochemical deposition of polyaniline nanoparticles on a highly ordered pyrolytic graphite (HOPG) anode [82]. The dimension of the nanoparticles was controlled by adjusting the charge density. For nanoparticles with diameters ~20 nm, the charge density of 5.7 $\mu\text{C}/\text{cm}^2$ (10 ms pulse) was applied. To produce larger nanoparticles ~60 nm in diameter, the applied charge density was 19.3 $\mu\text{C}/\text{cm}^2$ (100 ms pulse). In other reports, uniformly oriented polyaniline nanowires were electrochemically synthesized without the need for any templates [83, 84]. The process consisted of two steps to control the polymer nucleation and growth. Initially polyaniline nuclei were grown by applying high current density (0.08 mA/cm^2) or voltage (0.75 V). Then a stepwise decrease of the applied current density (0.04 mA/cm^2 followed by 0.02 mA/cm^2) or a one step reduction in the applied voltage (0.65 V) allowed the growth of oriented one-dimensional nanostructures from the deposited polyaniline nuclei.

In a recent study, oriented array of polypyrrole nanowires, 40–120 nm in diameter, has been synthesized through template-free electropolymerization [85]. The electrolyte consisted of a mixture of weak acidic anions (hydrogen phosphate) and non-acidic anions (perchlorate). It was shown in an earlier report that in the case of utilizing weak acidic anions only, an over-oxidized polypyrrole thin film is deposited that does not contain any

nonostructured morphology [86]. Presumably in the presence of both anions, O₂ nanosized bubbles are formed during the electropolymerization [85]. These bubbles prevent the over-oxidation of polypyrrole by the solution hydroxyl radicals that leads to the formation of a compact film instead of a nanostructured film.

Chemical Polymerization

Bulk quantities of CPs nanostructures dispersed into solutions can be produced through controlling the parameters of the chemical reactions. This process was pioneered by Richard B. Kaner's group at the University of California, Los Angeles [87]. Polyaniline with nanofibrillar morphology was the first to be prepared in this manner. The procedure starts by preparing two separate solutions, one for the monomer and one for an oxidant such as APS. Then the two solutions are fed to the reaction vessel [88]. The reaction kinetics plays a major role in the evolution of the polyaniline nanostructures. In the case of feeding the oxidant solution slowly into the monomer solution via a buret or a syringe pump, an instant interfacial polymerization occurs that leads to the formation of polyaniline nanofibers at the interface between the aniline/APS solutions. The evolution of nanosized structures can be correlated to whether the polymer chains nucleate homogeneously or heterogeneously during polymerization [89]. In the interfacial polymerization of aniline, both homogeneous and heterogeneous nucleation occurs. At the beginning of polymerization, only homogeneous nucleation of polymer chains takes place since the solution is still empty of any hetero-nuclei. At this stage only nanofibrillar structures are obtained. As the polymerization goes on, the new chains may grow on existing nuclei through heterogeneous nucleation or form new nuclei by continuing the process of homogeneous nucleation. It was found that as the polymerization continues, heterogeneous nucleation prevails over homogeneous nucleation leading to a coral-like structures [89]. Hence the irreversible agglomeration can be attributed to the secondary growth of polymer chains from the existing one-dimensional structures through the heterogeneous nucleation.

To overcome the problem of secondary growth, the reaction should be fast enough to promote the homogeneous nucleation and suppress the heterogeneous nucleation. Speeding the polymerization process was accomplished through the method of rapid-mix reaction [67]. It is a straightforward procedure where the oxidant and the monomer solutions are poured together into the reaction vessel followed by shaking the mixture vigorously for 30 s [90]. This leads to an instant consumption of the oxidant molecules in the process of homogeneous nucleation of polymer chains throughout the solution. By this way only the one-dimensional nanostructures growth is allowed and the secondary

growth of polymer chains is minimized due to the depletion of oxidant molecules into the solution. This synthetic route produced high quality polyaniline nanofibers with diameters of 30–50 nm uniformly dispersed into the solution [91]. Implementing this procedure to produce nanostructures of other CPs required the use of oligomers to speed up the polymerization even further in order to prevent the heterogeneous nucleation [92-94].

2.3 Gas Sensors Based on Conducting Polymers

Employing CPs in the development of gas sensors is an active research area with an increasing number of published studies over the past years. This can be attributed to the unique electrical, electrochemical and optical properties of CPs. Oxidizing gases such as NO₂ and SO₂ withdraw electrons from CPs films, while reducing gases like H₂ and NH₃ donate electrons to these films. CPs based gas sensors produce measurable signal in response to the presence of target gases in their environment at room temperature, whereas gas sensors with metal oxides' sensitive films have almost no sensitivity at room temperature. This feature allows the fabrication of low power consumption gas sensors [39].

Despite the worldwide attention on developing gas sensors with CPs' sensitive films, the fabrication of gas sensors based on nanostructured CPs has not been fully explored yet due to the ongoing research and development of the synthesis methods of these nanomaterials as explained in the previous section. Consequently the author of this dissertation was motivated to add to the body of knowledge by developing novel hydrogen gas sensors based on nanostructured polythiophene, polypyrrole, polyaniline and its derivatives as well as graphene/polyaniline nanocomposite. The experimental work and results for these sensors will be covered in the upcoming chapters. In this section the author will review the published literature on gas sensors employing pure CPs. A review on composite materials for gas sensing applications will be the subject of section 2.4.

2.3.1 Polythiophene

The unsubstituted form of polythiophene and its derivatives have been recognized for their processibility, stability in air and high doped state conductivity [95]. They have been utilized in several applications such as organic transistors [96], polymer LEDs [97], solar cells [49] and chemical sensors [38]. The parent polymer, polythiophene, has a remarkable thermal stability of 42% weight loss at 900 °C and a conductivity range of

10^{-10} – 10^{-3} S/cm depending on the type of the doping anions [51]. However it has been revealed that the synthesis of polythiophene and its derivatives require higher oxidation potentials during polymerization compared to other CPs such as polypyrrole and polyaniline due to the presence of the inert sulfur atom in the molecules thiophene and its derivatives [98]. At high oxidation potentials, it would be hard to control the polymer growth and confine the structure into low dimensionality. Perhaps this hurdle limited the number of reported gas sensors based on polythiophenes, since the sensitive films' morphologies are of utter importance from the sensing perspective as was explained earlier in this chapter.

The first published report on polythiophene based gas sensors was the work of Hanawa et al in 1989 [99]. They electrodeposited polythiophene films on ITO glass and subsequently peeled the films and fixed them on a regular glass slide with adhesive tapes. Later on they sputtered platinum over the entire surface except a 5 mm² area of bare polythiophene was left and they bonded wires to the platinum area to form a polythiophene chemiresistor. They exposed the sensor towards NO₂ and H₂S balanced in N₂ by using one test gas at a time. The film resistance decreased in the presence of NO₂ and increased during the interaction with H₂S. They observed a weaker interaction of the polythiophene film with H₂S than that with NO₂. They suggested that during the interaction of polythiophene with H₂S a quenching of the positive charge carriers may occur through the electrostatic binding with adsorbed H₂S molecules and/or from annihilation by electron injection from the adsorbed H₂S molecules. Despite the noticeable shift in film resistances during the interaction with NO₂ and H₂S, the sensor did not recover after removing the test gas. The author of this dissertation believes that the lack of recovery was caused by the poor porosity and large thickness of their polythiophene film as well as the permanent replacement of some ClO₄⁻ dopant anions with NO₂⁻ anions according to their optical spectroscopies' results.

In another approach, polythiophene derivatives such as poly (decanoate thiophene) (PEDT), poly (propanoate thiophene) (PEPT) and poly (octyl thiophene) (POT) have been deposited on 6 MHz quartz crystal microbalances (QCM) using Langmuir-Blodgett technique and tested for their sensitivities towards NO₂ gas [100]. During the exposure to 550 ppm of NO₂, the QCMs with PEDT, PEPT and POT thin films responded by a frequency shift of ~20 Hz, ~40 Hz and ~90 Hz respectively. After removing the NO₂ gas, the recovery of these sensors was only 5–10% of the total frequency shifts. The different molecular structures for these polymers especially in the ester linkage of the side chains were thought to be responsible for the different sensitivity towards NO₂ gas.

There are several reports on employing regioregular (alkyl-substituted) polythiophenes in the development of room temperature volatile organic compound (VOC) vapors sensors. Li et al developed several conductometric gas sensors based on poly(3-hexylthiophene), poly(3-hexylthiophene)-b-polystyrene, poly(3-hexylthiophene)-b-poly(methylacrylate), poly(hexylthiophene)-b-poly(butylacrylate) and poly(3-dodecylthiophene)-ran-3-methylthiophene). Each sensor was tested for its response towards methanol, ethanol, 2-propanol, acetone, n-hexane, cyclohexane, methylene chloride, acetonitrile, toluene and benzene vapors [101]. These sensors were sensitive towards both of the polar and non-polar VOC vapors. All sensors produced fast and reproducible responses towards VOCs at room temperature unlike the sensors in other reports [96, 102, 103]. The amplitude and polarity of the sensors' responses were dependant on the molecular structure of the sensing layer and the type of VOC being tested. The largest shift in conductivity was observed with the poly(3-hexylthiophene)-b-polystyrene sensor towards toluene [101]. The authors attributed the responses to the physisorption of VOCs molecules and excluded the possibility of chemisorption due to the fast recovery at room temperature. Multiple sensing mechanisms were expected to be simultaneously involved in the physical interactions between the polymers and the VOCs vapors. For instance, it is anticipated that the adsorption of a polar VOC vapor can induce a dipole moment. This dipole moment causes reduction in the average polymer molecule spacing distance, namely, increasing the density of states for interchain polaron hopping, leading to an increase in the sensitive film conductivity [104].

Polythiophenes based organic thin-film transistors (OTFTs) have been developed by several research groups to function as gas sensors. Li et al developed OTFTs with nanostructured regioregular poly(3-hexylthiophene) (P3HT) thin films [105]. Their VOCs vapors sensing results were directly related to the gate biasing field. Changing the gate voltages altered the source-drain current magnitude and polarity for the same vapor. These results were substantially different than that published by another group where the responses of (P3HT) OTFTs towards VOCs vapors were either positive or negative [106]. Perhaps the difference in morphologies between the sensitive films in these reports was responsible for the changes in response mechanism [105]. Another factor is that the range of applied gate voltages $|V_{GS}|$ by Li et al (0–40V) was much larger than that used by Chang et al (0–20V), which can largely affect the sensing mechanism. In a recent study, inorganic oxidizing gases (NO_2 , Cl_2 and SO_2) were sensed by using the parent (unsubstituted) polythiophene nanofibers that were in situ chemically polymerized on poly(ethylene terephthalate) (PET) sheets [107]. They have found that

the polythiophene conductivity increased by ~20% during the exposure to NO₂ gas with the concentration of 100 ppm. However the polymer did not recover to its original conductivity after removing the NO₂ gas. Instead they exposed the sensitive film to a 254 nm UV light to reverse the response to its baseline value. Concentrations as low as 250 ppb of NO₂ gas could be sensed. Reversible responses were also observed for Cl₂ and SO₂ gases with detection limits of 5 ppm and 25 ppm respectively. Although their optical spectroscopy results for polythiophene sensitive film did not show any photo-bleaching or photo-oxidative changes to the polymer backbone during the UV irradiation over multiple cycles of gases exposures, these effects may be observed if the sensor is used over a prolonged period of time. A morphological change in the polymer nanostructured film due to the extended exposure to UV light is also possible, which can ultimately degrade the sensor's sensitivity towards target gases.

A new technique for the in situ monitoring of amine vapors physisorption into polybutylthiophene and polydecylthiophene thin films has been reported by Liao et al [108]. In this technique, X-ray reflectivity (XPR) measurements were conducted to accurately determine the sensitive films' thickness changes during the gas exposure. A reversible increase in the films thicknesses was observed during the exposure to amine vapors, which confirms the physical interaction between the gaseous molecules and the polymer films. In other words, a reversible polymer swelling was taking place during the interaction with amine vapors.

It is evident from the previous discussions that gas sensors based on nanostructures of the parent polythiophene have not been thoroughly investigated in literature. Probably the absence of facile methods for synthesizing nanostructures of the parent polythiophene is the main reason behind this lack of studies. Hence the author of this dissertation was motivated to add to the body of knowledge by developing novel hydrogen gas sensors based on chemically and electrochemically synthesized polythiophene nanofibers. For instance, the author reported a layered SAW hydrogen gas sensor with polythiophene nanofibers as the sensitive layer [109]. The nanomaterial characterization and gas sensing results of the polythiophene based hydrogen gas sensors developed by the author will be presented in Chapter 6 and Chapter 7 respectively.

2.3.2 Polypyrrole

Polypyrrole (PPY) is a heteroaromatic CP that attracted a great deal of research attention due to its high conductivity and environmental stability [110]. It has been used in many applications such as chemical sensors, anticorrosive coatings, actuators,

electrochromic devices and polymer-based artificial muscles [111]. PPY is usually prepared through chemical or electrochemical polymerization. During this process, continuous oxidation of the conjugated structure takes place leading to a p-type doped polymer because of the formation of polarons and bipolarons. At low oxidation levels, polarons are predominant over bipolarons. Whereas at high oxidation levels, most of the ionic species are bipolarons. In such oxidation levels, the bipolaronic energy states overlap leading to the formation of intermediate band structures between the conduction and valance bands [110]. Therefore It has been suggested that the electrical conduction in PPY can be attributed to the presence of bipolarons [112]. The neutral form of PPY has a large band gap of 3.16 eV. However the insulating regime of neutral PPY can be easily reversed to a metallic one at room temperature by doping [110]. This feature makes PPY an interesting material for gas sensing applications.

Soon after the first report on PPY electropolymerization [113], Kanazawa et al. reported that the conductivity of doped PPY decreased from the baseline value by a factor of 10 during the exposure to ammonia gas [114]. Original PPY conductivity value was restored after removing the NH_3 gas leading to the conclusion that a weak interaction was taking place. In another report, Nylander et al. found that the exposure of PPY impregnated filter paper to NH_3 gas with concentrations of (0.5–5%) diluted in either argon or oxygen-argon mixture increased the polymer resistance [115]. Linear response was observed with a 30% resistance change per one percent of NH_3 concentration. It was proposed that NH_3 gas causes depletion of the charge carriers in PPY or restriction to their mobility leading to a decrease in the overall film conductivity [116]. Alternatively Blanc et al. suggested that the conductivity changes of PPY film during the interaction with NH_3 gas consisted of two subsequent events, which are an initial fast decrease in conductivity due to a superficial adsorption followed by a relatively slower diffusion process [117]. More detailed discussion on the theoretical aspects of gas diffusion into CPs thin films will be provided in Chapter 3. In recent studies, it has been reported that concentrations as low as 5 ppm of NH_3 gas can be sensed with conductometric gas sensors based on PPY nanoparticles [118, 119]. Kwon et al. investigated the gas sensing properties of PPY nanostructured films with nanoparticles diameters of 20 nm, 60 nm and 100 nm [118]. They have found that decreasing the nanoparticles size produced a noticeable increase in the sensitivity towards NH_3 gas. It was anticipated that the enhanced sensitivity can be attributed to the higher surface-to-volume ratio of the 20 nm nanoparticles compared to the 60 nm and the 100 nm nanoparticles.

Mass changes in PPY film during the interaction with NH_3 gas was monitored by several workers. Slater et al. electrochemically deposited PPY thin films on QCMs and

observed the frequency changes during the exposure to NH_3 gas [120]. Instant decrease of the QCM frequency was observed with the exposure to NH_3 gas with the concentration of 1% indicating that mass loading of the PPY thin film was taking place. They correlated the mass increase during the interaction with the NH_3 gas with the decrease in PPY conductivity observed by them and other workers. It was anticipated that swelling of the polymer causes a reduction of the activation energy for the electrons hopping between PPY chains resulting in a decrease in its conductivity. In an alternative approach, Penza et al. developed a surface acoustic wave (SAW) based NH_3 gas sensor [121]. Langmuir-Blodgett method was employed to deposit the PPY sensitive layer. The SAW gas sensor outperformed its QCM counterpart by the ability to detect as low as 46 ppm of NH_3 gas. This study suggested that both of the mass loading and the elastic loading were jointly contributing to the decrease in SAW velocity. Further discussions on the theory of SAW gas sensors are provided in Chapter 3.

PPY sensitivity towards a range of VOC vapors had been investigated in a number of studies [122-126]. Bartlett et al. observed the interaction of PPY films with methanol, ethanol, acetone, ether and toluene vapors at room temperature [122]. Out of all the vapors tested, the response towards methanol vapor was fast and reproducible. It was observed that PPY conductivity decreased during the exposure to these VOC vapors. The response times were in the range of (40 – 60) s. The strong interaction between PPY and methanol vapor was confirmed by Slater et al. through their measurements of PPY mass and conductivity changes during the exposure to methanol, hexane and 2,2-dimethylbutane vapors [123]. In fact, they have reported that the QCM frequency shift upon the exposure to methanol vapor was about ten times greater than that for other vapors. Perhaps the ease of hydrogen bonding between methanol and the solvation sheath surrounding the PPY doping anions resulted in a solvent type interaction for methanol leading to an increase in the polymer dimensions, whereas other tested vapors did not have this effect on the polymer. The swelling of PPY is usually associated by a transition from the glassy state of the polymer to the rubbery state. In contrast to methanol vapor, PPY response towards ethanol vapor is much slower [122, 124, 125]. The responses in these studies did not show that the adsorption of ethanol vapor into PPY films reached the state of equilibrium regardless of the amount of the exposure time employed. Also continuous drift of the baseline was observed despite allowing the sensors to recover for 30 minutes after each ethanol exposure [124]. De Souza et al. studied the effect of utilizing different doping agents during PPY chemical synthesis on the resultant films sensitivities towards seven VOCs vapors [126]. Out of all the synthesized PPY films, camphor sulfonic acid (CSA) and lithium perchlorate doped PPY

films showed the highest sensitivities towards the tested vapors. They demonstrated that the PPY sensitivity towards polar VOC vapors was noticeably higher than that for non-polar vapors.

On the contrary to the interaction between nucleophilic gases such as NH_3 and PPY films, electrophilic gases like PCl_3 , SO_2 , NO_2 and I_2 withdraw electrons from polarons along the PPY backbone causing an increase in the overall film conductivity [37, 127-129]. It was also suggested that the interaction between PPY films and electrophilic gases can lead to the chemical doping of PPY with ionic species such as NO_2^- [127-129]. The degree of anion doping for PPY during gas exposure is dependant on the electron affinity of that particular gas. Since the electron affinity of PCl_3 , SO_2 , NO_2 and I_2 gases are 0.8 eV, 1.1 eV, 2.1–2.5 eV and 2.5–2.6 eV respectively, it was observed that PPY responded with larger shift in resistance during the exposure to NO_2 and I_2 gases compared to the response towards PCl_3 and SO_2 gases [129]. In this work, the PPY films resistances did not recover to the baseline values after removing the target gases. However it was reported earlier that reversible responses were obtained during the interaction of PPY films with NO_2 and H_2S gases [37]. Probably different doping anions employed during the PPY electropolymerization in these reports is the main factor behind this dissimilarity in gas sensing results.

In another report, Liu et al. developed a CO gas sensor based on PPY thin film [130]. The sensitivity was low at room temperature. However at the operating temperature of 300 °C, the sensor's sensitivity was 6.5% towards 500 ppm of CO gas and the response was reproducible. Since this report did not include a study of the PPY morphology changes due to the operation at 300 °C, it was difficult to explain their observation. Torsi et al. reported the reversible decrease in PPY film resistance due to the exposure to CO gas at room temperature [131]. However in this study much higher concentration of CO gas was employed (20000 ppm). It is evident that further investigation is needed to elucidate the gas sensing properties of PPY thin films towards CO gas.

Apart from toxic gases sensing, environmental groups developed PPY based gas sensors for monitoring the concentration of CO_2 gas in the ambient [132, 133]. It has been proposed that during the interaction between CO_2 and PPY the π -electronic structure of PPY is disturbed by a weak chemisorption of CO_2 molecules causing a decrease in PPY conductivity [133]. Due of the chemisorption process, the sensors' recovery from the CO_2 exposure was slow in the range of (1560–1770) s.

In contrast to the well studied PPY sensitivity towards all the above mentioned gases, the sensitivity of pure PPY films towards H_2 gas has not been widely investigated. Most of the reported H_2 gas sensors were based on PPY films with the inclusion of copper,

palladium or platinum particles. For instance, Torsi et al. electropolymerized PPY films with Pd or Cu inclusions and investigated their sensitivities towards NH_3 , H_2 and CO gases [131]. During the exposure to H_2 gas, the resistance of the Pd-PPY film decreased from its baseline value whereas that of Cu-PPY film increased. Apparently the metal inclusions were dominating the response towards H_2 gas. In a recent work, a composite of PPY and Pt was chemically synthesized and deposited in situ on a flexible conductometric transducer [134]. It was found that the highest sensitivity towards H_2 gas was obtained when the concentration of Pt nanoparticles in the sensitive film was 20000 ppm. Due to the nonporous structure of the pure PPY film developed through this approach, including the Pt nanoparticles provided a catalytic effect by dissociating the H_2 molecules leading to a substantial PPY protonation. Hence the sensitivity of Pt decorated PPY film towards H_2 gas with the concentration of (0.02–0.5%) was twice the order of magnitude of the undecorated PPY film. However the response of the Pt/PPY based gas sensor was extremely slow. A response time of 330 s (5.5 minutes) was observed towards H_2 gas with the concentration of 0.1%, which can be attributed to the slow chemisorption of H_2 molecules. Therefore this sensor is not practical in terms of real life situations where fast detection of any H_2 gas leak is of utmost importance in protecting lives and properties from the devastating explosions that can be caused by the highly flammable H_2 gas.

In another approach, amperometric H_2 gas sensor was developed which consisted of PPY films deposited via chemical vapor deposition on Pd/Nafion[®] and Pt/Nafion[®] electrodes [135]. It was observed that the aging problems of Nafion[®] electrodes were significantly decreased after coating with PPY films. However this improvement in the anti-aging properties was associated by a decline in the electrodes' sensitivities towards H_2 gas compared to the uncoated ones.

In this dissertation, the author has developed novel H_2 gas sensors based on pure PPY nanofibers. In one published report, the author fabricated a conductometric gas sensor and tested its response towards H_2 gas with the concentration of (0.06 – 1.0%) at room temperature [136]. In another journal article, the author reported a layered SAW H_2 gas sensor [137]. The nanostructured PPY films employed in these sensors prompted fast responses towards H_2 gas. The response times of 43 s and 39 s towards H_2 gas with the concentration of 1% were recorded for the conductometric and the layered SAW gas sensors respectively. Whereas during the exposure to H_2 gas with the concentration of 0.06%, the response times of the conductometric and the layered SAW gas sensors were 72 s and 79 s respectively. More detailed discussions on these sensors will be provided in the upcoming chapters.

2.3.3 Polyaniline

One of the widely investigated CPs is polyaniline (PANI) for its environmental stability, simplicity of synthesis and remarkable insulator to conductor switching properties [59]. It was found useful in many applications such as lightweight battery electrodes, electromagnetic shielding devices and anticorrosion coatings [138-142]. Especially its capability to switch between an insulating regime to a conducting one and vice versa in response to certain species in the surrounding medium made it attractive for chemical sensing purposes. The doped (conducting) form of PANI is known as emeraldine salt and can be obtained through treatments with acids. On the contrary, PANI is dedoped during the interaction with bases and takes the insulating form which is the emeraldine base. This process is accompanied by a color change of the PANI film from light green for the doped state to dark blue for the dedoped form. For instance, it was observed that the HCl doped PANI had a maximum optical absorbance at ~800 nm that shifted towards ~620 nm upon the exposure to NH₃ gas because of the color change from green to blue and this optical response was reversible [143]. The doping and dedoping process of PANI is illustrated in Figure 2.3 [67, 89, 144].

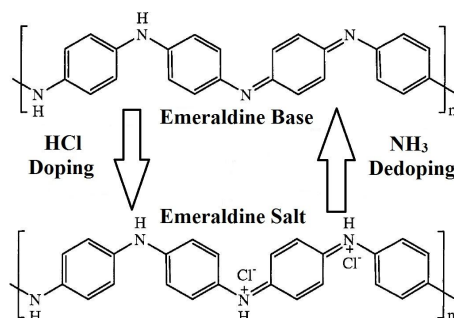


Figure 2.3. Doping and dedoping of polyaniline [144].

Since the reversible process of doping/dedoping described above occurs at room temperature, many research groups were interested in developing gas sensors based on PANI thin films. For instance, it has been established that electron-donating gases like NH₃ deprotonate PANI leading to a drop in its conductivity [145-147]. Agbor et al. reported the PANI conductivity increase during the interaction with oxidizing gases such as NO₂ [148]. They compared the gas sensing performance of PANI films deposited via thermal evaporation, spin coating and Langmuir-Blodgett (LB) techniques. It was observed that the thermally evaporated PANI film had higher sensitivity and faster response compared to the spun film. No reversible response was obtained for the PANI film deposited by the LB technique. In contrast to the 1-D nanostructured films, the sensitivity of the 3-D (bulk) thin films towards target gases is largely affected by the

sensitive film thickness. Hence the different PANI films thicknesses obtained by thermal evaporation, spin coating and LB techniques contributed to the difference in gas sensing results. Another factor to consider was the different oxidation states of PANI films obtained from these deposition methods. The spun PANI films were in the emeraldine base state, whereas the thermally evaporated films were in the leucoemeraldine state. The interaction of PANI films with H₂S and SO₂ gases also produced an increase in PANI films conductivities. These results are interesting because H₂S is a reducing gas and it should decrease the PANI conductivity by injecting electrons. Apparently the dissociation of H₂S into H^+ and HS^- onto the polymer surface caused a protonation of the PANI backbone resulting in an increase of the film conductivity instead of a decrease.

In another report, PANI and its alkyl-substituted derivatives of poly(*o*-toluidine), poly(*o*-anisidine), poly(*N*-methylaniline), poly(*N*-ethylaniline), poly(2,3 dimethylaniline), poly(2,5 dimethylaniline) and poly(diphenylamine) were investigated for their sensitivities towards methanol, ethanol, propanol, butanol and heptanol vapors [149]. The interaction between these polymers and either methanol, ethanol or propanol vapors resulted in an increase in their conductivities, whereas the exposure to butanol and heptanol vapors produced the opposite response. The values of the changes in films resistances and the response time were dependent on each polymer's chemical structure and the chain length of the alcohol vapor under test.

In recent years, an increasing number of studies have been published on utilizing nanostructured forms of PANI as gas sensitive films. Gas sensors based on PANI nanofibers offered higher sensitivities towards a range of vapors and gases such as HCl, hydrazine, chloroform, methanol and H₂S compared to those based on bulk PANI thin films [63, 144, 150-152]. In another report, gas sensors were developed by depositing a single PANI nanowire on conductometric transducers through electrospinning technique [153]. The sensors responded reversibly towards low concentrations of NH₃ gas with a detection limit of 0.5 ppm. It was also found that changing the nanowire diameter affected the response times of the developed sensors. Their comparison results showed that as the PANI nanowire diameter was made smaller, the response became faster. This was attributed to the rapid diffusion of gas molecules into the nanowire with small diameter.

In other reports, PANI nanofibers synthesized via chemical and electrochemical methods were utilized to develop conductometric and SAW H₂ gas sensors [64, 84, 154, 155]. A template-free chemical reaction was employed to develop PANI nanofibers suspended in a solution that was airbrushed on conductometric and QCM transducers

after heating them to a 100 °C [64]. Heating the substrates was necessary for this deposition technique in order to obtain a uniform distribution of nanofibers. For the conductometric sensor, the interaction with H₂ gas caused a decrease in its resistance. A 3% decrease in the film resistance was observed during the exposure to H₂ gas with the concentration of 1% diluted in nitrogen gas. This response was about an order of magnitude higher than that produced by the conventional 3-D PANI thin film towards the same concentration of H₂ gas due to the high porosity and surface-to-volume ratio of the nanofibrillar film. Reversible H₂ mass uptake by camphorsulfonic acid (CSA) doped PANI nanofibers was also confirmed with an average QCM frequency shift (Δf) of 182 ± 8 Hz observed during the exposure to H₂ gas with the concentration of 1% [64]. The mathematical expression relating the mass loading (Δm) and the frequency response (Δf) of a QCM with an operational frequency of F_0 and an active gas sensing area of A is given by Sauerbrey equation [156]:

$$\Delta m = \frac{-\Delta f \times A}{2.3 \times 10^6 \times F_0^2}$$

In another study, the performances of layered SAW H₂ gas sensors based on HCl and CSA-doped PANI nanofibers were compared [154]. The diameters of the HCl-doped PANI nanofibers were ~30 nm, whereas those doped with CSA were ~50 nm. The sensor based on HCl-doped PANI nanofibers showed faster response and recovery towards H₂ gas concentrations of (0.06–1)% than the other sensor. However the response (Δf) of the CSA-doped PANI nanofibers based sensor towards 1% of H₂ gas was 14.6 kHz, which was much higher than the 3 kHz response of the sensor based on HCl-doped PANI nanofibers for the same concentration of H₂ gas. Since the CSA-doped PANI nanofibers were thicker, they offered larger number of adsorption sites for H₂ molecules but the HCl-doped PANI nanofibrillar film was more porous due to its thin nanofibers and producing a faster response as a result. In an alternative approach, template-free electropolymerization was employed to deposit PANI nanofibers directly on the gold IDTs of SAW transducers and investigated for their sensitivities towards H₂ gas [84, 155]. In both reports 1M HCl was used as the supporting electrolyte during synthesis to obtain the doped PANI nanofibers. Yu et al. investigated the response of the (as deposited) doped PANI nanofibers based sensor towards H₂ gas [155]. While Arsat et al. dedoped the PANI nanofibers with NaOH before starting the H₂ gas sensing experiments [84]. The SAW gas sensor based on doped PANI nanofiber operating at ~ 111.133 MHz responded with a frequency shift of 7.8 kHz towards H₂ gas with the concentration of 1%. Whereas the dedoped PANI nanofibers based SAW gas sensor

produced a 9.2 kHz shift from a 102.325 MHz baseline towards the same concentration of H₂ gas.

Recently, the author of this thesis published a report on a layered SAW H₂ gas sensor based on nanoporous PANI [157]. The novel nanoporous PANI structure had larger surface area than nanofibers. Consequently, the developed gas sensor outperformed those reported in literature with a 48.86 kHz frequency shift from a 94.41 MHz baseline during the exposure to H₂ gas with the concentration of 1%.

In contrast to the parent polymer (PANI), PANI derivatives received little attention in the field of gas sensors. Consequently, the author of this dissertation was keen to publish reports of layered SAW H₂ gas sensors based on nanostructured polyanisidine and polyethylaniline films [158, 159]. The experimental details and the outcomes of these investigations will be discussed in the upcoming chapters.

2.4 Gas Sensors Based on Composites of Conducting Polymers and Organic or Inorganic Materials

Great deal of research endeavor has been devoted towards the development of new materials that combine CPs with organic or inorganic compounds. These composites can offer either new or enhanced chemical properties to be exploited in many applications such as gas sensors and biosensors. Composites of CPs with either metal oxides, carbon nanotubes or un-conjugated polymers have been investigated for gas sensing applications [160-171]. The inclusion of metal oxides nanoparticles into the CPs backbones can produce *n-p* hetero junctions with depletion regions. The interaction with target gases causes reversible changes to the depletion regions and hence modulating the composite conductivity [163, 165, 172, 173]. Combining poly(3-hexylthiophene) with ZnO nanowires caused the chemical reduction of poly(3-hexylthiophene) and therefore improving its sensitivity towards oxidizing gases such as NO₂ gas [169].

In particular, several researchers developed gas sensors based on composites of PANI and metal oxides to achieve room temperature operation. For instance, PANI/In₂O₃ nanocomposite was synthesized through template-free chemical polymerization and deposited on the surface of a ZnO/64° YX LiNbO₃ SAW transducer for gas sensing applications [174]. The sensor responded with frequency shifts of ~11 kHz, 2 kHz and 2.5 kHz towards H₂ gas with the concentration of 1%, CO gas with the concentration of 500 ppm and NO₂ gas with the concentration of 2.12 ppm balanced in synthetic air from a baseline frequency of 107.2 MHz, respectively. The 90% response time was in the

range of 24–30 s. It was also observed that the sensor was faster in responding to high concentrations of target gases compared to its response towards low concentrations of the same gases.

In another report, similar gas sensor was developed by depositing PANI/WO₃ nanocomposite on the surface of a ZnO/64° YX LiNbO₃ SAW transducer [175]. The sensor's response towards H₂ gas with the concentration of 1% was a 7 kHz decrease from its 107.2 MHz baseline frequency with a response time of 40 s. It was shown in a recent study that using high weight percentage of WO₃ compared to the aniline monomer during the chemical polymerization resulted in the dominance of WO₃ nanoparticles in the observed morphology of the nanocomposite [176]. The sensitivity of the developed conductometric gas sensor towards H₂ gas with the concentration of 1% was ~4%. The sensor's response time was found to be 60 s. It was anticipated that the high volume of WO₃ nanoparticles in this nanocomposite caused a decrease in the deposited film porosity which resulted in the observed slow response.

In a recent article, PANI/TiO₂ composite with a nanofibrillar morphology was synthesized and employed for sensing low concentrations of NH₃ gas in the range of 25 – 200 ppb [177]. It was found that the sensitivities of the sensors were directly related to the composite constituents' concentrations. The highest sensitivity towards NH₃ gas was obtained when the composite contained 40.74 wt% of PANI nanofibers to TiO₂ nanoparticles. Also they demonstrated that the composite based sensor was more sensitive than the sensor based on pure PANI.

In another approach, CP/CNT nanocomposites have been utilized in developing gas sensors. A CNT may be conceptually viewed as a graphite sheet that is rolled into a nanoscale tube to form a single walled carbon nanotube (SWCNT), or a multiwalled carbon nanotube (MWCNT) with additional graphene coaxial tubes around the SWNT core [178]. Depending on their diameter and the helicity of the orientation of graphite rings along the nanotube length, CNTs can exhibit semiconducting or metallic behavior. CNTs are also known for their high surface-to-volume ratio, which is a favorable feature for gas sensing application. CP/CNT nanocomposites are expected to enhance the physical properties of CPs by integrating them into the nanoscale hollow molecular symmetry of CNTs [179]. These enhanced properties can be beneficial in many applications including the fabrication of highly sensitive chemical sensors.

By employing the electrospinning polymer deposition method, Wanna et al. deposited PANI/MWCNT nanocomposite doped with maleic acid on a conductometric transducer to function as a CO gas sensor [180]. The sensor produced reversible response during the exposure to CO gas with the concentration of 100–500 ppm at room temperature. They

have found that the sensitivity of the nanocomposite based sensor towards CO gas was more than two orders of magnitude higher than the sensor with PANI sensitive film deposited by solvent casting. High surface-to-volume ratio of the nanocomposite can be responsible for its high sensitivity.

The high sensitivity of the CNTs and PANI nanocomposites compared to that of PANI was also observed by Srivastava et al. for conductometric H₂ gas sensors [181]. Their gas sensing results showed that the SWNT/PANI nanocomposite achieved higher sensitivity towards H₂ gas with the concentration of 2% compared to the MWNT/PANI nanocomposite and pure PANI. However the dynamic responses of their sensors were distorted suggesting unstable performance and consequently they couldn't assess their sensors' reproducibility. These poor dynamic responses can be caused by the large distance (1 mm) between the conductometric transducer's consecutive electrodes. Due to the large distance between electrodes, most of the generated responses were attributed by only the adsorption sites close to the electrodes because of the poor charge transport throughout the sensitive films. This was evident from the high baseline resistances of their gas sensors.

Despite all the reported work on gas sensors based on CP/CNT nanocomposites, the author of this dissertation was the first to publish a report on graphene/polyaniline nanocomposite based H₂ gas sensor according to the best of the author's knowledge [182]. The author's informed decision to develop this novel gas sensor was made after reviewing the literature provided in the upcoming subsection.

2.4.1 Graphene/Polyaniline Nanocomposite

Graphene is a two-dimensional sheet of carbon atoms bonded through sp² hybridization [31]. Several studies have reported on the excellent properties of graphene including Young's modulus ~1100 GPa [183], thermal conductivity ~5000 Wm⁻¹K⁻¹ [184], mobility of charge carriers of up to 200,000 cm²/Vs [185], specific surface area (a calculated value of 2630 m²g⁻¹) [186] and interesting transport phenomena such as the quantum Hall effect [187]. The first successful experimental preparation of graphene was reported in 2004 by Novoselov et al. through the mechanical exfoliation of small mesas of highly oriented pyrolytic graphite [188]. However, this method has a very low yield, which is not suitable for large scale production as well as it is difficult to control the number of exfoliated layers. Other methods have been reported in the literature such as chemical vapor deposition (CVD) and epitaxial growth which often require very high temperatures ~1000 °C, ultra-high vacuum equipment and/or lengthy purification procedures [189-191]. An alternative promising approach is the chemical modification of

graphene/graphite oxide or graphite fluoride to generate homogeneous colloidal suspensions known as chemically modified graphene (CMG) [192]. This approach has the advantages of being an economical solution suitable for large-scale production and simultaneously viable for chemical functionalization. Due to the disruption of the 'graphitic' networks, CMGs are electrically insulating and hence reduction of the graphene oxide by chemical means such as hydrazine is needed to restore electrical conductivity [193]. Through the CMG approach, aqueous dispersions of graphene nanosheets were recently prepared without the inclusion of any stabilizers or surfactants [194]. Instead, electrostatic repulsion between negatively charged graphene oxide sheets was found to be responsible for generating a stable aqueous suspension.

There is a growing interest in the scientific community on the development of sensors based on graphene for its unique properties [195]. Novoselov et al. investigated mechanically exfoliated graphene for sensing individual gas molecules [196]. Concentrations as low as 1 part per million (ppm) of NO₂, NH₃ and CO gases could be sensed. Thermally reduced graphene oxide has also been tested for NO₂ and NH₃ gas sensing [197]. A sensitivity of ~1.56 for NO₂ gas was recorded. However, the NH₃ gas sensor did not produce a coherent response when it was tested after 2 months. Further analysis suggested non-ohmic contact between the gold electrode and the graphene oxide due to an asymmetric I-V curve, which was likely responsible for the alteration of the response through variations in the adsorbate-induced Schottky barrier. In contrast, gas sensors based on graphene from the CMG approach maintained ohmic contacts between graphene and metal electrodes during interaction with NO₂ and NH₃ [33]. In another report, a surface acoustic wave gas sensor based on chemically modified graphene-like nanosheets was fabricated and used to sense H₂ and CO gases [32]. It was observed that the sensor achieved higher sensitivity towards these gases at room temperature than at 40 °C. On the contrary the dynamic response of the sensor was faster at the elevated temperature compared to the response at room temperature. They suggested that the changes in the sensitive film's conductivity and the mass loading were responsible for the responses towards H₂ gas and CO gas respectively.

Recently, several reports have been made on incorporating graphene into polymer matrices to produce novel nanocomposite materials [198, 199]. It was found that a homogeneously dispersed graphene nanofiller in a polymer matrix provided nanocomposites with enhanced mechanical, electrical, thermal and other properties due to the high aspect and surface-to-volume ratios of the nanofiller. It was also suggested that graphene nanosheets can provide more active nucleation sites for polyaniline as well as excellent electron transfer pathways [199]. To the best knowledge of this thesis

author, a graphene/polyaniline nanocomposite has not been investigated for gas sensing application before. Therefore the author reported a novel H₂ gas sensor based on graphene/polyaniline nanocomposite [182]. Due to the high surface-to-volume ratio of the incorporated graphene nanosheets, the developed sensor has higher sensitivity towards H₂ gas than that of only graphene and polyaniline nanofibers based gas sensors. The nanocomposite's characterization results and the gas sensing results will be discussed in Chapter 6 and Chapter 7 respectively.

2.5 Summary

A critical review of literature on CPs synthesis methods and their application in the field of gas sensing was presented in this chapter. It was highlighted that traditionally the template-based synthesis was the major known method for developing nanostructured CPs. However in recent years, the template-free method has emerged overcoming the problems of template-based synthesis such as treatment with harsh chemicals and the collapse of nanostructures after removing the template. Due to the disadvantages of the template-based methods for developing nanostructured CPs, the author of this PhD dissertation adopted template-free synthesis method that is conducted through chemical or electrochemical polymerization of monomer units.

It was also demonstrated that gas sensors based on compact and nanostructured CPs received a great deal of attention from researchers around the globe. A comprehensive understanding of published work in this area, which was presented in this chapter, was crucial for the author to make informed decisions regarding the development of novel processes for fabricating nanostructured CPs based gas sensors that will be presented in the next few chapters. In addition to the CPs, after reviewing the literature on gas sensors based on composites, the author of this thesis also decided to develop novel gas sensor based on graphene/polyaniline nanocomposite. Detailed theoretical background behind CP based gas sensors will be provided in Chapter 3.

Chapter 3

Theoretical Background on Conductometric and SAW Gas Sensors

AFTER surveying the literature on the field of conducting polymer based gas sensors in the past chapter, the present chapter will cover the theoretical aspects of the conductometric and SAW gas sensors. It is essential to mention here that the conduction mechanism in conducting polymers is quite different than that of inorganic semiconductors such as silicon. Several conduction models have been proposed to interpret the charge transport in conducting polymers and the matter is still being investigated in academia. The most adopted model is the Variable Range Hopping (VRH) which will be described in section 3.1. The theory of conductometric gas sensors based on conducting polymers will be the subject of section 3.2. While the theory of SAW gas sensors will be discussed in section 3.3. Finally section 3.4 will provide the summary of the chapter.

3.1 Variable Range Hopping Model

This model was developed by Mott in 1968 to describe the conductivity in non-crystalline, disordered, materials [200]. Hopping conduction is defined as the process in which charge carriers transport by thermally activated tunneling from an occupied site to an empty site. Charge transport in disordered conducting polymers is attributed to

the hopping process between localized states [67]. This process is associated with the formation of polarons and bipolarons on the polymer backbone [201-203]. Prigodin et al. has studied the variable range hopping model for conducting polymers with nanostructured morphology (1-D) as well as for higher dimensionalities (2-D and 3-D) [204]. Table 3.1 summarizes the DC and AC electrical responses of localized electrons with respect to different dimensionalities of conducting polymers' systems.

Table 3.1. Electrical response of localized electrons in systems of different dimensionality [204].

Response	One	Quasi-1D	$(1+s)$ -fractal	$d = 2,3$
$\frac{\sigma_{dc}(T)}{\sigma_0}$	$\frac{v_{ph}}{T_0} \exp\left[-\frac{T_0}{T}\right]$	$\frac{\omega_{\perp}^0 v_{ph}}{T_0^2} \exp\left[-\left(\frac{T_0}{T}\right)^{1/2}\right]$	$\frac{v_{ph}}{T_0} \exp\left[-\left(\frac{T_0}{sT}\right)^{1/2}\right]$	$\left(\frac{T_0}{T}\right)^{2/(d+1)} \exp\left[-\left(\frac{T_0}{T}\right)^{1/(d+1)}\right]$
$\frac{\text{Re } \sigma_{ac}(\omega)}{\sigma_0}$	$\frac{T}{T_0} \left \frac{\omega}{v_{ph}} \right ^{1-(T/T_0)}$	$\frac{T}{T_0} \left \frac{\omega}{v_{ph}} \right ^{1-(T/T_0)}$	$\frac{\sigma_{dc}(T)}{\sigma_0} \exp\left[\left(\frac{sT_0}{T}\right)^{1/2} \left \frac{\omega}{v_{ph}} \right ^{s/2}\right]$	$\frac{T}{T_0^2} \left \ln \frac{v_{ph}}{\omega} \right ^{d+2}$

The parameters in the above table are defined in the following equations:

$$\sigma_0 = \left(\frac{e^2}{\hbar} \right) \xi^{2-d} \quad (3.1)$$

$$T_0 = B_d \left(N(E_F) \xi^D \right)^{-1} \quad (3.2)$$

where, e is the charge of electron, \hbar is the Dirac constant, ξ is the localization radius, $N(E_F)$ is the density of state at the Fermi level, B_d is the percolation constant, v_{ph} is the phonon frequency taken as 10^{12} Hz, D is the diffusion coefficient, $(s \ll 1)$ is the polymer chain fractal dimensionality and ω_{\perp}^0 is the inter-chain hopping frequency. Since the variable range hopping model is the best known model so far to describe the charge transport in conducting polymers, it will be considered as the basis for the subsequent analysis of conducting polymers based gas sensors.

3.2 Modeling of Conductometric Gas Sensors Based on Conducting Polymers

Conducting polymers are considered an attractive class of materials for the development of gas sensors according to the literature survey provided in the last chapter. Since their conductivities change noticeably during the exposure to various organic and inorganic gases, a gas sensor can be easily made by depositing a conducting polymer layer on the surface of a conductometric transducer. A conductometric transducer is fabricated by patterning a pair or a number of conductive electrodes on an insulating substrate. Due to the high resistivity of the insulating substrate, the transducer would have an infinite resistance value. After the deposition of the sensitive layer, the new resistance value is related to the conductivity of the sensitive film only. Detailed description of the fabrication process that was employed by the author to fabricate the conductometric transducers will be provided in Chapter 4.

Despite the interest in the development of conducting polymers based gas sensors, there is no complete understanding of the mechanism behind the changes of conducting polymers' conductivities during the exposure to various gases. Gardner and Bartlett developed a model to analyze the adsorption and desorption of gas molecules into and out of a homogeneous conducting polymer thin film deposited on a conductometric transducer [205-207]. Their model assumes the existence of fixed sites into the polymer backbone that interact with the diffusing chemical species. Based on the kinetics of diffusion, the model analyzes the process through six analytical cases. The analytical expressions from these six cases provide an estimation of the site occupancy in each case, which is directly related to the film conductivity at that particular case. The author of this thesis believes that this model provides a good interpretation of the reversible changes in sensors' resistances during the interaction with target gases.

3.2.1 Gas Diffusion Model

A gas sensor with semi-infinite electrodes is shown in Figure 3.1. The thickness of the polymer film is L . In the sensor's environment, there is a gas with species A mixed with air. If there are N immobile adsorption sites distributed uniformly in the polymer film, then the adsorption process can be described by the Langmuir adsorption isotherm [206]:



where k_f and k_b are the forward and backward reaction rates respectively. From these reaction rates the equilibrium constant (K) can be calculated as:

$$K = \frac{k_f}{k_b} \quad (3.4)$$

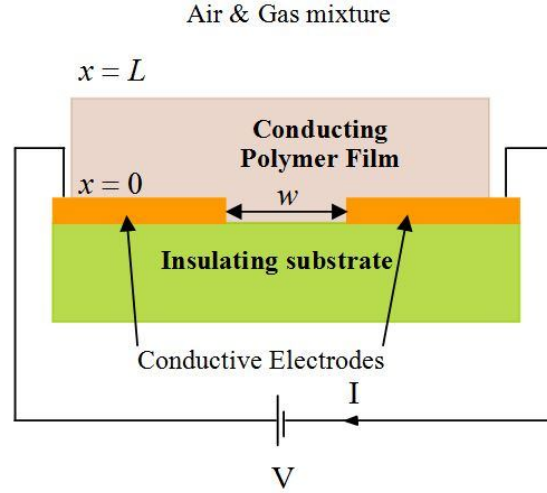


Figure 3.1. Schematic diagram of a gas sensor with semi-infinite electrodes; reproduced from ref.: [206].

The equilibrium constant is considered a measure of the affinity of the polymer sites to the gas species A . For a high value of K , low concentration of gas species would be sufficient to saturate all the sites. While at low values of K , a weak interaction occurs and a high gas concentration is needed to fill all the sites.

In Figure 3.1, x is the diffusing distance for gas species A into the polymer film at a time t . At the interface between the polymer film and the conductive electrode $x=0$. While at the interface between the polymer and the gas/air mixture $x=L$. If we define $\theta(x,t)$ as the fraction of occupied sites at a particular time, then the diffusion reaction equation for the gas species A can be written as follows [207]:

$$D \frac{\partial^2 a}{\partial x^2} - k_f a(1-\theta)N + k_b \theta N = \frac{\partial a}{\partial t} \quad (3.5)$$

where $a(x,t)$ is the concentration of the diffusing gas species A at a particular time and distance into the polymer thin film and N represents the polymer sites concentration. In the presence of a certain concentration of the target gas in the sensor's environment, let's assume that there is a constant concentration, a_∞ , of gas molecules in the environment for that particular concentration and D is the rate of diffusion constant. Then the adsorption and desorption kinetics can be expressed as follows:

$$N \frac{\partial \theta}{\partial t} = k_f a (1 - \theta) N - k_b \theta N \quad (3.6)$$

For the purpose of the development of the adsorption and desorption analytical expressions, the following dimensionless parameters are introduced:

$$\chi = \frac{x}{L} \quad (3.7)$$

$$\tau = \frac{Dt}{L^2} \quad (3.8)$$

$$\gamma = \frac{a}{a_\infty} \quad (3.9)$$

$$\kappa = \frac{k_f N L^2}{D} \quad (3.10)$$

$$\lambda = K a_\infty \quad (3.11)$$

$$\eta = K N \quad (3.12)$$

Here κ represents the ratio between the adsorption and diffusion kinetics. When $\kappa \gg 1$, the adsorption happens at a much faster rate than the diffusion. The parameter λ is related to the status of equilibrium. At $\lambda \ll 1$, a large number of unoccupied sites exist at equilibrium. While for $\lambda \gg 1$, all of the existing sites are filled at equilibrium. The parameter η is the the equilibrium constant multiplied by the concentration of sites. The parameter τ is the diffusion time in dimensionless form. The parameter γ is the normalized concentration of target gas.

By considering the above dimensionless parameters, equations (3.5) and (3.6) are rewritten as follows:

$$\frac{\partial^2 \gamma}{\partial \chi^2} - \frac{\partial \gamma}{\partial \tau} = \frac{\eta}{\lambda} \left(\frac{\partial \theta}{\partial \tau} \right) \quad (3.13)$$

$$\eta \frac{\partial \theta}{\partial \tau} = \kappa \lambda \gamma (1 - \theta) - \kappa \theta \quad (3.14)$$

There is no exact analytical solution to the nonlinear partial differential equations of (3.13) and (3.14). However, Bartlett et al derived the expressions for the adsorbed gas concentration $\gamma(\chi, \tau)$ and the site occupancy $\theta(\chi, \tau)$ during adsorption and desorption for six analytical cases as listed below in Table 3.2 and Table 3.3 respectively.

Table 3.2. The analytical expressions for the adsorbed gas concentration and sites occupancy during adsorption; adopted from ref: [207].

Case No.	$\gamma(\chi, \tau)$	$\theta(\chi, \tau)$
I	$\gamma(\chi, \tau) \approx 1 - \frac{2}{\pi} \sum_{n=0}^{\infty} \frac{\cos\left[\left(n + \frac{1}{2}\right)\pi\chi\right] \exp\left[-\left(n + \frac{1}{2}\right)^2 \pi^2 \tau\right]}{(-1)^n \left(n + \frac{1}{2}\right)}$	$\theta(\chi, \tau) \approx \lambda\gamma$
II	$\gamma(\chi, \tau) \approx 1 - \frac{2}{\pi} \sum_{n=0}^{\infty} \frac{\cos\left[\left(n + \frac{1}{2}\right)\pi\chi\right] \exp\left[-\left(n + \frac{1}{2}\right)^2 \pi^2 \tau / \eta\right]}{(-1)^n \left(n + \frac{1}{2}\right)}$	$\theta(\chi, \tau) \approx \lambda\gamma$
III	$\gamma(\chi, \tau) \approx 1 - \frac{2}{\pi} \sum_{n=0}^{\infty} \frac{\cos\left[\left(n + \frac{1}{2}\right)\pi\chi\right] \exp\left[-\left(n + \frac{1}{2}\right)^2 \pi^2 \tau\right]}{(-1)^n \left(n + \frac{1}{2}\right)}$	$\theta(\chi, \tau) \approx \lambda \left[1 - \exp\left(\frac{\kappa\tau}{\eta}\right)\right]$
IV	$\gamma(\chi, \tau) \approx 1 - \frac{2}{\pi} \sum_{n=0}^{\infty} \frac{\cos\left[\left(n + \frac{1}{2}\right)\pi\chi\right] \exp\left[-\left(n + \frac{1}{2}\right)^2 \pi^2 \tau\right]}{(-1)^n \left(n + \frac{1}{2}\right)}$	$\theta(\chi, \tau) \approx 1 - \exp\left(\frac{\lambda\gamma\kappa\tau}{\eta}\right)$
V	$\gamma(\chi, \tau) \approx 1 - \frac{2}{\pi} \sum_{n=0}^{\infty} \frac{\cos\left[\left(n + \frac{1}{2}\right)\pi\chi\right] \exp\left[-\left(n + \frac{1}{2}\right)^2 \pi^2 \tau\right]}{(-1)^n \left(n + \frac{1}{2}\right)}$	$\theta(\chi, \tau) \approx \frac{\lambda\gamma}{1 + \lambda\gamma}$
VI	$\begin{aligned} \gamma(\chi, \tau) = & 1 + \frac{2}{\pi} \sum_{n=1}^{\infty} \frac{\cos(n\pi) - 1}{n} \sin\left(\frac{1}{2}n\pi(\chi + 1)\right) \exp\left(-\frac{1}{4}n^2\pi^2(\tau - \tau_*)\right) \\ & + 2 \sum_{n=1}^{\infty} \sin\left(\frac{1}{2}n\pi(\chi + 1)\right) \exp\left(-\frac{1}{4}n^2\pi^2(\tau - \tau_*)\right) \\ & \times \int_0^1 \gamma_2(\chi', \tau_*) \sin\left(\frac{1}{2}n\pi(\chi + 1)\right) d\chi' \end{aligned}$	$\theta(\chi, \tau) \approx \frac{\lambda\gamma}{1 + \lambda\gamma}$

Table 3.3. The adsorbed gas concentration and sites occupancy analytical expressions during desorption; adopted from ref: [207].

Case No.	$\gamma(\chi, \tau)$	$\theta(\chi, \tau)$
I	$\gamma(\chi, \tau) \approx \frac{2}{\pi} \sum_{n=0}^{\infty} \frac{\cos\left[\left(n + \frac{1}{2}\right)\pi\chi\right] \exp\left[-\left(n + \frac{1}{2}\right)^2 \pi^2 \tau\right]}{(-1)^n \left(n + \frac{1}{2}\right)}$	$\theta(\chi, \tau) \approx \lambda\gamma$
II	$\gamma(\chi, \tau) \approx \frac{2}{\pi} \sum_{n=0}^{\infty} \frac{\cos\left[\left(n + \frac{1}{2}\right)\pi\chi\right] \exp\left[-\left(n + \frac{1}{2}\right)^2 \pi^2 \tau / \eta\right]}{(-1)^n \left(n + \frac{1}{2}\right)}$	$\theta(\chi, \tau) \approx \lambda\gamma$
III	$\gamma(\chi, \tau) \approx \frac{2}{\pi} \sum_{n=0}^{\infty} \frac{\cos\left[\left(n + \frac{1}{2}\right)\pi\chi\right] \exp\left[-\left(n + \frac{1}{2}\right)^2 \pi^2 \tau\right]}{(-1)^n \left(n + \frac{1}{2}\right)}$	$\theta(\chi, \tau) \approx 1 - \lambda \left[1 - \exp\left(-\frac{\kappa\tau}{\eta}\right)\right]$
IV	$\gamma(\chi, \tau) \approx \frac{2}{\pi} \sum_{n=0}^{\infty} \frac{\cos\left[\left(n + \frac{1}{2}\right)\pi\chi\right] \exp\left[-\left(n + \frac{1}{2}\right)^2 \pi^2 \tau\right]}{(-1)^n \left(n + \frac{1}{2}\right)}$	$\theta \approx \frac{\exp(-\kappa(\tau - \tau_d)/\eta)}{1 + \exp(-\kappa(\tau - \tau_d)/\eta)}$ $\tau_d = \frac{4 \ln(4\lambda/\pi)}{\pi^2}$
V	$\gamma(\chi, \tau) \approx \frac{2}{\pi} \sum_{n=0}^{\infty} \frac{\cos\left[\left(n + \frac{1}{2}\right)\pi\chi\right] \exp\left[-\left(n + \frac{1}{2}\right)^2 \pi^2 \tau\right]}{(-1)^n \left(n + \frac{1}{2}\right)}$	$\theta(\chi, \tau) \approx \frac{\lambda\gamma}{1 + \lambda\gamma}$
VI	$\gamma(\chi, \tau) \approx \frac{2}{\pi} \sum_{n=0}^{\infty} \frac{\cos\left[\left(n + \frac{1}{2}\right)\pi\chi\right] \exp\left[-\left(n + \frac{1}{2}\right)^2 \pi^2 \zeta / \eta\right]}{(-1)^n \left(n + \frac{1}{2}\right)}$ $\zeta = \tau + 2\lambda \int_0^\tau \operatorname{erf}\left[\frac{\eta^{1/2}}{2(1+\lambda)\tau^{1/2}}\right] d\tau + \lambda^2 \int_0^\tau \operatorname{erf}^2\left[\frac{\eta^{1/2}}{2(1+\lambda)\tau^{1/2}}\right] d\tau$	$\theta(\chi, \tau) \approx \frac{\lambda\gamma}{1 + \lambda\gamma}$

The six cases presented in Table 3.2 and Table 3.3 describe the kinetics of diffusion and binding of molecules with sites into the polymer film. In case I ($\lambda < 1, \eta < 1, \kappa > \eta$) the film is still unsaturated with the gas molecules when equilibrium is reached and hence the chemical reaction is much faster than the diffusion. Therefore the amount of bound gas molecules in this case is smaller than the amount of free gas molecules into the film. In case II ($\lambda < 1, \eta > 1, \kappa > 1$) the large number of bound gas molecules results in a lower value for the diffusion coefficient and hence the diffusion time is higher by a factor of η than that for case I. For case III ($\lambda < 1, \kappa < 1, \kappa < \eta$) the diffusion of gas molecules becomes much faster than the chemical reaction. So this case constitutes the linear, unsaturated, part of the Langmuir isotherm ($\theta \ll 1$). The diffusion continues to be faster than the reaction in case IV ($\lambda > 1, \kappa < \eta / (1 + \eta)$), which corresponds to the saturated part of the isotherm ($\theta \approx 1$). In case V ($\lambda > 1, \lambda^2 > \eta, \kappa > \eta / (1 + \eta)$) there is a large number of occupied sites and the area of the filled by the bound molecules is dependent on the concentration of the target gas. Here the chemical reaction does not affect the process of diffusion. Both of the reaction and the diffusion are fast for this case. For case VI ($\lambda > 1, \lambda^2 < \eta, \kappa > \eta / (1 + \eta)$) a more complex state exists due to the nonlinear kinetics of diffusion and chemical reaction. Here the reaction is faster than the diffusion. Since a significant amount of gas molecules are already bound to immobile sites into the upper part of the polymer film, all new gas molecules have to diffuse deeper into the polymer film to fill unoccupied sites [207, 208]. Therefore, the reaction front is constantly moving inwards, but the velocity of its movement is dependant on the difference between the flux of the diffusing species and the flux of the reacting species.

3.2.2 Gas Sensor Conductance Model

As mentioned earlier in this chapter, that till this moment there is no complete understanding of the charge transport mechanism in conducting polymers. This can be attributed to several factors including the young age of this relatively new class of materials that was discovered at late seventies, the diversity of molecular structures between one conducting polymer and another, and the medium surrounding the polymer such as polar solvents or the ambient. However the most plausible model so far is the variable range hopping model discussed in section 3.1. By examining the equations in Table 3.1, it can be noticed that the conductivities of conducting polymers have profound temperature dependency. Hence a conducting polymer film can be visualized as a three dimensional array of N identical resistors linked together. A simplified representation

of this network is shown in Figure 3.2 (A). Each resistive link can be resembled as a barrier to the electron hopping from one conjugated backbone to another. During the polymer/gas interaction, some of these links (n) are affected by the imposed oxidizing or reducing target gas since these gases either withdraw or donate electrons to the film. If we interpret that process in terms of the site occupancy θ discussed in previous section, then we can conclude that there is $n\theta$ of these gas modified resistive links. Also at the same time there are $(N - n\theta)$ of unmodified resistive links who are maintaining there baseline resistance R_0 .

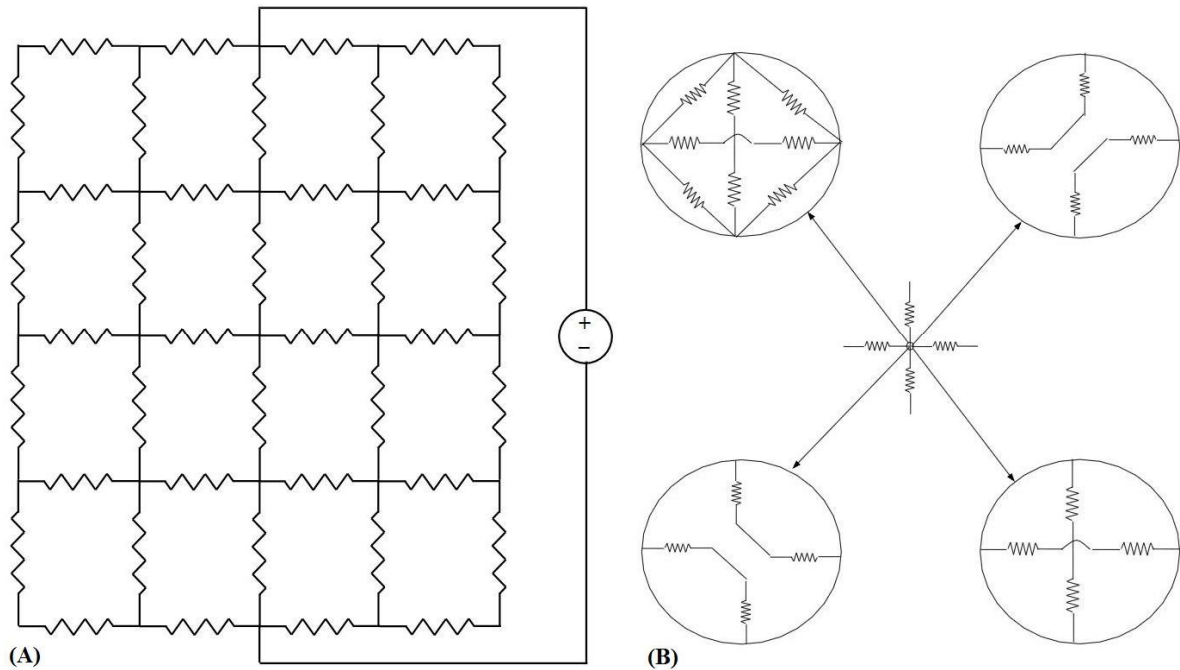


Figure 3.2. (A) Schematic diagram of the resistive network [209] (B) Possible node connections [210].

The macroscopic resistance of the polymer film is determined by the node connections method as shown in Figure 3.2 (B). For instance, the total resistance of the resistors connected in series is proportional to the site occupancy. While in the case of connection in parallel, the overall conductance is proportional to the site occupancy. For more complicated networks, the 3-D models demonstrate that above the percolation threshold the total conductance is approximately proportional to the square of the site occupancy. For simplicity, let us consider the following linear formula that relates the polymer film conductivity $\sigma(\chi, \tau)$ and the site occupancy $\theta(\chi, \tau)$ [206]:

$$\sigma(\chi, \tau) = \sigma_0 [1 - S\theta(\chi, \tau)] \quad (3.15)$$

In the equation above, S is the sensitivity coefficient and σ_0 is the baseline film conductivity. For the sensor shown in Figure 3.1, if the conductive electrode length is b where $b \gg w$ then the electric field bisecting these semi-infinite electrodes can be derived using the Schwartz-Christoffel transformations [211]:

$$E_1(\chi, 0) = \frac{V}{L\pi\sqrt{\chi^2 + w^2/4L^2}} \quad (3.16)$$

where V is the applied voltage between the electrodes, L is the polymer film thickness, χ is the dimensionless distance parameter and w is the electrode separation distance. This equation has been verified elsewhere in a study implementing the finite element method [212]. The baseline film conductance G_0 can be expressed in terms of the device geometry as follows [206]:

$$G_0 = \frac{\sigma_0 b}{\pi} \ln \left[\frac{1 + \sqrt{1 + w^2/4L^2}}{w/2L} \right] \quad (3.17)$$

By rearranging equations (3.15) and (3.17), the sensor's response towards the target gas is determined by the following expression [206]:

$$\frac{G(\tau) - G_0}{G_0} = -S \frac{\int_0^1 \theta(\chi, \tau) / \sqrt{\chi^2 + w^2/4L^2} d\chi}{\ln[1 + \sqrt{\chi^2 + w^2/4L^2} / (w/2L)]} \quad (3.18)$$

The conductometric transducers, which are fabricated and employed for gas sensing by the author of this dissertation consist of an array of interdigitated electrodes. The electric field associated with this system can be approximated by the electric field generated from a pair of finite coplanar electrodes with a width of d each as shown in Figure 3.3. The electric field for this structure can be written as [206]:

$$E_2(\chi, 0) = \frac{V}{2A^*L^2} \left[(\chi^2 + w^2/4L^2)(M^2\chi^2 + w^2/4L^2) \right]^{-0.5} \quad (3.19)$$

In equation (3.19) the following parameters can be defined:

- The geometrical modulus which is:

$$M = \frac{w}{w + 2d} \quad (3.20)$$

- The conformal transformation of the electrode, which is a first kind Jacobean elliptical integral:

$$A^* = \frac{2}{w} \int_0^1 \left((1 - t^{*2})(1 - M^2 t^{*2}) \right)^{-0.5} dt^* \quad (3.21)$$

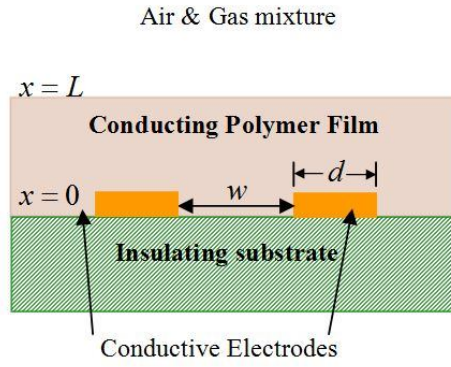


Figure 3.3. Schematic diagram of a gas sensor with finite coplanar electrodes; reproduced from ref.: [206].

The baseline conductance and the sensor's response during exposure to target gases can be expressed as follows [206]:

$$G_0 = \frac{\sigma_0 b}{2A^* L} \int_0^1 d\chi / \sqrt{(\chi^2 + w^2 / 4L^2)(M^2 \chi^2 + w^2 / 4L^2)} \quad (3.22)$$

$$\frac{G(\tau) - G_0}{G_0} = -S \frac{\int_0^1 \theta(\chi, \tau) d\chi / \sqrt{(\chi^2 + w^2 / 4L^2)(M^2 \chi^2 + w^2 / 4L^2)}}{\int_0^1 d\chi / \sqrt{(\chi^2 + w^2 / 4L^2)(M^2 \chi^2 + w^2 / 4L^2)}} \quad (3.23)$$

It is worthy to mention here that the site occupancy $\theta(\chi, \tau)$ in equations (3.18) and (3.23) can be obtained from Table 3.2 and Table 3.3 for the six analytical cases of diffusion discussed in the previous section. The steady-state response is independent of the conductive electrode geometry and can be determined through the following equation [206]:

$$\frac{G_{\tau \rightarrow \infty} - G_0}{G_0} = -S \theta_\infty = -S \frac{K a_\infty}{1 + K a_\infty} \quad (3.24)$$

where a_∞ is the target gas concentration in the sensor's environment. From equation (3.24), it is evident that the gas sensing is limited by the sensitivity coefficient, the equilibrium constant and the gas concentration only.

The models presented above were verified experimentally by Ingleby et al in their study on conductometric sensing for ethanol vapor using polypyrrole and polyaniline sensitive films [125]. They also modified the conductance model to accommodate the influence of humidity as some sites into the polymer film are occupied by water molecules. Their experimental results on ethanol sensing demonstrated adsorption-rate kinetics that are confined into the linear part of the Langmuir isotherm, which agrees with case III kinetics presented in previous section. Another significant factor that was investigated experimentally in this study was the impact of changing the electrodes spacing on the

device performance. They fabricated transducers with the conductive electrode spacing ranging from 18 μm to 64 μm and electrochemically deposited each polymer on these transducers. By maintaining the deposition time an identical polymer film profile has been achieved for all the developed sensors. Their results proved that, for constant temperature and humidity, the sensors steady-state responses were almost identical. The time constant did not change for the transducers with different conductive electrodes spacing. This experimental observation was supported by the theoretical expression given in equation (3.24).

Based on the above discussion the author of this dissertation made an informed decision regarding the design of the conductometric transducers utilized in this study. Since the spacing between the conducting electrodes does not have a proven impact on the developed sensors' response, the author chose the distances of 50 μm and 200 μm for the electrodes spacing of the developed transducers. The 50 μm transducers were developed specifically to suit the process of electropolymerization. While the 200 μm were fabricated to be used with chemically prepared conducting polymers and nanocomposites. The transducers fabrication will be explained in details in the following chapter. The syntheses of the novel nanostructured conducting polymers investigated for hydrogen gas sensing in this thesis will be discussed in chapter 5.

As mentioned earlier in this chapter that the understanding of charge transport within the conducting polymer and with its surrounding medium is still under investigation. The author opinion regarding the models presented so far in this thesis is that they best describe the physisorption kinetics of target gas molecules into the conducting polymer film and do not cover any catalytic chemical reaction that may occur at the polymer/gas interface. This effect may exist during the interaction between the conducting polymer and low molecular weight gases such as hydrogen. For instance, it is believed that hydrogen gas molecules dissociate during the interaction with polyaniline which render the atomic hydrogen to protonate the polyaniline film. Furthermore in order to simplify the complex diffusion-reaction problem, the models assume that the charge mobility is merely originated from charge carriers generation and ignore any polymer inter-chain or intra-chain charge mobility as well as any possible reaction with the doping cations. Hence the author will discuss the proposed gas sensing mechanism for every developed sensor individually in Chapter 7.

3.3 Theory of SAW Gas Sensors

Surface acoustic wave (SAW) devices with deposited conducting polymer films along the acoustic wave propagation path can provide sensors for monitoring gases and vapors

with very good sensitivity [154, 213]. SAW refers to a unique acoustic mode in which the acoustic wave propagation is confined to the surface of the piezoelectric crystal. In a SAW transducer, the acoustic wave is generated and received by a pair of input and output interdigital transducers (IDTs) as shown earlier in Figure 1.2.

The centre frequency of the excited wave (f_0) relies on the SAW propagation velocity (v) and the transducer period (d):

$$f_0 = \frac{v}{d} \quad (3.25)$$

It is worthy to mention here that the transducer period must match the wavelength of the propagating acoustic wave in order for the SAW device to operate at the center frequency.

After the deposition of a sensitive thin film on the surface of a SAW transducer, the SAW propagation characteristics such as the wave velocity (v) and the attenuation (α) become directly affected by the deposited film properties. A number of factors can perturb the SAW velocity such as [214]:

$$\frac{\Delta v}{v_0} = \frac{1}{v_0} \left(\frac{\partial v}{\partial m} \Delta m + \frac{\partial v}{\partial c} \Delta c + \frac{\partial v}{\partial \sigma} \Delta \sigma + \frac{\partial v}{\partial \varepsilon} \Delta \varepsilon + \frac{\partial v}{\partial T} \Delta T + \frac{\partial v}{\partial p} \Delta p + \dots \right) \quad (3.26)$$

where v_0 is the unperturbed SAW velocity. The factors in equation (3.26) that affect the SAW velocity and can be responsible for the SAW sensor's response are listed below:

- m : is the mass.
- c : is the stiffness.
- σ : is the conductivity.
- ε : is the dielectric coefficient.
- T : is the temperature.
- p : is the pressure.

However some of these factors have small contribution to the overall sensor sensitivity compared to others. Based on the factors with large contributions to sensitivity, three main sensing mechanisms can be distinguished [215]:

- Mass sensitivity
- Elastic and viscoelastic sensitivities
- Conductometric sensitivity

In the upcoming subsections the author will provide a brief description for each of the above interaction mechanisms.

3.3.1 Mass Sensitivity

For SAW sensors, this mechanism was first proposed by Wohltjen to describe their sensitivities towards gases and vapors [216]. According to this mechanism, physisorbed or chemisorbed molecules modify the sensitive layer mass density. Any change to the surface mass density ρ_s directly affects the kinetic energy U_k of the propagating SAW according to the following relation [217]:

$$\Delta U_k = \frac{\rho_s}{4} (v_{x0}^2 + v_{y0}^2 + v_{z0}^2) \quad (3.27)$$

where v_{x0} , v_{y0} and v_{z0} represent the displaced piezoelectric particles velocities in the x , y , z directions respectively. When acoustic waves pass through a volume, the energy density is expressed in terms of the incident power (P) and the transit time (τ):

$$U = P\tau = \frac{P}{v} \quad (3.28)$$

By combining equations (3.27) and (3.28), the variations of the acoustic wave velocity due to the mass loading of the sensitive layer can be expressed as [218]:

$$\frac{\Delta v}{v_0} = -\frac{\omega v_0 \rho_s}{4} \left(\frac{v_{x0}^2}{\omega P} + \frac{v_{y0}^2}{\omega P} + \frac{v_{z0}^2}{\omega P} \right) \quad (3.29)$$

where ω is the angular frequency of the propagating wave ($\omega = 2\pi f_0$). Equation (3.29) can be simplified by defining the mass sensitivity factor (c_m):

$$c_m = \frac{\pi v_0}{2} \left(\frac{v_{x0}^2}{\omega P} + \frac{v_{y0}^2}{\omega P} + \frac{v_{z0}^2}{\omega P} \right) \quad (3.30)$$

Therefore the perturbation of the propagating SAW velocity due to the mass sensitivity can be written as follows [217]:

$$\frac{\Delta v}{v_0} = -c_m f_0 \rho_s \quad (3.31)$$

Equation (3.31) explains the dependence of the SAW velocity on the surface layer mass, which can be largely affected by the diffusion and binding of gas molecules as discussed in section (3.2.1).

However for the SAW sensor's mass loading, it was assumed that the sensitive film is infinitesimally thin and its mechanical properties effects are negligible. Thus according to this assumption, there is no signal attenuation imposed by the sensitive film. But actual sensitive films do have finite thickness and elastic properties. The effects of the mechanical properties of the sensitive film on the SAW propagation parameters will be discussed in the next subsection.

3.3.2 Elastic and Viscoelastic Sensitivities

The SAW sensor's gas sensitive layer can be classified as acoustically thin film with elastic loading or acoustically thick film that has viscoelastic loading. For an isotropic polymer film deposited on the surface of a SAW transducer, two key mechanical properties of the sensitive material can be defined here [219]:

$$K = K' + jK'' \quad (3.32)$$

$$G = G' + jG'' \quad (3.33)$$

In the above equations, K is the bulk modulus and G is the shear modulus. The real parts (K' and G') are the in-phase stress and strain that contribute to energy storage in the film and are referred to as the storage moduli. While the imaginary components (K'' and G'') are the 90° out of phase stress and strain responsible for the power dissipation in the film and hence known as the loss moduli.

In an acoustically thin film, a uniform particles displacement occurs for the entire thickness in synchronization with the propagating SAW. As a result the film becomes subject to elastic effects. The SAW velocity perturbation due to the elastic sensitivity can be expressed as follows [217]:

$$\frac{\Delta v}{v_0} = -\omega h \left[c_1 \left(\rho - \frac{\mu}{v_0^2} \right) + c_2 \rho + c_3 \left(\rho - \frac{4\mu}{v_0^2} \left(\frac{\lambda + \mu}{\lambda + 2\mu} \right) \right) \right] \quad (3.34)$$

where (λ, μ) are the Lamé constants, h is the sensitive film thickness, ρ is the film mass density and (c_1, c_2, c_3) are the SAW-film coupling parameters calculated from the following equation [218]:

$$c_i = \frac{v_{i0}^2}{4k_0 P} \quad (3.35)$$

where k_0 is the acoustic wave number for SAW ($k_0 = \omega / v_0$) and P is the SAW acoustic power density. The surface particle velocity v_{i0} is expressed in terms of the surface particle displacement in each direction (u_x, u_y, u_z) as follows:

$$v_{i0} = j\omega u_{i0} \quad (3.36)$$

For an acoustically thick film, a non-uniform displacement of particles occurs across the film thickness due to the lagging of the particles in the upper portions of the film behind the particles at the film/substrate interface. Hence viscoelastic deformation of the film is the dominant effect in this condition. The formula describing the SAW velocity perturbations due to the viscoelastic sensitivity is [219]:

$$\frac{\Delta v}{v_0} \cong -\omega h \left((c_1 + c_2 + c_3) \rho - \left(\frac{c_1 + 4c_3}{v_0^2} \right) G' \right) \quad (3.37)$$

The deformation in such a case is attributed to both of the in-plane and cross-film gradients. But the cross-film gradients are the dominant ones.

3.3.3 Conductometric Sensitivity

During the SAW propagation onto the surface of a piezoelectric substrate, it forms a band of surface bound charges that produces an evanescent electric field. The generated current per surface area (I_0) can be expressed as [218]:

$$I_0^2 = 2K^2 \omega k^2 (\varepsilon_0 + \varepsilon_s) P \quad (3.38)$$

where K^2 is the electromechanical coupling coefficient which represents the efficiency of acoustic energy transformation into electrical energy, $(\varepsilon_0, \varepsilon_s)$ are the air and substrate dielectric permittivities respectively, k is the acoustic wave number, and P is the power density. After depositing the sensitive film on the SAW transducer, the charge carriers in the film redistribute due to the electric field generated by the surface bound charges. The acoustic power dissipation due to the variation in film conductivity during gas sensing is [218]:

$$P_T = -\frac{I_0^2}{2} \left(\frac{k^2 \sigma_{sh}}{j\omega k c_s (k^2 \sigma_{sh} + j\omega k c_s)} \right) \quad (3.39)$$

where P_T is the complex power flow, σ_{sh} is the sensitive film sheet conductivity and c_s is the surface capacitance. The effects of the sensitive film conductivity on the velocity and attenuation of the propagating SAW can be described as follows [214]:

$$\frac{\Delta v}{v_0} = -\frac{K^2}{2} \left(\frac{\sigma_{sh}^2}{\sigma_{sh}^2 + v_0^2 c_s^2} \right) \quad (3.40)$$

$$\frac{\Delta \alpha}{k} = \frac{K^2}{2} \left(\frac{v_0 c_s \sigma_{sh}}{\sigma_{sh}^2 + v_0^2 c_s^2} \right) \quad (3.41)$$

The plots of the fractional SAW velocity perturbation and the acoustic wave attenuation due to the changes in film conductivity can be found in several references such as [214], [215], [218] and [217]. The maximum changes to SAW velocity occurs at a critical sheet conductivity value defined as:

$$\sigma_{sh} = v_0 C_s = v_0 (\varepsilon_0 + \varepsilon_L) \quad (3.42)$$

where $(\varepsilon_0, \varepsilon_L)$ are the free space and SAW sensor layers permittivities respectively.

Unlike the mass sensitivity, the acoustoelectric coupling (conductometric sensitivity) is

not affected by the physical continuity of the deposited sensitive film [214]. From this observation, the author believes that the conductometric sensitivity is the dominant mechanism for the SAW sensors based on nanostructured conducting polymers sensitive films reported in this dissertation due to their high porosity. This idea is supported by the study conducted by Martin et al to distinguish between the mass and conductometric sensitivities for SAW sensors [220]. For mass sensitivity no attenuation change was found over the entire film thickness range. However they reported the presence of attenuation for the conductometric sensitivity. The author of this dissertation verified the existence and measured the attenuation in all of the developed sensors utilizing the network analyzer. The results from these measurements will be provided in Chapter 7.

It is evident from equation (3.40) that the sensor response can be enhanced by increasing the value of (K^2). Shoji et al showed that the deposition of Zinc oxide (ZnO) layer on LiNbO₃ or LiTaO₃ substrates increased (K^2) by 1.5 times compared to that of the uncoated substrates [221]. Since ZnO is a piezoelectric material, so an intermediate layer of ZnO can serve as a guiding layer for the propagating SAW by confining the acoustic energy to the surface region of the transducer. Therefore more sensitive transducers to SAW perturbations are obtained. Another important function to the ZnO layer is that it serves as a protective coating to the gold IDTs. Depending on the doping level of conducting polymers, they can be highly conductive. Hence if a conducting polymer was deposited on a non-layered SAW transducer it can short circuit the input and output IDTs. Therefore the author of this dissertation concentrated his efforts on developing layered SAW sensors with ZnO thin film as the intermediate layer as shown in Figure 3.4.

The author employed the oscillator circuit configuration shown in Figure 3.4 to evaluate the SAW velocity perturbation during gas sensing by recording the SAW sensor operational frequency (f) since $v = f\lambda$. There are two essential conditions need to be met in order to obtain a stable oscillator performance:

- The total phase shift around the loop must be an integer number of 2π radians. This condition can be expressed as follows [222]:

$$\tau_g 2\pi f_A + \phi_a + \phi_c = 2\pi N \quad (3.43)$$

where τ_g is the delay time between phase centers, f_A is the allowable oscillation frequency, ϕ_a is the amplifier phase shift, ϕ_c is the phase shift through the coaxial cables connecting the sensor and the amplifier, and N is an integer number.

- The amplifier gain must be greater than the losses of the SAW sensor.

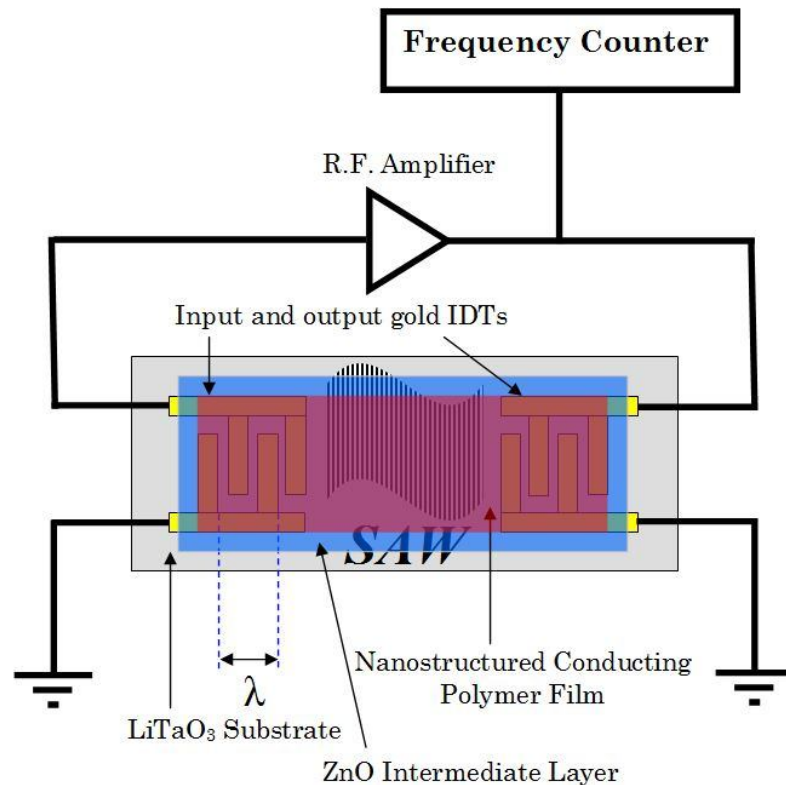


Figure 3.4. Layered SAW sensor oscillator circuit configuration.

3.4 Summary

The main purpose of this chapter was to discuss the theory behind the conductometric and SAW gas sensors. After careful consideration of the information presented here, the author made important decisions regarding the transducers' fabrication.

The knowledge in conducting polymers' conduction mechanisms and their gas sensing properties is still being developed by researchers around the world. Nevertheless, VRH as the most favorable conduction mechanism was explained briefly in section 3.1. The model was tailored to accommodate for (1-D) nanostructured conducting polymers as well as for higher dimensionalities.

The theory of conductometric gas sensors based on conducting polymers was discussed in section 3.2 through two linked models. The first model analyzes the physisorption of gas molecules onto a homogeneous conducting polymer film. As there is no exact solution to the nonlinear partial differential equations for the gas diffusion, six analytical cases were proposed to solve the problem. The expressions for the normalized gas concentration and the site occupancy during adsorption and desorption were presented in Table 3.2 and Table 3.3 respectively. Then a conductance model for the gas sensors with semi-infinite and coplanar electrodes was discussed. The conductance

model mainly relies on the site occupancy profiles provided by the gas diffusion model. These models were verified experimentally with conductometric sensors based on polyaniline and polypyrrole thin films for ethanol vapor sensing. Conductometric transducers with different electrodes spacing were investigated. The studies concluded that the electrodes separation distances do not have any impact on the developed sensors' sensitivities. Having in mind the practicalities regarding the microfabrication processes, the author of this thesis decided to design and fabricate conductometric transducers with 50 and 200 μm electrode separation distances for the purpose of electrochemical and chemical polymer deposition techniques, respectively.

In section 3.3 the principle of operation for SAW gas sensors was explained. These sensors can respond through changes in the mass, conductivity, elastic or viscoelastic properties of their gas sensitive films. From the discussions provided in this section, the author of this dissertation decided to develop layered SAW gas sensors. The process of the transducers' microfabrication will be described in Chapter 4.

Chapter 4

Transducers Microfabrication

THEORETICAL background on the gas sensors' principles of operation was presented in Chapter 3. As explained in Chapter 1, each developed sensor consisted of two physical components namely the transduction platform in the lower part and the active chemical sensing layer on the surface. This chapter will provide a detailed description of the microfabrication process employed by the author to fabricate the conductometric and layered SAW transducers used in this project. Patterned gold Interdigital Transducers (IDT) are the main element for both types of transducers. In section 4.1, the author will describe the overall process of IDT microfabrication. The preparation of the photolithographic mask will be discussed in section 4.2. The details of every microfabrication step will be provided in sections 4.3–4.9. Testing of the developed transducers will be described in section 4.10. Section 4.11 will summarize the microfabrication work presented in this chapter.

4.1 Introduction to IDT's Microfabrication

For the purpose of this research, different IDT patterns have been fabricated by the author. The work was undertaken utilizing the facilities of the Microelectronics and Materials Technology Centre (MMTC) at RMIT University. Figure 4.1 displays the overall microfabrication steps, which are widely adopted in the field of microelectronics for the development of Integrated Circuits (IC). A mistake in any microfabrication step results in an irreversible error and the whole process has to be restarted.

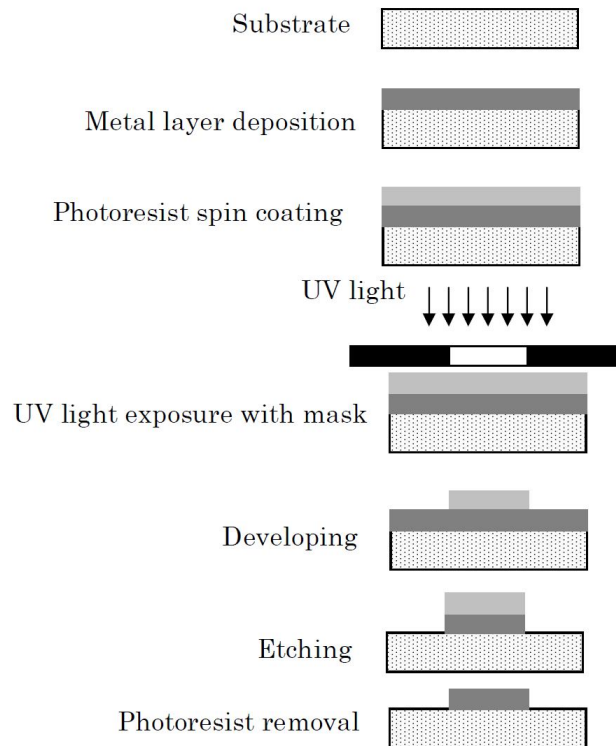


Figure 4.1. Microfabrication steps for the IDTs of conductometric and SAW transducers.

It is worthy to mention here that all the developed sensors in this research project operate at room temperature. This feature offer a simplification in the transducers microfabrication process compared to that of the transducers designed for high temperature operation due to the elimination of the heater microfabrication on the backside of the substrate.

For the purpose of conductometric transducers' microfabrication, the substrate material must be nonconductive and withstands treatments with harsh chemicals as well as heat treatment up to 90 °C. The author has chosen the following substrates to fabricate the conductometric IDTs:

- Fused quartz silicon dioxide (SiO_2) substrates which are 2.75 inches (70 mm) in diameter each.
- Silicon coated with a thick layer (300 nm) of SiO_2 . The diameter of each substrate was 3 inches (76.2 mm).

For the layered SAW transducers microfabrication, 36° YX LiTaO_3 substrate was chosen for its high thermal stability and electromechanical coupling [222].

For the conductometric transducers, two IDT patterns have been microfabricated by the author, which were suitable for the subsequent polymer deposition techniques that will be discussed in great detail in Chapter 5. Fine IDT pattern with a gold electrodes width of 50 μm and spacing of 50 μm between electrodes as well as larger features IDT with

200 μm in electrodes width and 200 μm spacing between electrodes were microfabricated.

For the microfabrication of layered SAW transducers on 36° YX LiTaO_3 substrates, a two-port resonator structure was chosen over the delay line structure due to its higher phase slope that contributes to better oscillation stability [222]. The input and output IDTs consisted of 38 electrode pairs with reflective gratings. In each reflective grating there are 160 electrodes. The aperture width was 700 μm with the periodicity of 40 μm . By implementing these IDT parameters, the SAW transducer center operational frequency was ~ 94 MHz. A batch of SAW transducers with bare IDTs were supplied by an external contractor in China according to these parameters. The author deposited the ZnO thin film to achieve the layered SAW structure which will be explained in more details in section 4.8.

4.2 Preparation of Photolithographic Masks

For the purpose of photolithography, which will be discussed in an upcoming section, specially designed masks are used for patterning of IDTs. The mask designed by the author for the fabrication of conductometric transducers as well as the layout of a single conductometric transducer are shown in Figure 4.2.

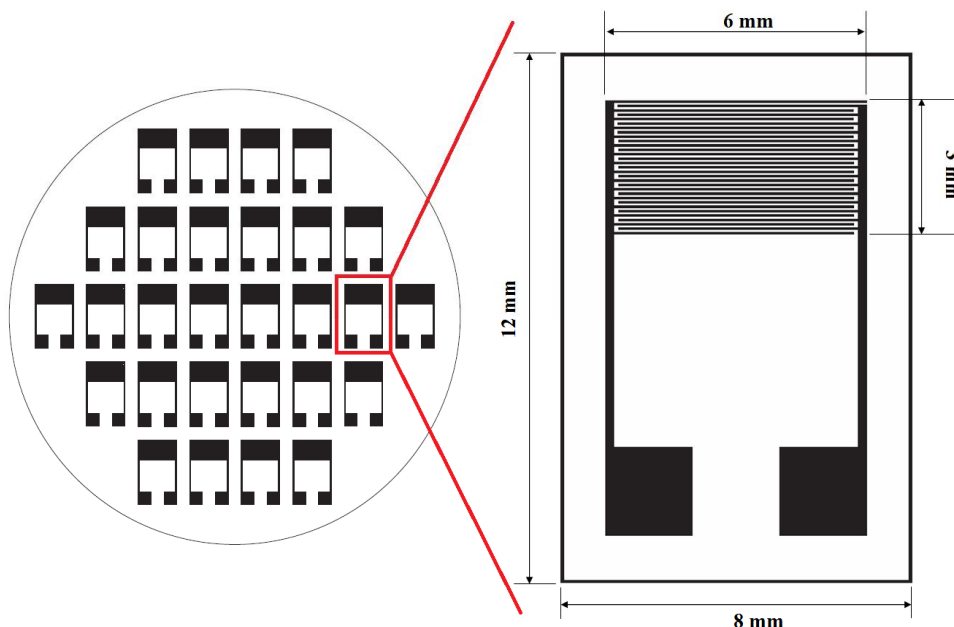


Figure 4.2. Conductometric transducers mask and the overall device layout.

The IDTs patterns were drawn using the *Adobe Illustrator® CS4* software according to the parameters specified in section 4.1. After taking extra care in generating and checking the IDT patterns' computer files, they were printed on transparent sheets.

4.3 Substrate Cleaning

Due to the micron sized features of the IDTs, the microfabrication process is largely affected by redundant organic or inorganic particles introduced to the substrate during manufacturing or improper handling or from dust in the air [223]. Hence the microfabrication of IDTs was performed by the author in class 1000 clean rooms at RMIT University.

At the beginning of the process, the substrate was rinsed with acetone for five minutes to remove any organic contaminants. Acetone is a well known volatile organic compound that evaporate quickly leaving stains behind. Therefore the substrate was washed with isopropyl alcohol (IPA) for two minutes before the complete evaporation of the acetone. Running deionized (DI) water was used to clean the substrate from any IPA residue. Then the substrate was dried by blowing it with compressed nitrogen gas.

After this process, the substrate was inspected thoroughly under the optical microscope to determine whether further cleaning is necessary. If more cleaning was needed, the substrate was soaked in a bath containing quick strip AZ-100 solution that was heated up to 80 °C for 30 minutes. Meanwhile the substrate was wiped constantly from both sides with clean room lint tissues. After the period of 30 minutes the heat source was removed and the bath was allowed to cool down at room temperature for 15 minutes. Then the substrate was rinsed with fresh quick strip AZ-100 solution, washed with DI water, and dried with compressed nitrogen gas.

The substrate cleaning is repeated until there are no more particles can be found during the inspection with the optical microscope. Before engaging in the next microfabrication step, the substrate was completely dehydrated by placing it on a 100 °C hot plate for five minutes in order to prevent any staining caused by the slow evaporation of water droplets.

4.4 Metal Thin Film Deposition

For the conductometric IDT on a quartz substrate, chromium (Cr) and gold (Au) thin films were deposited using Balzers™ electron beam evaporator. Cr was deposited first to provide good adhesion medium for the Au thin film. The thickness of the Cr thin film was 50 nm. Then a 100 nm Au thin film was deposited. For the microfabrication of conductometric IDT on a silicon wafer, a thick layer (300 nm) of SiO₂ was deposited before starting the deposition of Cr and Au. The purpose of the SiO₂ is to provide complete insulation between the IDT and the semiconducting silicon.

Gold was chosen as the transducers' surface material because it is highly inert to most of the target gases. Hence the output signal of the developed sensors can be attributed merely to the changes in the sensitive films properties during the interaction with target gas molecules.

4.5 Photolithography

Photolithography is a process widely utilized in the IC industry [223]. It is the process of transferring a pattern from the mask to the substrate. The author performed the photolithography inside the clean room facility at RMIT University with a maintained room temperature of 22 °C and relative humidity of 38%.

The procedure starts with cleaning of the substrate after the deposition of metal layers. The cleaning process was described in section 4.2. Dehydration of the substrate was performed by placing it on a 100 °C hot-plate for 5 minutes. The substrate was allowed to cool down on the bench for about 10 minutes. Then the liquid positive photoresist (AZ1512) was dispensed on the substrate using an adjustable micro-dispenser. With the micro-dispenser the amount of the dispensed photoresist is adjusted depending on whether the whole wafer is being microfabricated or a small portion to produce only one transducer. After casting the photoresist the substrate was spun at 3000 rpm for 20 s to produce a uniform coating of ~0.5 µm in thickness. In order to cure the wet photoresist, the substrate was placed inside a 90 °C oven for 20 minutes. Then the substrate was allowed to cool down for few minutes. In the mean time the mask was wiped with a lint-free tissue containing some methanol to remove any remaining photoresist stuck to it from previous usage. Subsequently the mask was placed inside the *Carl Suss MRK-3* mask aligner and the substrate underneath it. The alignment of the substrate and the mask was achieved through adjusting the alignment knobs. The substrate was locked in the final position providing a complete contact with the mask. Afterwards a UV light exposure was performed for 12 s. It is well known from literature that positive photoresists become soluble when exposed to UV light [223]. However the areas that are covered by the mask pattern remain insoluble, which is the main principle behind photolithography.

In order for the pattern to appear, the substrate was immersed in diluted (1:4) chemical developer (AZ400) for 20 s. In this process a selective dissolving of the cured photoresist took place. Since a positive photoresist (AZ1512) was used, the IDT pattern remained on the substrate and all the rest was dissolved in the developer. Then the substrate was washed with running DI water and dried with compressed nitrogen gas. The transferred pattern was inspected under the microscope. Any mistake found through the microscope

inspection can be corrected by the total removal of the photoresist through washing the substrate with acetone, IPA, and DI water followed by restarting the photolithography process.

Subsequently the substrate was hard backed at 110 °C for 20 minutes. The hard backing removes any residual solvents and anneals the patterned photoresist to promote interfacial adhesion of the photoresist that has been weakened by the developer penetration along the photresist/substrate interface. It also improves the hardness of the photoresist and makes it ready for the next microfabrication step, which is the chemical etching.

4.6 Chemical Etching

For the IDT pattern to be permanently printed on the wafer, two steps of chemical etching are needed. The first step is the etching of the gold thin film. Gold etching was achieved by dipping the substrate in aqua-regia solution, which is a 1:3 mixture of the highly concentrated nitric (69%) and hydrochloric (32%) acids. In order to prepare this solution the acids were poured straightaway from the manufacturer bottles, *Biolab*, with no further dilution. With this strong solution, only 15 s was needed to etch the 100 nm gold layer from the areas that were not patterned. After this quick gold etching, the substrate was washed thoroughly with running DI water and dried with compressed nitrogen gas.

The second step is etching the chromium layer. For that purpose, a solution consisting of 5 grams ceric ammonium nitrate, 4 ml of highly concentrated nitric acid (69%) and 50 ml of DI water was used. The substrate was immersed in this solution for about 60 s until the chromium layer was visibly gone and only the patterned gold IDTs were left on the substrate. Then the substrate was washed with running DI water. Subsequently, the microfabricated substrate was cleaned from any residual photoresist through rinsing with acetone, IPA and DI water followed by drying with compressed nitrogen gas.

4.7 Wafer Dicing

Due to the rigorous nature of the wafer dicing process, the wafer was spin-coated with photoresist at 3000 rpm for 20 s and baked at 90 °C for 20 minutes before starting the dicing in order to protect the microfabricated IDTs. Then a *Tempress (Model 602)* dicing saw was used to cut the wafer into small rectangular pieces (8 mm × 12 mm). In the case of the 200 μm IDT, the photolithographic mask was developed in conjunction with another research project at RMIT University and contained many different patterns.

Hence in order to microfabricate this type of IDT, the photoresist coated wafer had to be diced before starting the photolithography process. After dicing the transducers were microfabricated one by one according to the previously mentioned steps. An image of a developed conductometric sensor based on the 200 μm IDT will be shown in Chapter 5. Figure 4.3 displays a microfabricated and diced silicon/SiO₂ substrate, which has 28 conductometric transducers. Each transducer consists of a 50 μm gold IDT.

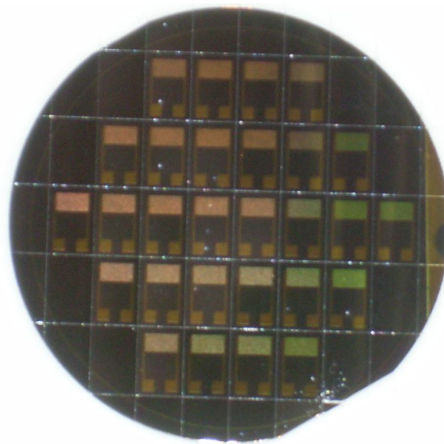


Figure 4.3. Microfabricated and diced silicon/SiO₂ wafer with 50 μm IDTs.

4.8 ZnO Sputtering on SAW Transducers

In this work, the author sputtered ZnO thin films on the purchased 36° YX LiTaO₃ transducers as shown in Figure 4.4.

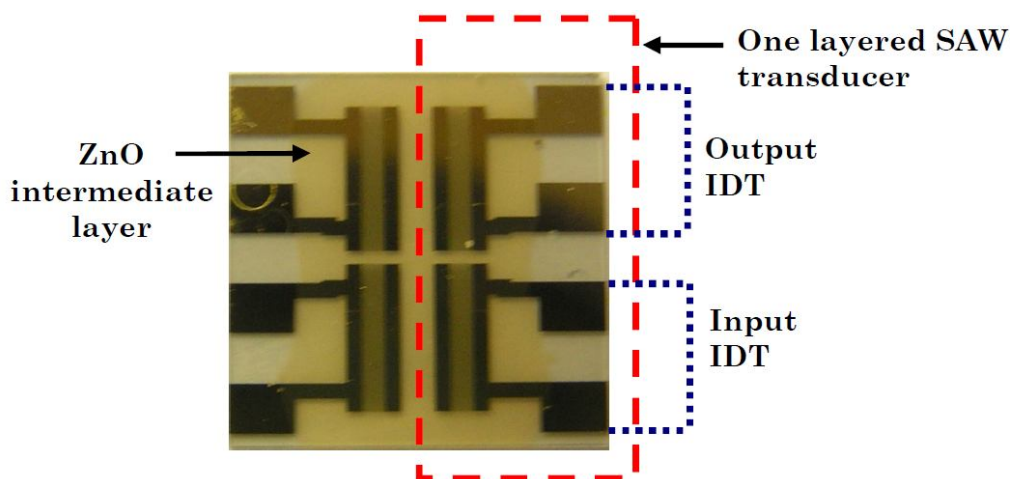


Figure 4.4. A microfabricated 36° YX LiTaO₃ substrate with sputtered ZnO thin film.

A radio frequency (RF) magnetron sputterer was used to sputter ZnO from a pure (99.99%) ZnO target. The forward RF power was 120 W. The matching circuit was carefully tuned to achieve ~0 W of reflected power. The sputtering gas was 40% O₂ in Ar with the pressure of 1×10^{-2} torr. The substrate temperature was 260°C. It was shown in an earlier study that the ZnO/36° YX LiTaO₃ structure would have a maximum K^2 value at a ZnO film thickness ~1–2.5 μm [224]. The deposited ZnO film thickness was measured with the *Ambios XP-2 Stylus* profilometer and found to be ~1.2 μm after 60 minutes of deposition.

4.9 Gold Wire Bonding

Connection of the developed transducers to external equipment was achieved by bonding gold wires to the transducers' rectangular gold pads. Before starting the process of wire bonding, the transducers must be prepared in a certain manner depending on their type. For conductometric transducers cleaning was necessary to remove the photoresist, which was deposited before the wafer dicing. This was achieved by rinsing the transducers with acetone, IPA and DI water followed by drying with compressed nitrogen gas. While in the case of layered SAW transducers, etching of the ZnO layer from the pads area was needed. For this purpose a diluted (1.0 M) nitric acid solution was used. A small cotton bar was dipped in the solution and used to wipe the pads area very slowly and carefully. Then the transducers were washed with running DI water and inspected under the optical microscope to confirm the removal of the ZnO layer from the gold pads.

In this project, 50 Ft long spooled 99.99% gold wire rolls were purchased from the *Semiconductor Packaging Materials (SPM) CO. INC.* based in New York, USA. The silver conductive epoxy *EPO-TEK® EE 129-4* was used to bond the gold wires. The author chose to order this particular silver epoxy since it cures at room temperature ~ 23 °C in 24 hours.

The silver epoxy consists of two parts named as part A and part B which are kept in separate containers. For wire bonding, equal amounts of each part were mixed thoroughly. A needle was used to cast small drops of the mixture on the transducers' gold pads. Then the gold wires were attached carefully. The attachment of the gold wires was verified by inspection with the optical microscope. In some cases some mistakes happened during the wire attachment and the silver epoxy bridged the gap between the gold pads. To rectify this, the wires were removed and the pads area was cleaned with a small cotton bar containing acetone. Then the transducer was inspected under the microscope again before reapplying the silver epoxy to the gold pads.

4.10 Transducers Testing

Before proceeding with the deposition of the sensitive layer, the developed transducers were tested. For conductometric transducers, the testing was made with conventional multimeter. The resistance between the gold pads was measured. The functional conductometric transducer must be open circuit before the deposition of any sensitive layer. If the multimeter displays any value for the resistance, that transducer is rejected.

The network analyzer is the most suitable instrument for testing SAW devices. An *Anritru 37369A* 50 Ω vector network analyzer equipped with picoprobe manipulators was used for testing the layered SAW transducers. Measurement of the scattering matrix parameters (S_{11} , S_{21} , S_{12} , S_{22}) allows the determination of both the phase velocity and the insertion loss of the transducer over a given frequency range. Since the deposition of the conducting polymer layer increases the insertion loss, any ZnO/36° YX LiTaO₃ SAW transducer with insertion loss more than 15 dB (before depositing the polymer sensitive film) was rejected. After the sensitive layer deposition, every sensor was tested again with the network analyzer to specify the overall sensor center frequency and insertion loss. The network analyzer results for all the developed gas sensors will be presented in Chapter 7.

4.11 Summary

The transducers microfabrication process was discussed in this chapter. It started with the rigorous cleaning of the substrates before the deposition of metal layers. Specially designed masks were needed to fabricate the transducers. Then the IDTs were microfabricated through the photolithography and chemical etching procedures. Dicing saw was used to separate the transducers from each other. ZnO thin films were deposited on the SAW transducers by RF magnetron sputtering to confine the acoustic wave energy. This process was followed by the gold wires bonding. Testing the developed transducers allowed the elimination of the faulty transducers before proceeding with the sensitive layer deposition. In the next chapter, the deposition of the gas sensitive nanomaterials will be discussed.

Chapter 5

Synthesis and Deposition of Nanostructured Materials

NANOSTRUCTURED conducting polymers can be mainly synthesized via template or template-free methods as discussed earlier in Chapter 2. Out of these methods, the template-free synthesis is currently receiving an increasing attention from researchers around the world since it eliminates the need for post-synthetic template removal process that usually requires treatment with harsh chemicals. The template-free synthesis of nanostructured conducting polymers, which is considered in this thesis, can be achieved by chemical oxidative polymerization or electropolymerization of monomer solutions.

In the previous chapter, the fabrication of conductometric and layered SAW transducers was described. The purpose of this chapter is to detail the experimental steps for nanomaterials' preparation and their deposition on transducers' surfaces. In section 5.1, the author will introduce the concept of polymerization by which individual monomer molecules bind together to form the polymer backbone. The deposition of nanomaterials on the surfaces of conductometric and layered SAW transducers will be discussed in section 5.2. Sections 5.3, 5.4, 5.5, 5.6, and 5.7 will explain the syntheses and deposition of nanostructured polythiophene, polypyrrole, polyaniline, derivatives of polyaniline and graphene/polyaniline nanocomposite respectively. Then the chapter will be concluded by a summary in section 5.8.

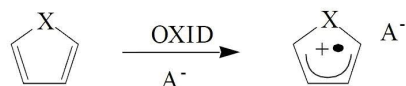
5.1 Polymerization Concept

Polymers are usually formed by binding a large number of monomer aromatic rings to form macromolecules in a process known as polymerization. This process involves monomer oxidation by chemical or electrochemical means. Chemical polymerization is carried out in a solution containing the monomer and a dissolved chemical oxidant. When the chemical reaction ends, the insoluble polymer particles precipitate at the bottom of the reaction vessel. While in the case of electropolymerization, the polymer is deposited directly on a conductive substrate placed as the working electrode of an electrochemical cell.

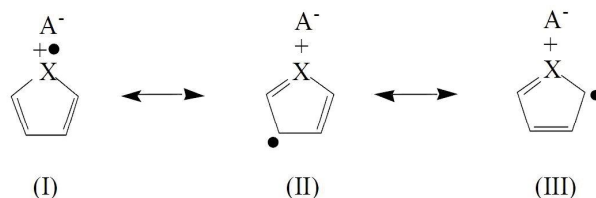
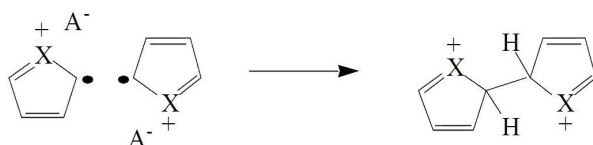
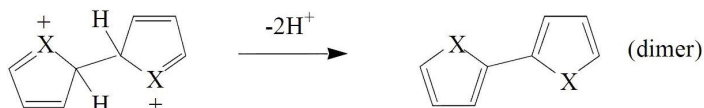
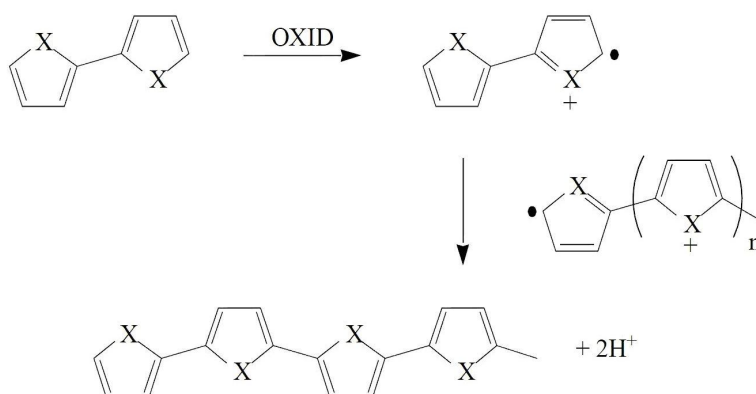
Despite the experimental difference between the chemical and the electrochemical polymerization, the mechanism by which monomer units bind together to form the polymer backbone is similar for both cases. It is a stepwise process that can be summarized by the following steps [53, 225]:

- Oxidation of monomer molecules to produce radical cations.
- Coupling between every two radical cations at the α -position of the aromatic rings.
- Deprotonation by the expulsion of two protons from each radical cations causing the formation of dimer molecules.
- Chain propagation to form the polymer through coupling between dimer molecules due to the continuous oxidation.

The first step in this process, which is the monomer oxidation, is slow [59]. Whereas the coupling of radicals, deprotonation and dimer oxidation steps are fast. Although the chain starts to grow in the solution, it loses solubility when it reaches a certain length and begins to precipitate in the reaction vessel during chemical polymerization and on the working electrode during electropolymerization. A schematic diagram illustrating the polymerization mechanism for heterocyclic monomers such as thiophene and pyrrole is provided in Figure 5.1, where X represents a heteroatom such as S for thiophene or N for pyrrole and A^- is an anion released by the chemical oxidant during chemical polymerization or by the electrolyte during electropolymerization. This mechanism also applies for a monomer consisting of a benzene ring such as aniline [66]. The polymerization of aniline is conducted in an acidic medium. After the formation of aniline radical cations through oxidation, consecutive rearomatization produces aniline dimer. When the chain oxidation is completed, the green emeraldine salt (the conducting form of PANI) is precipitated in the vial after consuming all the oxidant in the chemical polymerization or on the working electrode surface during electropolymerization.

Step 1. Monomer Oxidation

Resonance forms:

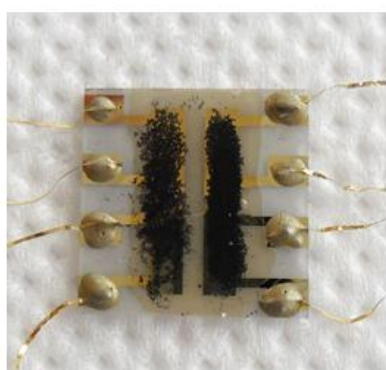
**Step 2. Radical-Radical Coupling****Step 3. Deprotonation/Re-Aromatization****Step 4. Chain Propagation****Figure 5.1. Polymerization steps of a heterocyclic monomer [59].**

The morphology of the resultant polymer is largely dependant on the experimental conditions for the chemical or electrochemical polymerization. For nanostructured CPs synthesis, the polymerization process should be fast in order to promote homogeneous nucleation of polymer chains to restrict the growth into one dimension and suppress the secondary growth that leads to the formation of three dimensional structures [68]. A review on the growth methods for nanostructured CPs was provided in section 2.2. For the nanostructured CPs synthesized in this project, speeding the polymerization process was achieved by either the inclusion of an oligomer such as a dimer or trimer during

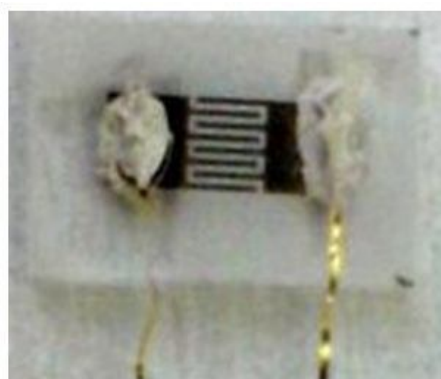
polymerization as well as careful adjustment of electrochemical parameters such as the applied potential as well as the type and concentration of the electrolyte.

5.2 Deposition Techniques

Template-free method for synthesizing nanostructured CPs is adopted throughout this dissertation. Chemically synthesized CPs nanostructures are usually suspended in the solvent used during polymerization and can be deposited on conductometric and layered SAW transducers through either drop casting or airbrushing. In drop casting, the author used a micropipette to cast a fixed amount of the polymer solution on transducers' surfaces and left them to dry in the clean room overnight. Alternatively, airbrushing technique was employed to obtain more uniform distribution of nanostructures over the entire transducer's surface. In this deposition technique, the transducers were placed on a 60 °C hot plate. Nitrogen gas was used for airbrushing since it is an inert gas. The distance between the airbrush tip and the transducer surface was maintained at about 10 cm. The deposited films thicknesses were measured with an Ambios XP-2 Stylus profilometer and found to be ~500 nm. Figure 5.2 shows a layered SAW and a conductometric sensors based on chemically synthesized nanostructured CPs.



(A)



(B)

Figure 5.2. Gas sensors based on chemically synthesized nanostructured conducting polymers: (A) Layered SAW sensor, (B) Conductometric sensor.

On the other hand, electropolymerization allows for a controllable in situ deposition of a CP thin film on a conductive substrate placed as the working electrode in an electrochemical cell. It was demonstrated in earlier reports that this technique can be employed for developing conductometric and SAW gas sensors based on CPs thin films [61, 84]. By adjusting the deposition parameters such as the applied potential, the

deposition time and/or the electrolyte constituents, the deposited film morphology and thickness can be optimized in order to achieve high sensitivity of the developed sensor towards target gases. In order for the deposition on conductometric transducers to occur, the distance between conductive fingers must be in the order of several tens of micrometers [39]. Specially designed conductometric transducers were employed for this purpose with a 50 μm of gold finger width and spacing between fingers. Further details on the fabrication of these transducers were provided in the previous chapter. The transducers were short-circuited during the electrodeposition in order to obtain a closed loop for the current to flow between electrodes. After the electrodeposition the short-circuit wires were removed. Electropolymerization can be conducted inside a two-electrodes or three-electrodes electrochemical cell. Both of them have been used in this research project for depositing sensitive films on conductometric transducers as shown in Figure 5.3.



Figure 5.3. (A) A sensor based on nanostructured polythiophene deposited by two-electrodes cell, (B) A sensor based on polypyrrole nanowires deposited by a three-electrodes cell.

Due to the deposition of ZnO acoustic guiding layer on SAW transducers, only chemically synthesized nanostructured CPs could be deposited on these transducers and electropolymerization was not feasible in this case. In the upcoming sections, syntheses of the nanostructured materials investigated for their sensitivity towards H_2 gas in this research project will be detailed.

5.3 Polythiophene Nanostructures

Synthesis of nanostructured polythiophene has attracted the attention of several research groups. Polythiophene nanowires have been prepared through different

techniques. Densely packed monolayers found in Langmuir-Blodgett (LB) films of amphiphilic polythiophenes can spontaneously fold when compressed beyond the collapse point of the LB-trough to give polythiophene nanowires with diameters of about 60 nm [226]. Liu and co-workers have synthesized di- and tri- block copolymers of regio-regular poly(3-alkylthiophene) using atom transfer radical polymerization (ATRP) which self-assembles to form polythiophene nanowires [227]. Scanning probe microscopy based lithography has been an alternative method of making nanowires. Using Electrochemical Dip-Pen Nanolithography (E-DPN), polythiophene nanolines with line width of 50 nm were obtained [228].

Chemically, polythiophene nanowires with diameters of 50–100 nm have been developed through the oxidative polymerization followed by one hour of gamma radiation [229]. Although the process succeeded in producing nanofibrillar morphology, but the structures tend to merge with each other to form sub-micron sized coral-like structures. In a recent study, polythiophene nanoparticles with diameters of 60–100 nm were synthesized through an oxidative emulsion polymerization catalyzed by copper (II) salts. The process resulted in high yields (86–98%) of polythiophene nanoparticles uniformly suspended in an aqueous solution [230]. Template synthesis of polythiophene nanotubes with diameters range of 20–200 nm has been reported by some researchers [78, 79]. The scanning electron microscopy (SEM) results in both reports demonstrate the collapse of the stand-alone nanotubes after the removal of the alumina membrane and sticking to each other into bundles of micron sized clusters.

Hence, the author of this dissertation made an informed decision to develop gas sensors based on polythiophene nanostructured synthesized through template-free method. For this purpose both of the electrochemical and chemical polymerizations were employed for synthesizing polythiophene nanostructures as described in the upcoming subsections. Characterization results for the deposited polythiophene nanostructures are provided in Chapter 6.

Electropolymerization

For gas sensors based on nanostructured thin films, a uniform distribution of nanostructures over the entire transducer surface is essential for a stable sensor performance. Therefore, the author developed a novel technique for controllable deposition of polythiophene nanostructures on conductometric transducers through template-free electropolymerization. The deposited film thickness can easily be controlled by adjusting the electropolymerization time. The author electrodeposited polythiophene nanostructures on transducers' surfaces in the Microelectronics and

Materials technology Centre (MMTC) at RMIT University. Several deposition parameters were varied for comparison between the deposited films' characterization and gas sensing results in order to find the deposition parameters that lead to the optimum sensor performance. For these experiments, a two-electrodes electrochemical cell was utilized. The conductometric transducer was used as the working electrode (the anode) and a (3 × 3) cm² platinum sheet as the counter-electrode (the cathode). The electrodes were separated by a 3 cm span. A 50 mL of acetonitrile was used as the organic solvent in each experiment. The concentrations of the monomer, thiophene, and the oligomer, terthiophene, were fixed throughout the experiments at 0.15 M and 1 mM, respectively.

First of all, the author investigated the effect of anion type on the resultant polymer morphology. For that purpose, the polythiophene thin films' morphologies obtained by using FeCl₃ electrolyte that release Cl⁻ anions and lithium perchlorate (LiClO₄) electrolyte that produce ClO₄⁻ anions were compared. Since LiClO₄ is a much weaker oxidant (corrosive class 5.1) than FeCl₃ (corrosive class 8), higher concentration of LiClO₄ (0.5 M) and potential (1.3 V DC) were needed to start the polymerization compared to that of FeCl₃ (1.2 mM, 0.75 V DC). The electro-deposition on conductometric transducers was performed for one hour with each electrolyte. At lower concentration of LiClO₄ and applied potential, no deposition of polythiophene could occur despite running the experiment for several hours.

After analyzing the characterization and gas sensing results of the above sensors, the author decided to conduct further investigations on the electropolymerization of polythiophene using FeCl₃ electrolyte. The effect of varying the electrolyte concentration and the amplitude of applied potential was investigated with one hour of deposition for each case. Deposition on conductometric transducers was conducted for each of FeCl₃ solution concentrations of 0.6 mM, 0.9 mM, 1.2 mM, 1.5 mM and 1.8 mM. The deposition was conducted using a fixed applied potential of 0.75 V DC for all of them. After observing the characterization and gas sensing results for these sensors, the author concluded that the concentration of 1.2 mM of FeCl₃ was the optimum value for deposition. Hence this concentration was fixed for the investigation of different applied potentials. For this study, the deposition on five transducers was conducted using one of 0.65 V, 0.7 V, 0.75 V, 0.8 V or 0.85 V each time. The characterization and gas sensing results demonstrated that the best deposition voltage was 0.75 V.

Also the author investigates the effect of depositing different thicknesses for the sensitive films on the developed sensors' performances. For this investigation, four sensors were developed using 1.2 mM of FeCl₃ as an electrolyte and 0.75 V of applied

voltage. In this case different deposition time was applied for each sensor, which were 10, 20, 30 and 60 minutes respectively. Table 5.1 lists the measured film thicknesses. No further steps were taken between 30 minutes and 60 minutes of deposition time due to the high measured film thickness after 30 minutes.

Table 5.1. Deposition time versus film thickness of electrochemically deposited nanostructured polythiophene films.

Deposition Time (Minutes)	Film Thickness (μm)
10	0.2
20	1.5
30	3.7
60	10

Chemical Polymerization

Chemical synthesis of polythiophene nanofibers was performed in University of California, Los Angeles in USA according to an established collaboration with RMIT University. Polythiophene nanofibers were synthesized through a template-free chemical oxidative polymerization. This synthetic route yields pure nanofibers suspended in the reaction solvent that can easily be dispersed onto interdigitated transducers (IDT) to function as a sensitive layer for gas sensors. The introduction of an initiator in the reaction mixture speeds up the polymerization process. This in turn produces nanofibrillar morphology by promoting homogeneous nucleation of the polymer chains thereby suppressing subsequent growth of new polymer chains on top of one another (secondary growth) [93].

Polythiophene nanofibers were synthesized by dissolving 100 mg of the oxidant, which was iron (III) chloride (FeCl_3) in 3 mL of acetonitrile. This solution was added to a 3 mL solution of o-dichlorobenzene containing 42 mg of thiophene and 2 mg of terthiophene (the polymerization initiator). The reaction was shaken vigorously for 10 s and left unagitated for one day after which the crude product was purified by centrifugation and washed with copious amounts of acetonitrile. The solution containing polythiophene nanofibers was then drop-cast onto a ZnO/36° YX LiTaO₃ layered SAW transducer using a micropipette and left to dry for one day.

5.4 Polypyrrole Nanostructures

The production of nanostructured PPy was studied using templated synthetic methods employing mesoporous silica, anodized aluminum oxide membranes, and particle track-etched membranes [231, 232]. Also, a bulk growth approach using V_2O_5 seeds as a template was reported [233]. Fibrillar and tubular morphologies of polypyrrole was observed when β -naphthalene sulfonic acid (NSA) or p-toluenesulfonate acid (TsOH) is used as a dopant during the synthesis process [234]. These fibers and tubes had diameters in the range of 50–2000 nm and were formed presumably as a result of the solution aggregation of the dopant anions. In general, a straightforward bulk synthesis of nanofibers of polypyrrole directly from pyrrole monomer with average fiber diameter less than 100 nm, has been difficult to achieve. Therefore, the author of this thesis made an informed decision to develop gas sensors based on polypyrrole nanofibers and nanowires polymerized via template-free approach. Characterization results of these nanostructures will be given in Chapter 6.

Electropolymerization

Electrochemical deposition of polypyrrole nanowires was performed in Pierre and Marie Curie University, Paris in France according to an established collaboration with RMIT University. The pyrrole electropolymerization was conducted in a three-electrode electrochemical cell. The conductometric transducer was used as the working electrode. The counter electrode was a platinum wire. Saturated calomel electrode (SCE) was used for the reference electrode. The polymerization solution contained 0.15 M of pyrrole monomer, 0.2 M of Na_2HPO_4 and 0.002 M of $LiClO_4$. Three sensors were developed and compared. The anodic potential was kept at 0.85 V/SCE during deposition. However different anodic charge settings were employed. The anodic charge during deposition of polypyrrole nanowires on transducers (A), (B) and (C) were 13, 55 and 90 mC respectively. Film deposition time was kept at 60 minutes for these sensors. However due to the difference in the charge quantity passing between the electrodes (electropolymerization current), different thicknesses for the deposited films was observed. The sensitive films thicknesses of sensors (A), (B) and (C) were measured and found to be ~ 3 μm , 4 μm and 10 μm respectively. Characterization and gas sensing results for these sensors will be provided in the upcoming chapters.

Chemical Polymerization

Chemical synthesis of polypyrrole nanofibers was performed in University of California, Los Angeles. All chemicals in the synthesis of polypyrrole nanofibers were purchased from Sigma-Aldrich. Monomers were distilled prior to use. Reactions were performed in 20 mL glass vials in which pyrrole (50 mg, 0.74 mmol) and bipyrrrole (3 mg, 0.023 mmol) were dissolved in 10 mL of methanol and rapidly mixed with a separate solution of FeCl_3 (120 mg, 0.74 mmol) in 10 mL of deionized water. The reaction mixture was vigorously shaken for several seconds and then left un-agitated for one day. The crude product was purified by centrifugation and washed multiple times with deionized water. The purified product was typically resuspended in deionized water to a concentration of 2 g/L. The solution containing polypyrrole nanofibers was then drop-cast onto a $\text{ZnO}/36^\circ \text{ YX LiTaO}_3$ layered SAW transducer using a micropipette and left to dry for one day.

5.5 Nanoporous Polyaniline

Recently there has been much interest in the preparation of nanoporous materials owing to their wide range of applications in sensors, catalysis, separation membranes, photonic devices and so forth [235]. For gas sensing applications, a nanoporous material can allow for a deep penetration of gas molecules for the interaction with adsorption sites throughout the bulk of the sensitive film leading to a high sensitivity of the developed gas sensor.

Layered SAW hydrogen gas sensor based on the nanoporous polyaniline was fabricated and tested herein. Nanoporous polyaniline was chemically synthesized through a template-free approach at Sejong University, Seoul in Korea according to an established collaboration with RMIT University. From the characterization results that will be provided in the next chapter, nanoporous polyaniline had higher surface area compared to that of other nanostructures for the same polymer.

Nanoporous polyaniline was synthesized directly from anilium salts in a template-free reaction. In a typical procedure, aniline (8.6 mmol) was dissolved in chloroform (10 mL) and ammonium peroxydisulfate (APS, 1 mmol) was dissolved in 10 mL of 4M HCl. Each solution was cooled at -25°C for one hour. The pre-cooled APS solution was slowly added to the cooled aniline solution at -25°C without stirring and left to react for 5 days. The resulting product was washed with acetone and 0.1M HCl solution three times, respectively. The solution containing nanoporous polyaniline was airbrushed on the surface of the heated $\text{ZnO}/36^\circ \text{ YX LiTaO}_3$ layered SAW transducer.

5.6 Derivatives of Polyaniline

Polyaniline derivatives such as polyanisidine (also known as polymethoxyaniline) and polyethylaniline can exhibit enhanced properties compared to polyaniline including improved dispersability in organic solvents like methanol [236, 237]. Furthermore, polyaniline derivatives often have a higher resistance against microbial and chemical degradation [238, 239]. In this dissertation, novel layered SAW hydrogen gas sensors based on polyanisidine and polyethylaniline nanofibers were developed for the first time, to the best of author's knowledge.

Template-free chemical syntheses of these nanostructured polyaniline derivatives were achieved in the University of California, Los Angeles. Polyanisidine nanofibers were synthesized by dissolving 0.4 g of anisidine in 10 mL of 1M HCl. This solution was mixed with 5–6 mg of aniline dimer dissolved in a minimal amount of methanol which serves as an initiator for the reaction. Then a 0.18 g of ammonium peroxydisulfate (oxidant) in 10 mL 1M HCl was added to the solution. The resulting dark green crude product was allowed to react for one day and then purified by dialysis versus deionized water. The solution containing polyanisidine nanofibers was then drop cast onto the ZnO/36° YX LiTaO₃ SAW transducer using a micropipette and left to dry for one day.

The chemical synthesis of polyethylaniline nanofibers was conducted in a 20 mL scintillation vial. Ethylaniline (0.39 g, 3.2 mmol) was dissolved in 10 mL of 1 M HCl along with p-phenylenediamine (5.2 mg, 0.05 mmol) which was pre-dissolved in a minimal amount of methanol. A separate solution of 10 mL of 1M HCl containing dissolved ammonium peroxydisulfate (0.18 g, 0.8 mmol) was rapidly mixed with the solution containing the monomer and initiator. The mixture was vigorously shaken for 15 seconds and left unagitated for 1 day after which time the crude product was purified by dialysis against deionized water. The pure polymer was collected and adjusted to a concentration of 2 g/L. In order to conduct UV-Vis spectroscopy, the doped polymer was washed with 0.1 M NH₄OH, dried, and dissolved in N-methyl-2-pyrrolidone (NMP). Subsequently, the polymer solution was airbrushed onto the surface of the ZnO/36° YX LiTaO₃ layered SAW transducer.

5.7 Graphene/Polyaniline Nanocomposite

It was demonstrated earlier that a homogeneous dispersion of a graphene nanofiller into a polymer matrix provided nanocomposites with enhanced mechanical, electrical, thermal and other properties due to the high aspect and surface-to-volume ratios of the nanofiller [198]. It was also suggested that graphene nanosheets can provide more

active nucleation sites for polyaniline as well as excellent electron transfer pathways [199].

In this thesis, a hydrogen gas sensor featuring a graphene/polyaniline nanocomposite as the sensitive layer was developed for the first time, to the best of the author's knowledge. From the gas sensing results that will be exhibited in Chapter 7, the developed sensor has higher sensitivity towards H₂ gas than that of only graphene and polyaniline nanofibers based gas sensors due to the high surface-to-volume ratio of the incorporated graphene nanosheets.

The graphene/polyaniline nanocomposite was synthesized through template-free chemical polymerization at Sejong University, Seoul. At the beginning, graphite oxide (GO) was synthesized through graphite oxidation with sulfuric acid and potassium permanganate (H₂SO₄-KMnO₄). Reduction of GO to graphene was achieved via refluxing GO with hydrazine in N,N-dimethylformamide (DMF). The graphene was sonicated for one hour in 10 ml of ethylene glycol in the presence of 1 mmol of aniline and 0.05 mmol of N-Phenyl-1,4-phenylenediamine. Then 0.25 mmol of APS in 10 mL of 1.0 M HCl was rapidly added to the mixture. The resulting solution was magnetically stirred overnight to produce the graphene/polyaniline nanocomposite.

For comparison, graphene nanosheets were also synthesized, characterized and employed as a sensitive material for H₂ gas. Aqueous graphene dispersions were synthesized from graphite oxide via a CMG approach as reported by Li et al. [194]. Graphene nanosheets were obtained through hydrazine reduction. The optimum hydrazine:GO ratio of 7:10 by weight was employed to obtain a stable solution, since an excessive hydrazine concentration may cause restacking of the graphene sheets.

In order to obtain a complete evaluation of the graphene/polyaniline based H₂ gas sensor performance, a sensor based on doped polyaniline nanofibers was also tested towards H₂ gas. The synthesis conditions for the polyaniline nanofibers were identical to that of the polyaniline in the graphene/polyaniline nanocomposite. Hence the same doping degree of polyaniline for both materials was carefully maintained by utilizing an identical type and concentration of the doping acid during synthesis, which was 1.0 M HCl. Further details on the synthesis process, characterization and gas sensing of polyaniline nanofibers are provided elsewhere [240]. The deposition of graphene/polyaniline, graphene nanosheets and polyaniline nanofibers was performed by the author through airbrushing on conductometric transducers heated at 60 °C.

5.8 Summary

In this chapter, the fundamentals and experimental details of the nanomaterials' syntheses were provided. Generally, the polymerization of monomers to produce polymers is a stepwise process. It starts by monomer oxidation to form radicals followed by radical-radical coupling, deprotonation by losing two protons and finally chain propagation. The chains start to form in the solution and then begin to precipitate on the bottom of the reaction vessel during chemical polymerization or on the working electrode in the case of electropolymerization when they lose their solubility after reaching a critical length. The deposition of chemically synthesized nanostructured polymers on transducers' surfaces was achieved by drop casting the solution or through airbrushing. On the contrary, in situ deposition of polymer chains on a transducer's surface occurs during electropolymerization when the transducer is used as the working electrode.

Chemical and electrochemical syntheses of nanostructured polythiophene and polypyrrole were described in this chapter. Additionally, the chemical syntheses details of nanoporous polyaniline, polyanisidine nanofibers, polyethylaniline nanofibers and graphene/polyaniline nanocomposite were provided herein. All of these nanomaterials were characterized to evaluate their physical and chemical properties. The results of nanomaterials characterization will be presented in the next chapter. The gas sensing results of the developed gas sensors based on these nanomaterials will be provided in Chapter 7.

Chapter 6

Characterization of Nanostructured Materials

THE performance of gas sensors is largely dependant on the physical and chemical properties of the sensitive films according to the literature reviewed in Chapter 2. Following the deposition of nanostructured films on conductometric and layered SAW transducers described in Chapter 5, characterization of each sensitive film was performed, which will be detailed in the present chapter.

An introduction to the characterization techniques considered in this research will be provided in section 6.1. Sections 6.2, 6.3, 6.4, and 6.5 will discuss the characterization results of nanostructured polythiophene, polypyrrole, polyaniline as well as its derivatives and graphene/polyaniline nanocomposite respectively. Finally the chapter will be concluded by a summary in section 6.6.

6.1 Characterization Techniques

Nowadays, there is a range of techniques that can be implemented for characterizing nanostructured conducting polymers. For morphological studies, the most widely used techniques are the scanning electron microscopy (SEM) and the transmission electron microscopy (TEM) [9]. Optical spectroscopic techniques such as ultraviolet-visible spectroscopy (UV-vis), Fourier transform infrared spectroscopy (FT-IR) and Raman spectroscopy can be employed to obtain information on the reduction/oxidation status and the chemical bonding for nanomaterials [62]. In order to determine the chemical

and electronic states of the elements within the first few layers of a nanostructured material's surface, X-ray photoelectron spectroscopy (XPS) can be utilized [9]. A combination of these characterization techniques was employed to analyze the properties of every nanostructured material developed during this research project. In the upcoming subsections, the author will provide a brief explanation of these techniques.

6.1.1 Scanning Electron Microscopy (SEM)

One of the largely utilized techniques for nanostructured materials' characterization is the scanning electron microscopy. Similar to an ordinary optical microscope, the SEM produces topographical information of the specimen being investigated but with nanoscale resolution.

An SEM microscope operates by scanning the sample with an electron beam focused into a small spot size of ~5 nm [62]. The electrons are accelerated by an applied voltage ranging from few hundred volts to 30 kV and the beam is steered via built-in deflection coils. The interaction between the electron beam and the sample's surface leads to the emission of secondary electrons, backscatter electrons, and X-rays. A detector inside the microscope picks up these emitted electrons and photons and converts them to an SEM image to study the morphology or an energy dispersive X-ray (EDX) spectrum to analyze the chemical composition of the sample.

6.1.2 Transmission Electron Microscopy (TEM)

In this microscopy technique, a beam of electrons accelerated with a 100 kV potential or higher (up to 1 MV) is focused on a very thin layer of the material under investigation (usually less than 200 nm in thickness) [62]. Most of the bombarded high energy electrons are transmitted through the sample and collected by a detector on the lower part of the microscope. This characterization technique provides information on the sample's morphology, crystallography, and its elemental composition at ultrafine resolution of 1 nm or even smaller [9].

A TEM operates by projecting electrons onto the nanomaterial which is deposited on a special TEM micro grid through condenser lenses. These electrons penetrate the sample either deflected or without deflection. The scattering of electrons during their transmission determines the kind of collected information from the sample. Through elastic scattering, electrons do not lose energy during transmission and in this case diffraction patterns of the sample can be obtained [62]. Whereas the inelastic interaction

between the projected electrons and the sample's electrons at heterogeneities of the nanostructures (like grain boundaries, dislocations, second-phase particles, defects, density variations, etc.) causes a complex absorption and scattering effects that produce spatial variations in the intensity of the transmitted electrons which can be distinguished by the detector during image formation [62]. Switching between the diffraction patterns' viewing mode and the imaging mode can be achieved by altering the intermediate lens's strength. For studying the morphology of a nanostructured material, a TEM is recommended when images with higher resolution than that produced by SEM are essential to analyze the nanostructures.

6.1.3 Ultraviolet-visible (UV-vis) Spectroscopy

One of the largely utilized techniques to characterize conducting polymers is the UV-vis spectroscopy. In this technique a sample is irradiated with electromagnetic waves in the ultraviolet and visible wavelengths and the sample's absorbance is analyzed through the output spectrum [9]. The positions of peaks in this spectrum provide information regarding the oxidation state of the polymer being investigated [241].

Typically, adsorption peaks at wavelengths in the range of 200–380 nm are associated with the π - π^* molecular transitions in conducting polymers [242]. Whereas adsorption peaks in the visible region of the electromagnetic spectrum at the wavelengths of 380–800 nm are related to the polaron–bipolaron transformations [242].

Depending on the conditions of the chemical or electrochemical synthesis, the resultant polymers can have different oxidation states. Therefore, the UV-vis spectroscopy is utilized throughout this thesis to determine the oxidation state of the conductive polymers employed for gas sensing application.

6.1.4 Fourier Transform Infrared (FT-IR) Spectroscopy

Infrared spectroscopy is a popular chemical characterization technique in which a sample is exposed to a mid-infrared radiation to measure its absorption of the infrared frequencies. For conducting polymers, an infrared spectrum provides information on the presence of single and conjugated bonds by analyzing the absorption peaks. Also information regarding the incorporation of dopant, doping level, chains linkage and side branching into a conducting polymer can be extracted through this characterization technique [53].

In principle, the covalent bonds holding molecules together are in continuous vibration [9]. The frequencies of these vibrations are in the range of 10^{12} – 10^{14} Hz (3–300 μm in

wavelength), which matches the frequencies of the mid-infrared radiation in the electromagnetic spectrum [62]. During the sample's exposure to infrared radiation, some of the incident frequencies are in resonance with the molecular vibration frequencies. This resonance allows for the exchange of energy between the incident electromagnetic wave and the mechanical molecular vibrations. Since the vibration of molecules represents a characteristic property for a particular type of bonds and the atoms included, the absorbed infrared frequencies recorded in the obtained spectrum can be regarded as a fingerprint indentifying that particular compound [9, 62, 243].

In the old technology of infrared spectroscopy, the spectrometers relied on prisms or grating to separate the radiation frequencies emitted from an infrared source and were referred to as dispersive spectrometers. However a new technology was later introduced by the production of Fourier-transform spectrometers. This type of spectrometers contains an interferometer that produces a signal that has all the infrared frequencies encoded through the implementation of the well established mathematical process of Fourier transformation [243]. By utilizing the FT-IR spectroscopy, a significant improvement to the quality of infrared spectra and acquisition time was achieved [243]. In this thesis, FT-IR spectra of chemically synthesized nanostructured conducting polymers were analyzed for chemical bonding characterization.

6.1.5 Raman Spectroscopy

Raman spectroscopy is a technique based on measuring the intensity and wavelength of the light scattered inelastically from a sample's surface illuminated by a source with known polarization and wavelength (generally in the visible or infrared regions) [9]. Inelastic scattering of light refers to the frequency shift between the incident light and the remitted light from the sample, which is also known as the Raman effect [9]. Typically Raman spectrometers employ intense monochromatic lasers as the exciting illumination due to the weak signal of the Raman scattering [62]. This technique is widely adopted technique to nondestructively characterize crystalline and noncrystalline materials by analyzing the lengths, strengths and arrangements of chemical bonds [62]. For instance, Raman spectroscopy can be employed to study sp^2 and sp^3 hybridization of carbon atoms in amorphous carbon nanostructures [244].

Both of the infrared and Raman spectroscopic techniques are based on the interaction between the incident radiation and the sample's molecular vibrations but differs in the mechanism by which energy is exchanged between the photons and the molecular vibrations [245]. In infrared spectroscopy, the absorbed low energy photons are in resonance with the molecular vibrations. Whereas in Raman spectroscopy, the incident

photons have much greater energy than that of the molecular vibrations. Consequently, part of the incident photons energy is transferred to the molecular vibrations and the remaining energy is reemitted from the sample. In Raman spectroscopy, the interaction between the incident light and a sample is an off-resonance condition involving Raman polarizability of the sample's molecules [245]. Raman spectroscopy is largely utilized in analyzing carbon nanostructures such as garphene.

6.1.6 X-Ray Photoelectron Spectroscopy (XPS)

XPS is a technique utilized for quantifying the chemical and electronic states of the elements within the top atomic layers of a material's surface [9]. In an XPS experiment, the sample is exposed to a beam of X-rays that can be absorbed by the sample's electrons leading to the ejection of photoelectrons [9]. By measuring the kinetic energy of the ejected photoelectron an elemental analysis can be performed as well as the determination of the material's oxidation level. For conducting polymers, XPS technique has been widely utilized to investigate the polymers' chemical composition and the incorporation of doping anions.

The characterization techniques described so far have been employed in this thesis to investigate the physical and chemical properties of the developed nanostructured gas sensitive thin films. The results from these investigations will be discussed in the upcoming sections.

6.2 Charaterization Results of Polythiophene Nanostructures

In this thesis, polythiophene nanostructures have been synthesized through template-free electrochemical and chemical polymerization methods. Through the electropolymerization of polythiophene nanostructures, the author conducted a comparative study on gas sensors utilizing conductometric transducers. Chemically synthesized polythiophene nanofibers were deposited on the surface of ZnO/36° YX LiTaO₃ layered SAW transducer for gas sensing application. The characterization results of polythiophene nanostructures synthesized through these methods are provided in the following subsections.

6.2.1 Electropolymerized Polythiophene Nanostructures

As described in Chapter 5, a comparative study on electropolymerized polythiophene nanostructures was conducted by the author of this dissertation. In this study,

polythiophene nanostructures were directly deposited on conductometric transducers. The gas sensing performance of these sensors will be analyzed in Chapter 7. In this section, analysis of the characterization results for the deposited thin films will be provided.

Initially, the effect of the type of anions in the electrolyte on the nanostructures' morphologies was investigated. Following this study, the author analyzed the effects of changing the electrolyte concentration and the applied deposition potential by varying one parameter at a time. Also the evolution of polythiophene nanostructures was monitored through investigating the morphology of the nanostructures at different deposition times.

Characterization of nanostructured polythiophene was performed entirely at RMIT University. The morphologies of the deposited polythiophene nanostructured thin films were all inspected by the author via FEI Nova NanoSEM. UV-Vis spectroscopy of the synthesized polythiophene was conducted by the author with an Oceanoptics HR4000 spectrophotometer and a Micropack DH2000 UV-VIS-NIR light source. The spectral data were logged to an adjacent computer running Spectrasuite software (2007 edition). The elemental composition of nanostructured polythiophene was investigated through XPS measurements. The XPS experiments were carried out with the assistance of Professor Johan Du Plessis utilizing Thermo K-Alpha spectrometer employing an Al-K α source with a spot size of 400 μm . Charging was minimized by a low energy electron ion flood gun. Individual peaks were scanned at 200 eV pass energy with an energy step of 1.0 eV. By analyzing the characterization results from the abovementioned studies, the author was able to make an informed decision regarding the optimum electrodeposition parameters.

The Effect of Electrolyte's Anion Type

In this investigation, polythiophene nanostructures electrodeposited in a 1.2 mM iron (III) chloride (FeCl_3) solution were compared with those deposited by utilizing 0.5 M lithium perchlorate (LiClO_4) solution. In both experiments, the solvent was acetonitrile and the deposition time was fixed at one hour. The electropolymerization currents shown in Figure 6.1 were recorded using a Keithley 2001 multimeter connected to a computer running a LabVIEW program that saves the current data at an acquisition interval of one second. By inspecting Figure 6.1, it can be noticed that the two electrolytes have different electrochemical reactivity. The author of this thesis observed that by employing LiClO_4 solution, the electropolymerization was not possible at a concentration lower than 0.5 M or at a deposition potential below 1.3 V.

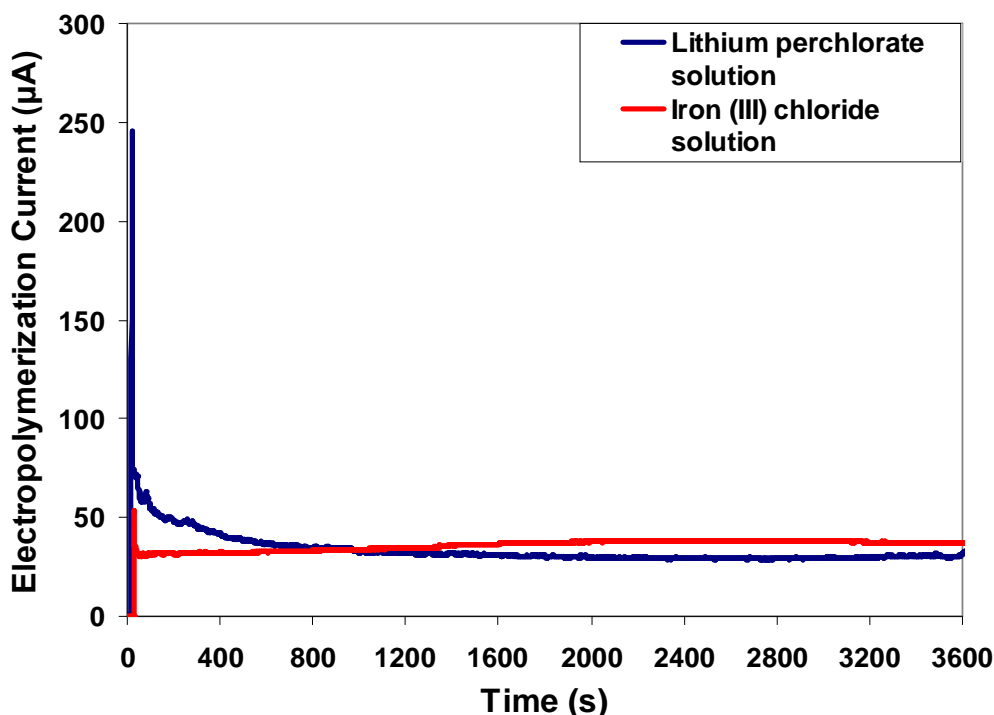


Figure 6.1. Polythiophene electropolymerization currents utilizing 1.2 mM FeCl_3 and 0.5 M LiClO_4 electrolytes.

The electropolymerization current for the deposition with LiClO_4 solution shows a sharp spike of 243.6 μA at the instant of applying 1.3 V DC. Then the current curve descends exponentially to a steady-state value of 30 μA . For the FeCl_3 solution, the electropolymerization current peaked at 52.6 μA at the moment of applying 0.75 V DC. Following this switching spike, the current was gradually rising towards the value of 37 μA . In this case, the current was rising gradually in contrast to the current observed with the LiClO_4 solution that was decreasing. SEM images of the deposited polythiophene by employing these electrolytes are shown in Figure 6.2. From Figure 6.2, it is evident that the type of electrolyte's anion has a significant impact on the resultant film's morphology. Utilizing LiClO_4 solution resulted in the deposition of polythiophene with a granular morphology as shown in Figure 6.2 (A). It is anticipated that the high current value for the first 10 minutes of electropolymerization, as shown in Figure 6.1, caused the instantaneous creation of a large number of nucleation sites that contribute to the compactness of the polymer [246]. Since the electropolymerization current was constantly decreasing, the polymerization process became slower promoting heterogeneous nucleation that caused secondary growth responsible for the formation of 3-D structures as discussed earlier in Chapter 2. By employing FeCl_3 solution, the deposited film consisted of a porous structure as shown in Figure 6.2 (B).

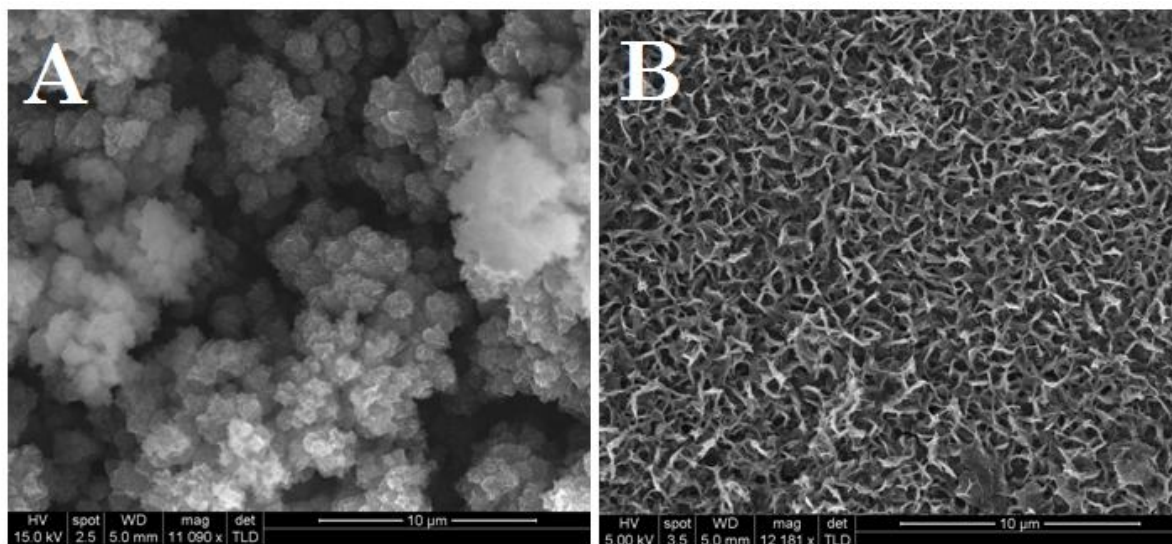


Figure 6.2. SEM images of electropolymerized polythiophene nanostructures using: (A) 0.5 M LiClO₄ solution, (B) 1.2 mM FeCl₃ solution.

A high magnification SEM image is displayed in Figure 6.3. The nanostructured polythiophene film consisted of nanofibers with diameters in the range of 26–40 nm and ~230 nm in length. These nanofibers are merging together in a network-like structure.

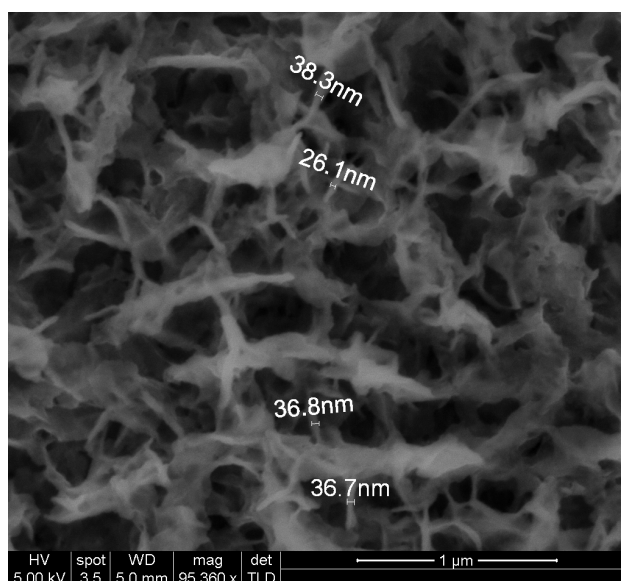
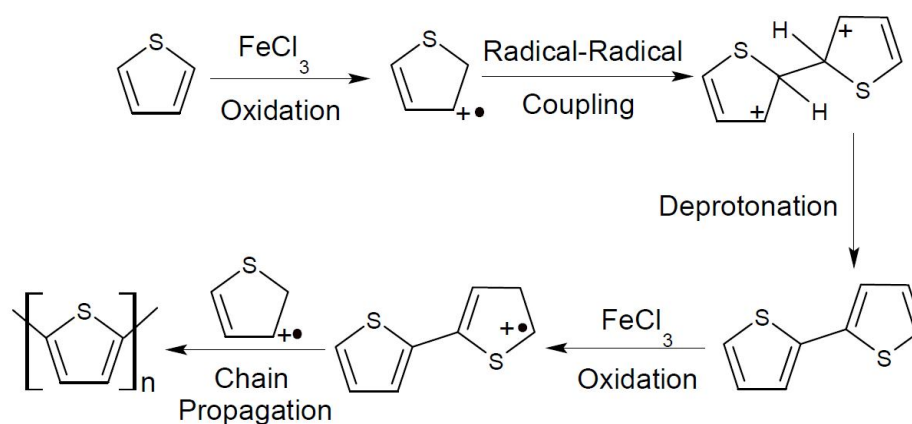


Figure 6.3. Magnified SEM image of polythiophene electropolymerized utilizing 1.2 mM FeCl₃ solution.

Referring to the current curve of electropolymerization with FeCl₃ solution shown in Figure 6.1, it can be concluded that the heterogeneous nucleation has been suppressed in this case by restricting the flow of the high current at the beginning of the electropolymerization and maintaining a stable high value of current throughout the

deposition period. Therefore, fast polymerization process was taking place leading to the domination of homogeneous nucleation in this case allowing the formation and uniform distribution of 1-D polythiophene nanostructures on the surface of the conductometric transducer placed as the working electrode.

Another important factor differentiating the two electrolytes is the capability of FeCl_3 to oxypolymerize thiophene monomer according to the following scheme [247]:



To the best knowledge of the author of this dissertation, this is the first time in which FeCl_3 solution was employed as an electrolyte for the electropolymerization of polythiophene. In this novel technique, the oxidizing property of FeCl_3 solution was advantageous in initializing the nucleation into the solution before starting the electropolymerization process. In such manner, the high electropolymerization current peak observed with the other solution was omitted as shown in Figure 6.1. For that purpose, the FeCl_3 solution concentrations adopted in this study were carefully selected to be in such low values (0.6–1.8 mM) that the solution does not have enough oxidizing anions to proceed with the polymerization chemically. Instead, the FeCl_3 solution maintained its clarity of any suspended chemically polymerized particles during the whole period of electropolymerization experiments and the deposition on conductometric transducer could not be commenced before applying the external potential. However at concentrations higher than 1.8 mM, chemical polymerization of thiophene is clearly visible by the formation of polythiophene chains suspended into the solution as shown in Figure 6.4.

From the results discussed so far, the author was able to decide on the type of electrolyte that promotes nanostructures formation during electropolymerization which was FeCl_3 . Also the concentration range of FeCl_3 solution to be considered for further investigation was determined.

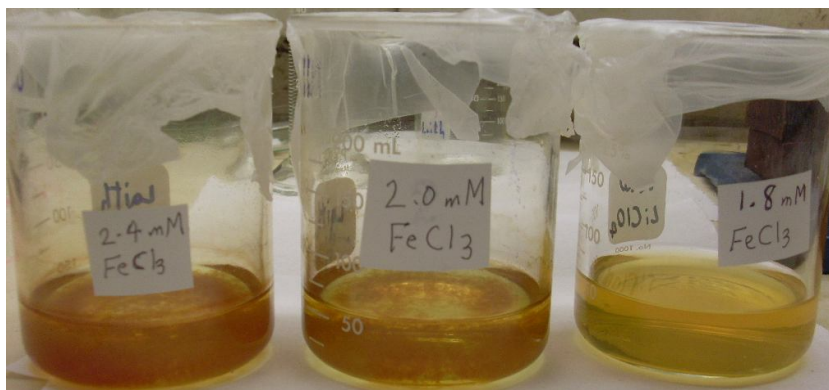


Figure 6.4. The effect of utilizing FeCl₃ concentration higher than 1.8 mM.

Electropolymerization with Different Electrolyte's Concentrations

The FeCl₃ solution concentrations selected for this investigation were 0.6 mM, 0.9 mM, 1.2 mM, 1.5 mM and 1.8 mM. All other deposition parameters were fixed. The electropolymerization currents were measured and plotted in Figure 6.5. SEM images of the deposited polythiophene films are shown in Figure 6.6.

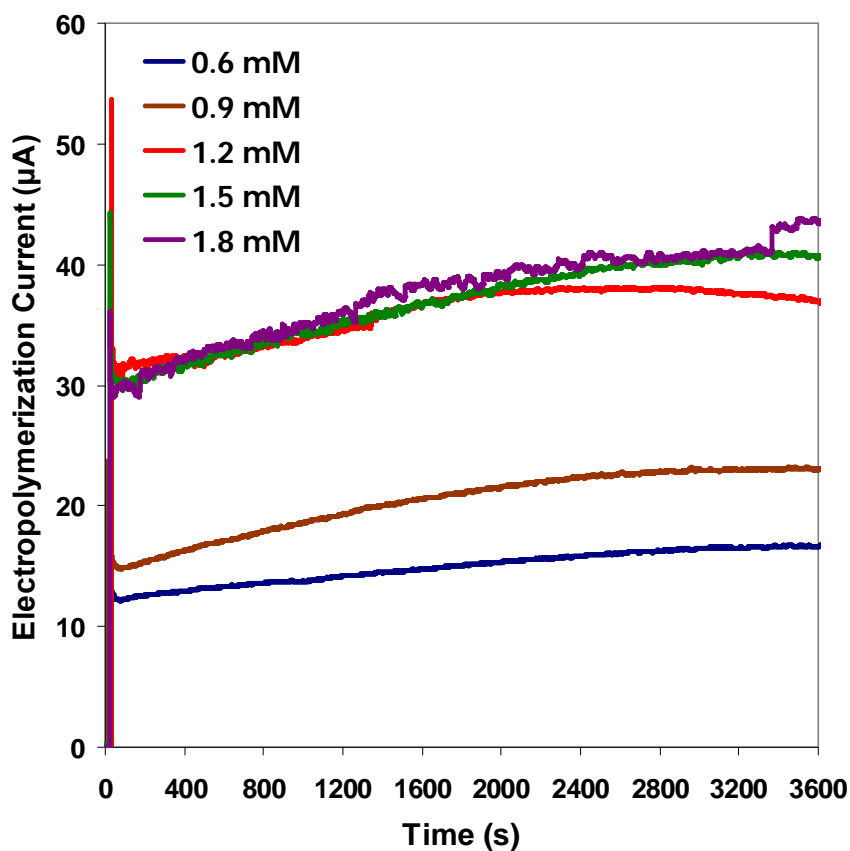


Figure 6.5. Electropolymerization currents during polythiophene deposition with different FeCl₃ solution concentrations.

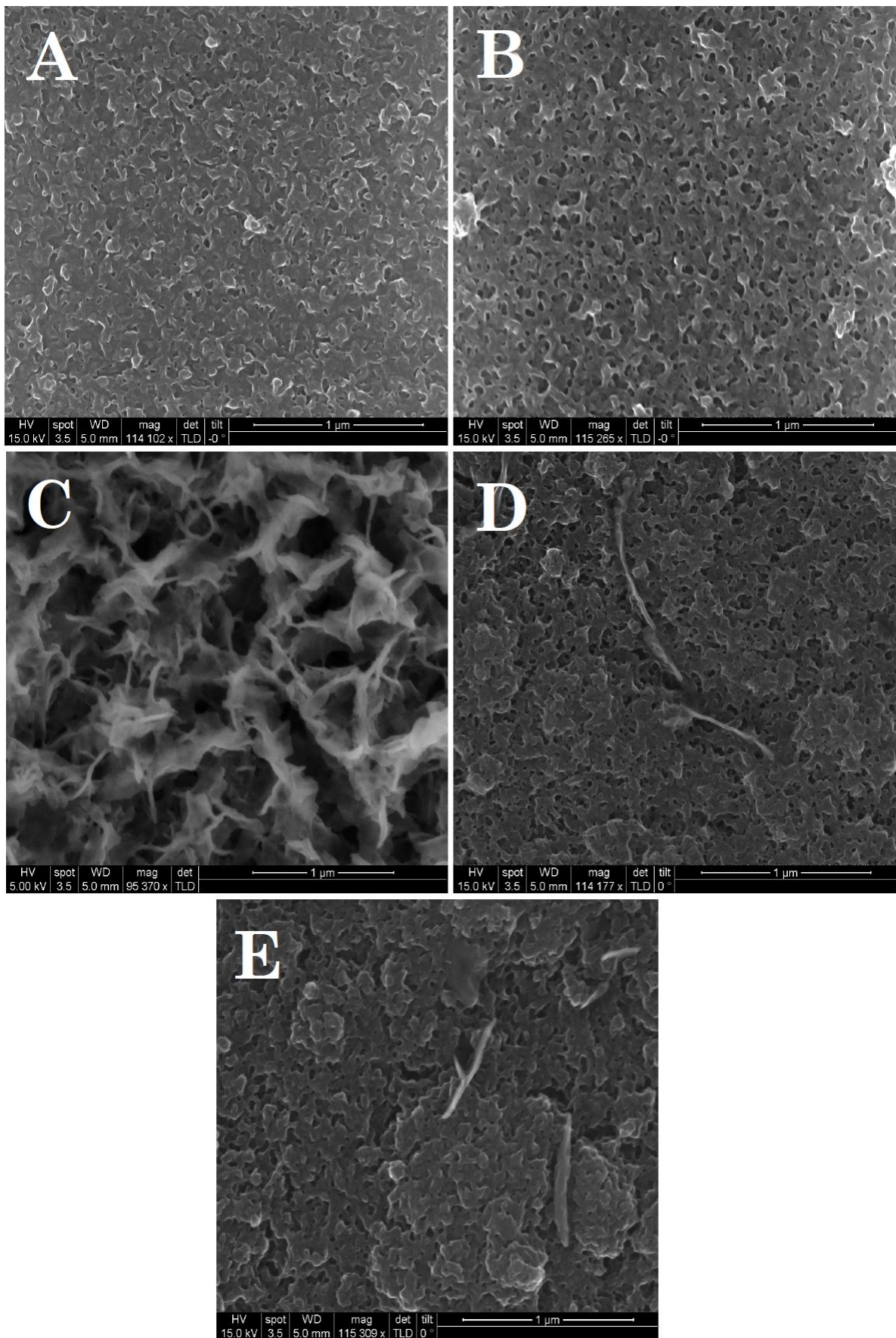


Figure 6.6. SEM images of electropolymerized polythiophene at FeCl_3 solution concentrations of: (A) 0.6 mM, (B) 0.9 mM, (C) 1.2 mM, (D) 1.5 mM, (E) 1.8 mM.

It is evident from the above figures that changing the electrolyte's concentration causes a change in the redox property of the solution that leads to some differences in the deposited polythiophene morphology. At the concentration of 0.6 mM of FeCl_3 solution, the current during electropolymerization was gradually rising to a steady-state value of 16.6 μA . In this case, the deposited film was compact and consisted of irregular shaped particles as shown in Figure 6.6 (A). By employing 0.9 mM of FeCl_3 solution, the electropolymerization current reached a steady-state value of 23 μA . The deposited film was porous as demonstrated in Figure 6.6 (B) and featured the evolution of short nanofibers ~ 80 nm in length and ~ 32 nm in diameter. At higher concentration of FeCl_3 solution (1.2 mM), the deposited polythiophene film consisted of nanofibers with diameters in the range of 26–40 nm and ~ 230 nm in length as exhibited in Figure 6.6 (C). In this case, the current reached a steady-state value of 37 μA . It is clear from Figure 6.5, that a further increase in the electrolyte's concentration did not provide significant increase in the electropolymerization current with the recorded maximum current values were 40 μA and 43 μA for the concentrations of 1.5 mM and 1.8 mM respectively. This observation is an indication of the dominance of the oxidative polymerization over the electropolymerization at FeCl_3 concentrations higher than 1.2 mM. Since the oxidative polymerization is not governed by charge transport between the electrodes inside the electrochemical cell, monomer units are consumed in a faster rate than that during the electrochemical polymerization. Therefore the overgrowth of polymer chains in these cases reduces the porosity of the deposited polythiophene film, which is clear from Figure 6.6 (D) and (E). It is also evident from these figures that this three dimensional growth increases by increasing the FeCl_3 solution concentration with more dense structures deposited by using 1.8 mM than that of 1.5 mM. Despite the agglomeration of the polythiophene deposited with the 1.8 mM FeCl_3 electrolyte, the presence of scattered nanofibers (~ 10 nm in diameter and ~ 258 nm in length) was evident as demonstrated in the high magnification SEM image shown in Figure 6.7.

By comparing the polythiophene films' structures shown in Figure 6.6, it can be established that the film with the largest surface-to-volume ratio was obtained utilizing 1.2 mM FeCl_3 electrolyte. At this concentration a balance between the chemical and electrochemical polymerization has been achieved. Also it is worthy to mention here that the nanostructured polythiophene synthesized by this method has larger surface-to-volume ratio than those synthesized in recent reports through electropolymerization of thiophene monomer in acetonitrile solution containing tetrabutylammonium hexafluorophosphate (TBAPF_6) [248], or via the chemical oxidative polymerization of thiophene in an aqueous FeCl_3 solution [249]. Gas sensitive films with high surface-to-

volume ratios are crucial for optimum performance of gas sensors as discussed earlier in Chapter 2.

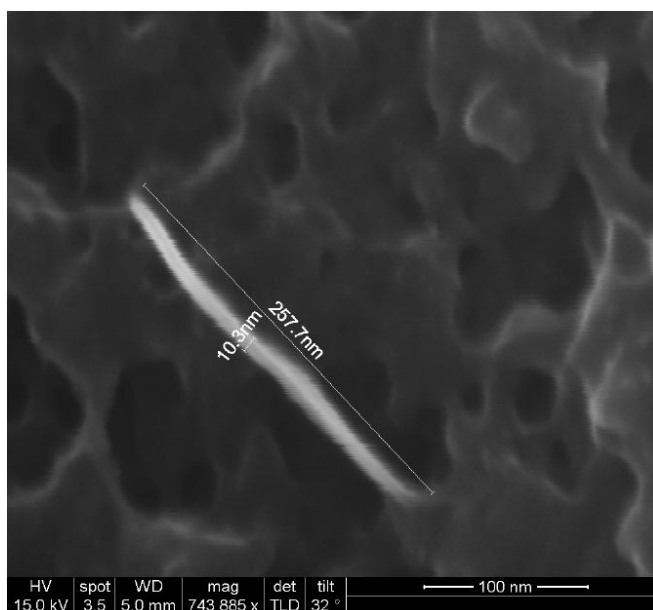


Figure 6.7. SEM image of polythiophene nanofiber segment obtained through electropolymerization with 1.8 mM FeCl₃ electrolyte.

Optical spectroscopy (UV-vis) has been also implemented to characterize the synthesized nanostructured polythiophene films. For that purpose, polythiophene electrodeposition with the aforementioned FeCl₃ concentrations was conducted for 20 minutes each time on optically transparent fluorine doped tin oxide (FTO) glass cuts. The UV-vis spectra for the nanostructured polythiophene films deposited utilizing the FeCl₃ concentrations of 0.6–1.8 mM are shown in Figure 6.8. At 0.6 mM of FeCl₃, oxidation of monomer units occurred at a slow rate leading to the deposition of almost transparent polythiophene thin film on the FTO glass. Hence the absorbance of that polythiophene thin film was minimal as shown in Figure 6.8. By the increase in the concentration of FeCl₃ solution, the rate of polymerization also increases leading to the deposition of more dense and therefore darker thin films than that deposited with the concentration of 0.6 mM. This observation is supported by the UV-vis spectra in Figure 6.8 with the evident rise in the absorbance by the increase of the FeCl₃ concentration utilized for depositing polythiophene nanostructured films.

From Figure 6.8, it can be seen that the spectra contain a broad absorption band at ~300–570 nm, which can be attributed to the characteristic $\pi - \pi^*$ electronic transition for the conjugated polythiophene molecules [249]. For the nanostructured polythiophene film deposited by utilizing 0.9 mM of FeCl₃, another absorption band is evident in Figure 6.8 at a wavelength ~700 nm indicating that the deposited polymer was in a partially

oxidized (doped) state [250]. By increasing the concentration of FeCl_3 , this adsorption band starts to diminish gradually as the deposited polythiophene nanostructured films become more doped until it disappears at the polythiophene film deposited with the concentration of 1.8 mM of FeCl_3 .

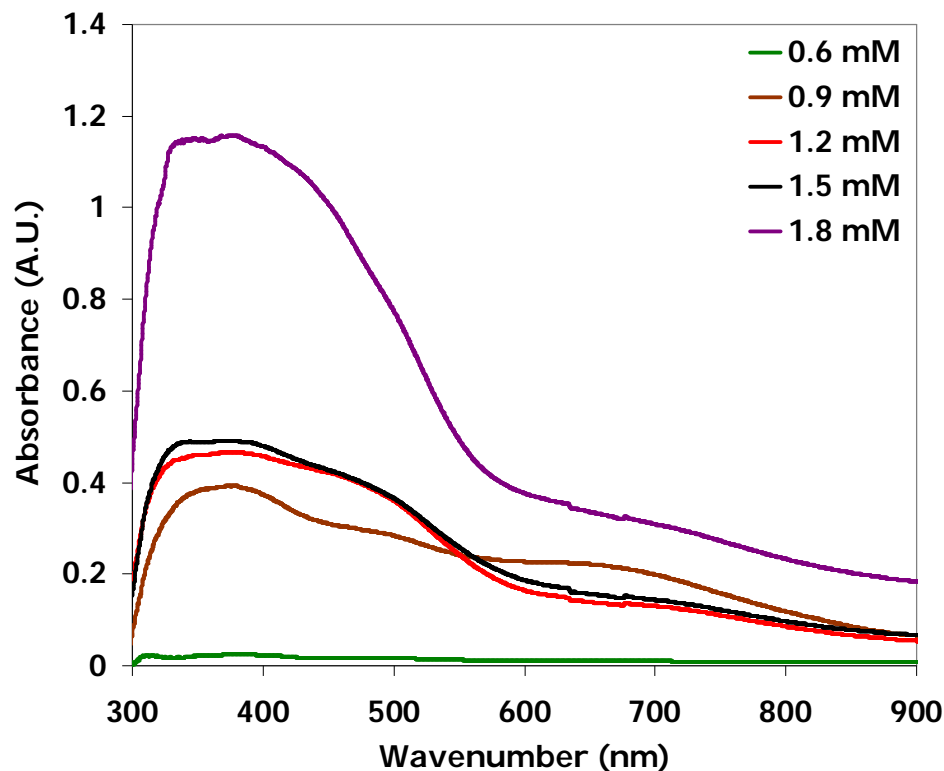


Figure 6.8. UV-vis spectra of polythiophene nanostructured films deposited with different electrolyte's concentrations.

The band gap energy (E_g) for conjugated polymers can be determined from lowest excitation energy, which can be extracted from the onset value at the lower energy edge for the $\pi - \pi^*$ adsorption band [251-253]. In this work, the E_g value for the deposited polythiophene films was obtained from the $\pi - \pi^*$ adsorption edge at ~ 583.43 nm for the spectra of Figure 6.8 and found to be 2.13 eV. This E_g value is characteristic to polythiophene according to Table 2.1 as well as other reports in literature such as the work of Alakhras et al., where they reported an E_g of 2.10 eV for the electropolymerized bulk polythiophene [253].

Through careful consideration of the characterization results for the effect of changing the electrolyte's concentration in the past discussions, the author of this dissertation chose the FeCl_3 concentration of 1.2 mM for further investigations. At this particular concentration the deposited film consisted mainly of 1-D nanostructures with high surface-to-volume ratio according to the SEM results. Also at this concentration, the

synthesized polythiophene nanostructured film exhibited a semiconducting property according to the UV-vis results due to the presence of an adsorption band at ~700 nm. This particular feature is favorable in the field of gas sensing since a semiconducting material can easily change its conductivity during the interaction with target gases that either donate or withdraw electrons from the gas sensitive layer.

Electropolymerization with Different Applied Potentials

To analyze the effect of the deposition voltage on the resultant polythiophene films' structure, five electropolymerization experiments were conducted by choosing a different deposition voltage each time. Hence polythiophene synthesis was carried out utilizing either 0.65 V, 0.7 V, 0.75 V, 0.8 V, or 0.85 V. Other deposition parameters such as monomer concentration, electrolyte concentration and deposition time were the same for these experiments. A similar approach to the previous study was adopted in this investigation. The electropolymerization currents were recorded as shown in Figure 6.9 and the deposited films' morphologies were studied by analyzing the corresponding SEM images which are exhibited in Figure 6.10.

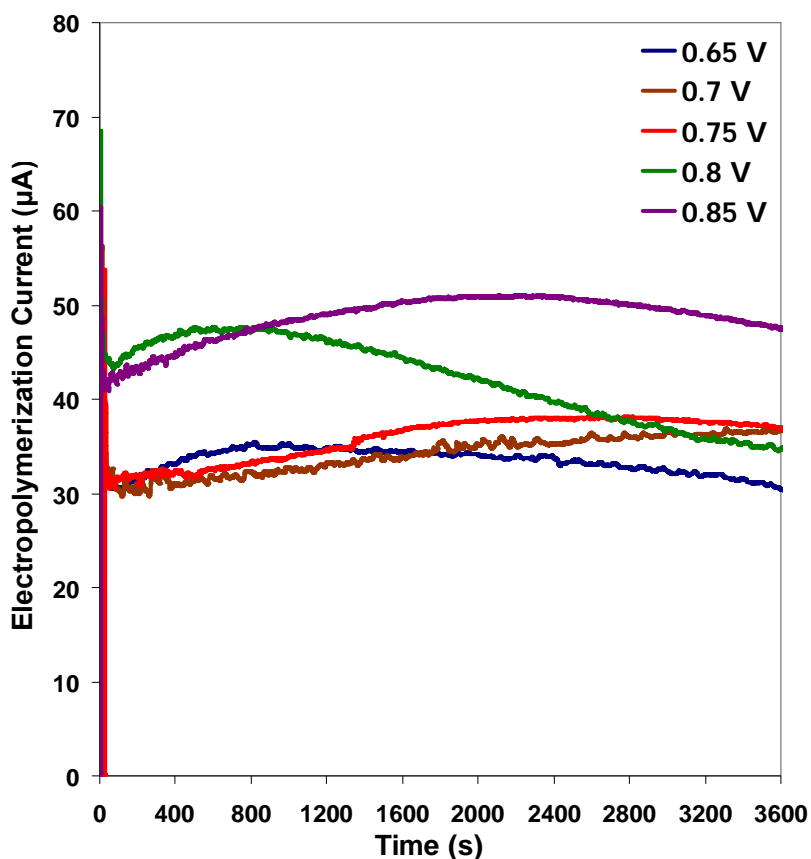


Figure 6.9. Electropolymerization currents recorded during polythiophene deposition with different deposition potentials.

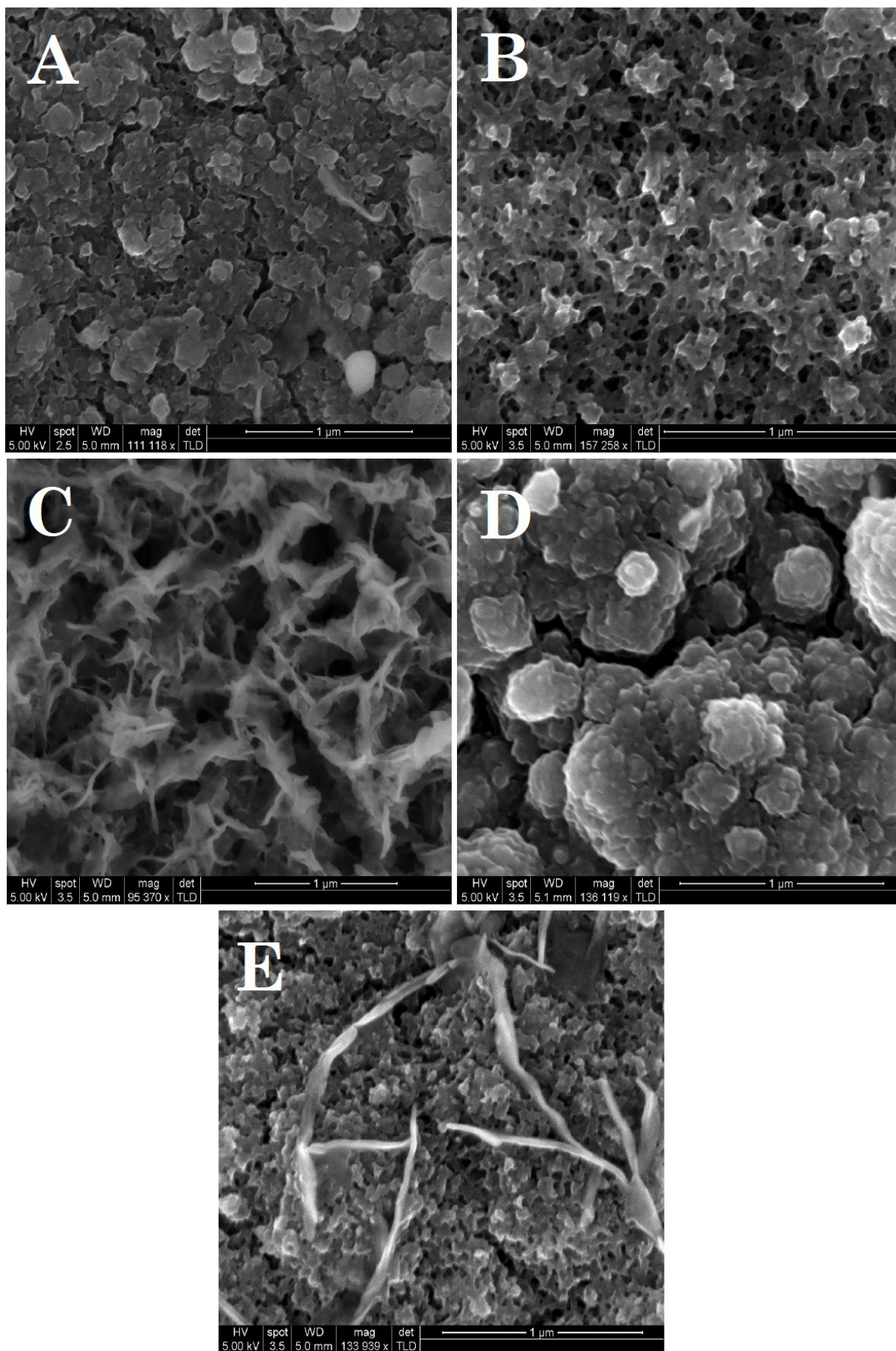


Figure 6.10. SEM images of electropolymerized polythiophene at deposition potentials of: (A) 0.65 V, (B) 0.7 V, (C) 0.75 V, (D) 0.8 V, (E) 0.85 V.

From a close inspection of the above figures, it can be seen that the choice of the deposition potential affects the morphology of the deposited polythiophene film. In analogy to the findings of the previous study on the effect of the electrolyte's concentration, the morphological changes can be analyzed with respect to the recorded currents during electropolymerization. At the deposition voltage of 0.65 V, the current was gradually rising from an initial value of $\sim 30 \mu\text{A}$ to the value of $35.4 \mu\text{A}$ after ~ 13 minutes of electropolymerization. Then the current started to drop continuously until it became $30.5 \mu\text{A}$ at the end of the selected deposition time of 60 minutes. Similar trend of the current curve was observed at the deposition voltage of 0.8 V. The current peaked at $47.6 \mu\text{A}$ from an initial value of $44 \mu\text{A}$ after ~ 8 minutes of electropolymerization and then gradually decreased to the value of $34.7 \mu\text{A}$ after 60 minutes of deposition. In both cases, the deposited films' structures consisted of accumulated spherical submicron sized polythiophene particles as shown in Figure 6.10 (A) and (D). This 3-D growth of the polymer chains is probably attributed to the limited number of nucleation sites formed during the period of high current and when the current drops the growth continues from these sites in all directions to produce stacked spherical shapes. Whereas for the deposition voltages of 0.7 V and 0.75 V, the currents were continuously rising during the electropolymerization period of 60 minutes from $\sim 31.5 \mu\text{A}$ to $\sim 37 \mu\text{A}$. However it is evident from Figure 6.9 that the current curve at the deposition voltage of 0.7 V was much noisier than that of the 0.75 V. This observation suggests that the solution's electrochemical property is affected by the marginal change in the deposition voltage. At these voltages, the resultant films had a nanofibrillar morphology as shown in Figure 6.10 (B) and (C). By selecting the value of 0.85 V as the deposition voltage, the current peaked at $\sim 51 \mu\text{A}$ before dropping to $\sim 47.6 \mu\text{A}$ at the end of 60 minutes of deposition. In this case, a mixture of the granular structures and nanofibers were deposited. The nanofibers were $\sim 40 \text{ nm}$ in diameter and $\sim 1 \mu\text{m}$ in length as shown in Figure 6.10 (E). Therefore, it can be concluded from Figure 6.10 that the polythiophene film with the highest surface-to-volume ratio was obtained through applying 0.75 V as the deposition potential.

The influence of different electropolymerization potentials on the resultant polythiophene films was also investigated through UV-vis spectroscopy as shown in Figure 6.11. The absorption band at $\sim 300\text{--}480 \text{ nm}$ can be attributed to the $\pi - \pi^*$ electronic transition. The presence of the adsorption band $\sim 700 \text{ nm}$ in these spectra confirms the semiconducting property (partially oxidized state) of the deposited polythiophene films since the FeCl_3 solution concentration was fixed at 1.2 mM in these experiments. Also it is evident from the spectra of Figure 6.11 that the optical

absorbance increases with the rise in the applied electropolymerization potential. Therefore the darkness of the deposited polythiophene film on the FTO glass increases by the increase of the deposition potential because of the rise in the corresponding polymerization rate.

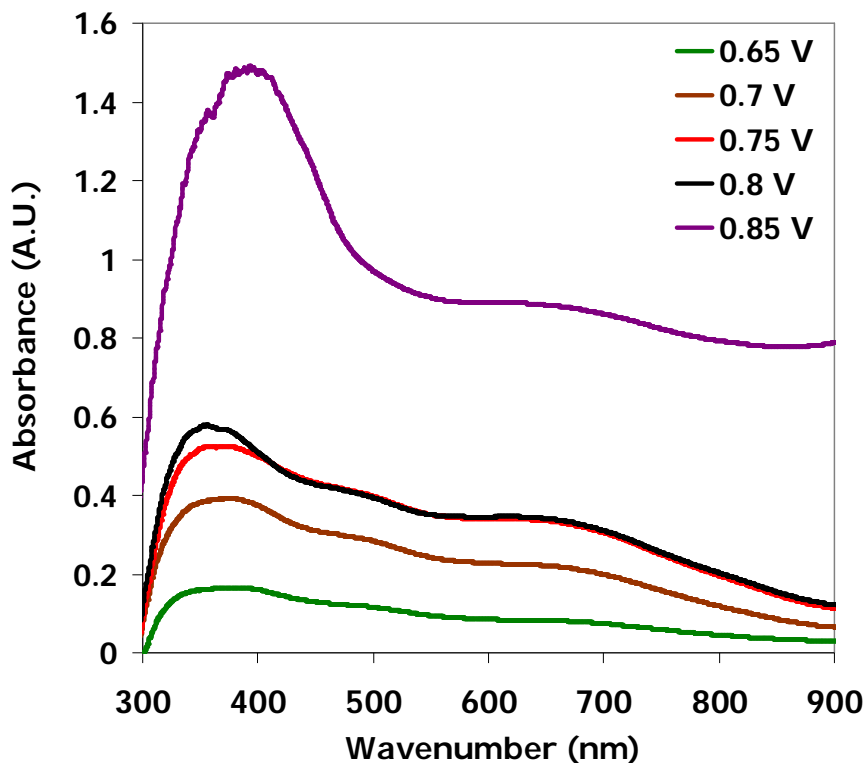


Figure 6.11. UV-vis spectra of polythiophene nanostructured films electropolymerized with different applied potentials.

The Effect of Electropolymerization Time

In the synthesis of the nanostructured polythiophene films discussed so far, the deposition time was fixed at 60 minutes in every electropolymerization experiment. After finding the optimum concentration of the FeCl_3 solution and the best deposition voltage, it was interesting to investigate if there is any effect of the deposition time on the synthesized polythiophene morphology. For that purpose, electropolymerization of polythiophene was conducted for 20 minutes utilizing the concentration of 1.2 mM for the FeCl_3 solution and the deposition voltage of 0.75 V. SEM images of the deposited nanostructured polythiophene film are shown in Figure 6.12. It is evident that a seeding layer in the form of a compact thin film was initially deposited at the beginning of the electropolymerization. As the process continues, nanofibers start to evolve from nuclei in the deposited thin film. These segments of nanofibers are scattered along the polythiophene film as shown in Figure 6.12 (A). The diameters of the synthesized

nanofibers were ~19–26 nm and they were ~200–900 nm in length. The magnified SEM image in Figure 6.12 (B) is showing a couple of these polythiophene nanofibers. At longer deposition time such as 60 minutes, more dense nanofibers were formed that tend to merge with each other as shown earlier in this study in Figure 6.2 (B).

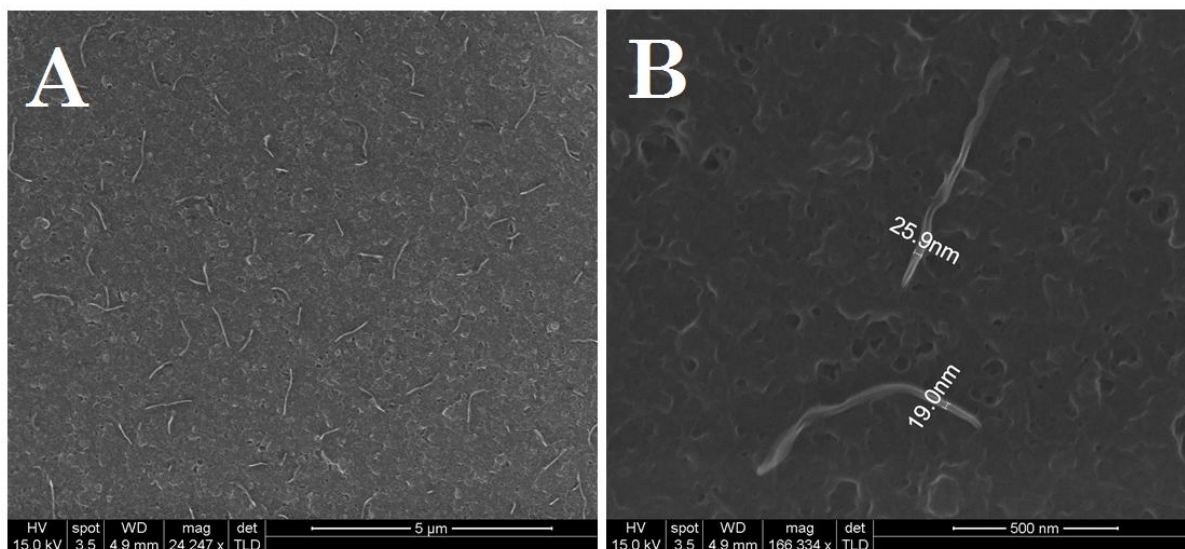


Figure 6.12. SEM images for the nanostructured polythiophene film electropolymerized with 1.2 mM FeCl₃ solution, 0.75 V of applied potential and 20 minutes of deposition time, (A) low magnification, (B) high magnification.

Elemental composition of the synthesized polythiophene nanostructures has been investigated by XPS as shown in Figure 6.13. It proves that the developed polythiophene has an identical conformation to that reported in literature [229, 248]. The atomic percentage of each element in the developed polythiophene macromolecules is listed in Table 6.1.

Table 6.1. Elemental composition of the nanostructured polythiophene.

Element	Binding Energy (eV)	Atomic (%)
C	284.6	71.08
S	164 – 165	22.91
Cl	198.4 – 200.2	4.60
O	532	1.29
Fe	711.6	0.12

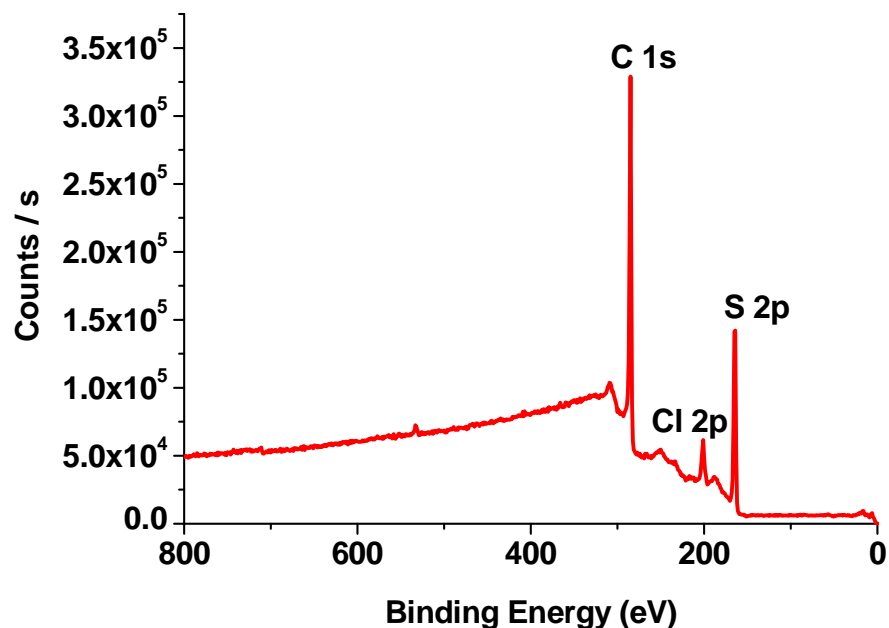


Figure 6.13. XPS spectrum of the synthesized nanostructured polythiophene.

Similar to other conjugated polymers, a sharp and intense peak for the C(1s) component can be observed from Figure 6.13 at a binding energy (BE) of 284.64 eV. Since this peak is characteristic to the XPS of all conductive polymers, further analysis of the C(1s) XPS core level deconvolution will be provided in the upcoming sections. The high resolution S(2p) core level spectrum is shown in Figure 6.14 and it consists of two spin-orbit splitting doublets, $S(2p_{3/2})$ and $S(2p_{1/2})$, at BE of ~164 eV and 165 eV respectively.

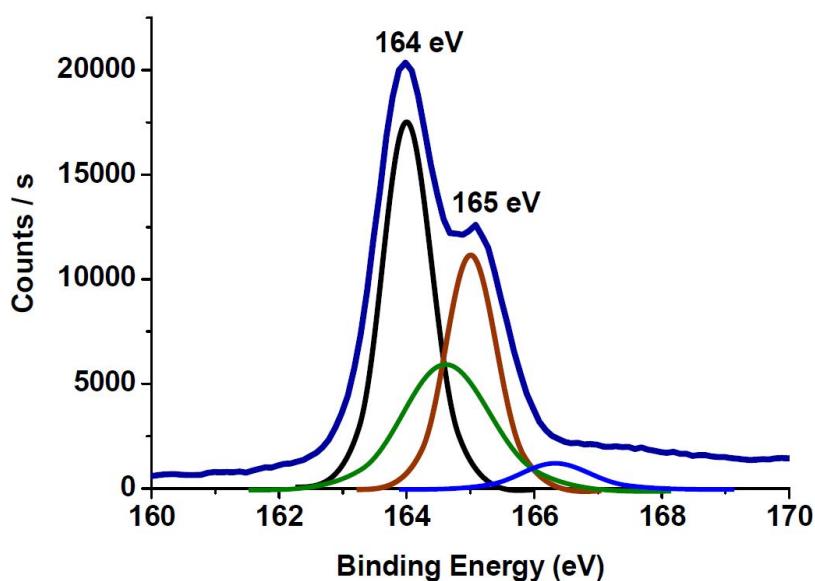


Figure 6.14. S(2p) core level deconvolution for polythiophene.

The presence of these doublets is typical to FeCl_3 -doped heterocyclic polymers with sulfur hetero atom [254-256]. The positive shift of (+1 eV) between these components is attributable to electrons extraction from some thiophene rings and hence localization of positive charges on these rings that may result in a positive polarization or partial charging of sulfur atoms [254].

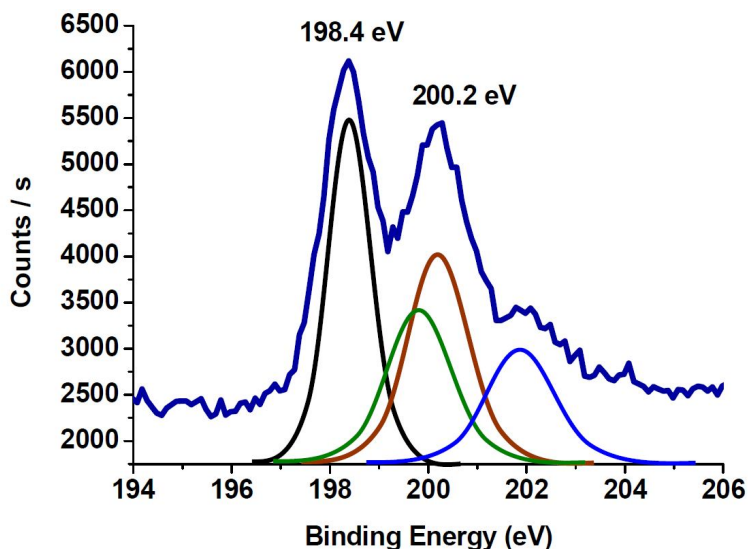


Figure 6.15. Cl(2p) core level deconvolution for electropolymerized nanostructured polythiophene.

Deconvolution of the high resolution Cl(2p) spectrum is shown in Figure 6.15 and it proves the involvement of two chloride species in the doping of polythiophene. The peak at BE of 198.4 eV can be attributed to the incorporation of FeCl_4^- anions [256]. This suggestion is supported by the presence of iron atoms according to the elemental composition data provided in Table 6.1. Due to the small iron's atomic portion of only 0.12%, no peak is visible for the $\text{Fe}(2p_{3/2})$ component at BE of 711.6 eV in the XPS survey spectrum shown in Figure 6.13. The other peak of the Cl(2p) core level spectrum at the BE of 200.2 eV is attributed to the chlorination of the polythiophene backbone through the covalent bonding with chlorine atoms ($\text{C}-\text{Cl}$) [255].

Despite the use of anhydrous acetonitrile as the organic solvent and the extra care taken to prevent moisture interference during electropolymerization, the effect of moisture is evident from the presence of some oxygen atoms with an atomic percentage of 1.29% according to Table 6.1. This can be attributed to the formation of carbonyl and hydroxyl groups on the polythiophene's backbone [247].

From all the abovementioned XPS results, it can be concluded that the chemical composition of the synthesized nanostructured polythiophene matches those in earlier

reports [229, 247, 248, 254, 256]. All the nanostructured polythiophene films developed herein were investigated for their hydrogen gas sensing performances and the results from these investigations will be discussed in Chapter 7.

6.2.2 Chemically Synthesized Polythiophene Nanofibers

The morphology of the polythiophene nanofibers obtained through chemical polymerization was investigated by the author of this thesis utilizing FEI Nova NanoSEM. Figure 6.16 shows an SEM image of the polythiophene nanofibers. It can be seen that the nanofibers' diameters were in the range of 60–110 nm with lengths in the order of several microns.

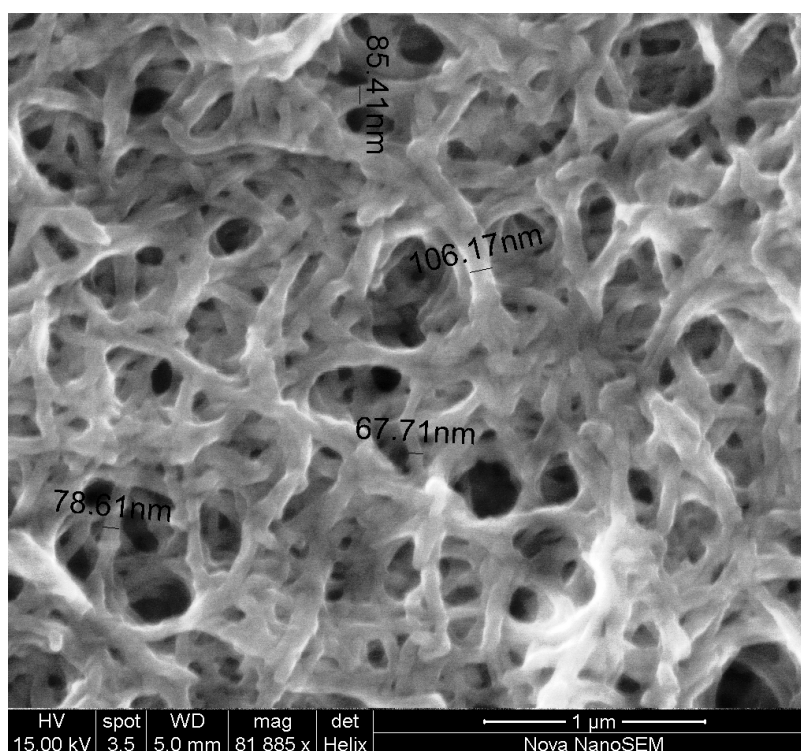


Figure 6.16. SEM image of the chemically synthesized polythiophene nanofibers.

Chemical analysis of polythiophene nanofibers was performed through FT-IR spectroscopy. The FT-IR spectrum of polythiophene nanofibers was collected in University of California, Los Angeles/USA with a JASCO FT/IR-420 spectrometer using a pressed potassium bromide (KBr) pellet for sample preparation. The FT-IR spectrum of polythiophene nanofibers is provided in Figure 6.17. It can be seen that the dominant thiophene ring vibrational modes were evident from the peaks at around 688, 780 and 1000 cm^{-1} which are in agreement with previously published results [257]. There was a

low intensity peak present at around 3100 cm^{-1} which can be attributed to the C–H stretching vibrations [229]. The rest of the peaks can be assigned to some low molecular weight oligomers in the polymer solution. The FT-IR spectrum of the developed nanofibers exhibits the molecular fingerprint of polythiophene and is comparable to that of the bulk material.

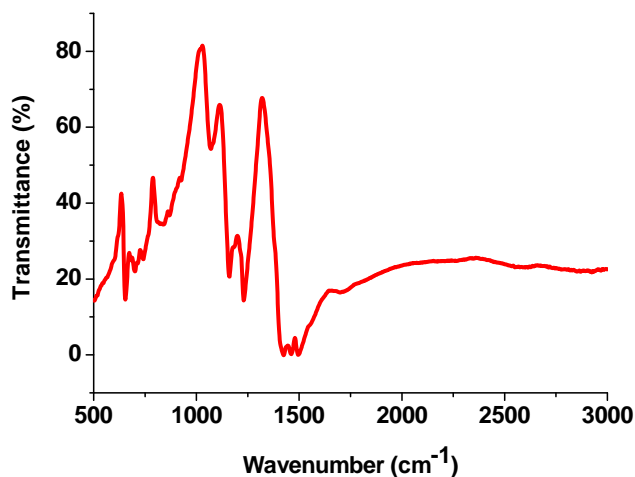


Figure 6.17. FT-IR spectrum of chemically synthesized polythiophene nanofibers.

6.3 Characterization Results of Polypyrrole Nanostructures

In this dissertation, polypyrrole (PPY) nanostructures were synthesized utilizing template-free techniques and investigated for their hydrogen gas sensing performances. Both of the electropolymerized and chemically synthesized PPY nanostructures were characterized to determine their morphologies and their chemical properties. The following subsections will provide a detailed discussion of these results.

6.3.1 Electropolymerized Polypyrrole Nanowires

As a result of a collaborative work between RMIT University in Melbourne/Australia and Pierre and Marie Curie University in Paris/France, three gas sensors based on electropolymerized PPY nanowires were developed and compared. The author of this thesis has published these results in an article in the *Journal of Physical Chemistry C* [258]. In every deposition of PPY nanowires, a conductometric transducer was utilized as the working electrode in a three-electrode electrochemical cell. All the electropolymerization parameters were identical except the anodic charge. The sensitive films of sensors A, B and C were deposited with an anodic charge of 13, 55 and 90 mC respectively.

Utilizing the FEI Nova NanoSEM at RMIT University, the author of this thesis investigated the deposited PPY nanowires on the surfaces of the conductometric transducers as shown in Figure 6.18 [258]. The nanowires diameters were in the range of 40–90 nm and lengths in the order of several tens of micrometers.

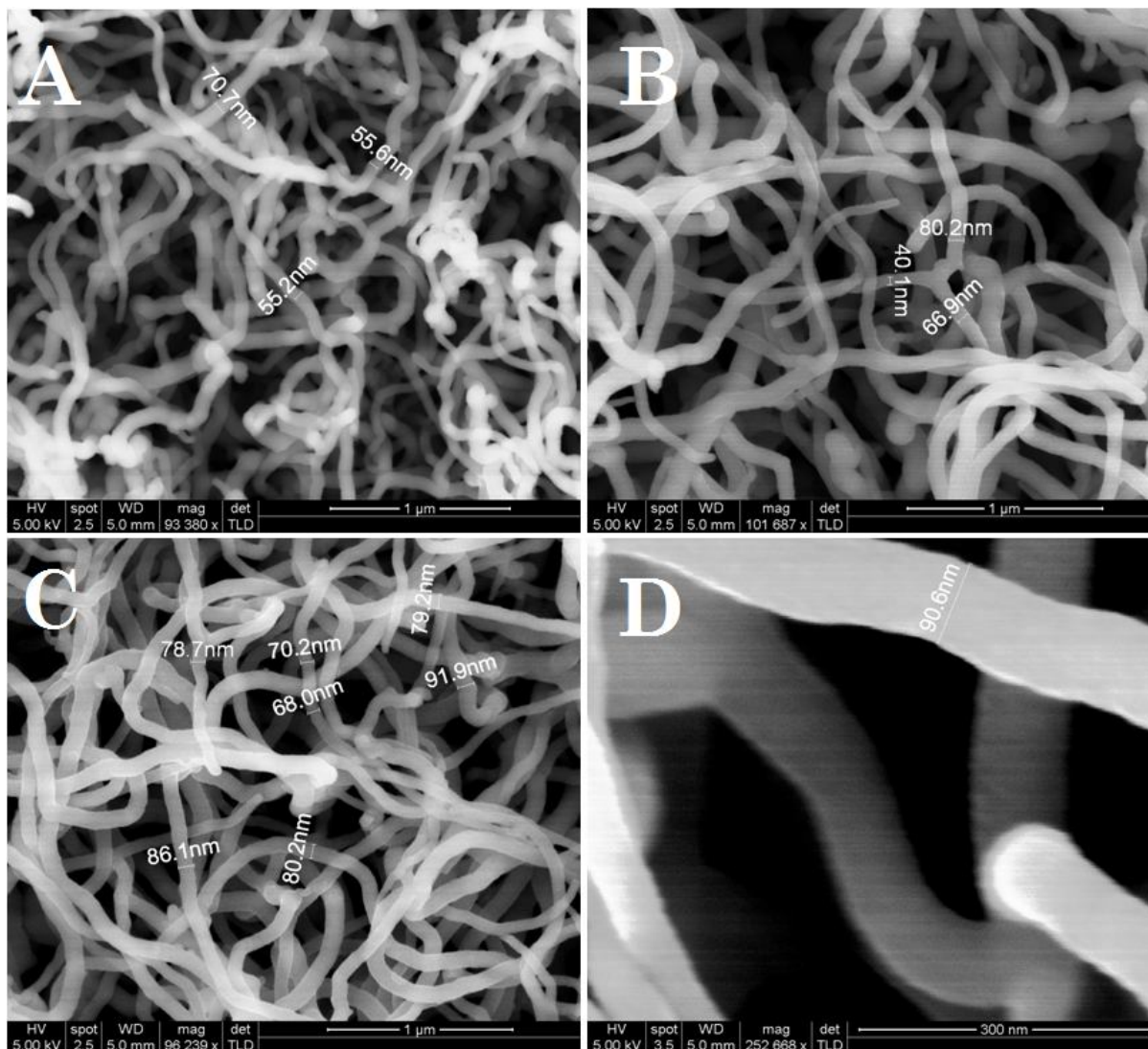


Figure 6.18. High magnification SEM images of PPY sensitive films for: (A) Sensor A (13 mC), (B) Sensor B (55 mC), (C) Sensor C (90 mC) and (D) Magnified SEM image of the PPY nanowires on Sensor C.

Despite the similarity between the morphologies of the three sensitive films, it is evident from Figure 6.18 (A) that the sensitive film of sensor A consisted of a mixture of short and long PPY nanowires merging with each other in some places to form irregular shaped lumps. The difference can be analyzed by referring to the electropolymerization mechanism. The process consists of consecutive steps starting from the monomer

oxidation followed by the radical-radical coupling, deprotonation and finally the chain propagation through further oxidation [59]. The rate of polymerization has a significant impact on the structure of the conducting polymer film precipitated on the anode surface [59]. It is anticipated that an increase in anodic charge would produce a rise in the rate of polymerization. Increasing the rate of polymerization promoted the formation of one-dimensional structures of conducting polymers in template-free synthesis as discussed in Chapter 2 [68]. At high polymerization rate, the homogeneous nucleation is dominant over the heterogeneous nucleation and therefore suppressing the secondary growth of polymer chains [259]. By prohibiting the secondary growth, the polymer chains can only grow to form one-dimensional nanostructures. Whereas at low polymerization rate, the heterogeneous nucleation is the dominant phase and merely three-dimensional structures are formed [89]. The minimal structural difference between the sensitive films of the developed novel gas sensors can also be interpreted in terms of the nucleation phase. For the sensitive film of sensor A, the polymerization was slow due to the low anodic charge of (13 mC). This condition allowed for some secondary growth through heterogeneous nucleation leading to the formation of three-dimensional irregular shaped lumps throughout the deposited film. While for the sensitive films of sensors B and C, homogeneous nucleation was dominant which prevented the formation of irregular shaped structures due to the elimination of secondary growth of polypyrrole chains.

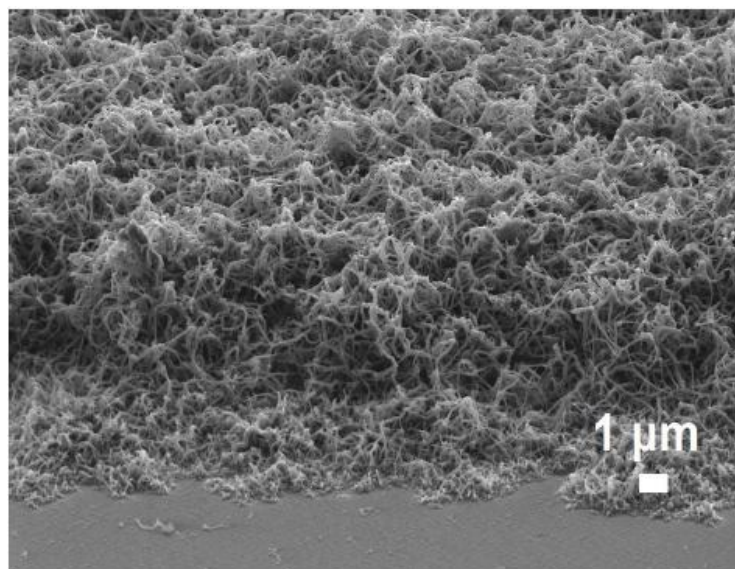


Figure 6.19. An SEM image showing a 65° tilted view for the deposited PPY nanowires on a conductometric transducer.

The nanowires grow vertically from the PPY zones which were protected from the hydroxyl radicals by the O₂ nano-bubbles that prevented over-oxidization [85]. Figure 6.19 shows the growth of PPY nanowires on a gold finger of the conductometric IDT.

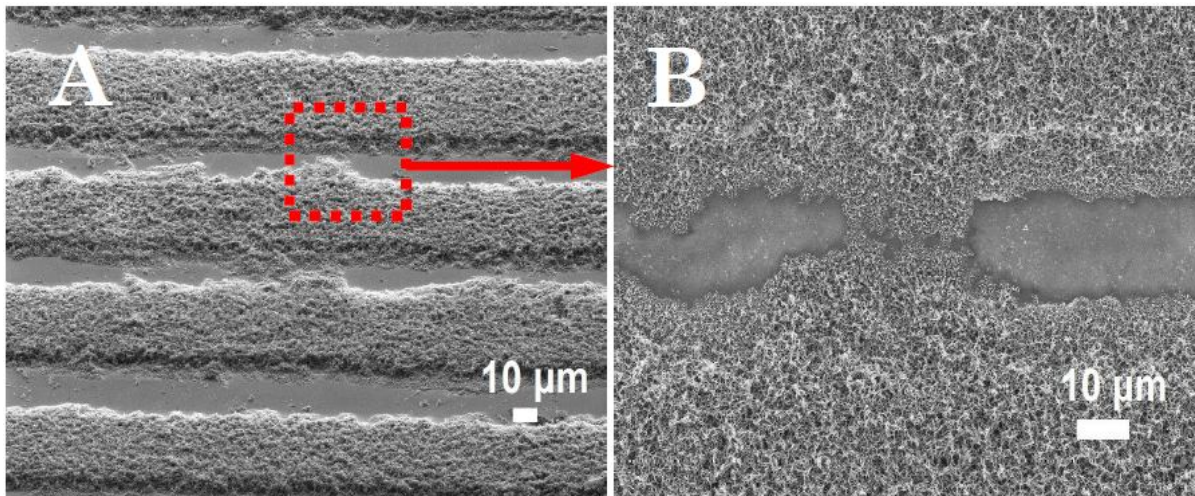


Figure 6.20. SEM images showing the formation of PPY nanowires bridges between the gold fingers of conductometric IDT.

After packing of the gold IDT with nanowires due to the vertical growth, PPY nanowires started to grow horizontally. This type of growth allows nanowires initiated from neighbouring gold fingers to intersect with each other forming a bridge over the insulating gap between the gold fingers, which is the quartz substrate for these sensors as shown in Figure 6.20 (A) and (B). Obviously, without the formation of these bridges of PPY nanowires, the sensor's resistance value would remain infinite. The SEM images in Figure 6.19 and Figure 6.20 were acquired utilizing Ultra55 Zeiss field emission scanning electron microscope at the Pierre and Marie Curie University in Paris.

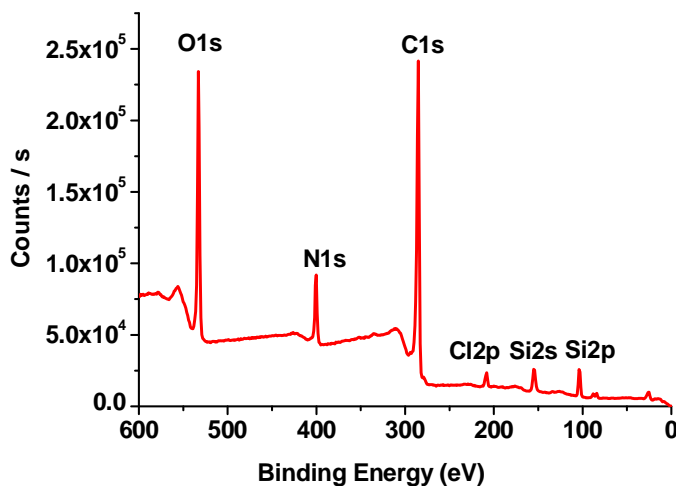


Figure 6.21. XPS spectrum of electropolymerized PPY nanowires.

The PPY nanowires' chemical composition was investigated by the author of this dissertation utilizing XPS spectroscopy at RMIT university. The experimental setup was identical to that outlined in section 6.2.1. The presence of the incorporated perchlorate anion into the PPY matrix is evident from the Cl 2p peak at binding energy of 208 eV [260]. The presence of Si 2s and Si 2p peaks in Figure 6.21 can be attributed to the striking the SiO₂ substrate with scattered X-ray beams.

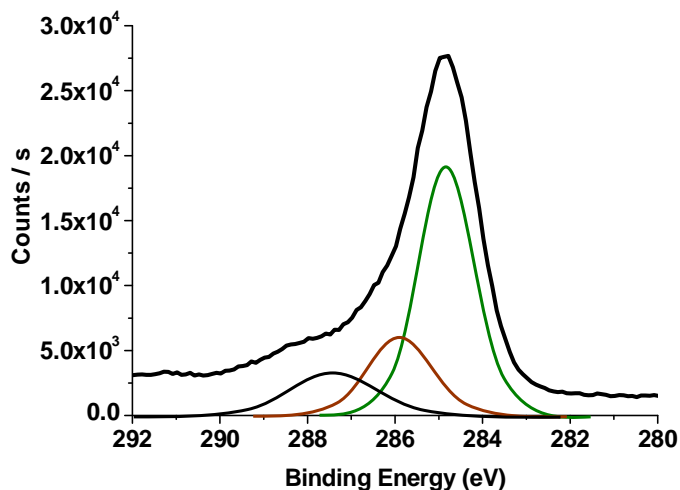


Figure 6.22. Deconvolution of C(1s) core level for electropolymerized PPY.

Deconvolution of C1s spectrum shown in Figure 6.22 consists of three component peaks. The main peak at binding energy of 284.8 eV is assigned to the aromatic C, the peak at 286.3 eV is assigned to C–N, and the peak at 288 eV is assigned to C=O [86, 260].

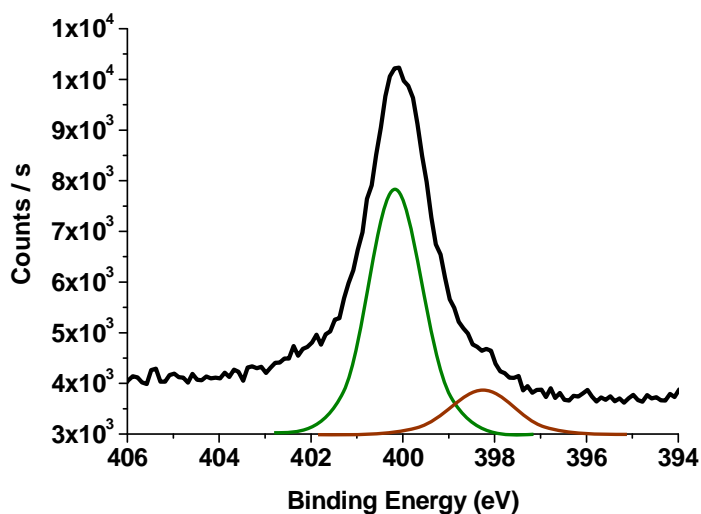


Figure 6.23. N(1s) core level deconvolution of electropolymerized PPY.

The N 1s spectrum shown in Figure 6.23 is deconvoluted into two peaks. A large peak is centred at binding energy ~400 eV and a smaller peak at a binding energy ~398 eV can be assigned to the neutral N atom and the imine nitrogen (=N-) respectively [132]. The O 1s spectrum shown in Figure 6.24 can be deconvoluted into a peak centred at binding energy ~533 eV that is assigned to perchlorate anion and a peak at a binding energy ~532 eV which is attributed to C=O [132].

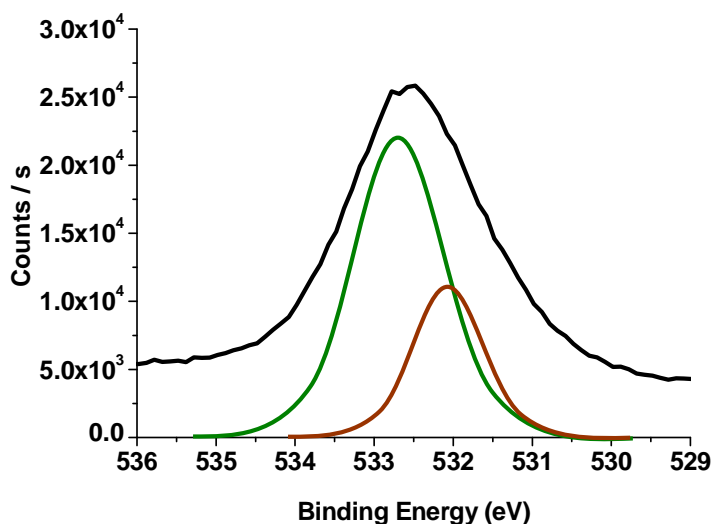


Figure 6.24. Deconvolution of O(1s) core level for electropolymerized PPY.

From the above discussion, it can be observed that the chemical composition of the deposited PPY nanowires is comparable to that of chemically and electrochemically synthesized PPY films reported in earlier studies [132, 260, 261].

6.3.2 Chemically Synthesized Polypyrrole Nanofibers

In this dissertation, novel conductometric and layered SAW gas sensors based on chemically polymerized PPY nanofibers were developed and reported by the author in journal articles [136, 137]. This work was conducted in a collaborative project between RMIT University in Melbourne, Australia and University of California in Los Angeles, USA. Characterization of PPY nanofibers was performed in the laboratories of University of California.

The morphology of PPY nanofibers was analyzed with a JEOL JSM-6700F field emission scanning electron microscope by drop casting a ~2 g/L dispersion of PPY nanofibers solution onto a silicon wafer and allowing it to dry in a clean room environment. Transmission electron microscopy (TEM) (JEOL 100CX) was also used to characterize the PPY nanofibers. The SEM and TEM images shown in Figure 6.25 suggests that a

mat of PPY nanofibers has been synthesized and deposited. The PPY nanofibers had an average diameter of 18 nm. The lengths of individual nanofibers were on the order of several microns.

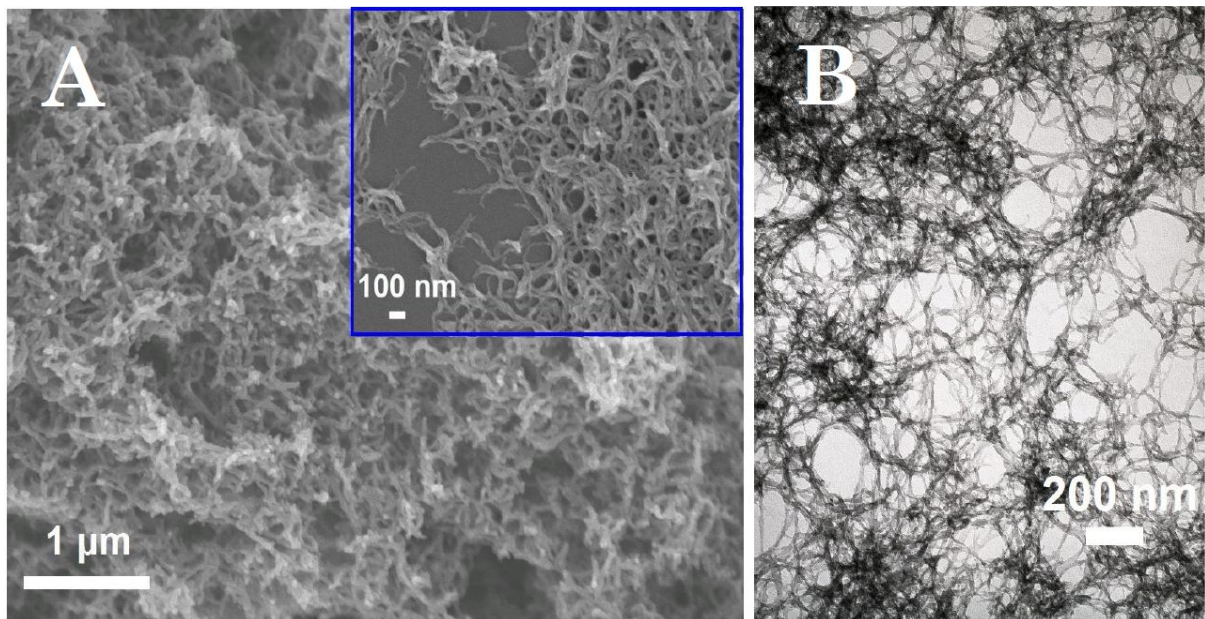


Figure 6.25. (A) SEM images of PPY nanofibers with high magnification image in the inset, (B) TEM image of PPY nanofibers.

Fourier transform infrared spectroscopy (FT-IR) was used to analyze dispersions of the solution containing PPY nanofibers. FT-IR spectra were obtained with a JASCO FT/IR-420 using pressed potassium bromide (KBr) pellets. The spectrum shown in Figure 6.26 reveals the characteristic bands of PPY nanofibers.

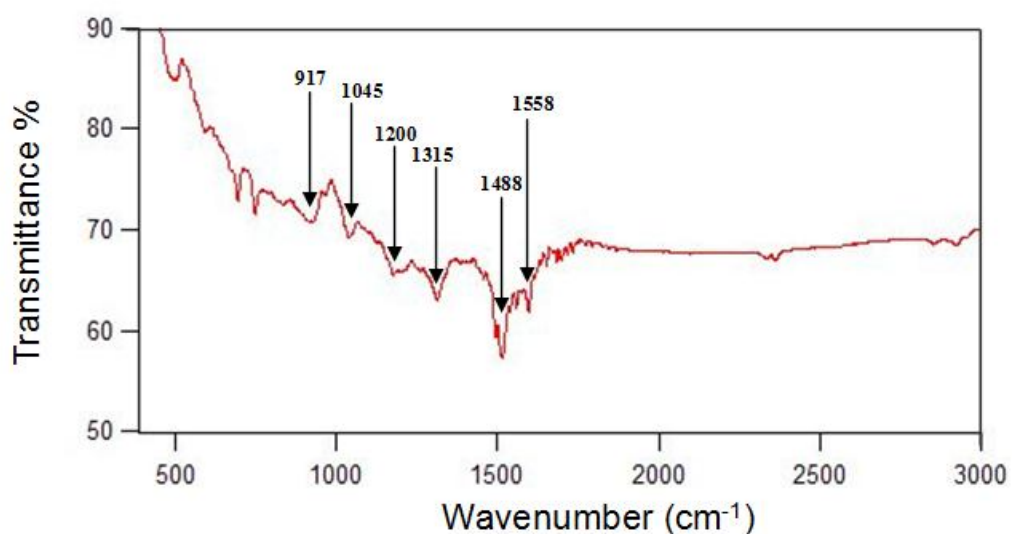


Figure 6.26. FT-IR spectrum of PPY nanofibers.

The characteristic absorption bands were observed at 1488 and 1558 cm^{-1} (stretching vibrations of the pyrrole ring), 917 and 1200 cm^{-1} (stretching vibrations of doped PPY), and 1045 and 1315 cm^{-1} (C–N stretching vibrations and C–H deformations, respectively), indicating that the PPY nanofibers share the same molecular structure as that obtained from established methods for synthesizing PPY [127].

Elemental analysis was conducted with a Thermo Electron/Flash EA1112 elemental analyzer. It revealed that the ratio of C/N of the PPY nanofibers (3.5) was consistent with the theoretical C/N ratio of pure PPY (3.43) and lends further support that the observed nanofibers were polypyrrole.

6.4 Characterization Results of Nanostructured Polyaniline and its Alkyl-Substituted Derivatives

Novel layered SAW hydrogen gas sensors based on nanoporous polyaniline (PANI), polyanisidine nanofibers and polyethylaniline nanofibers have been developed in a collaborative endeavor and reported by the author of this thesis [157-159]. Characterization of the nanoporous PANI was conducted in Sejong University, Seoul in Korea. Whereas the characterization results of polyanisidine nanofibers and polyethylaniline nanofibers were collected in University of California, Los Angeles. The characterization results of these nanostructured materials are presented in this section.

6.4.1 Nanoporous Polyaniline

The SEM study of nanoporous PANI revealed the nanoscale morphology. An SEM image of nanoporous PANI is shown in Figure 6.27 [157].

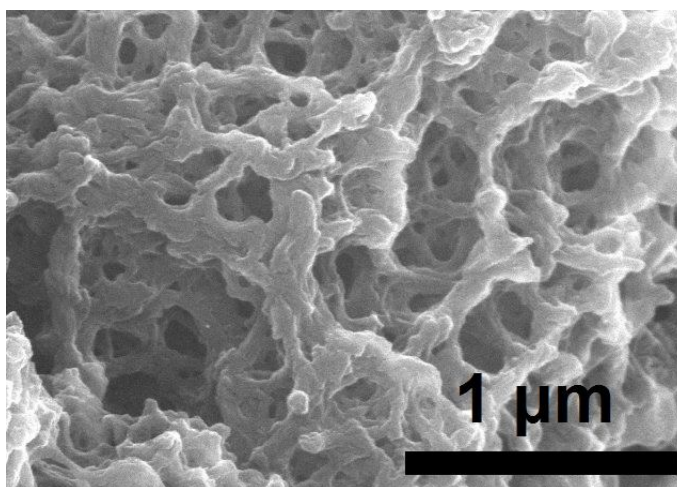


Figure 6.27. SEM image of the deposited nanoporous PANI film.

From Figure 6.27, it can be observed that the average pore size is about 45 nm. Furthermore, the Brunauer-Emmett-Teller (BET) nitrogen gas adsorption technique was employed to measure the surface area of nanoporous PANI. It was found that the nanoporous PANI had a surface area of 161 m²/g which is more than three times the previously reported BET surface area of PANI nanofibers of 49.3 m²/g and much higher than that of bulk PANI films of 0.2 m²/g [63].

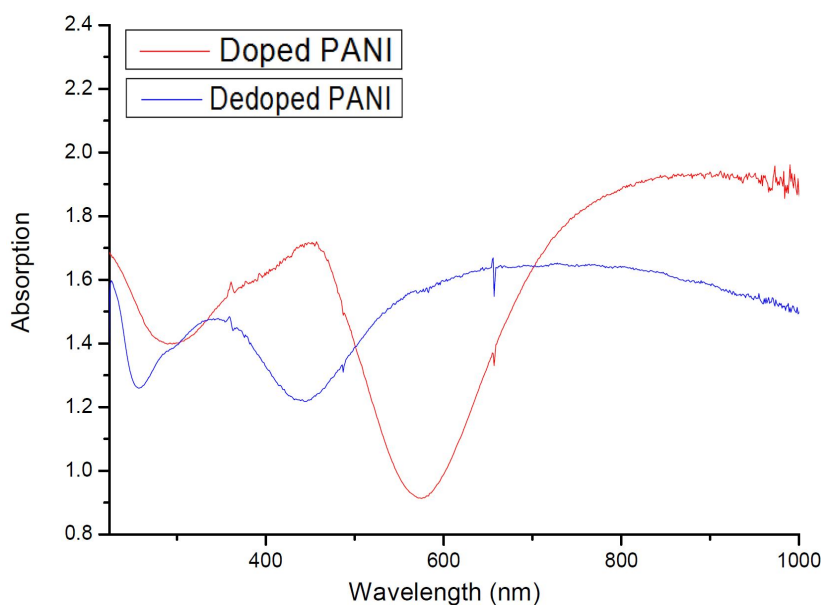


Figure 6.28. UV-vis spectra of doped and dedoped nanoporous PANI films.

The UV-vis spectra of the doped and dedoped nanoporous PANI is shown in Figure 6.28 [157]. For the spectrum of the doped nanoporous polyaniline, the peaks at 430 nm and the broader absorption at 869 nm correspond to electronic transition from valence band to polaron band which is a characteristic of the doped emeraldine oxidation state of PANI [262]. This is consistent with the green color of the deposited thin film. While for the dedoped nanoporous PANI, the $\pi-\pi^*$ absorption maxima were shifted towards lower wavelengths and can be found at 340 nm and 638 nm. These peaks are characteristic to the dedoped form of the polymer [263].

6.4.2 Polyanisidine Nanofibers

The chemically synthesized polyanisidine nanofibers were characterized using SEM microscopy and UV-vis spectroscopy. The SEM image of polyanisidine nanofibers is shown in Figure 6.29 [158].

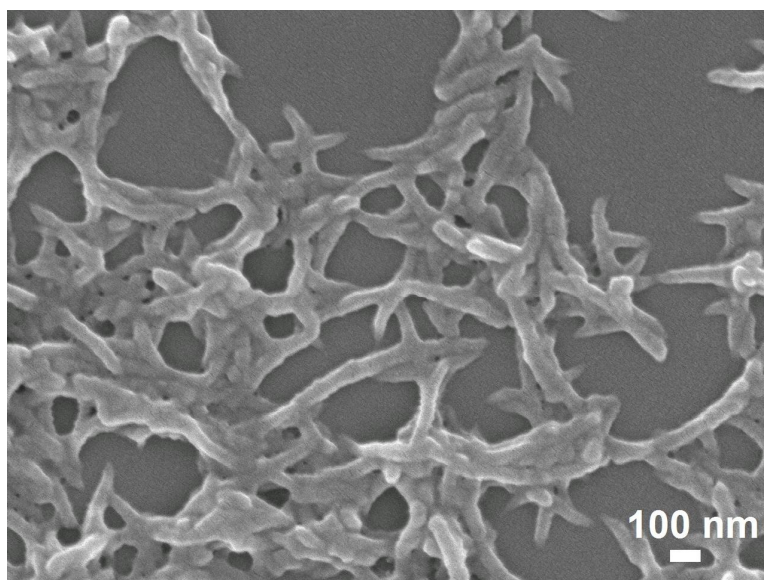


Figure 6.29. SEM image of polyanisidine nanofibers.

The average nanofiber diameter is approximately 55 nm with an average length of several microns. It was previously shown that the presence of an initiator such as aniline dimer is crucial to the formation of nanofibers of polyaniline derivatives [92]. In the case of polyanisidine, when the reaction was performed in the absence of an initiator, only large micron sized agglomerates were observed. However, when aniline dimer was introduced into the reaction between anisidine and ammonium peroxydisulfate, a drastic change was observed in the morphology of the purified product from micron sized agglomerates to a nanofibrous mat consisting of strands of nanofibers that are highly interconnected. The change in morphology is attributed to an increased reaction rate with the introduction of an initiator which facilitates the growth of polymer chains from homogeneous nucleation sites instead of heterogeneous nucleation sites which leads to agglomerated particles [90].

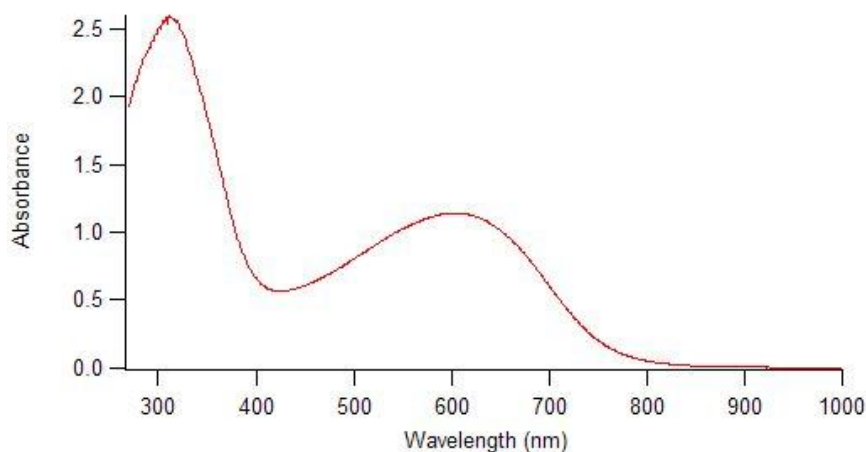


Figure 6.30. UV-vis spectrum for polyanisidine.

The UV-vis spectrum of polyanisidine in its doped state is shown in Figure 6.30 [158]. The spectrum presents two absorptions: one with maximum at 634 nm (1.96 eV) and another at 320 nm (3.75 eV). This spectrum indicates that the polymer was in the emeraldine oxidation state.

6.4.3 Polyethylaniline Nanofibers

SEM analysis of the synthesized polymer confirmed the nanofibrous morphology of the deposited polyethylaniline with an average nanofiber diameter of 47 nm. Figure 6.31 shows SEM images for polyethylaniline nanofibers at low and high magnification [159].

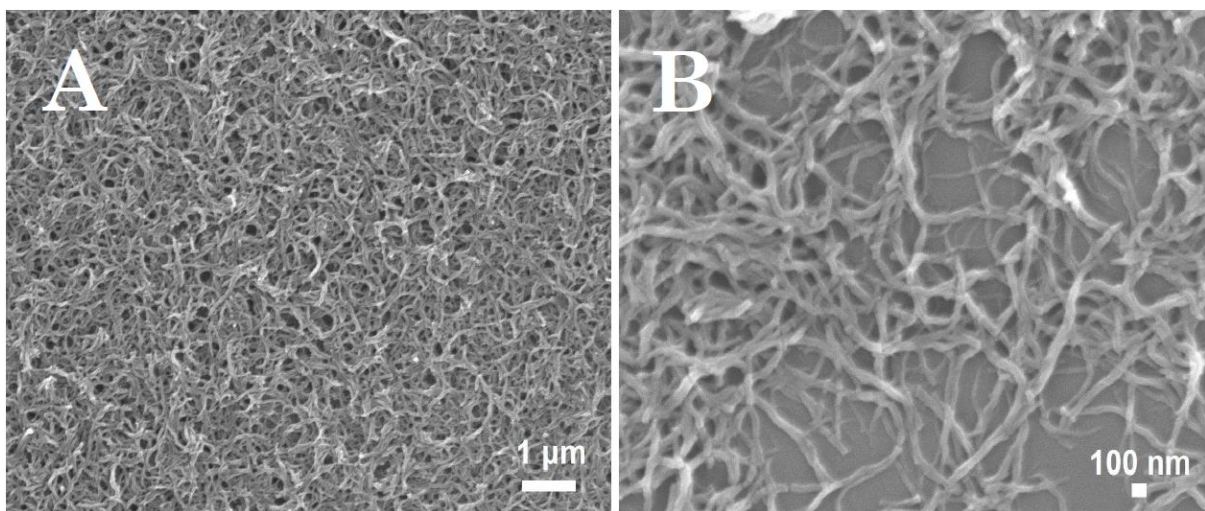


Figure 6.31. SEM images of polyethylaniline nanofibers.

UV-vis spectrum of polyethylaniline nanofibers is provided in Figure 6.32 [159]. It shows two adsorption peaks at the wavenumbers of 270 nm and 619 nm.

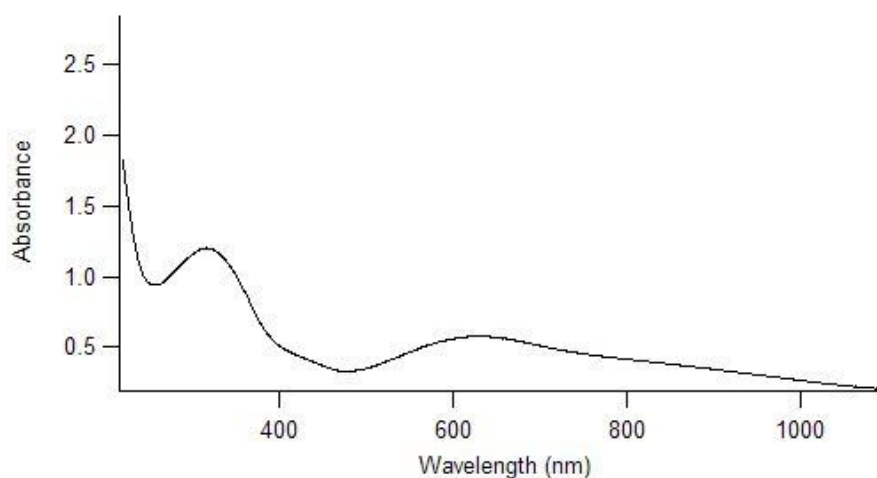


Figure 6.32. UV-vis spectrum of polyethylaniline.

There is a noticeable shift in the excitonic transition (λ_{\max}) to 619 nm compared to that of the parent polymer, polyaniline, located at 630 nm. This observation confirms that polyethylaniline has a slightly higher oxidation state than that of the ideal emeraldine oxidation state [94].

6.5 Characterization Results of Graphene/Polyaniline Nanocomposite

Based on a collaborative project between RMIT University in Australia, Monash University in Australia, Sejong University in Korea and University of California (Los Angeles) in USA, an investigation on the hydrogen gas sensing properties of graphene/PANI nanocomposite compared to that of graphene and PANI nanofibers has been conducted. The outcomes of this study have been published by the author of this dissertation in a joint article in the Journal of Physical Chemistry C [182], which received ~50 citations (ref: Scopus/ November 2012). SEM images of the graphene/PANI nanocomposite were obtained in Sejong University. Whereas TEM imaging was conducted at UCLA. Raman spectroscopy was performed at RMIT University using a Ramanstation 400F Dispersive Raman Spectrometer (Perkin Elmer) operating at 785 nm and 350 mW near infrared laser with a cooled CCD detector. The XPS investigation was conducted at RMIT University utilizing the experimental setup described in section 6.2.1.

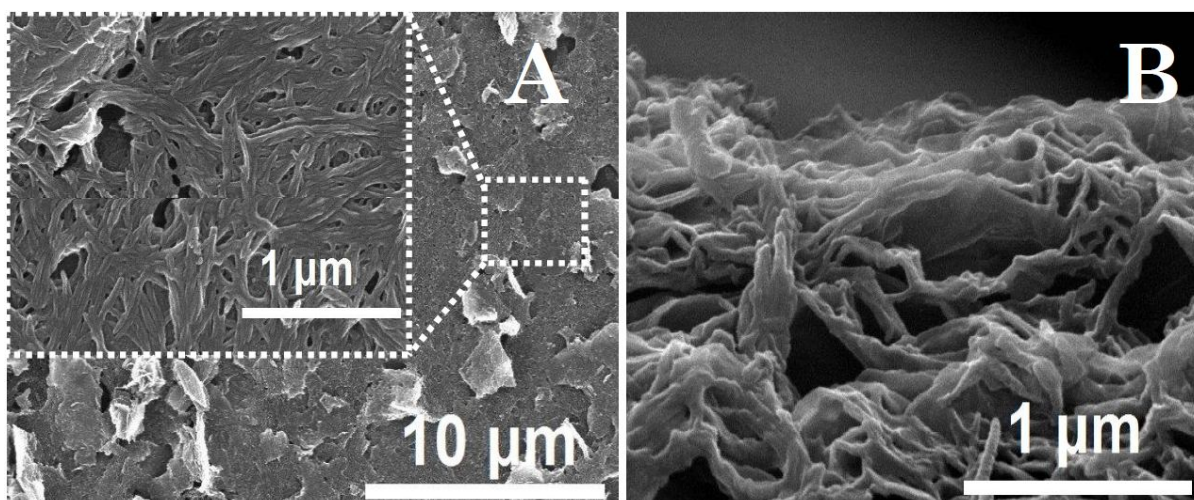


Figure 6.33. SEM images of graphene/PANI nanocomposite: (A) top view, (B) tilted view (45°).

The morphology of the graphene/PANI nanocomposite was investigated by SEM and TEM microscopies as shown in Figure 6.33 and Figure 6.34. It can be seen that PANI

nanofibers on the order of 25–50 nm have been grown on the surface of the graphene nanosheets which has been confirmed by the TEM observation.

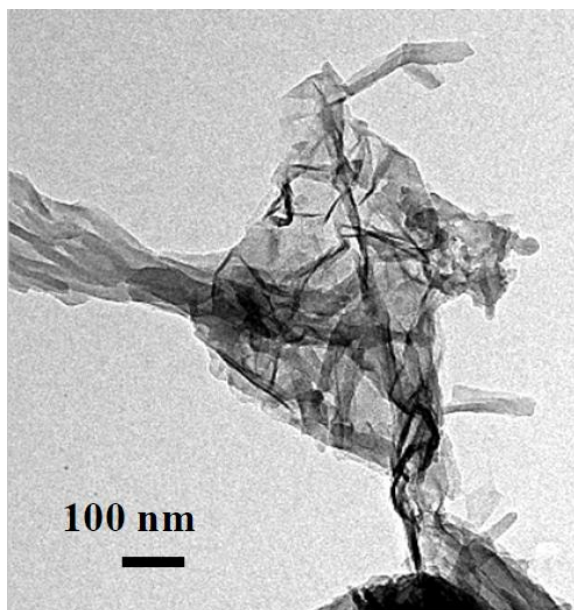


Figure 6.34. TEM image of graphene/PANI nanocomposite.

In analyzing the morphology of the graphene/PANI nanocomposite, it is important to take into consideration the electron transport properties of both graphene and aniline monomer in order to determine the molecular binding mechanism. Graphene is an electron acceptor, analogous to other forms of carbon such as the zero-dimensional fullerene (C_{60}) or one-dimensional single-walled carbon nanotubes [264]. Aniline, on the other hand, is an electron donor [199]. It was reported earlier that C_{60} and CNTs can form donor-acceptor complexes in the liquid state when dissolved in tertiary amines and substituted anilines forming stable CNT-aniline complexes [265].

In the likely mechanism for the formation of nanofibers on the graphene nanosheets, the aniline monomer is first adsorbed onto the surfaces of the graphene nanosheets due to electrostatic attractions. Oxidation of aniline by ammonium peroxydisulfate (APS) in the presence of the aniline dimer, N-Phenyl-1,4-phenylenediamine, results in a product with the nanostructure shown in Figure 6.33 and Figure 6.34. It was reported earlier that a rapid reaction promotes homogeneous nucleation of growing PANI chains and thus the formation of uniform PANI nanofibers [240]. It is anticipated that the N-Phenyl-1,4-phenylenediamine has accelerated the polymerization of the aniline monomer and results in a nanofibrillar morphology on the surface of the graphene nanosheets. Hence, the graphene nanosheets can be considered as a support material for PANI growth providing a large number of active nucleation sites [199].

The Raman spectra for the developed graphene/PANI nanocomposite as well as for graphene and PANI are shown in Figure 6.35. The Raman spectra of pure graphene and the graphene based nanocomposite have very distinctive peaks for the D and G bands. The D band peak which can be found in Figure 6.35 at around 1318 cm^{-1} is attributed to the K-point phonons of A_{1g} symmetry, while the G band peak at around 1592 cm^{-1} is usually assigned to zone center phonons of E_{2g} symmetry [244]. Characteristic vibrational peaks of PANI are also evident in the graphene/PANI nanocomposite spectrum. For the doped form of the polymer, both polaronic and bipolaronic structures are expected to coexist and hence the vibrational modes of both structures contribute to the overall spectrum. However, a slight deviation from the theoretical values is always anticipated [266].

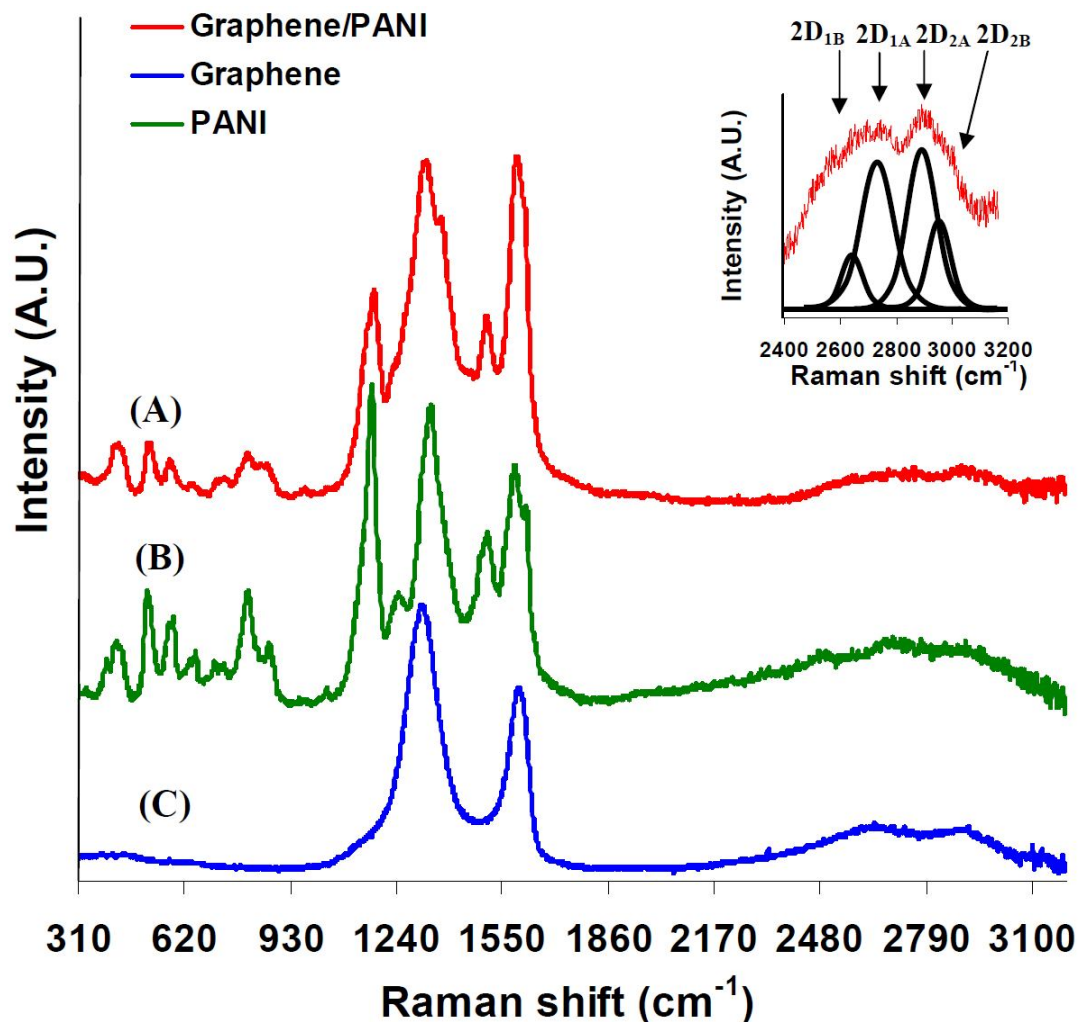


Figure 6.35. Raman spectra of: (A) graphene/PANI nanocomposite, (B) PANI and (C) graphene; the 2D band in the Raman spectrum of graphene/PANI nanocomposite is analyzed in the inset.

In the graphene/PANI nanocomposite spectrum presented in Figure 6.35, the bipolaronic N–H bending vibration can be seen at 1504 cm^{-1} . The peak at 1372 cm^{-1} can be attributed to the C–N stretching vibration of the cation radical species indicating an intermediate level of doping. The peak at 1172 cm^{-1} can be attributed to the C–H bending of the quinoid ring. A minor polaronic peak at 856 cm^{-1} is a characteristic benzene ring deformation. The peaks observed at 806 cm^{-1} , 712 cm^{-1} , 640 cm^{-1} and 576 cm^{-1} can be attributed to bipolaronic quinoid ring deformations, bipolaronic C–C ring deformations, bipolaronic benzene ring deformations, and bipolaronic amine deformations, respectively. The peak at 518 cm^{-1} can be correlated to a polaronic amine deformation, while the peak related to the polaronic C–N–C torsion can be found at 418 cm^{-1} [266].

It was demonstrated in earlier studies that the number of graphene layers can be determined through examining the 2D band of the Raman spectrum [267, 268]. Raman measurements for the graphene/PANI sample could not be taken using a micro Raman system with a spot size of $\sim 350\text{ nm}$ due to the nanofibrillar morphology. Instead the Raman measurements were conducted using a Raman system with a spot size of $100\text{ }\mu\text{m}$. The inset to Figure 6.35 shows the 2D band of the graphene/PANI nanocomposite spectrum. It appears that the graphene in the graphene/PANI nanocomposite consists of a variety of sheets containing from just few layers up to several tens of layers [269, 270]. However, because of the nanofibrillar morphology and high overall coverage of the PANI nanofibers, the number of graphene layers cannot be accurately determined from either the Raman measurements or SEM images. According to a study conducted by Ferrari [271], the number of graphene layers can be verified by identifying the four components of the 2D band which were named as $2D_{1B}$, $2D_{1A}$, $2D_{2A}$, and $2D_{2B}$. For the graphene/PANI nanocomposite, these four components can be found in the inset to Figure 6.35. The $2D_{1A}$ and $2D_{2A}$ peaks have higher relative intensities than the other two peaks. The relatively strong $2D_{1A}$ corresponds to the presence of single or bi-layer graphene sheets in the nanocomposite [269, 270]. However, the intensity of $2D_{2A}$ is also large, which can correspond to the presence of multi-layer graphene sheets [269, 270]. Further complication arises from the fact that the Raman spectrum of PANI itself exhibits an elevated intensity in the same wavenumber range of the 2D band due to its aromatic structure, which further distorts the number of layers measurement using Raman spectroscopy.

It was mentioned earlier in this study that the graphene/PANI nanocomposite can function as a donor-acceptor structure from the electron transport point of view. However for a graphene/ TiO_2 nanocomposite, it was found that further chemical

reduction occurred due to electron transfer to graphene oxide [272, 273]. In order to clarify this point and for further understanding of the graphene/PANI nanocomposite chemical composition, XPS measurements were conducted.

Figure 6.36 shows the C(1s) XPS spectrum of the graphene/PANI composite. Curve fitting of the C(1s) reveals a high intensity peak centered at a binding energy of 284.6 eV that corresponds to C–C, C=C and C–H bonds. It is reported that the peaks, found at shifts of +1.5, +2.5 and +4.0 eV from the main peak, can be attributed to the functional groups C–OH, C=O, and O=C–OH, respectively [274, 275]. In this work, these peaks are found at 286.08, 287.38, and 288.18 eV, respectively.

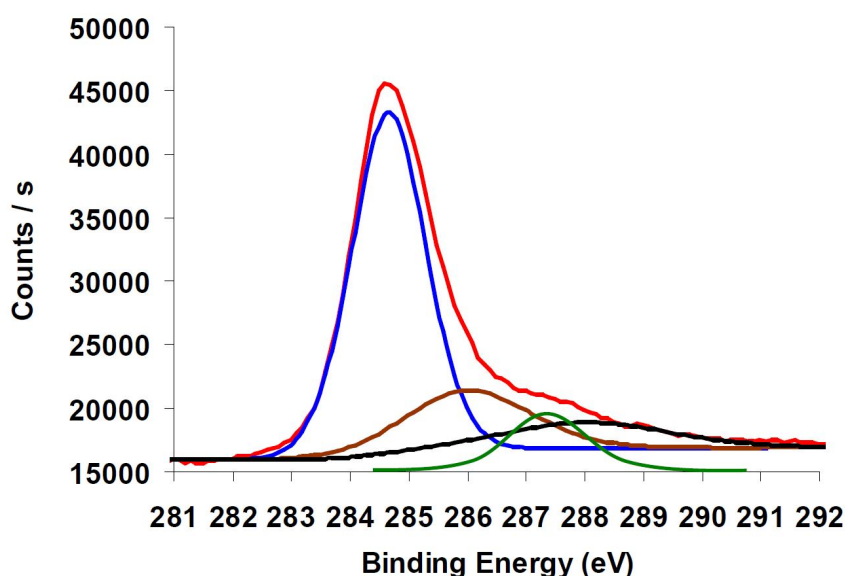


Figure 6.36. Peak deconvolution of the C(1s) XPS core level for the graphene/PANI nanocomposite.

It is also important to examine the O(1s) XPS spectrum in order to determine the chemical reduction state of the graphene/PANI composite as shown in Figure 6.37. The deconvolution of the O(1s) spectrum results in three peaks, which are comparable to those found in earlier reports [274, 275]. The peak with the lowest intensity at a binding energy of ~530 eV can be attributed to the C=O and O=C–OH functional groups, while the main peak with a binding energy of ~532 eV can be assigned to the C–OH bond. The third peak is from bound water at a binding energy of ~533.1 eV. The relatively high intensity of the H₂O bond peak can be attributed to the fact that the chemically prepared graphene/PANI nanocomposite is suspended in water and the deposited films were not exposed to any heat treatment to avoid changing or decomposing the PANI.

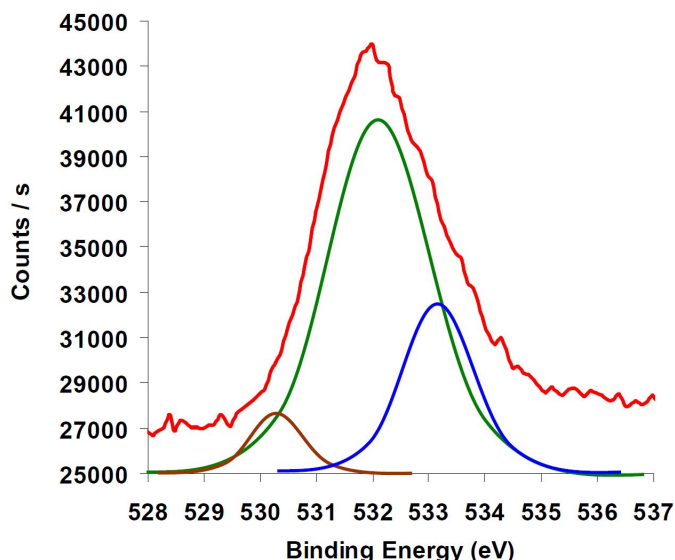


Figure 6.37. Peak deconvolution of the O(1s) XPS core level for the graphene/PANI nanocomposite.

In a recent published study, Akhavan prepared graphene films from graphene oxide nanosheets following two heat treatment methods [275]. The deconvolution of the O(1s) spectrum of graphene films obtained in that work showed a minimum intensity for the peak assigned to the C=O and O=C–OH functional groups. For the graphene/PANI nanocomposite, It was also noticed a minimum intensity for that peak as a result of chemical reduction. It can be noticed that the shape of the O(1s) spectrum herein is very similar to the shapes of the O(1s) spectra of graphene films obtained by heat treatment [275]. Hence, the graphene in the synthesized nanocomposite is a reduced graphene.

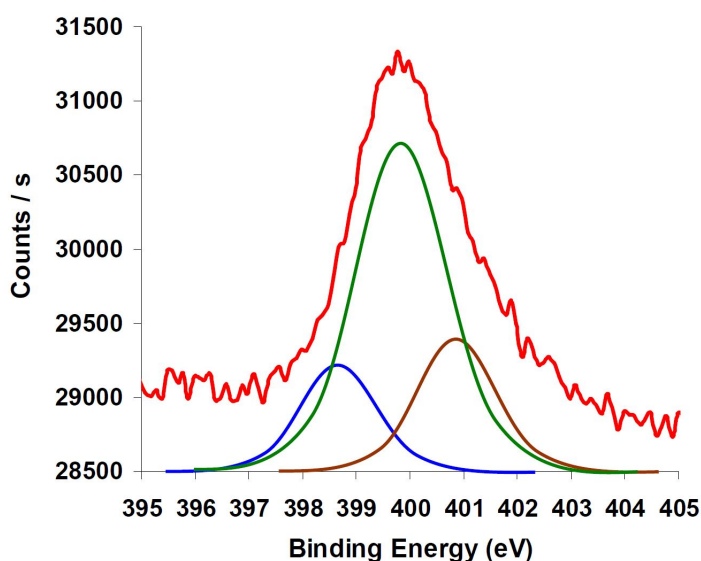


Figure 6.38. Peak deconvolution of the N(1s) XPS core level for the graphene/PANI nanocomposite.

The deconvolution of the N(1s) core level spectrum for graphene/PANI is shown in Figure 6.38. It consists of three components. The quinoid amine is found at a binding energy of 398.3 eV. The main benzenoid amine peak can be found at a binding energy of 399.7 eV. The nitrogen cationic radical (N⁺) component can be found at a binding energy of 401.1 eV. The deconvolution of the N(1s) core level spectrum presented here is comparable to the typical XPS N(1s) deconvolution of PANI reported in literature [276]. It can be concluded from this study that the graphene/PANI nanocomposite can outperform both of graphene and PANI in its gas sensing performance because of the large surface area of this nanomaterial as demonstrated in Figure 6.33 and Figure 6.34. Also it is evident from the Raman spectra in Figure 6.35 that the graphene/PANI nanocomposite spectrum contained a mixture of graphene and PANI vibrational peaks leading to the proposition that this nanocomposite has the chemical and physical properties of both materials combined. Therefore a stronger interaction between hydrogen gas and the nanocomposite compared to that with graphene and PANI alone is anticipated due to the large number of adsorption sites available from the two combined nanomaterials. This proposition has been experimentally proven and the hydrogen gas sensing results of the graphene/PANI nanocomposite compared to that of graphene and PANI individually will be provided in Chapter 7.

6.6 Summary

The physical and chemical properties of the nanostructured materials utilized for gas sensing application in this dissertation were analyzed throughout the present chapter. An introduction to the employed characterization techniques was provided in section 6.1 followed by an extended analysis of the characterization results for the nanostructured conductive polymers and graphene/PANI nanocomposite. The key findings are summarized below:

- Polythiophene nanostructures: characterization results of the electropolymerized and chemically polymerized nanostructured polythiophene by the author of this thesis revealed the following outcomes:
- Electropolymerization of thiophene in LiClO₄ based electrolyte produced granular 3-D structures of polythiophene. On the contrary, utilizing FeCl₃ solution promoted the formation of polythiophene nanofibers with diameters in the range of 10–40 nm as demonstrated in the SEM images. From analyzing the electropolymerization current curves, it can be suggested that the heterogeneous nucleation has been suppressed in this case of FeCl₃ solution by restricting the flow of the high current at the beginning of the electropolymerization that was

observed in the case of LiClO_4 based electrolyte and instead maintaining a stable high value of current throughout the deposition period.

- Comparison of the polythiophene films' morphologies synthesized with different concentrations of the FeCl_3 electrolyte 0.6–1.8 mM revealed that the optimum concentration was 1.2 mM. It can be proposed that a balance between the chemical and electrochemical polymerization of thiophene monomer has been established at this particular concentration. UV-vis spectra of the deposited polythiophene films exhibited a direct relationship between the FeCl_3 electrolyte concentration and the doping level. The band gap of the synthesized polymer was calculated from the UV-vis spectra and found to be 2.13 eV, which is typical for polythiophene according to previous reports.
- The choice of the electropolymerization potential (0.65–0.85 V) had a profound impact on the resultant polymer morphology. This observation can be attributed to the increase of polymerization rate with the rising deposition potential. Supporting this explanation was the evident increase in the UV-vis absorbance for the deposited polythiophene films with the rise in the applied electropolymerization potential. Nevertheless, the presence of the adsorption band ~700 nm in the UV-vis spectra confirmed the semi-doped state of the deposited polythiophene films since the FeCl_3 electrolyte concentration was fixed at 1.2 mM in these experiments. Comparing the films' structures deposited with different potentials revealed that the optimum nanostructured polythiophene film's morphology was obtained by selecting 0.75 V as the electropolymerization potential.
- At the beginning of the electrodeposition, a seed layer of polythiophene is deposited followed by the growth of nanofibers from nucleation sites as demonstrated by the SEM images taken after 20 minutes of polythiophene electropolymerization. By increasing the deposition time, the number of grown nanofibers increased as well as the overall nanostructured film's thickness.
- The chemical composition of the electropolymerized polythiophene nanostructures was characterized using XPS. The incorporation of the doping anion (Cl^-) into the polymer matrix was confirmed.
- The nanofibrillar morphology of the chemically synthesized polythiophene was verified by SEM microscopy. The polythiophene nanofibers were 60–110 nm in diameter and several micrometers in length. Characteristic vibrational peaks for polythiophene molecules were observed in the FT-IR spectrum.

- Polypyrrole nanostructures: the electropolymerized and chemically polymerized polypyrrole nanostructures were characterized in this chapter and the findings are summarized below:
- Electrochemical deposition of polypyrrole nanowires on three conductometric transducers was conducted using either 13, 55 or 90 mC of anodic charge each time. Consistent with the polythiophene electropolymerization results, the rise in the anodic charge is expected to increase the rate of polymerization. Hence the sensitive film deposited with 90 mC consisted of only polypyrrole nanowires with diameters in the range of 40–90 nm providing higher surface-to-volume ratio compared to the other films. It is anticipated that homogeneous nucleation was dominant over heterogeneous nucleation and consequently the secondary growth of polymer chains was suppressed at 90 mC of anodic charge. Bridges of polypyrrole nanowires over the insulating gaps between the gold electrodes were formed. Elemental composition of the electropolymerized polypyrrole nanowires was investigated utilizing XPS. The incorporation of the doping perchlorate anion into the polypyrrole matrix was noticed.
- Chemically synthesized polypyrrole nanofibers deposited on conductometric and layered SAW transducers were ~18 nm in diameter according to SEM and TEM images. The FT-IR spectrum exhibited the characteristic molecular vibrations for polypyrrole.
- Nanostructured polyaniline and its alkyl-substituted derivatives: chemically synthesized nanostructured polyaniline, polyanisidine and polyethylaniline were deposited on layered SAW transducers for gas sensing application. The characterization results for these nanomaterials are summarized below:
- The average pore size of nanoporous polyaniline was ~45 nm. Measured surface area was 161 m²/g, which was interestingly about three times that of polyaniline nanofibers. UV-vis spectra of doped and dedoped nanoporous polyaniline were comparable to that of the bulk form of the polymer reported in literature.
- Polyanisidine and polyethylaniline nanofibers were approximately 55 and 47 nm in diameter, respectively. The polymers were in the semi-doped state according to the analysis of the corresponding UV-vis spectra.
- Graphene/Polyaniline nanocomposite: characterization of chemically synthesized graphene/polyaniline nanocomposite was performed through SEM, TEM, Raman spectroscopy and XPS. The outcomes of these investigations are summarized below:

- SEM images demonstrated that polyaniline nanofibers ~25–50 nm in diameter were grown on the graphene nanosheets' surfaces as confirmed by the TEM observation.
- The Raman spectrum of graphene/polyaniline nanocomposite consisted of a combination of graphene and polyaniline vibrational modes. Therefore this nanocomposite has the chemical and physical properties of both materials.
- The single and conjugated carbon bonds as well as the characteristic functional groups for the graphene/polyaniline nanocomposite were analyzed by the XPS spectroscopy. Furthermore, the XPS results confirmed that the graphene was actually in its reduced form. Trapping of some water molecules into the graphene/polyaniline nanocomposite based sensitive film was evident.

To the best knowledge of this dissertation's author, conductometric and layered SAW gas sensors based on the above described nanomaterials have been developed for the first time in this PhD research project. The gas sensing results of these sensors will be discussed in the upcoming chapter.

Chapter 7

Gas Sensing Results and Discussions

NOVEL conductometric and layered SAW gas sensors based on nanostructured conjugated polymers and graphene/polyaniline nanocomposite were successfully fabricated as described in the past chapters. The gas sensing performance of these sensors towards different concentrations of hydrogen gas was investigated by the author of this dissertation and will be discussed in the present chapter. In addition to the gas sensors' electrical characterization, a discussion of the anticipated chemical sensing mechanisms for the nanostructured conductive polymers considered in this dissertation will be provided herein.

For conductometric gas sensors, the output signal is a measure of the instantaneous variation in the sensitive film's ohmic resistance during the interaction with the target gas. Whereas in SAW gas sensors, the deviation in the operational frequency due to the surface acoustic wave velocity perturbations during the exposure to the target gas is measured and regarded as the sensor's output. A description of the experimental set-up utilized for evaluating the gas sensing performances of the developed conductometric and layered SAW gas sensors will be provided in section 7.1. The gas sensing results for the nanostructured polythiophene, polypyrrole, polyaniline as well as its derivatives and graphene/polyaniline nanocomposite based gas sensors will be discussed in sections 7.2, 7.3, 7.4, and 7.5 respectively. Finally, the chapter will be concluded by a summary in section 7.6.

7.1 Gas Sensing System Configuration

Gas sensing experiments were conducted using the gas calibration system illustrated in Figure 7.1. A programmable 4-channel mass flow controller was utilized to control the exposure of the sensor under test to target gases with different concentrations diluted in synthetic air.

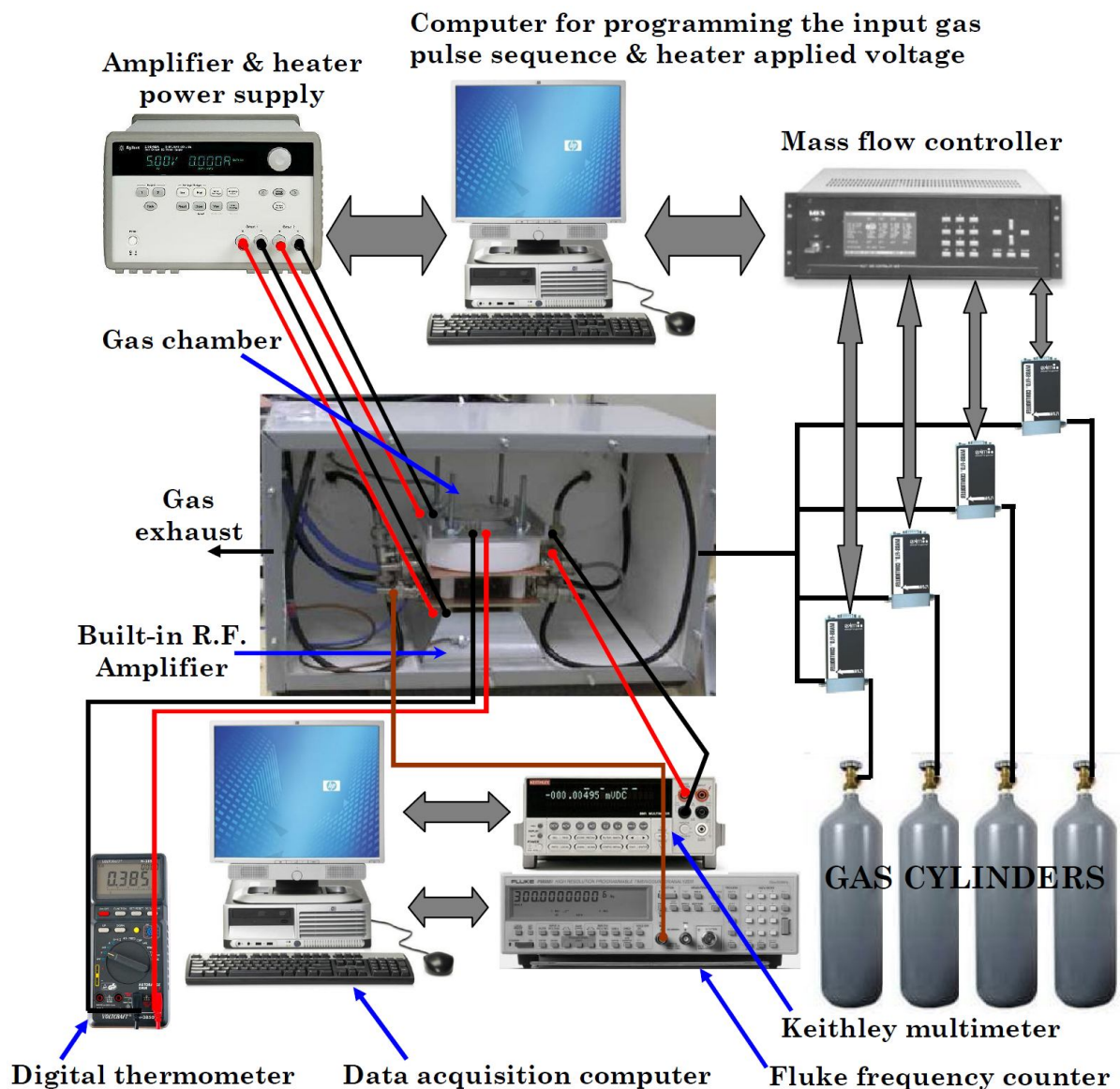


Figure 7.1. Schematic illustrating the gas sensors' testing system (the gray double-sided arrows represent data cables).

The gas/air mixture flow into the gas chamber was maintained at 200 SCCM throughout the experiments. All gas bottles used in this work contained dry gases only according to the manufacturer data sheets. The synthetic air used consisted of 79% nitrogen and 21%

oxygen as specified by the supplier, while the hydrogen gas bottle contained 1% (10000 ppm) of hydrogen gas balanced in synthetic air. Every gas sensor reported in this thesis was tested towards a pulse sequence of hydrogen gas balanced in synthetic air. Five concentrations of hydrogen gas were exposed to each sensor during testing, which were 0.06%, 0.12%, 0.25%, 0.5% and 1%. The synthetic air was used as the washing gas. The gas chamber was always placed inside an insulated steel box in order to eliminate any electromagnetic interference (EMI) as well as providing thermal stability to the sensor's environment.

In conductometric gas sensors testing, the sensor was connected to a Keithley 2001 multimeter in order to measure the variations in film resistance during the interaction with the target gas. The multimeter is connected to the data acquisition computer that runs a LabVIEW program.

Theoretical aspects of SAW gas sensors has been presented in Chapter 3. The developed layered SAW gas sensors were tested in an oscillator circuit configuration as described in Figure 3.4. For that purpose, the SAW delay line was placed in the positive feedback of an RF amplifier to overcome the device's insertion loss. Phase matching condition expressed in equation (3.43) was achieved by careful selection of the coaxial cables length for a $2\pi N$ phase shift. Hence, the SAW gas sensor was operating at the resonant frequency which was predetermined by the network analyzer analysis using 50Ω calibrated leads. A high resolution frequency counter, Fluke PM66860B, was used to measure the sensor operational frequency upon exposure to target gases. This approach for testing SAW gas sensors was adopted by several research groups [216, 277, 278].

The conductometric and layered SAW sensors' responses were displayed in real time on the data acquisition computer's screen and saved for off-line processing and analysis. In the upcoming sections, the developed gas sensors' performances will be discussed.

7.2 Gas Sensors with Nanostructured Polythiophene Sensitive Films

As discussed in earlier chapters that a comparative study has been conducted in this dissertation to analyze the effect of the electropolymerization parameters on the deposited polythiophene films' structures and consequently on the developed gas sensors' performances. Because of the (1.2 μm thick) ZnO acoustic guiding layer sputtered on the gold IDTs of each layered SAW transducer employed in this research, only conductometric transducers have been considered for the electropolymerization comparative study since a highly conductive surface in the working electrode is essential

for the electrodeposition to occur. On the other hand, a hydrogen gas sensor based on chemically synthesized polythiophene nanofibers deposited on the surface of a ZnO/36° YX LiTaO₃ SAW transducer has been developed and tested herein also. All of the developed nanostructured polythiophene based conductometric and layered SAW gas sensors were operating at room temperature. In the following subsections, the gas sensing results of these sensors will be presented.

7.2.1 Conductometric Gas Sensors Based on Electropolymerized Polythiophene Nanostructures

In this comparative study, the effects of electropolymerization parameters such as electrolyte's anion type, concentration of the electrolyte, applied potential and deposition time (sensitive film thickness) on the developed sensors' responses towards hydrogen gas are investigated for the first time to the best knowledge of this dissertation's author. The selection of the deposition parameters has a direct impact on the resultant polythiophene film morphology and optical properties as demonstrated in section 6.2.1. From gas sensing point of view, the effect of each parameter is discussed individually in the following subsections.

The Effect of Electrolyte's Anion Type

To elucidate the effect of the type of polythiophene's doping anion on the sensors' performances, two gas sensors have been developed and compared. The first sensor, referred to here as sensor (A), was developed through electrochemical deposition of polythiophene using LiClO₄ salt diluted in 50 mL of acetonitrile in order to dope the polymer with perchlorate (ClO_4^-) anions. It is worth to mention here that LiClO₄ is well known in literature for its role in the electropolymerization and electrochemical doping of polythiophene films [279-282]. However, to the best knowledge of this dissertation's author, ClO_4^- doped polythiophene has not been investigated for its sensitivity towards hydrogen gas before. For the second sensor, sensor (B), the electropolymerization was carried out using the same type and volume of the organic solvent but with diluted FeCl₃ salt instead as the supporting electrolyte to produce polythiophene sensitive film doped with chloride (Cl^-) anions. The dynamic responses of the two sensors are shown in Figure 7.2. Normalized resistance (R/R_0) is adopted herein as the basis for comparison between the sensors' dynamic performances, where R is the sensitive film's resistance during the exposure to hydrogen gas and R_0 is the film's resistance under synthetic air

only. It is evident from Figure 7.2 that sensor (B) had a much more stable operation compared to that of sensor (A). The baseline of sensor (A) was continuously drifting downwards despite the numerous attempts to stabilize it during the experiments. On the contrary, sensor (B) featured a stable baseline at all times during tests.

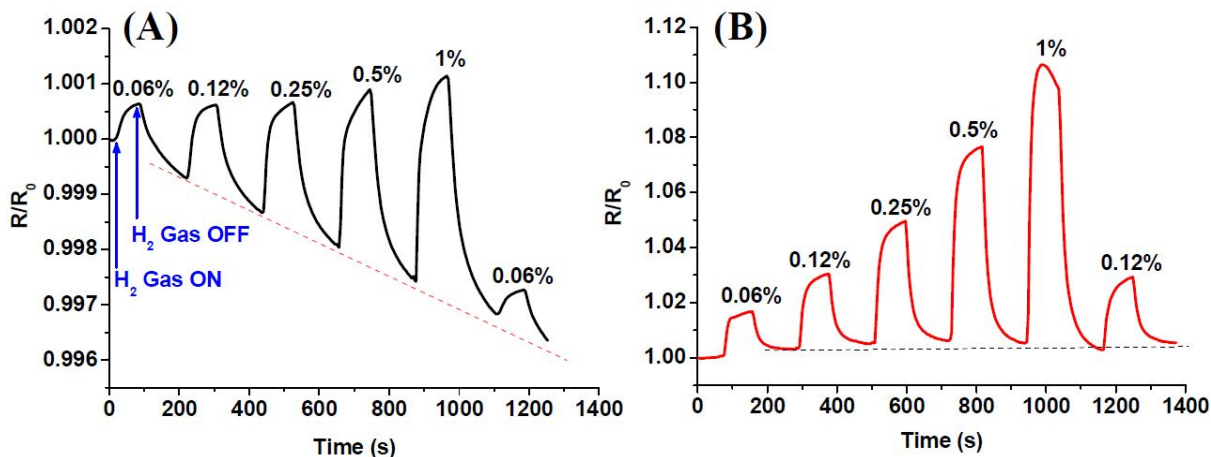


Figure 7.2. Dynamic responses of gas sensors: (A) Sensor (A) based on ClO_4^- doped polythiophene, (B) Sensor (B) based on Cl^- doped polythiophene.

The observed difference in the dynamic performance of these sensors can be interpreted in terms of the morphological difference between their sensitive films as shown earlier in Figure 6.2. The sensitive film of sensor (A) consists of granular structures closely packed on top of each other forming a rough surface that lacks porosity. Whereas the sensitive film of sensor (B) featured nanostructures containing nanofibers with diameters $\sim 10\text{--}40$ nm that are uniformly distributed as demonstrated in Figure 6.3. Therefore the new approach in synthesizing polythiophene adopted by the author of this thesis, which is the merge of chemical and electrochemical polymerizations into a single synthesis process, has resulted in an enhanced gas sensing performance as shown in Figure 7.2 (B) due to the large surface-to-volume ratio and high porosity of the sensitive film of sensor (B) compared that of sensor (A). Supporting this explanation is the fact that sensor (B) is faster in responding to hydrogen gas exposure than sensor (A). For instance, sensor (A) and sensor (B) responded in 79 s and 40 s towards hydrogen gas with the concentration of 1% balanced in synthetic air at room temperature respectively. The response time is usually defined as the 90% of the time needed by the sensor to reach saturation in responding to the target gas [118]. The overall output response of a conductometric gas sensor can be expressed by the relative change of its resistance [283]:

$$\text{Response (\%)} = \left| \frac{R - R_0}{R_0} \right| \times 100\% \quad (7.1)$$

A plot of the responses of sensor (A) and sensor (B) towards five concentrations of hydrogen gas is provided in Figure 7.3. It is evident that the response of the nanostructured and Cl^- doped polythiophene based sensor, sensor (B), is about three times higher than that of the sensor with conventional ClO_4^- doped polythiophene sensitive film. This finding can be attributed to the higher surface-to-volume ratio of the nanostructured polythiophene film compared to its conventional bulk counterpart as shown in Figure 6.2. Hence, the nanostructured film offers a higher number of adsorption sites for interaction with hydrogen gas. Also the hydrogen gas diffuses deep into the nanostructured polythiophene film because of its porosity, whereas the interaction is confined to the surface in the case of the conventional film. It can be anticipated that both of these factors are contributing to the observed larger response of sensor (B) compared to that of sensor (A).

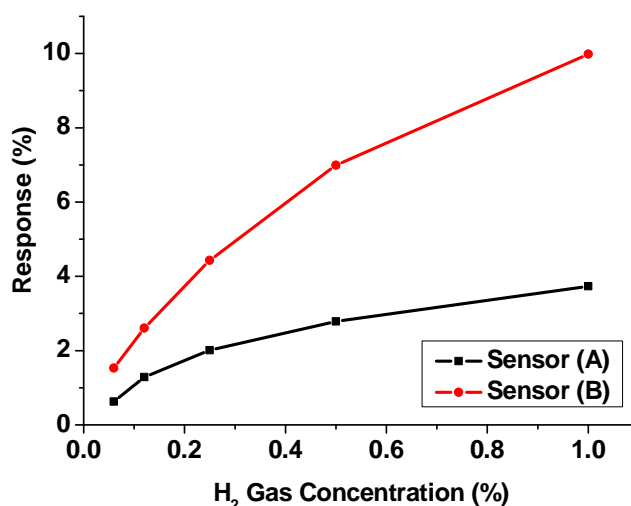


Figure 7.3. Responses of sensor (A) with ClO_4^- doped polythiophene and sensor (B) with Cl^- doped polythiophene.

For further understanding of the sensors' performances, it might be useful to refer to the conduction mechanism in heterocyclic conjugated polymers. At room temperature condition, conduction through polaron hopping is a plausible charge transportation mechanism in the backbone of polythiophene [104, 284]. However for the nanostructured polythiophene exhibited in Figure 6.3, two additional charge transportation mechanisms are possible [101]. The first mechanism is related to a particular nanostructure, for instance through the whole length of a nanofiber. The second mechanism is related to

the conduction between interconnected nanostructures i.e. at the boundaries of a nanofiber or any other nanostructure. Hence, the degree of crystalline order and the nanostructures' boundaries have a significant impact on the overall conductivity of the nanostructured polythiophene film. From the above discussion, it can be anticipated that a nanostructured polythiophene film would be relatively more conductive than the conventional film. This proposition is verified for the developed sensors herein. The nanostructured polythiophene film deposited on sensor (B) is more conductive than that of the conventional film deposited on sensor (A). The baseline resistance (R_0) for sensor (B) was 202.7 Ω , whereas R_0 for sensor (A) was 322 Ω .

During the gas exposure, a modulation to the conjugated polymer conductivity takes place. It has been suggested that considering the polymer characteristics such as the planarity of the conjugated polymer chains and the length of chains, multiple sensing mechanism may occur simultaneously during the exposure to the target gas [101]. A proposed hydrogen gas sensing mechanism for the developed sensors will be provided in an upcoming subsection.

From the above analysis, it can be deduced that polythiophene electropolymerization on conductometric transducers utilizing FeCl_3 solution can provide more sensitive sensors than employing LiClO_4 based electrolyte. Hence, Cl^- doped polythiophene films have been selected for further investigation. The influence of the FeCl_3 concentration, the anodic potential and the film thickness on the sensors' performances will be studied in the following subsections.

The Effect of Different Electrolyte's Concentrations

In the previous discussion, sensor (B) was developed through electropolymerization of thiophene monomer in a 1.2 mM FeCl_3 solution. In order to determine the optimum concentration of FeCl_3 to be adopted during electropolymerization from gas sensing perspective, four other sensors were developed and tested for the comparison with sensor (B) by utilizing the 0.6 mM, 0.9 mM, 1.5 mM and 1.8 mM concentrations of FeCl_3 solution. Figure 7.4 displays the response of these sensors towards five concentrations of hydrogen gas at room temperature. It can be seen that the sensor developed by utilizing 0.6 mM FeCl_3 has the worst baseline stability among the other sensors. According to the analysis in the above subsection, the dynamic performance of a gas sensor is largely inhibited by the morphology of its sensitive film. From the SEM investigation of the deposited sensitive films shown in Figure 6.6, it is evident that the film deposited with 0.6 mM FeCl_3 consisted of compact and irregular shaped polythiophene particles. Hence,

a drift of baseline would be expected in agreement with the gas sensing performance of the conventional film discussed in previous subsection. As the concentration of FeCl_3 increases, the baseline drift decreases because of the formation of nanostructures.

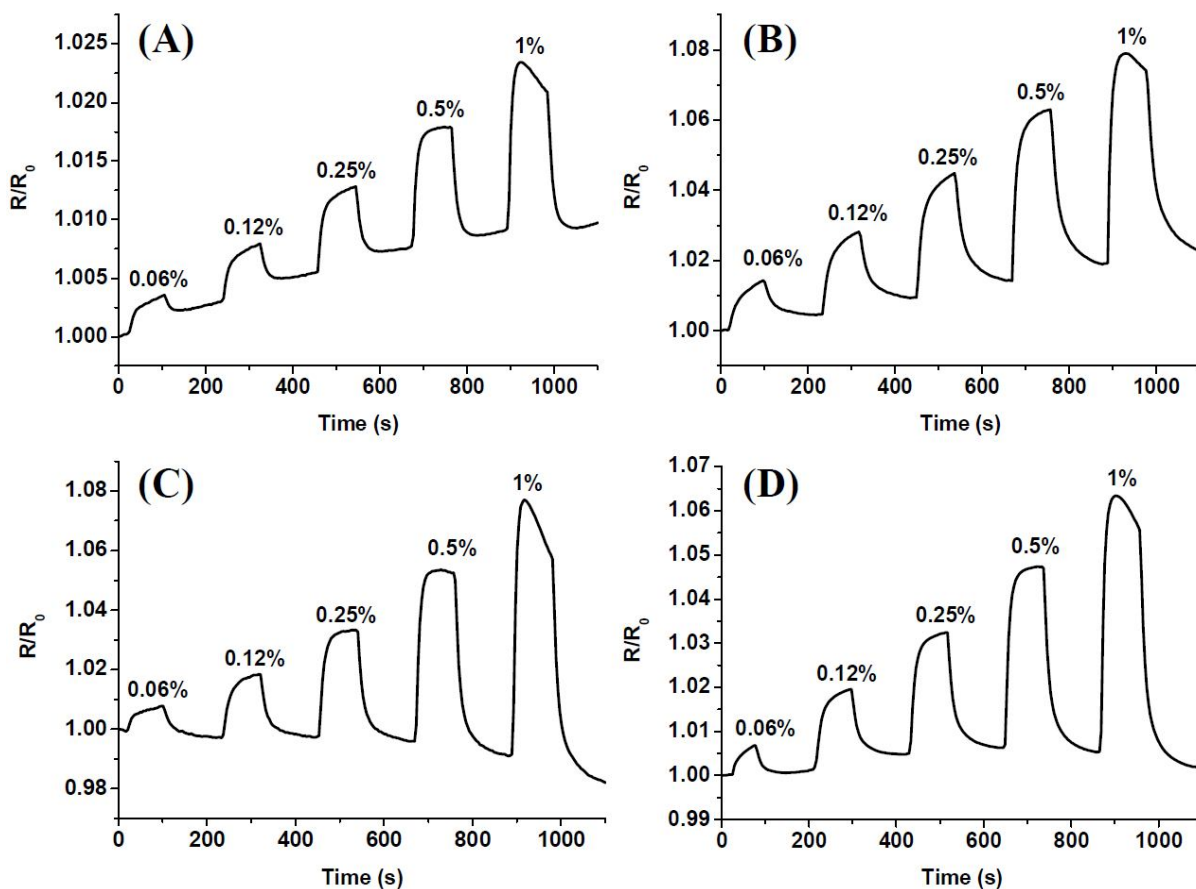


Figure 7.4. Dynamic responses of gas sensors based on polythiophene electropolymerized utilizing FeCl_3 concentrations of: (A) 0.6 mM, (B) 0.9 mM, (C) 1.5 mM, (D) 1.8 mM.

Nevertheless, similar response time was observed for the developed sensors regardless of the FeCl_3 concentration. During the exposure to hydrogen gas with the concentration of 1%, the sensors' response time was ~ 32 s and the sensors' signal recovered in 90 s to the baseline value after stopping the flow of hydrogen gas and pumping synthetic air instead. Since the shifts in sensitive films' resistances for these sensors are less than that of the sensor developed with 1.2 mM FeCl_3 , so it is expected that these sensors are a little bit faster in responding to hydrogen gas with an 8 s difference in response time towards hydrogen gas with the concentration of 1%.

The effect of selecting the FeCl_3 concentration during the electrodeposition of polythiophene nanostructures on the resultant gas sensors' responses can be assessed from Figure 7.5. It can be seen that the highest response was obtained when the

electrodeposition was conducted utilizing the concentration of 1.2 mM FeCl₃ and the lowest response was related to the electropolymerization at 0.6 mM FeCl₃.

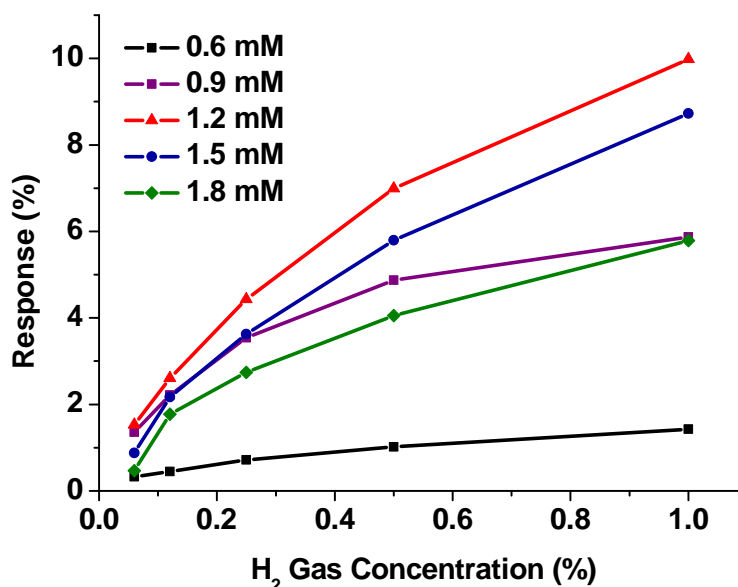


Figure 7.5. Responses of gas sensors based on polythiophene nanostructures electropolymerized with different concentrations of FeCl₃.

Comparing the gas sensors' response curves shown in Figure 7.5 with the SEM images of their sensitive films exhibited in Figure 6.6 reveals the relationship between the response of a gas sensor and the morphology of its sensitive film. As the concentration rises from 0.6 mM to 0.9 mM, the polythiophene film structure improves by the evolution of short nanofibers ~80 nm in length and ~32 nm in diameter as shown in Figure 6.6 (B) leading to an increase in response. The optimum morphology of the nanostructured polythiophene was achieved with the FeCl₃ concentration of 1.2 mM as exhibited in Figure 6.6 (C) and therefore the largest response was observed. By increasing the FeCl₃ concentration above 1.2 mM, the balance between chemical and electrochemical polymerizations breaks and an overgrowth of polymer chains was noticed in Figure 6.6 (D) and (E) causing a decline in the sensitive film porosity and ultimately its response towards hydrogen gas as shown in Figure 7.5.

The Effect of Electropolymerization's Potential

In previous discussions, the dynamic performance of sensor (B) shown in Figure 7.2 (B) was analyzed. The applied anodic potential during the electrodeposition of its sensitive film was 0.75 V. In order to determine the impact, if any, of the deposition voltage on the resultant sensor's performance, four other sensors were developed by applying either

0.65 V, 0.7 V, 0.8 V or 0.85 V during the electropolymerization each time. The concentration of FeCl_3 was kept constant at 1.2 mM in these experiments.

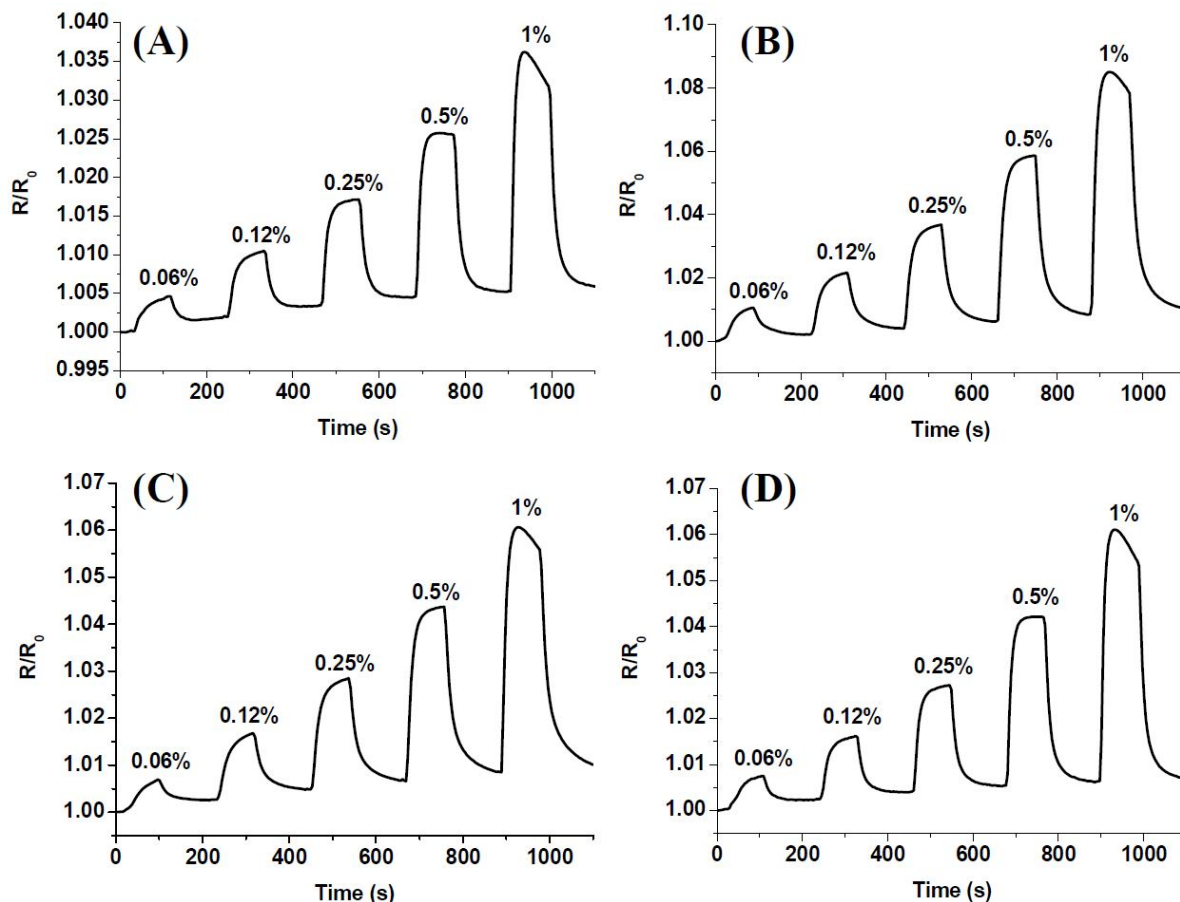


Figure 7.6. Dynamic responses of gas sensors based on polythiophene electropolymerized with the anodic potentials of: (A) 0.65 V, (B) 0.7 V, (C) 0.8 V, (D) 0.85 V.

Figure 7.6 displays the dynamic responses of the developed gas sensors. A stable baseline was observed for every sensor, since the deposition of a uniform nanostructured polythiophene sensitive film was achieved by using the 1.2 mM FeCl_3 solution as shown in Figure 6.2 (B). The response time of these sensors during the exposure to hydrogen gas with the concentration of 1% was measured and found to be 46 s. The recovery time from that concentration of hydrogen gas was 136 s. However, some differences in the response of these sensors can be noticed in Figure 7.7. The morphologies of the corresponding sensitive films were studied through SEM microscopy as shown in Figure 6.10. It has been reported earlier that increasing the oxidation voltage promotes the growth of polymer chains due to a rise in the amount of charges in the electrolyte [248]. From Figure 6.10, it can be seen that the optimum morphology in terms of 1-D nanostructures was obtained with the oxidation voltage of 0.75 V. As a result, the

response of the corresponding sensor is the largest among the others as evident in Figure 7.7. Applying higher than the optimum voltage, 0.8 V and 0.85 V, leads to overoxidation that breaks the balance between the chemical and the electrochemical polymerizations responsible for nanostructures' formation and promotes the 3-D growth of polymer chains as demonstrated in Figure 6.10 (D) and (E). The observed overgrowth decreases the surface-to-volume ratio and porosity of the sensitive films causing a reduction in their corresponding sensors' responses compared to the sensors developed by employing the deposition voltage of 0.7 V and 0.75 V as shown in Figure 7.7.

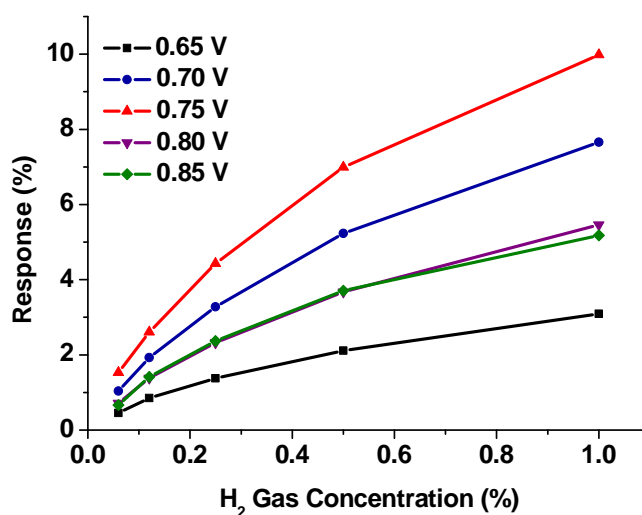


Figure 7.7. Responses of gas sensors based on polythiophene electropolymerized with the different anodic potentials.

The Effect of Nanostructured Film's Thickness

After specifying the optimum values for the FeCl₃ concentration and the applied potential during electropolymerization in terms of the resultant sensors' responses, the effect of different films' thicknesses deposited by employing the optimum concentration and potential on the sensors' responses was investigated. Therefore, four sensors based on different electrodeposition time were developed as listed in Table 5.1. Figure 7.8 shows the response graphs for these gas sensors. After running the electropolymerization for 10 minutes, a 200 nm thick polythiophene film was deposited on the surface of the conductometric transducer. The response of that sensor was the smallest among the others as shown in Figure 7.8. It has been established that at the beginning of electropolymerization, a smooth and compact polythiophene film is deposited on the working electrode due to the 2-D growth of polymer chains on the electrode's surface [285]. Therefore, the 200 nm thick sensitive film lacks porosity and

the sensor's response is generated by only the surface interaction with hydrogen gas. Nevertheless, this sensor produces a reversible change in its sensitive film's resistance during the exposure and removal of hydrogen gas as shown in Figure 7.9.

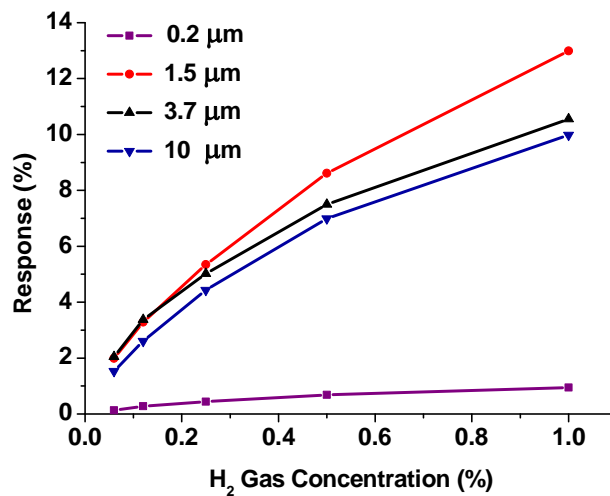


Figure 7.8. Responses of gas sensors based on nanostructured polythiophene films with different thicknesses.

The sensor based on 1.5 μm thick polythiophene film (20 minutes of deposition) has the largest response as seen in Figure 7.8. This large response can be attributed to the high surface-to-volume ratio of the nanofibers, 19–26 nm in diameter, grown from the bulk polythiophene film underneath (seed layer) as shown in Figure 6.12.

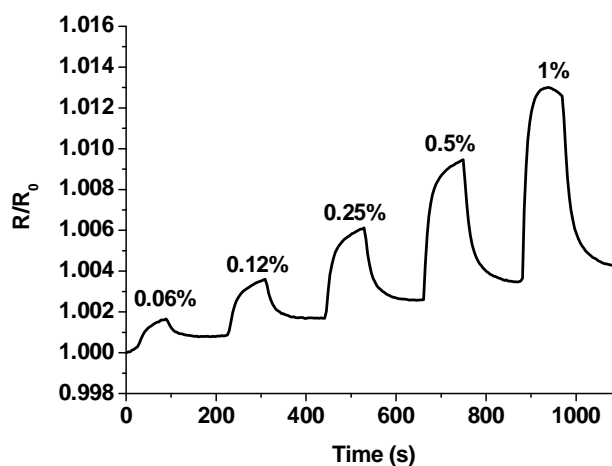


Figure 7.9. Dynamic response of the gas sensor based on 200 nm thick polythiophene film.

As the deposition time increases, the growth of nanostructures continues in addition to the increase in the overall film's thickness causing a reduction in the corresponding

sensor's response due to the close packing of nanostructures and hence affecting the film's porosity. However, it can be noticed from Figure 7.8 that increasing the film's thickness from 3.7 μm (30 minutes of deposition) to 10 μm (60 minutes of deposition) did not cause a large change in response. This phenomenon is one of the most significant advantages of employing a nanostructured film over the conventional compact film for gas sensing applications. Indeed, it was shown in an earlier study that changing the thickness of the polyaniline nanofibers based thin film from 0.2 μm to 2.0 μm did not change the sensitivity or the response time of the gas sensors towards HCl vapor with the concentration of 100 ppm [144]. They also demonstrated that the sensors based on compact polyaniline films were largely dependant on the sensitive film's thickness in their performance.

The response of the gas sensor based on 1.5 μm thick nanostructured polythiophene film is shown in Figure 7.10. Whereas the response of the sensor with 10 μm thick film is provided in Figure 7.2 (B). SEM images of these gas sensors are displayed in Figure 7.11. Both sensors have a reproducible response as shown in Figure 7.10 and Figure 7.2 (B) as evident from their response to a second exposure to hydrogen gas with the concentration of 0.12%. The sensor with the 10 μm thick film has a better baseline stability and is about 6 s faster in responding to hydrogen gas with the concentration of 1% than the sensor with 1.5 μm thick sensitive film. This can be attributed to the scarcity of nanostructures in the 1.5 μm thick film. But the sensor with 1.5 μm thick film outperforms the others in terms of response as seen in Figure 7.8 since its film is capable of sensing with whole individual nanofibers according to its morphology shown in Figure 6.12.

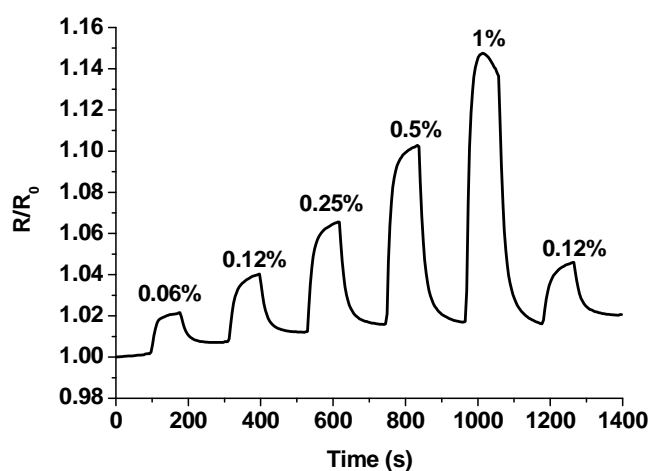


Figure 7.10. Dynamic response of the gas sensor based on 1.5 μm thick nanostructured polythiophene film.

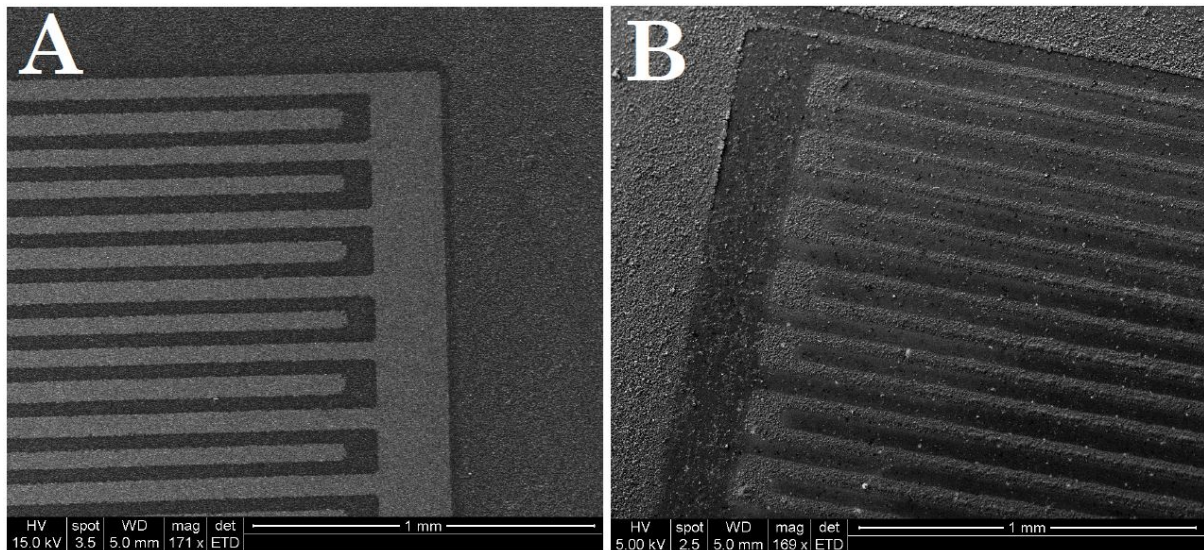


Figure 7.11. SEM images of the gas sensors based on the electropolymerized polythiophene nanostructures deposited for: (A) 20 minutes (1.5 μm thick film), (B) 60 minutes (10 μm thick film).

7.2.2 Layered SAW Gas Sensor with Chemically Synthesized Polythiophene Nanofibers Sensitive Film

The frequency response for the developed polythiophene nanofibers/ZnO/36° YX LiTaO₃ SAW gas sensor shown in Figure 7.12 were extracted through measuring the SAW scattering parameter S_{21} using a network analyzer. The sensor was operating in SH-SAW mode with a center frequency of 202.73 MHz and an insertion loss of -19.4 dB. The insertion loss is compensated by the built-in high gain RF amplifier with a power gain of ~ 30 dB as outlined in Figure 7.1.

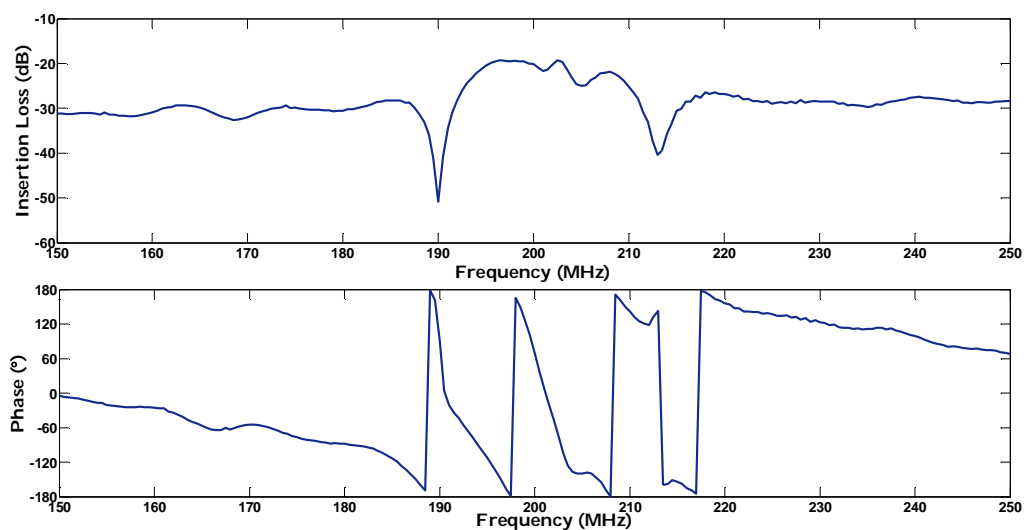


Figure 7.12. Frequency response of the layered SAW gas sensor with polythiophene nanofibers sensitive film.

During the sensor's exposure to the hydrogen gas concentrations of 0.06%, 0.125%, 0.25%, 0.5%, and 1% balanced in synthetic air, a shift in the operational frequency of 1 kHz, 2.86 kHz, 6.15 kHz, 10.74 kHz, and 16.92 kHz from the 202.73 MHz baseline was observed. The response time and recovery time for 1% hydrogen pulse were 36 s and 272 s, respectively.

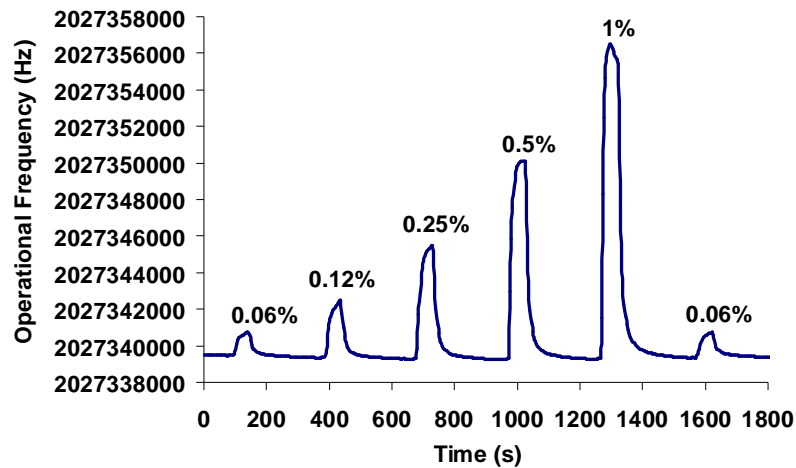


Figure 7.13. The dynamic response of the layered SAW gas sensor with polythiophene nanofibers sensitive film.

The sensor's dynamic response is shown in Figure 7.13, while the overall variation of the SAW operational frequency with hydrogen exposure is shown in Figure 7.14 [109]. The sensor was tested over a period of 2 days at room temperature and repeatable results were obtained as shown in Figure 7.13 with the start of a new pulse sequence of hydrogen gas diluted in synthetic air.

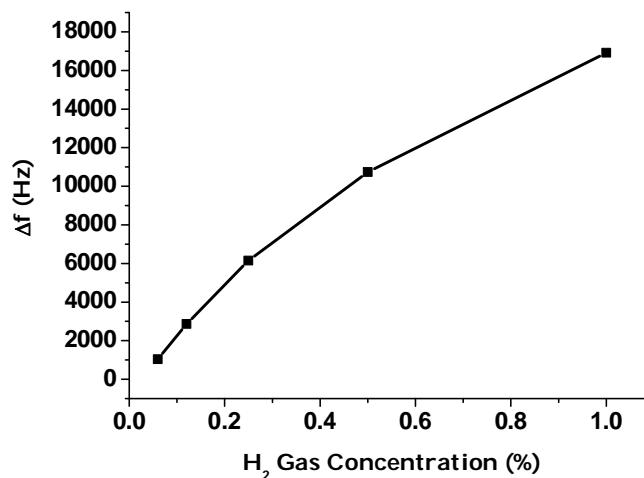


Figure 7.14. Frequency deviations of the polythiophene nanofibers based SAW gas sensor during hydrogen gas exposure.

It can be seen from Figure 7.14 that at lower concentrations of hydrogen, the frequency shift increases linearly with an increase in hydrogen gas concentration. However, at higher concentrations of hydrogen, the sensor response tends to saturate.

It was demonstrated in section 7.2.1 that the interaction between the nanostructured polythiophene sensitive film and hydrogen gas resulted in a decrease in the film's conductivity. According to the acoustoelectric coupling described in equation (3.40), it can be suggested that the conductometric sensitivity is responsible for the perturbation in the propagating SAW velocity. Furthermore, the deposited polythiophene nanofibers form a porous structure as shown in Figure 6.16 that does not satisfy the sensitive film's physical continuity condition essential for mass loading [214].

7.2.3 Gas Sensing Mechanism for Polythiophene

Since all the developed polythiophene based gas sensors were operating at room temperature with fast and completely recoverable responses, chemisorption of gaseous species remains a remote possibility. Therefore, the physisorption can be a plausible sensing mechanism instead. It has been suggested that the adsorption of polar organic vapors on poly(3-hexylthiophene) films can induce dipole moments leading to an electrostatic interaction with the polymer molecules [101].

Similarly, hydrogen gas molecules can interact with the polaron or bipolaron species on the polythiophene backbone [286]. Hence, the hydrogen molecules become polarized in the form of $H^{\delta+}-H^{\delta-}$ due to electron density induction with the polarons or bipolarons as illustrated in Figure 7.15. This electrostatic coupling restricts charge transportation along the polymer backbone causing a drop in the polythiophene conductivity in the presence of hydrogen gas. Purging the hydrogen gas with dry air flow removes the polarized hydrogen molecules, which increases the charge mobility on the polythiophene backbone. Consequently the polythiophene sensitive film's conductivity is recovered to its original value before the exposure to hydrogen gas.

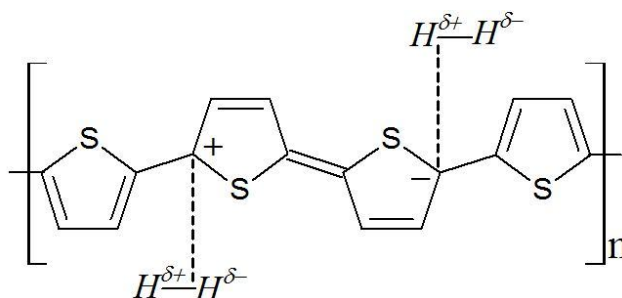


Figure 7.15. Scheme illustrating the proposed hydrogen gas sensing mechanism; reproduced for polythiophene from ref.: [286].

7.3 Gas Sensors Based on Polypyrrole Nanostructures

Both of conductometric and layered SAW gas sensors with nanostructured polypyrrole (PPY) sensitive films have been developed and tested herein. The gas sensing results for these sensors will be discussed throughout this section.

7.3.1 Conductometric Gas Sensors

The sensitive films of the conductometric gas sensors were prepared through electrochemical and chemical polymerization of PPY. Syntheses, deposition and characterization of the nanostructured PPY sensitive films have been discussed in previous chapters. Since the electropolymerization and the chemical polymerization are two different techniques for synthesizing conducting polymers, the developed gas sensors will be classified here accordingly.

Conductometric Gas Sensors Based on Electropolymerized Polypyrrole Nanowires

Three gas sensors were developed through electrodeposition of ClO_4^- doped PPY nanowires by applying the anodic charges of 13 mC, 55 mC and 90 mC and are named here as sensor A, sensor B and sensor C, respectively. The three sensors were tested at room temperature. The sensors' response curves are shown in Figure 7.16. For the purpose of this dissertation, the responses are displayed using normalized resistances. The responses with the ohmic resistance values can be found in the published Journal of Physical Chemistry C article [258].

It is evident from Figure 7.16 that sensor C had the largest response and the fastest response towards H_2 gas. For instance during the exposure to hydrogen gas with the concentration of 1%, the drop in resistance of sensor C reached saturation after 54 s. Whereas sensors A and B responded in 90 s and 86 s towards H_2 gas with the same concentration, respectively. Despite the fact that the three PPY sensitive films consist of structures in the form of nanowires, there is a slight morphological difference between them as shown in Figure 6.18. Therefore the large response of sensor C compared to the other sensors can be attributed to the high surface-to-volume ratio for its sensitive film that consists of long and uniform PPY nanowires as shown in Figure 6.18 (C) and (D). It is also worth to mention here that the dynamic response of sensor A exhibited in Figure 7.16 is rather noisy compared to that of other sensors. This difference can be caused by

the presence of a mixture of long and short nanowires in the sensitive film of sensor A that tend to tangle with each other as shown in Figure 6.18 (A).

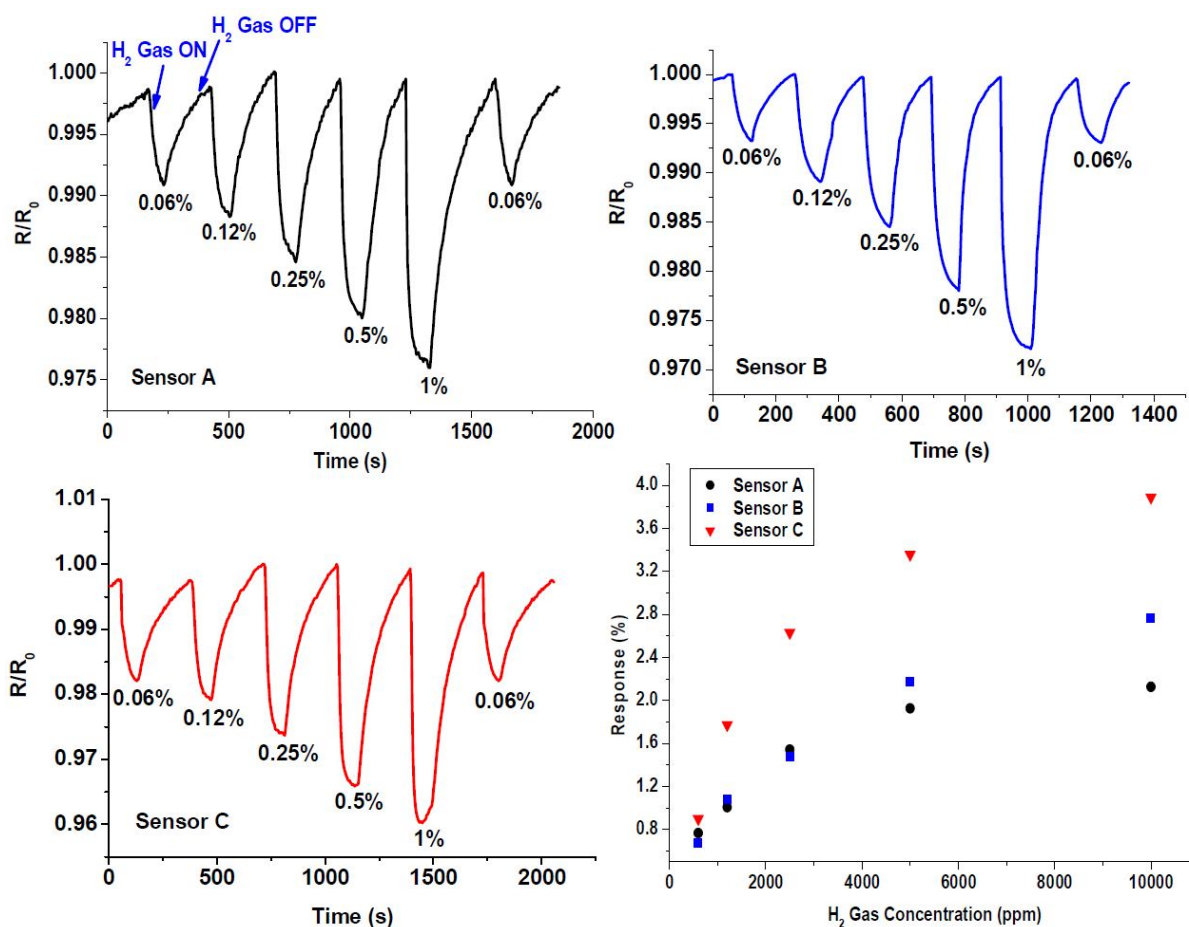


Figure 7.16. The responses of the hydrogen gas sensors based on electropolymerized ClO_4^- -doped polypyrrole nanowires.

Nowadays, there is a global interest in minimizing the use of fossil fuel to improve air quality. Hydrogen technology is playing a major role in that endeavour. In that perspective, gas sensors with a fast response to a hydrogen gas leak are critical. Although a highly sensitive H_2 gas sensor was reported by decorating PPY thin film with Pt nanoparticles, but the sensor response was slow (330 s towards hydrogen gas with the concentration of 0.1%) [134]. Whereas in this work, the response time of sensor C was 72 s during the exposure to hydrogen gas with the concentration of 0.06%. This improvement can be attributed to the high surface-to-volume ratio of the sensitive film based on PPY nanowires compared to that of the Pt decorated PPY thin film and therefore allowing for fast adsorption/desorption kinetics.

The effect of an interfering gas was also investigated in this study. For that purpose, CO gas was selected as the interfering gas. CO is a toxic gas produced as a result of incomplete combustion of petrol in conventional automobiles. In order to evaluate the

highest interference impact, the sensor with the lowest response towards H₂ gas in this study, sensor A, was chosen. Figure 7.17 shows the response of the gas sensor towards hydrogen gas with the concentration of 1% (10000 ppm) with and without the interference of CO gas with the concentration of 500 ppm.

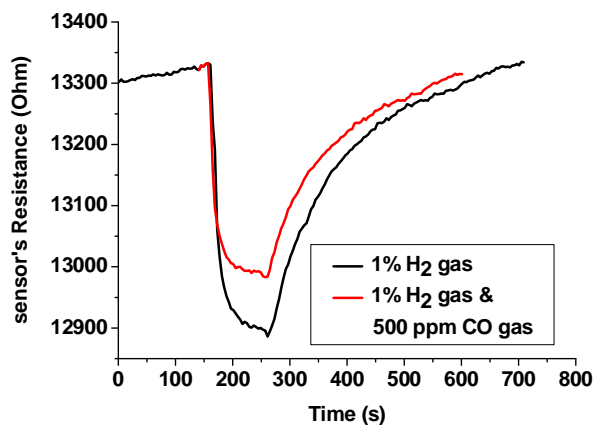


Figure 7.17. The performance of an H₂ gas sensor based on polypyrrole nanowires with and without CO gas interference.

Despite the presence of CO gas, the sensor produced a reversible decrease in its sensitive film resistance during the exposure to hydrogen gas with the concentration of 1%. However, the shift in the sensitive film resistance towards the H₂/CO gas mixture was less by 89 Ω compared to that towards pure H₂ gas. CO gas molecules can withdraw electrons from the nitrogen atoms in the pyrrole aromatic rings leading to the formation of polarons [287]. This reaction can decrease the number of adsorption sites available for interaction with H₂ gas in the bulk of the polymer film contributing to a lower response of the H₂ gas sensor during CO gas interference.

Conductometric Gas Sensor Based on Chemically Synthesized Polypyrrole Nanofibers

In this investigation, a conductometric gas sensor based on the Cl⁻ doped PPY nanofibers, shown in Figure 6.25, was tested towards different concentrations of hydrogen gas at five temperature settings (22, 38, 55, 75, and 100) °C in order to determine the optimum operating temperature for the sensor. The outcomes of this study were published in an article in the IEEE Sensors Journal [136], which received ~25 citations (ref: Scopus/ November 2012). Figure 7.18 shows the dynamic response of the sensor towards H₂ gas with different concentrations at room temperature (22°C). The response is displayed using normalized resistance for the purpose of this thesis and

the response with the actual resistance values can be found in the published report [136].

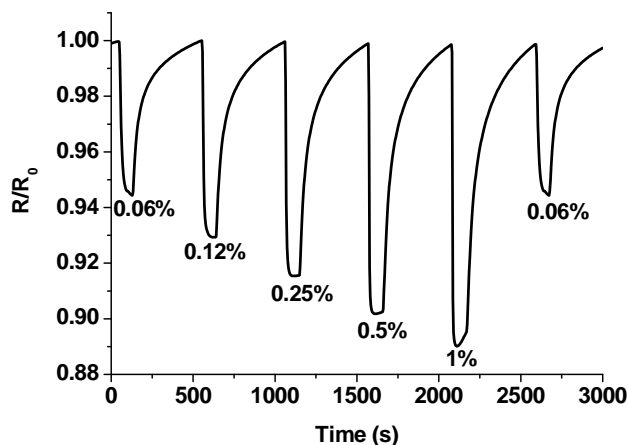


Figure 7.18. Dynamic response of the conductometric H₂ gas sensor based on Cl⁻-doped PPY nanofibers.

The sensor was found to have a response time of 43 s upon exposure to hydrogen gas with the concentration of 1% with a resistance change of 312 Ω . Resistance decreases of 157, 205, 245 and 282 Ω were obtained towards hydrogen gas with the concentrations of 0.06%, 0.12%, 0.25% and 0.5% and response times of 75, 72, 61, 61 s, respectively. Hence, it can be concluded that the largest response is obtained for 1% H₂ with the shortest response time. Recovery time was fixed at 7 min under synthetic air after the exposure to each H₂ gas pulse. The sensor's response at room temperature was calculated according to equation (7.1) and plotted in Figure 7.19.

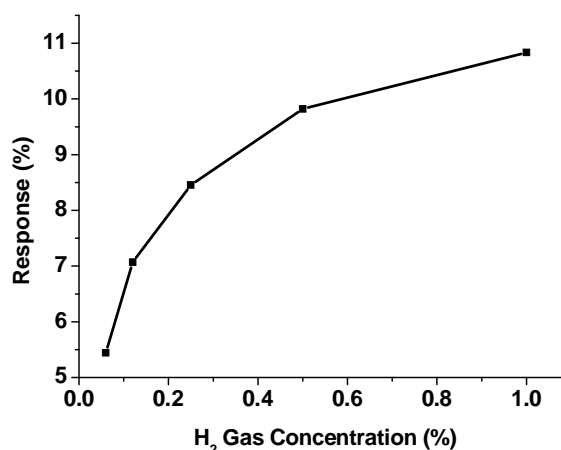


Figure 7.19. Room temperature response of the Cl⁻-doped PPY nanofibers based conductometric H₂ gas sensor.

It is evident from Figure 7.19 that the response of the Cl^- doped PPY nanofibers based sensor is about three times higher than the response of the ClO_4^- doped PPY nanowires shown in Figure 7.16, which is consistent with the observed gas sensing results for the electropolymerized polythiophene thin films discussed in section 7.2.1. This finding can be related to the difference in PPY thin film's redox property with the different molecular size for the incorporated anion. Walton et al. studied the effect of anion's molecular size on the redox properties of PPY films [288]. They observed that the PPY films doped with small anions, such as tetrafluoroborate BF_4^- , had a broad reduction peak suggesting a high mobility of the incorporated anions along the polymer backbone. On the contrary, a sharp reduction peak was found for the PPY doped with large anions, like *p*-toluenesulfonate PTS^- , due to the restricted mobility of anions. High mobility of anions in the PPY film makes the film more reactive and consequently creates large number of adsorption sites for hydrogen gas molecules. Therefore, the observed difference in response towards hydrogen gas can be related to the smaller size of the incorporated Cl^- anion compared to that of the ClO_4^- anion.

In this work, the effect of elevating the operating temperature on the gas sensor's response towards different concentrations of the hydrogen gas/synthetic air mixture was also studied. Under synthetic air only, the changes in film resistance as a function of increasing temperature from 22°C to 100°C are shown in Figure 7.20. It can be seen that the film resistance decreases, i.e. the conductivity increases, which can be related to the increase in the number of thermally activated carriers. Figure 7.21 presents the steady-state response of the sensor towards hydrogen gas at different operating temperatures.

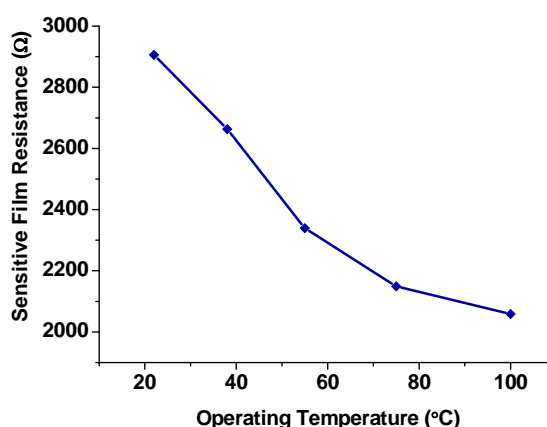


Figure 7.20. The effect of elevating the operating temperature on the polypyrrole nanofibers based conductometric sensor's resistance under synthetic air only (no hydrogen gas).

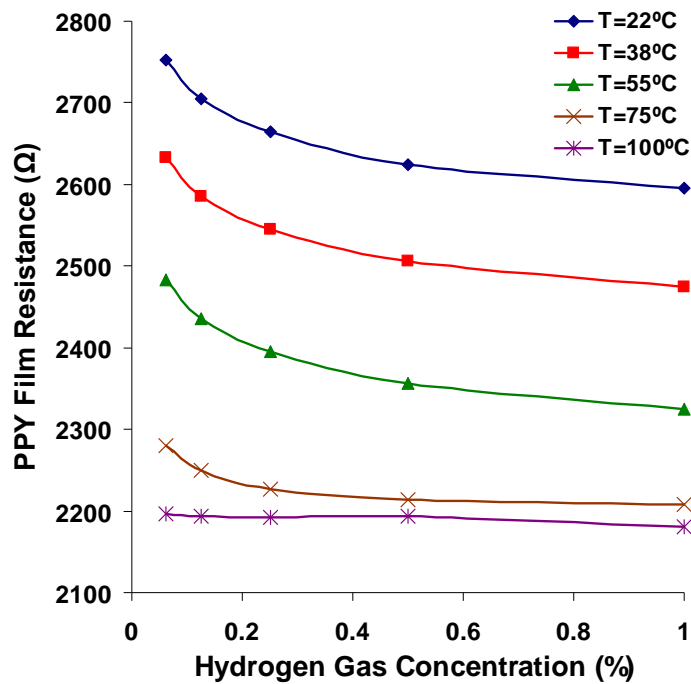


Figure 7.21. The steady-state response of the polypyrrole nanofibers based conductometric gas sensor at different operating temperatures.

The nonlinearity of the curves in the temperature range between 22°C to 55°C can be described by a Langmuir type isotherm as established in the literature [289]. At elevated temperatures, the increase in the film conductivity can be attributed to the increase of charge carriers hopping between localized states along the polymer chains in accordance with Mott's Variable Range Hopping (VRH) conduction model [290].

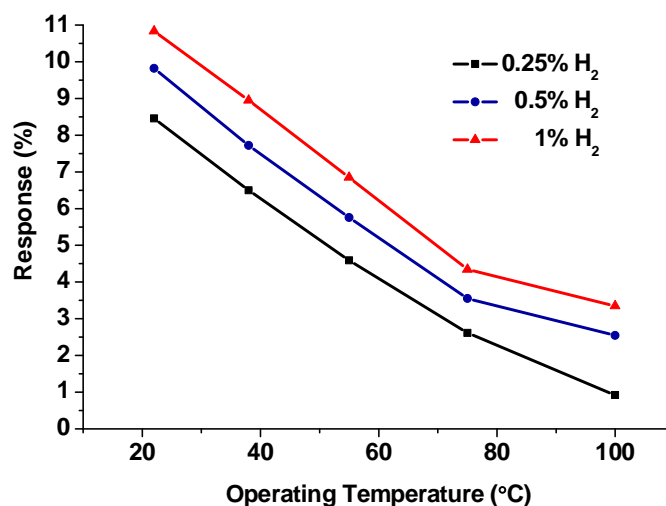


Figure 7.22. The polypyrrole nanofibers based conductometric gas sensor's response as a function of temperature increase during the exposure to 0.25%, 0.5% and 1% of hydrogen gas.

The high conductivity of the PPY nanostructured film at high temperatures makes the film inert to hydrogen gas similar to noble metals such as gold, which degrades the sensor response significantly as shown in Figure 7.21. The effect of different operating temperatures on the gas sensor response towards hydrogen gas with concentrations of 0.25%, 0.5% and 1% is shown in Figure 7.22. It can be seen that the largest response of the sensor towards hydrogen gas was observed during room temperature operation.

7.3.2 Layered SAW Gas Sensor Based on Polypyrrole Nanofibers

In addition to the conductometric sensors described in the previous section, the chemically synthesized PPY nanofibers shown in Figure 6.25 was also implemented as the sensitive film deposited on a ZnO/36° YX LiTaO₃ SAW transducer. The sensor performance towards a reducing gas (H₂) and an oxidizing gas (nitrogen dioxide NO₂) at room temperature was investigated. The outcomes of this study were published in an article in the Sensors and Actuators B: Chemical journal [137], which has been cited by ~40 articles (ref: Scopus/ November 2012).

The frequency response of the sensor was measured through the network analyzer and is shown in Figure 7.23. It was found that the sensor's center frequency was 90.92 MHz with an insertion loss of -19.48 dB. This allows for a ~10 dB of forward gain after the compensation from the built-in RF amplifier during the gas sensing experiments.

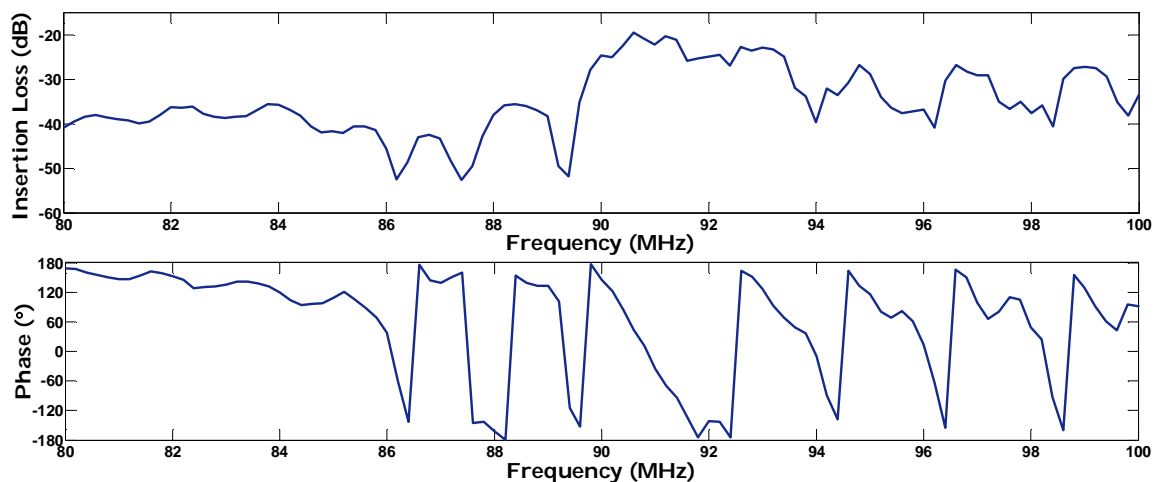


Figure 7.23. Frequency response of the layered SAW gas sensor with polypyrrole nanofibers sensitive film.

Figure 7.24 displays the dynamic response of the sensor towards H₂ gas with different concentrations mixed with synthetic air. Frequency deviations of 8.5 kHz, 12.1 kHz,

16 kHz, 18.7 kHz and 20.194 kHz were recorded during the sensor's exposure to H₂ gas with the concentrations of 0.06%, 0.12%, 0.25%, 0.5% and 1% respectively.

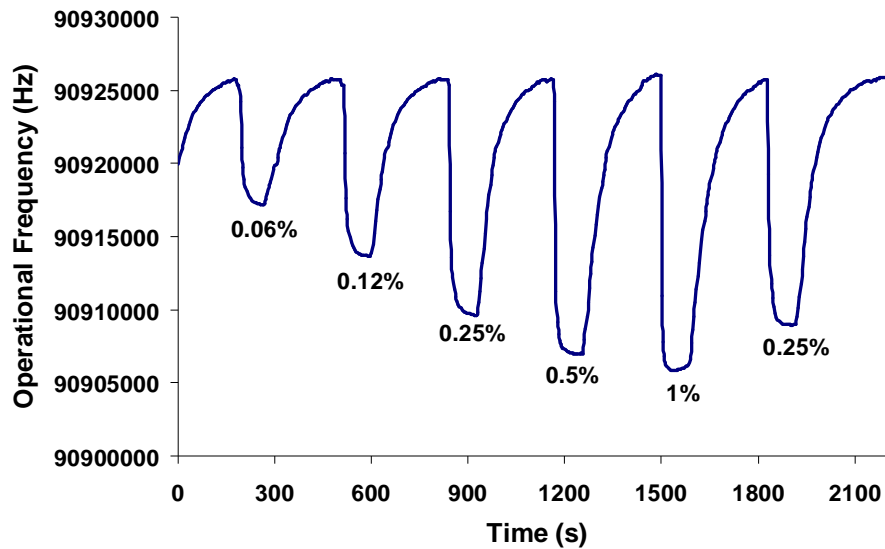


Figure 7.24. The dynamic response of the layered SAW gas sensor with polypyrrole nanofibers sensitive film towards hydrogen gas.

The response time was found to be 39 s and the recovery time was 219 s during the exposure to H₂ gas with the concentration of 1%. The overall variations of the SAW operational frequency with H₂ gas exposure is shown in Figure 7.25. It can be seen that the response is linear for low concentrations, while the sensor tends to saturate at higher concentrations.

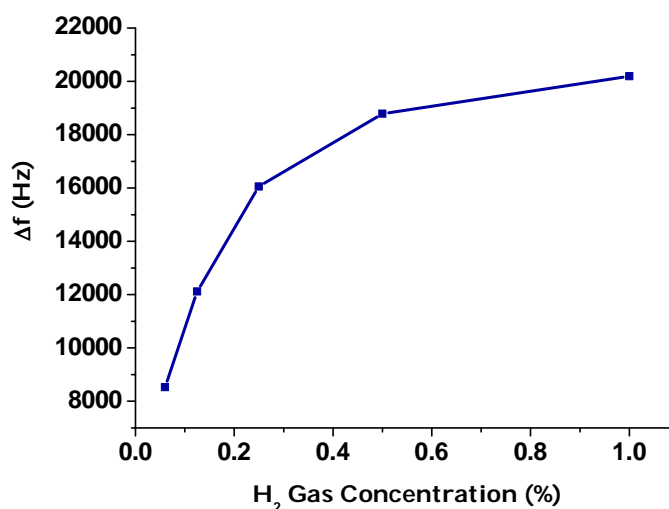


Figure 7.25. Frequency deviations of the polypyrrole nanofibers based SAW gas sensor during hydrogen gas exposure.

Nitrogen dioxide (NO_2) gas is a well-known air pollutant that is usually released during any combustion process that uses air as an oxidant such as automobile engines. It is harmful to humans by inhalation and therefore is being closely monitored by industries and governments around the world [291].

Testing the layered SAW gas sensor towards NO_2 gas revealed that the sensor was able to sense a low concentration of the toxic gas, which makes it useful for environmental studies that monitor air quality. A stable and repeatable frequency deviation of 4.5 kHz in response to a sequence of NO_2 gas pulses with a fixed concentration of 2.1 ppm was observed. Figure 7.26 shows the dynamic response of the sensor during the exposure to NO_2 gas. The 90% response time of the sensor towards 2.1 ppm of NO_2 diluted in synthetic air was 133 s and the 90% recovery time was 298 s. At higher concentrations of NO_2 no stable response was obtained perhaps due to the over-oxidation of polypyrrole that can disrupt its π -electron conjugation [127].

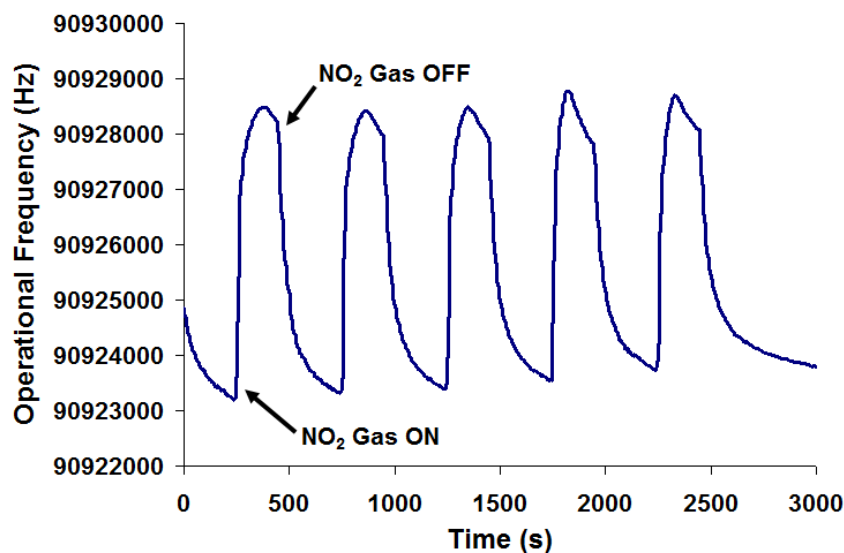


Figure 7.26. The polypyrrole nanofibers based layered SAW gas sensor's response towards 2.1 ppm of NO_2 gas diluted in synthetic air.

Despite the poisoning effect of NO_2 , the sensor surface recovered to its original state when left under the exposure of synthetic air overnight and all responses were reproducible the following day. Continuous testing at room temperature over a period of five days concluded that the sensor responses were repeatable. It was demonstrated earlier that the conductivity of a bulk PPY thin film can be affected by the presence of a reducing or oxidizing gas [117]. Therefore, it can be anticipated that the acoustoelectric coupling described by equation (3.40) is responsible for producing the observed responses of the layered SAW gas sensor.

7.3.3 Gas Sensing Mechanism for Polypyrrole

The gas sensing mechanism of PPY is still under further investigation. The interaction between PPY sensitive films and the adsorbed gas molecules can lead to a heterogeneous charge transfer. This charge transfer can release free anions in the polymer chains during the redox reactions according to the scheme shown in Figure 7.27:

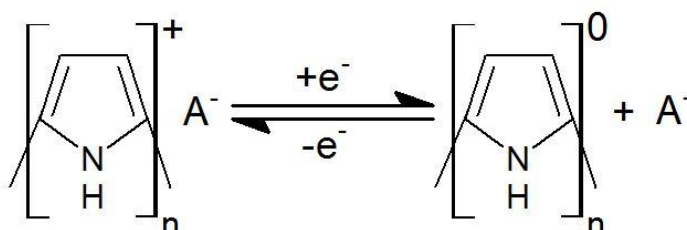


Figure 7.27. Scheme showing the redox reaction for polypyrrole [59].

Therefore a chemical modulation of the polymer doping level can occur leading to changes to the Fermi level of the organic semiconductor [292]. This effect produces variations to the electronic conductivity or the work function, Φ , of the polymer. The polarity of the response relies on the charge density exchange kinetics between the diffusing gas molecules and the polymer matrix through either oxidation ($\Delta\Phi > 0$) or reduction ($\Delta\Phi < 0$). Hence the gas molecules can be regarded as electron acceptors or donors, respectively. H_2 gas is a reducing gas. Hence it can be suggested that the interaction between PPY and H_2 gas causes the release of free anions according to the scheme in Figure 7.27 that are mobile along the polymer backbone. Therefore, the resistance of a PPY sensitive film is expected to decrease during the interaction with H_2 gas and increase during the exposure to an oxidizing agent such as NO_2 gas.

7.4 Layered SAW Gas Sensors Based on Nanostructured Polyaniline and its Alkyl-Substituted Derivatives

Three layered SAW gas sensors were developed by the author of this thesis based on nanoporous polyaniline, polyanisidine nanofibers and polyethylaniline nanofibers sensitive films. Due to the derivatisation of the of the parent polymer, polyaniline, with alkyl functional groups, these chemically synthesized conducting polymers exhibited different physical and chemical properties according to the characterization results discussed in section 6.4. The gas sensing performance of these sensors was investigated and the findings have been published by the author [157-159]. The gas sensing results of these sensors will be discussed in the upcoming subsections.

7.4.1 Layered SAW Gas Sensor Based on Nanoporous Polyaniline

The frequency response of the nanoporous polyaniline/ZnO/36° YX LiTaO₃ SAW gas sensor was measured by network analyzer and is shown in Figure 7.28. The center frequency of the sensor was found to be 94.41 MHz and the insertion loss was -15.32 dB.

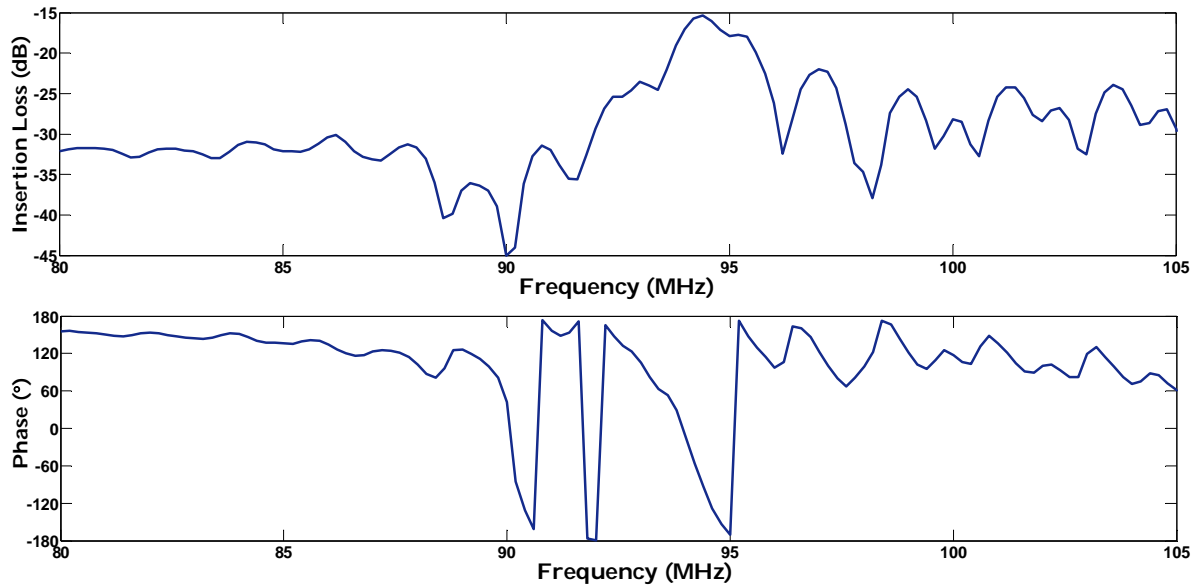


Figure 7.28. Frequency response of the layered SAW gas sensor based on nanoporous polyaniline.

The dynamic response of the nanoporous polyaniline based SAW hydrogen gas sensor is shown in Figure 7.29 [157]. While, the overall variation of the SAW operational frequency with hydrogen gas exposure is shown in Figure 7.30 [157].

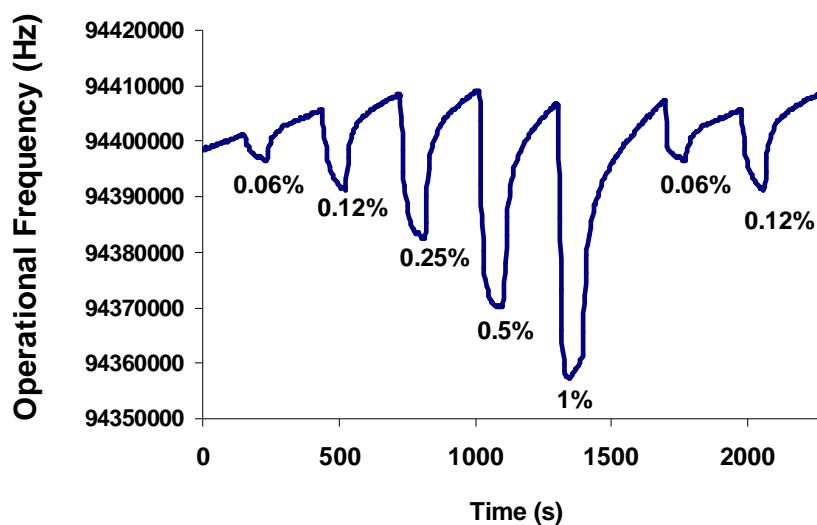


Figure 7.29. The dynamic response of the layered SAW gas sensor based on nanoporous polyaniline.

When hydrogen gas with the concentration of 0.06%, 0.12%, 0.25%, 0.5%, and 1% balanced in synthetic air were exposed to the sensor, a decrease in the operational frequency of 4 kHz, 14 kHz, 25.7 kHz, 37.6 kHz, and 48.86 kHz was recorded respectively. The response and recovery times of 46 s and 200 s were recorded during interaction with 1% of hydrogen gas, respectively. The sensor was tested over a period of 2 days at room temperature and repeatable results were obtained which is shown in Figure 7.29 with the start of a new pulse sequence beginning with the concentration of 0.06% of hydrogen gas diluted in synthetic air.

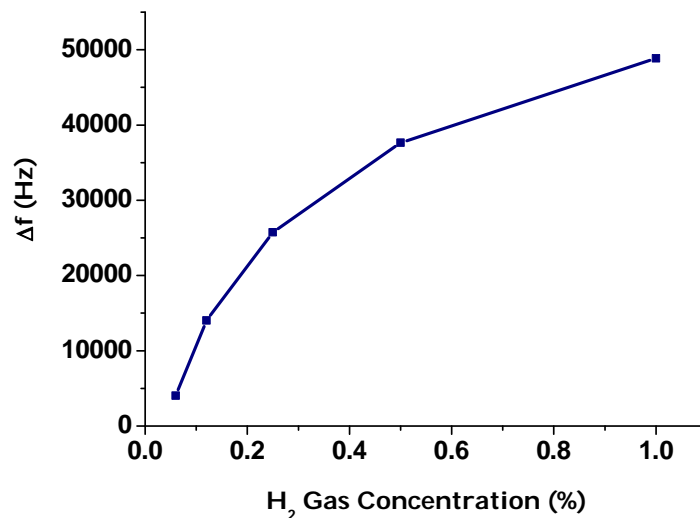


Figure 7.30. Frequency deviations of the nanoporous polyaniline based SAW gas sensor during the exposure to hydrogen gas at room temperature.

It was observed that the sensor's baseline shown in Figure 7.29 is rather unstable. This observation can be attributed to a number of factors. The most important factor is the physical nature of the sensitive film. The morphology of the sensitive film based on nanoporous polyaniline is shown in Figure 6.27. Fickian diffusion model for constant polymer film thickness on the surface of SAW device does not apply in this case because of the inability to determine the diffusion distance boundary conditions [218]. Another factor that may affect the baseline stability is the polyaniline capability of hydrogen storage [64, 293]. Furthermore due to the known high sensitivities of SAW sensors, noise and other electromagnetic interference can affect the output signal [218].

Nevertheless the response of the nanoporous polyaniline based layered SAW hydrogen gas sensor is much larger than that of the layered SAW hydrogen gas sensor based on polyaniline nanofibers presented in an earlier report [154]. The sensor based on HCl doped polyaniline nanofibers produced a response, Δf , of 3 kHz towards 1% of hydrogen gas, while the sensor based on nanoporous polyaniline produced a response of 48.86 kHz

towards the same concentration of hydrogen gas balanced in synthetic air. This significant increase in the sensor response towards hydrogen gas is directly related to the high surface area of the nanoporous polyaniline compared to the polyaniline nanofibers according to the BET results mentioned in section 6.4.1.

It has been established in literature that the conductivity of polyaniline nanofibers increases during the interaction with hydrogen gas [64, 240]. Also hydrogen uptake by polyaniline has been suggested [64, 293]. Therefore, both of the acoustoelectric coupling (conductometric sensitivity) and mass loading can be contributing to the layered SAW sensor's response. However, the hydrogen storage in the electrospun polyaniline fibers was mainly observed at high hydrogen gas pressure (~80 bar) exposure to heated polyaniline fibers at 100 °C or higher [293]. Whereas the layered SAW gas sensor based on nanoporous polyaniline in this thesis was tested at atmospheric pressure and room temperature. Therefore, it can be suggested that the acoustoelectric coupling is dominant over the mass loading in producing the response shown in Figure 7.29 since hydrogen uptake is negligible at these operating conditions.

7.4.2 Layered SAW Gas Sensor Based on Polyanisidine Nanofibers

The frequency response of the polyanisidine nanofibers/ZnO/36° YX LiTaO₃ SAW gas sensor is shown in Figure 7.31. The SAW sensor was operating in SH-SAW mode with a center frequency of 91.622 MHz and an insertion loss of (-13.07 dB).

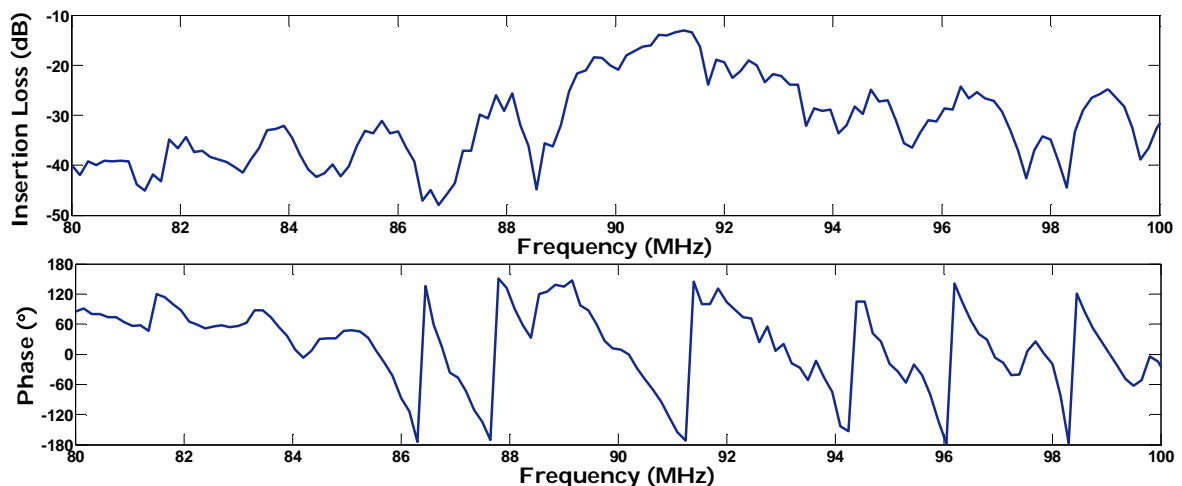


Figure 7.31. Frequency response of the layered SAW gas sensor based on polyanisidine nanofibers.

The dynamic response of the sensor towards different concentrations of the hydrogen gas/synthetic air mixture is shown in Figure 7.32 and the overall shifts in the SAW operational frequency during the interaction with hydrogen gas is shown in Figure 7.33.

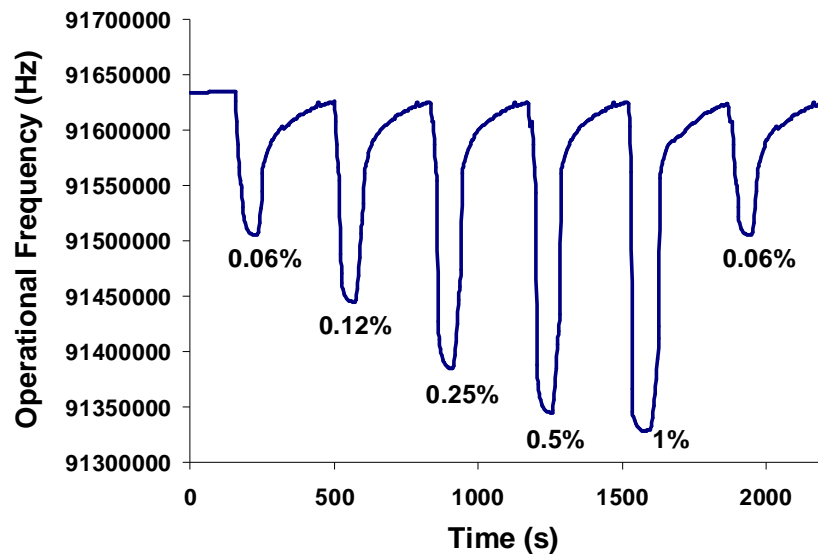


Figure 7.32. The dynamic reponse of the layered SAW gas sensor based on polyanisidine nanofibers.

By exposing the sensor to hydrogen gas with the concentrations of 0.06%, 0.125%, 0.25%, 0.5% and 1% balanced in synthetic air, a shift in its operational frequency of 127 kHz, 178 kHz, 239 kHz, 277 kHz and 294 kHz was observed respectively. The response time towards 1% H₂ was 72 s and the recovery time was 234 s.

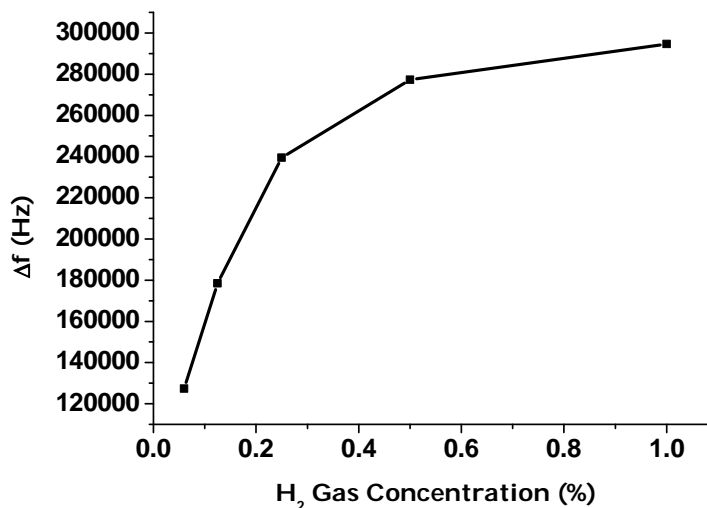


Figure 7.33. Frequency shifts of the SAW gas sensor based on polyanisidine nanofibers during the interaction with hydrogen gas.

The sensor was tested over a period of 2 days at room temperature and repeatable results were obtained which is shown in Figure 7.32 with the start of a new pulse

sequence beginning with the concentration of 0.06% of hydrogen gas diluted in synthetic air. The high frequency deviations of the sensor due to the interaction with hydrogen gas as observed in Figure 7.33 can be attributed to the high surface-to-volume ratio of the polyanisidine nanofibers as demonstrated in Figure 6.29. Also it can be seen from Figure 6.29 that the nanofibers are not densely packed with each other. This particular feature is very advantageous for gas sensing applications since it allows for deep penetration of target gas molecules. Also such separation between the polymer nanofibers makes gas sensing possible over the entire nanofiber length, which increases the sensor's response compared to that of its parent polymer, polyaniline, nanofibers [154]. Since the UV-vis spectrum for polyanisidine nanofibers shown in Figure 6.30 suggested that the polymer was in its emeraldine oxidation state, then the acoustoelectric coupling is expected to be responsible for the sensor's response.

7.4.3 Layered SAW Gas Sensor Based on Polyethylaniline Nanofibers

The network analyzer was utilized to measure the frequency response of the polyethylaniline nanofibers/ZnO/36°YX LiTaO₃ SAW gas sensor. The frequency response of the sensor is shown in Figure 7.34. It was observed that the sensor's center frequency was 83.958 MHz with an insertion loss of -19.64 dB.

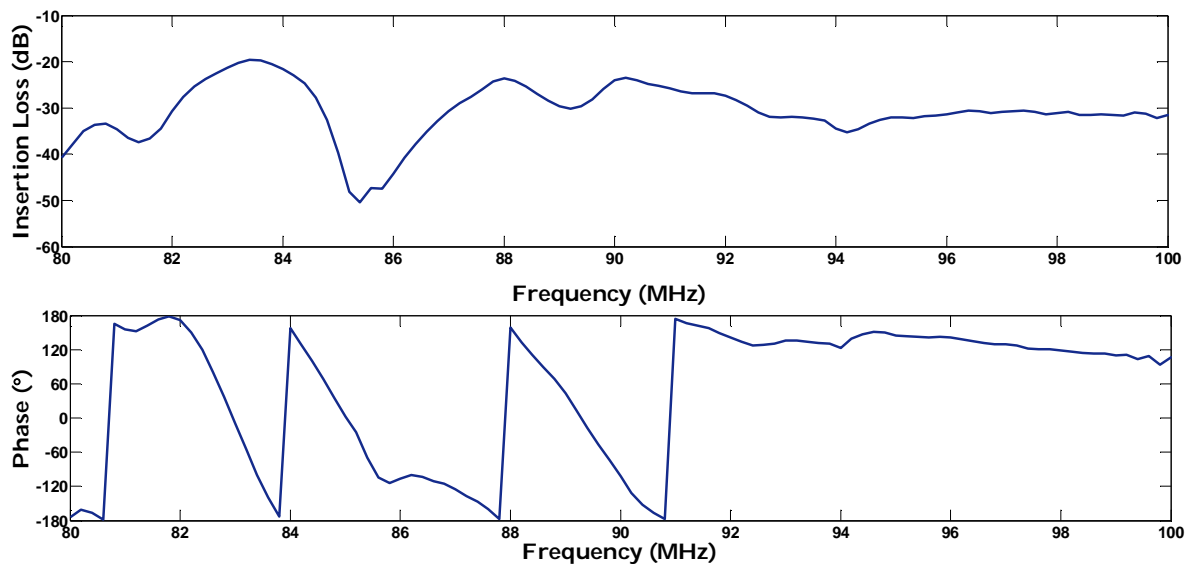


Figure 7.34. The frequency response of the polyethylaniline nanofibers/ZnO/36°YX LiTaO₃ SAW gas sensor.

The sensor was tested towards hydrogen gas with different concentrations at room temperature. Figure 7.35 presents the dynamic response of the sensor. It can be seen that the sensor has a stable baseline and the response is reproducible as evident from

the sensor's response to a second exposure of 0.12% of H₂ gas. The recorded frequency deviations with respect to hydrogen gas concentrations are shown in Figure 7.36.

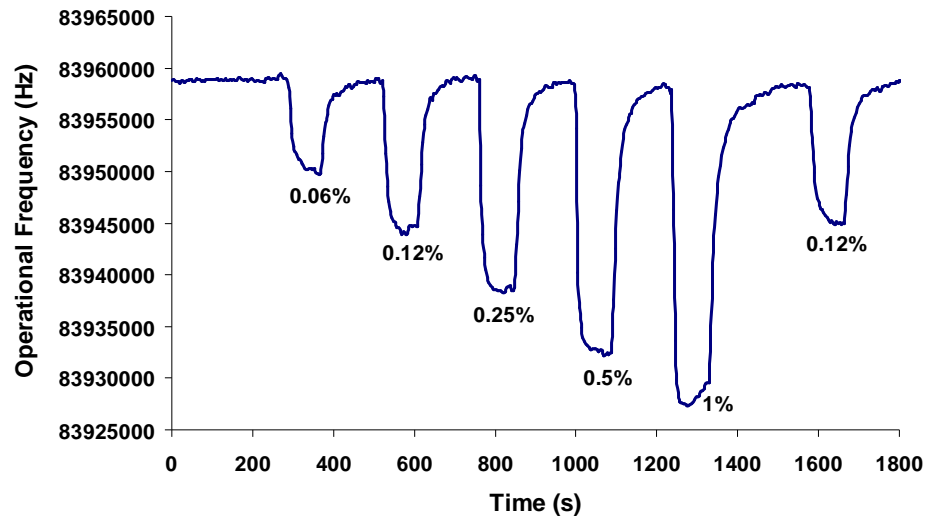


Figure 7.35. The dynamic response of the layered SAW gas sensor based on polyethylaniline nanofibers.

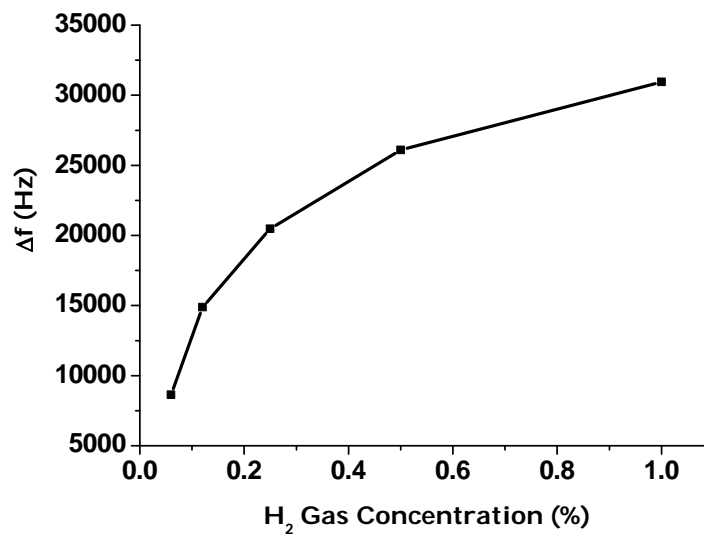


Figure 7.36. Frequency shifts of the layered SAW gas sensor based on polyethylaniline nanofibers during the interaction with hydrogen gas.

The frequency shifts of 8.6 kHz, 14.8 kHz, 20.5 kHz, 26.1 kHz and 31 kHz were recorded towards 0.06%, 0.12%, 0.25%, 0.5% and hydrogen gas with the concentration of 1% balanced in synthetic air respectively. The 90% response time was 54 s during the exposure to 1% H₂ and the recovery time was 148 s. It can be anticipated that the observed fast response and stable baseline were attributed to the high surface-to-volume ratio and porosity of the polyethylaniline nanofibers based sensitive film shown in

Figure 6.31. Similar to other conducting polymers, the acoustoelectric coupling is believed to be responsible for producing the observed SAW gas sensor's response.

7.4.4 Gas Sensing Mechanism for Polyaniline and its Alkyl-Substituted Derivatives

A proposed hydrogen gas sensing mechanism for polyaniline thin films is shown in Figure 7.37. In this mechanism, hydrogen gas molecules react with the charged amine nitrogen sites along the doped polyaniline chains. Consequently, the hydrogen bond dissociates and new N–H bonds are formed that can make bridges between surrounding polyaniline chains causing an increase in the charge transfer along the polymer backbone. Therefore the conductivity of polyaniline increases after hydrogen adsorption. Exposing the sensor to synthetic air releases the chemisorbed hydrogen molecules and returns the polymer to its original conductivity state.

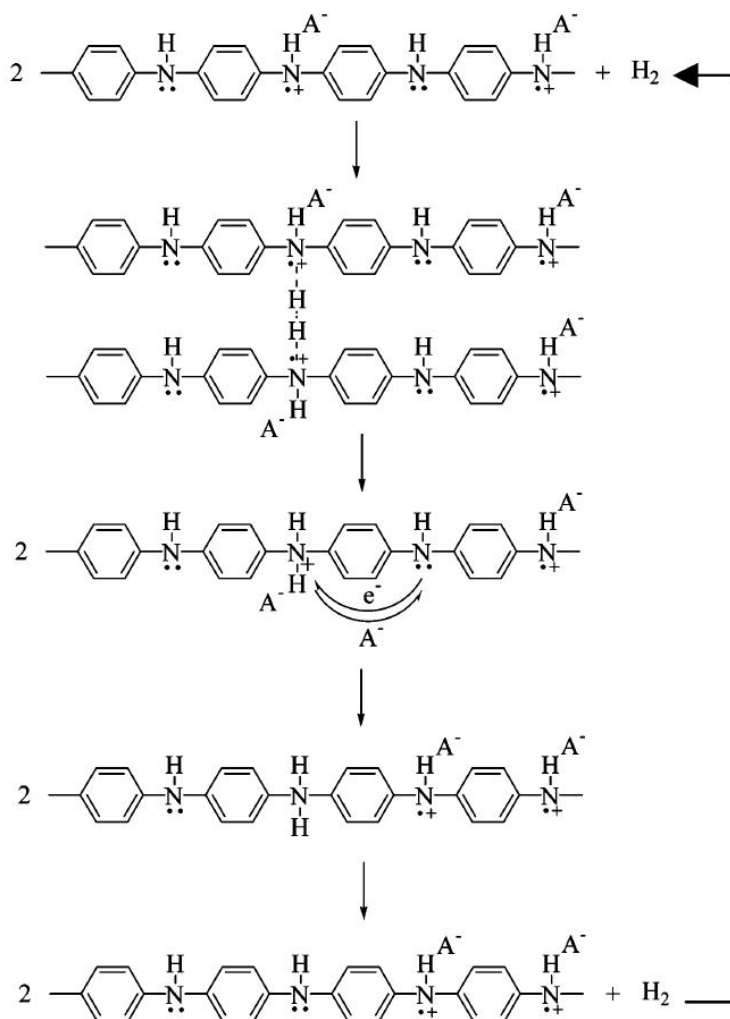


Figure 7.37. Scheme illustrating the proposed hydrogen gas sensing mechanism for polyaniline and its alkyl-substituted derivatives [64].

Since the chemisorption of hydrogen gas can only take place at the amine nitrogen sites on the polyaniline chain. Therefore, it can be suggested that this mechanism is also viable for polyaniline derivatives since the functional groups such as OCH_3 for polyanisidine and CH_3 for polyethylaniline are inert to the diffusing hydrogen gas.

7.5 Graphene/Polyaniline Nanocomposite Based Gas Sensor

In this dissertation, a gas sensor based on the graphene/PANI nanocomposite was fabricated and tested towards H_2 gas with different concentrations balanced in synthetic air. Since polyaniline (PANI) in its nanofibers form is a well known sensing material for H_2 gas [64, 240], another gas sensor was fabricated and tested based on PANI nanofibers with the same doping degree of the PANI as in the graphene/PANI nanocomposite in order to benchmark the graphene/PANI based sensor performance against a well known polymer system. Additionally for comparison purposes, an H_2 gas sensor based on graphene was also fabricated and tested under the same experimental conditions. Figure 7.38 displays the dynamic responses of the three gas sensors and their sensitivities are plotted in Figure 7.39 [182].

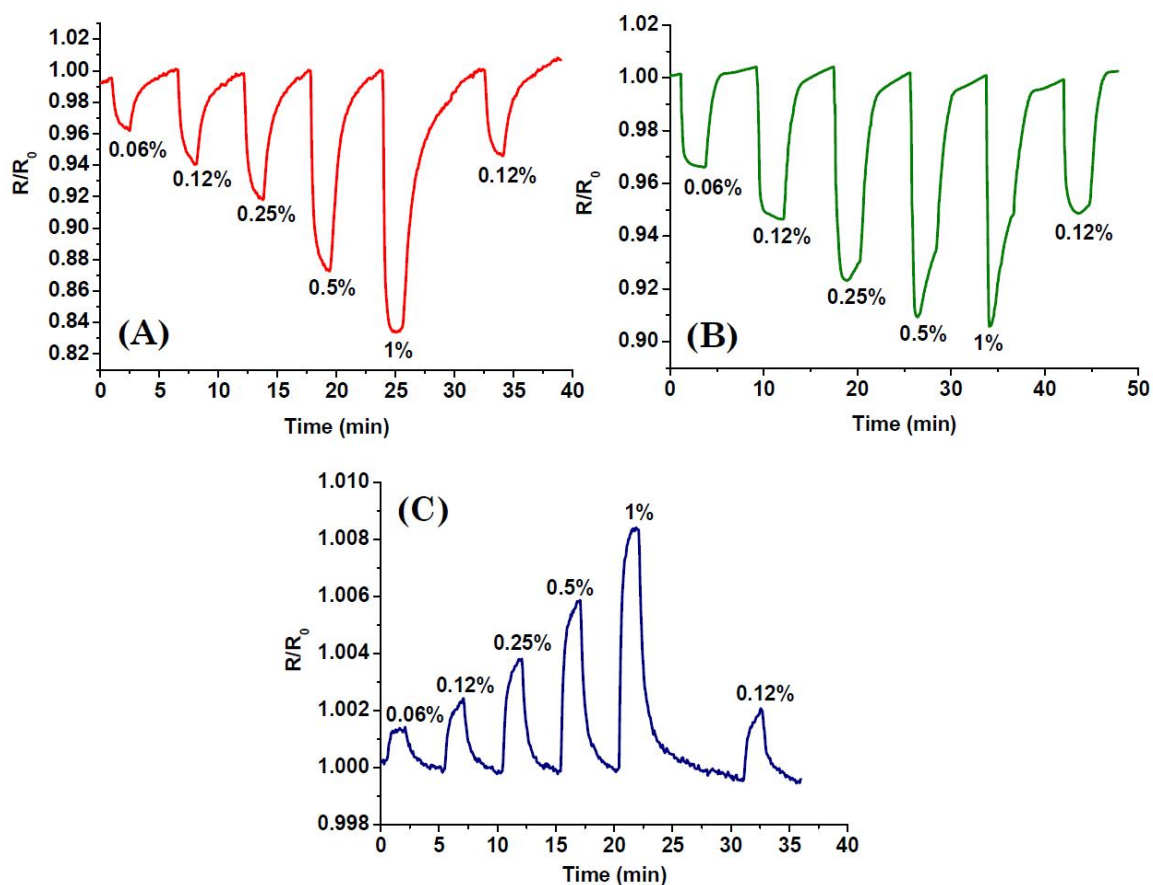


Figure 7.38. The dynamic responses of the conductometric H_2 gas sensors with sensitive layers of: (A) graphene/PANI, (B) PANI nanofibers and (C) graphene.

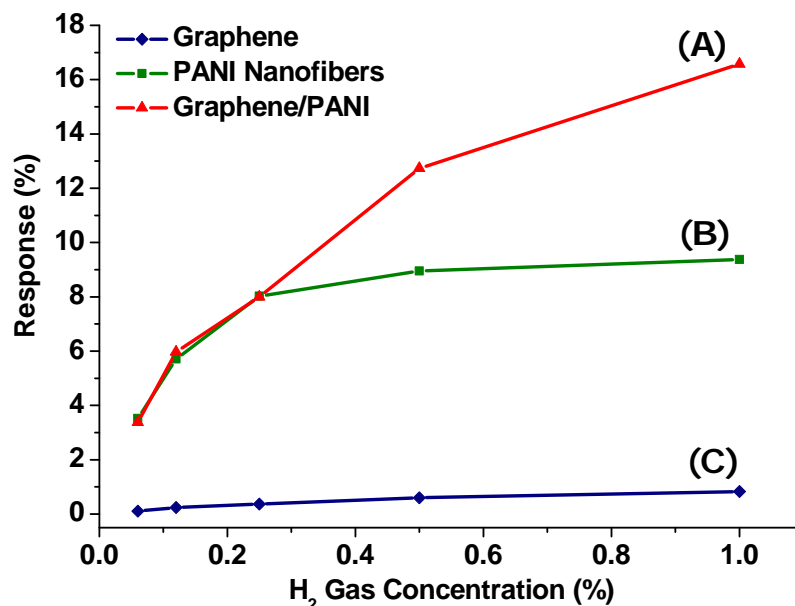


Figure 7.39. Responses of the conductometric H₂ gas sensors with sensitive layers of: (A) graphene/PANI, (B) PANI nanofibers and (C) graphene.

During the exposure to H₂ gas with the concentration of 1% balanced in synthetic air, the different sensors responded differently. The graphene based sensor's response was 0.83%. The response of the PANI nanofibers based sensor was 9.38%, while the graphene/PANI based sensor's response was 16.57%. It can be seen from Figure 7.39 that for low concentrations of H₂ gas (0.06%, 0.12%, 0.25%) the responses of the graphene/PANI nanocomposite and PANI nanofibers based sensors are similar. This similarity is caused by the fact that the same doping degree of PANI was achieved for both sensors. However for higher concentrations of H₂ gas, the PANI nanofibers based sensor response saturates. An earlier study suggested that the chemisorbed H₂ can react with oxygen from the sensor's environment to produce H₂O [294]. They also showed that the presence of H₂O ruins the ability of PANI to sense H₂. Similar effects might also deteriorate the response of the PANI sensor herein at high H₂ concentrations Figure 7.38 (B) due to the presence of 21% oxygen in the synthetic air. However, the presence of graphene nanosheets, which are employed to enhance the surface area of the overall nanostructure, resulted in the formation of PANI nanofibers with higher porosity than the pristine PANI nanofibers. As a result, the excess H₂O produced during the exposure to high concentrations of H₂ can be more easily released from the surface and hence the response does not deteriorate. This observation is supported by published results in literature, where it was found that the diameter of the PANI nanofibers has a direct effect on the H₂ gas sensing performance [154].

Hydrogen gas is a reducing agent and the mechanisms of its interaction with the sensitive materials considered herein are largely governed by the chemical properties of each material. For graphene synthesized through chemical modification, which is considered in this study, the residual epoxide and carboxylic groups in the product are electron-withdrawing and promote holes in the valence band [33]. Therefore, the interaction with a reducing (electron donating) type gas such as NH_3 would cause depletion of holes from the valence band and hence an increase in the materials' resistance [33, 197]. This mechanism is applicable to the graphene based sensor where the sensitive film resistance increases during the interaction with different concentrations of H_2 gas balanced in synthetic air as shown in Figure 7.38 (C).

Hence, both graphene and PANI interact with H_2 gas, but with opposite effects. For the graphene/PANI nanocomposite, the H_2 gas sensing mechanism will be governed by the dominant interaction. From the dynamic response of the graphene/PANI nanocomposite towards H_2 gas shown in Figure 7.38 (A), it can be concluded that the PANI gas sensing mechanism is the dominant one. This idea is also supported by the SEM study of the developed graphene/PANI nanocomposite as demonstrated in Figure 6.33. According to the SEM images, it is clear that PANI nanostructures cover the whole surface uniformly. Therefore the charged amine nitrogen sites on the PANI backbone are largely accessible to H_2 gas molecules resulting in the dominant PANI H_2 gas sensing mechanism.

It is evident from Figure 7.39 that the response of the graphene/PANI nanocomposite towards H_2 gas is noticeably higher than that of graphene and PANI individually due to the high surface-to-volume ratio of the graphene/PANI nanocomposite as shown in Figure 6.33 and Figure 6.34. Hence, the graphene/PANI nanocomposite's morphology permits deep penetration of H_2 gas molecules into the sensitive film.

Table 7.1. Response time and recovery time of the graphene/PANI, PANI nanofibers and graphene based gas sensors towards 1% of H_2 gas.

Sensitive Film	Response Time (s)	Recovery Time (s)
Graphene/PANI	68	444
PANI Nanofibers	36	308
Graphene	90	496

The response and recovery times of the developed gas sensors during the exposure to H₂ gas with the concentration of 1% are listed in Table 7.1. The slowest response was that of the graphene based sensor due to its weak interaction with H₂ gas as shown in Figure 7.38 (C) and Figure 7.39. The response time has improved with the graphene/PANI nanocomposite sensitive film because of the incorporation of PANI which features a fast response towards H₂ gas [240]. So it can be suggested that a compromise between the response time and the sensitivity has been achieved with the graphene/PANI nanocomposite based gas sensor.

7.6 Summary

The gas sensing results for the nanostructured conducting polymers and graphene/PANI nanocomposite based gas sensors have been discussed throughout this chapter. The experimental setup for testing the developed conductometric and layered SAW gas sensors was described in section 7.1. The gas sensing performance of every gas sensor has been analyzed by the author of this thesis in sections 7.2–7.5. The key outcomes are summarized as follows:

- Gas sensors based on nanostructured polythiophene thin films: the effects of polythiophene electropolymerization parameters on the gas sensing performance of conductometric gas sensors were investigated. On the other hand, chemically synthesized polythiophene nanofibers were employed as the sensitive film on a layered SAW gas sensor. Testing these gas sensors towards hydrogen gas at room temperature revealed the following findings:
 - Electropolymerization of thiophene utilizing FeCl₃ solution provided more sensitive and faster gas sensor than employing LiClO₄ based electrolyte. Indeed, the response time of the Cl⁻ doped polythiophene based gas sensor towards H₂ gas with the concentration of 1% was 40 s. On the contrary, the response time of the ClO₄⁻ doped polythiophene based gas sensor was 79 s towards the same concentration of H₂ gas. The observed dissimilarities between these gas sensors, including baseline stability, were attributed to the difference between the physical properties of a nanostructured sensitive film compared to its bulk counterpart.
 - The choice of the concentration of FeCl₃ solution during electropolymerization affected the developed gas sensor's performance. This observation was attributed to the morphological differences between the polythiophene films deposited with FeCl₃ concentrations of 0.6–1.8 mM as shown in Figure 6.6. The gas sensor with

the largest response was obtained by utilizing the 1.2 mM FeCl₃ solution during electropolymerization because of the formation of a nanostructured film containing nanofibers with diameters in the range of 10–40 nm.

- The effect of selecting the applied electropolymerization potential, (0.65–0.85 V), on the developed gas sensor performance was investigated. The gas sensor with the sensitive film deposited with 0.75 V achieved the highest sensitivity towards hydrogen gas due to the high surface-to-volume ratio of its nanostructured sensitive film. Nevertheless, a stable baseline was observed for all the sensors developed by polythiophene electropolymerization with different potentials. The response time of these gas sensors towards H₂ gas with the concentration of 1% was 46 s and the recovery time was 136 s.
- Gas sensors with different nanostructured polythiophene film's thickness have been evaluated. The gas sensor with the 1.5 μm thick polythiophene film had the largest response. This finding can be attributed to the high surface-to-volume ratio of the nanofibers (19–26 nm in diameter) grown from the bulk seed layer as shown in Figure 6.12. Increasing the film thickness above 1.5 μm did not cause a significant decrease in the sensors' responses towards H₂ gas, which is one of the merits of utilizing nanostructured films for gas sensing applications according to the literature review which was presented in Chapter 2.
- The layered SAW gas sensor based on chemically synthesized polythiophene nanofibers, with diameters in the range of 60–110 nm, had a stable baseline on 202.73 MHz. By exposing the sensor to H₂ gas with the concentration of 1%, a 16.92 kHz shift in its operational frequency was observed. The response and recovery times were 36 s and 272 s, respectively.
- Since the experimental observation herein suggested that the conductivity of polythiophene is dropping upon its interaction with H₂ gas, an H₂ gas sensing mechanism has been proposed based on polaron and bipolaron transportation restriction due to the electrostatic coupling of polarized H₂ gas molecules.
- Gas sensors based on nanostructured polypyrrole thin films: conductometric gas sensors and a layered SAW gas sensor based on polypyrrole nanostructures were fabricated and tested by the author of this thesis. The key findings of the gas sensing experiments on these gas sensors are summarized as follows:
 - The largest response for the conductometric gas sensors based on electrodeposited ClO₄⁻ doped polypyrrole nanowires was 3.9% towards H₂ gas with the concentration of 1% at room temperature. Whereas the conductometric gas sensor based on chemically synthesized Cl⁻ doped polypyrrole nanofibers

- had a response of 10.8% towards the same concentration of H₂ gas at room temperature. According to the published literature, this observation can be related to the difference in polypyrrole's redox property because of the different molecular size for the counterion.
- The performance of a conductometric gas sensor based on polypyrrole nanofibers at elevated operating temperatures (38–100 °C) was investigated. It was found that the polypyrrole film's resistance decreases at high temperatures before the exposure to H₂ gas due to the increase in the number of thermally excited charge carriers. However as the temperature rises and polypyrrole's conductivity increases, polypyrrole becomes similar to a noble metal and less sensitive to H₂ gas. Consequently, the sensor's response deteriorates at high temperatures. Therefore the largest response of the sensor towards H₂ gas was found to be at room temperature (22 °C).
 - Room temperature testing of the polypyrrole nanofibers/ZnO/36° YX LiTaO₃ SAW gas sensor towards H₂ gas with the concentration of 1% and towards NO₂ gas with the concentration of 2.1 ppm produced a deviation in its operational frequency of 20.194 kHz and 4.5 kHz from a 90.92 MHz baseline, respectively. The sensor's response times towards these concentrations of H₂ and NO₂ gases were 39 s and 133 s, respectively. The observed responses were reproducible.
 - The proposed gas sensing mechanism for polypyrrole is based on the chemical modulation of the polymer doping level due to a heterogeneous charge transfer. The interaction with a reducing gas such as H₂, free anions can be released and become mobile along the polymer backbone leading to an increase in its conductivity. This process is reversed during the interaction with an oxidizing gas such as NO₂.
- Gas sensors based on nanostructured polyaniline and its alkyl-substituted derivatives: layered SAW gas sensors were developed with nanoporous polyaniline, polyanisidine nanofibers and polyethylaniline nanofibers sensitive films. Testing these gas sensors towards H₂ gas at room temperature revealed the following findings:
- The nanoporous polyaniline/ZnO/36° YX LiTaO₃ SAW gas sensor responded to H₂ gas with the concentration of 1% with a frequency shift of 48.86 kHz from a 94.41 MHz baseline. The response time was 46 s and the recovery time was 200 s. The layered SAW gas sensor based on nanoporous polyaniline outperformed a similar sensor based on polyaniline nanofibers reported in

- literature due to the high porosity and surface area of the nanoporous polyaniline.
- During the exposure of polyaniline nanofibers/ZnO/36° YX LiTaO₃ SAW gas sensor to H₂ gas with the concentration of 1% at room temperature, a frequency shift of 294 kHz from a 91.62 MHz baseline was observed. The response time towards this H₂ gas concentration was 72 s and the recovery time was 234 s. Morphological analysis of the polyaniline nanofibers based sensitive film revealed that the nanofibers were not densely packed, which permits deep penetration of target gas molecules and makes gas sensing possible over the entire nanofiber length. Consequently, the response of this sensor towards H₂ gas was higher than the layered SAW gas sensors based on nanoporous polyaniline and polyethylaniline nanofibers.
 - The polyethylaniline nanofibers/ZnO/36° YX LiTaO₃ SAW gas sensor had a stable baseline of 83.958 MHz. A frequency shift of 31 kHz was observed during the exposure to H₂ gas with the concentration of 1%. The response and recovery times were 54 s of 148 s, respectively. The gas sensor produced repeatable responses towards H₂ gas.
 - The proposed hydrogen gas sensing mechanism for polyaniline and its alkyl-substituted derivatives is based on the chemisorption of hydrogen molecules at the charged amine nitrogen sites on the polymer backbone. The formation of new N–H bonds is anticipated that can make bridges between adjacent polyaniline chains leading to an increase in its conductivity. Upon the desorption of H₂ gas, these temporary bridges break and the polymer returns to its original conductivity state.
- Gas sensor based on graphene/polyaniline nanocomposite: the author of this thesis evaluated the performance of this conductometric gas sensor with respect to conductometric gas sensors based on polyaniline nanofibers and graphene. He found that the response of the graphene/polyaniline nanocomposite based gas sensor towards H₂ gas with the concentration of 1% was 16.57% at room temperature, which was larger than the room temperature responses of the gas sensors based on polyaniline nanofibers (9.38%) and graphene (0.83%). The response time of the graphene/polyaniline nanocomposite based gas sensor was 68 s and the recovery time was 444 s. The growth of the polyaniline nanofibers on the surface of graphene nanosheets as shown in Figure 6.33 and Figure 6.34 resulted in a high surface area for the graphene/polyaniline nanocomposite compared to that of polyaniline nanofibers. Therefore, a larger number of

adsorption sites for H₂ gas was available in the graphene/polyaniline nanocomposite compared to the polyaniline nanofibers and graphene. Consequently, the graphene/polyaniline nanocomposite based gas sensor outperformed the other two gas sensors in terms of its room temperature response to hydrogen gas.

Chapter 8

Conclusions and Future Work

THROUGHOUT the PhD research program presented in this dissertation, novel gas sensors based on nanostructured conducting polymers and graphene/polyaniline nanocomposite were developed and evaluated. The motivations for conducting this research and the objectives were outlined in Chapter 1. Then, an extended review of published work was presented in Chapter 2 in order to establish the original contributions of this research program to the body of knowledge. Theoretical aspects of the polymer based conductometric and layered SAW gas sensors were discussed in Chapter 3. The fabrication procedures for producing conductometric and layered SAW transducers were described in great detail in Chapter 4.

The final stage in the development of the novel gas sensors mentioned in this thesis was the deposition of the nanostructured sensitive films on the conductometric and ZnO/36° YX LiTaO₃ SAW transducers. For that purpose, template-free syntheses were performed via electropolymerization and chemical polymerization methods as detailed in Chapter 5. The following nanomaterials were successfully deposited and investigated for their gas sensing characteristics in this PhD dissertation:

1. Electropolymerized polythiophene nanostructures.
2. Chemically synthesized polythiophene nanofibers.
3. Electropolymerized polypyrrole nanowires.
4. Chemically polymerized polypyrrole nanofibers.
5. Chemically synthesized nanoporous polyaniline.
6. Chemically polymerized polyanisidine nanofibers.

7. Chemically polymerized polyethylaniline nanofibers.
8. Chemically synthesized graphene/polyaniline nanocomposite.

The physical and chemical properties of each nanostructured material were studied utilizing a combination of characterization techniques. SEM and TEM microscopies as well as UV-vis, FT-IR, Raman, and XPS spectroscopic techniques were employed in this research program. With these techniques, the deposited nanostructured sensitive films' morphologies and chemical bonding were studied by the author of this thesis and discussed in Chapter 6.

Evaluation of the developed gas sensors' performances during the exposure to different concentrations of hydrogen gas was conducted and analyzed in Chapter 7. Consequently, the gas sensors' static and dynamic parameters such as response, baseline stability, response time and recovery time were determined. Furthermore, the author discussed the anticipated gas sensing mechanisms for the developed gas sensors.

During this PhD program, the author of this dissertation was the first author of 5 refereed journal papers and a co-author of 3 refereed journal papers. Four of these papers were published in high impact factor journals. In particular, the author of this thesis was the first author on 2 papers published in *The Journal of Physical Chemistry C* (impact factor: 4.805, ref: Web of Knowledge/ November 2012). Also, the author of this dissertation was the first author and a co-author for 2 papers in *Sensors and Actuators B: Chemical* (impact factor: 3.898, ref: Web of Knowledge/ November 2012). The author also presented his work via 15 conference presentations in high quality international conferences such as Eurosenors, Asian Conference on Chemical Sensors, International Conference on Nanoscience and Nanotechnology (ICONN), etc. Consequently, the author of this thesis received the RMIT University's 2012 Vice-Chancellor's Higher Degree by Research Publication Excellence Award. Some of the author's journal articles received a large number of citations as listed below:

- The author's article published in the American Chemical Society journal, *The Journal of Physical Chemistry C*, on graphene/polyaniline nanocomposite based gas sensor has been cited by ~50 articles [182] (ref: Scopus/ November 2012). This article was also praised and hand-picked by two senior editors of the American Chemical Society for their editorial articles [295, 296].
- The author's article published in the Elsevier journal, *Sensors and Actuators B: Chemical*, on polypyrrole nanofiber based SAW gas sensor has so far been cited by ~40 articles [137] (ref: Scopus/ November 2012).

- The author's article published in the IEEE Sensors Journal on conductometric hydrogen gas sensor based on polypyrrole nanofibers has been cited by ~25 articles [136] (ref: Scopus/ November 2012).

As indicated throughout this PhD dissertation that the author was successful in conducting research work individually at RMIT University as well as within teams in a collaborative endeavors. The author was privileged to collaborate with the following institutions:

- Department of Chemistry and Biochemistry and California NanoSystems Institute, University of California, Los Angeles, USA.
- Laboratory of Interfaces and Electrochemistry Systems, National Center for Scientific Research, Pierre and Marie Curie University, Paris, France.
- Department of Applied Chemistry, Sejong University, Seoul, Korea.
- Department of Materials Engineering, Monash University, Melbourne, Australia.

The main goal of the present chapter is to highlight the findings observed in the past chapters. In section 8.1, the conclusions extracted from the author's research work are provided. Avenues of further investigations that can be adopted by other researchers in the field will be discussed in section 8.2.

8.1 Conclusions

The author of this dissertation has successfully fulfilled the PhD research objectives with the development of the novel nanostructured materials' based conductometric and layered SAW gas sensors. The observed conclusions from the characterization results for the synthesized nanomaterials are covered in subsection 8.1.1. Then, the gas sensing results for the conductometric and layered SAW gas sensors are concluded in subsections 8.1.2 and 8.1.3 respectively.

8.1.1 Characterization of Nanomaterials

Nanostructured Polythiophene

To the best knowledge of the author of this thesis, a comparative study on electropolymerized polythiophene nanostructures for hydrogen gas sensing was conducted for the first time in this dissertation. Furthermore, chemically synthesized polythiophene nanofibers were employed to develop a novel layered SAW gas sensor. The characterization results for the electropolymerized and chemically polymerized nanostructured polythiophene revealed the following findings:

- Electropolymerized ClO_4^- doped polythiophene thin film consisted of granular 3D structures. Whereas, the electropolymerized Cl^- doped polythiophene thin film contained nanofibers with diameters in the range of 10–40 nm. The author of this thesis suggested that the heterogeneous nucleation was suppressed in the case of the $FeCl_3$ solution by restricting the flow of the high current at the beginning of the electropolymerization that was observed in the case of the $LiClO_4$ based electrolyte.
- Analysis of the morphologies for the polythiophene thin films synthesized with different concentrations of the $FeCl_3$ electrolyte, 0.6–1.8 mM, concluded that the optimum concentration was 1.2 mM. A balance between the chemical and electrochemical polymerization of thiophene monomer was established at this particular concentration. The study of the UV-vis spectra by the author of this thesis revealed the doping level dependence of polythiophene on the selected $FeCl_3$ electrolyte concentration.
- The selection of the polythiophene's electropolymerization potential (0.65–0.85) V has an effect on the deposited film's morphology due to the increase in the polymerization rate with the rising deposition potential. Supporting this explanation is the evident increase in the UV-vis absorbance for the deposited polythiophene films with the rise in the applied potential. From comparison of the deposited films' structures, the author of this dissertation showed that the optimum polythiophene nanostructured film was obtained by selecting the deposition potential of 0.75 V.
- During the first 10–15 min of polythiophene electropolymerization, the author of this thesis observed that a bulk seed layer was deposited followed by the growth of nanofibers from the nucleation sites as the electropolymerization continues. By increasing the deposition time, the number of grown nanofibers increases as well as the overall nanostructured film's thickness.
- The chemical composition of the electropolymerized polythiophene thin films and the incorporation of the Cl^- doping anion were confirmed by XPS spectroscopy, which was an important finding governing the properties of these films for gas sensing.
- Template-free chemically synthesized polythiophene nanofibers were 60–110 nm in diameter. The characteristic vibrational peaks for polythiophene molecules were observed by the author of this thesis in the FT-IR spectrum.

Nanostructured Polypyrrole

For the first time, to the best knowledge of this dissertation's author, electropolymerized polypyrrole nanowires and chemically synthesized polypyrrole nanofibers were employed for hydrogen gas sensing in the work presented in this PhD dissertation and published by the author in journal articles [136, 137, 258]. Characterization of these nanostructured films revealed the following findings:

- Electrochemical deposition of ClO_4^- doped polypyrrole nanowires with the anodic charges of either 13 mC, 55 mC or 90 mC was conducted on three conductometric transducers. Consistent with the observations during the electropolymerization of polythiophene, the rate of polymerization is expected to increase with the rise in the anodic charge. The author of this thesis found that the sensitive film deposited with 90 mC consisted of only polypyrrole nanowires with diameters in the range of 40–90 nm. Whereas at much lower anodic charge (13 mC), some secondary growth through heterogeneous nucleation resulted in the formation of 3D irregular shaped lumps throughout the deposited film. With the 90 mC, it can be anticipated that homogeneous nucleation was dominant over heterogeneous nucleation and consequently the secondary growth of polymer chains was suppressed.
- The author of this PhD dissertation demonstrated that the electropolymerized polypyrrole nanowires grew densely at the gold fingers of the conductometric IDTs. Further growth of the polymer chains led to the formation of polypyrrole nanowires' bridges over the insulating quartz substrate separating adjacent gold fingers.
- Incorporation of the perchlorate anion into the electropolymerized polypyrrole nanowires matrix was revealed by the author of this thesis from the XPS spectroscopy results with the presence of the Cl 2p peak at the binding energy of 208 eV and a peak at the binding energy of ~533 eV that was observed through the deconvolution of O(1s) core level.
- Template-free chemically polymerized Cl^- doped polypyrrole nanofibers were ~18 nm in diameter. Analysis of the FT-IR spectrum by the author of this thesis revealed the characteristic absorption bands for polypyrrole molecules.

Nanostructured Polyaniline and its Alkyl-Substituted Derivatives

Nanoporous polyaniline, polyanisidine nanofibers and polyethylaniline nanofibers based SAW hydrogen gas sensors were developed by the author of this PhD thesis for the first

time according to the best knowledge of this dissertation's author. Characterization results for these nanostructured materials are highlighted below:

- Morphological analysis of the nanoporous polyaniline revealed that the average pore size was ~45 nm. The surface area of the deposited nanoporous polyaniline was 161 m²/g, which is about three times that of polyaniline nanofibers. The UV-vis spectra of doped and dedoped nanoporous polyaniline were comparable to that of the conventional form of polyaniline.
- The average diameter for polyanisidine nanofibers was ~55 nm. Polyethylaniline nanofibers were ~47 nm in diameter. The polymers were in the semi-doped state according to the analysis of the corresponding UV-vis spectra.

Graphene/Polyaniline Nanocomposite

According to the best knowledge of this dissertation's author, graphene/polyaniline nanocomposite based gas sensor has been developed for the first time in the research work presented in this PhD thesis. Characterization of the graphene/polyaniline nanocomposite was performed utilizing SEM microscopy, TEM microscopy, Raman spectroscopy and XPS spectroscopy. The key outcomes are summarized below:

- Polyaniline nanofibers with diameter ~25–50 nm were grown on the graphene nanosheets' surfaces according to the SEM results and verified by the TEM findings.
- Both of the graphene and polyaniline vibrational modes were evident in the graphene/polyaniline nanocomposite's Raman spectrum. So the nanocomposite has the chemical and physical properties of both materials.
- Analysis of the XPS spectra by the author of this PhD thesis revealed the graphene/polyaniline nanocomposite's single and conjugated carbon bonds as well as the characteristic functional groups. Also, the XPS results confirmed that the graphene was actually in its reduced form. Water molecules trapping into the dried sensitive film was observed since the nanocomposite was suspended in water before depositing it on the conductometric transducer's surface.

8.1.2 Electrical Characterization of Conductometric Gas Sensors

Nanostructured Polythiophene Based Gas Sensors

Novel room temperature hydrogen gas sensors based on nanostructured polythiophene films were reported for the first time in this PhD thesis, according to the best knowledge of this dissertation's author. The impact of several electropolymerization parameters on

the gas sensors' static and dynamic characteristics was investigated. The following conclusions were drawn from this comparative study:

- The response of the nanostructured Cl^- doped polythiophene based gas sensor was about three times higher than that of the gas sensor with compact ClO_4^- doped polythiophene sensitive film. This finding can be attributed to the higher surface-to-volume ratio of the nanostructured polythiophene film compared to its bulk counterpart. Furthermore, the gas sensor based on the nanostructured Cl^- doped polythiophene had more stable baseline and faster response towards hydrogen gas than the compact ClO_4^- doped polythiophene based gas sensor.
- The author of this PhD dissertation showed that the value of the $FeCl_3$ concentration utilized during the electropolymerization of polythiophene affects the gas sensor's performance. The gas sensors' baseline stability gradually improved as the concentration value approached the optimum value in terms of the deposited film's morphology. The largest response was observed when the electrodeposition was conducted utilizing the concentration of 1.2 mM $FeCl_3$ (1.53% and 9.98% towards H_2 gas with the concentration of 0.06% and 1%, respectively). The lowest response was related to the electropolymerization at 0.6 mM $FeCl_3$ (0.33% and 1.43% towards H_2 gas with the concentration of 0.06% and 1%, respectively).
- The selection of the applied electropolymerization potential, (0.65–0.85) V, had an evident effect on the resultant gas sensor's response. The gas sensor with the sensitive film electrodeposited with 0.75 V had the largest response towards H_2 gas due to the high surface-to-volume ratio of its nanostructured sensitive film. The observed response time for these gas sensors towards 1% of H_2 gas was 46 s and the recovery time was 136 s with good baseline stability.
- Investigation of the effect of the nanostructured polythiophene film's thickness on the gas sensors' responses was carried out by the author of this thesis. It was found that the gas sensor with the 1.5 μm thick polythiophene film had the largest response (2% and 13% towards H_2 gas with the concentration of 0.06% and 1%, respectively). This finding can be attributed to the sensitive film's capability of gas sensing through the entire length of its nanofibers due to the limited number of nanofibers grown after 20 min of electropolymerization according to the SEM results. Increasing the film thickness above 1.5 μm did not result in a significant decrease in the sensors' responses towards H_2 gas, which is one of the merits of utilizing nanostructured films for gas sensing applications according to literature.

Nanostructured Polypyrrole Based Gas Sensors

Gas sensors based on electropolymerized polypyrrole nanowires and chemically synthesized polypyrrole nanofibers were developed and tested by the author of this PhD dissertation. The conclusions of these investigations are provided below:

- The optimum response of the electropolymerized ClO_4^- doped polypyrrole nanowires based gas sensors towards H_2 gas with the concentration of 1% at room temperature was 3.9%. While the chemically polymerized Cl^- doped polypyrrole nanofibers based gas sensor had room temperature response of 10.8% towards H_2 gas with the concentration of 1%. This finding was attributed to the difference in the polypyrrole's redox property because of the different molecular size of the counterion.
- The polypyrrole nanofibers based gas sensor performance at elevated operating temperatures (38–100) °C was studied by the author of this thesis. With the increase of thermally excited charge carriers at high temperatures, it was found that the polypyrrole film's resistance decreases. However as the conductivity of polypyrrole increased, it became more and more inert to H_2 gas. Consequently, the sensor's response deteriorated at high temperatures. Therefore the largest response of the sensor towards H_2 gas was found to be at room temperature (22 °C).

Graphene/Polyaniline Nanocomposite Based Gas sensor

It was found that the developed graphene/polyaniline nanocomposite based gas sensor was more sensitive to H_2 gas than the polyaniline nanofibers and graphene based gas sensors at room temperature. The key outcomes of this investigation that was conducted by the author of this PhD thesis are the following:

- During the exposure to H_2 gas with the concentration of 1%, the graphene/polyaniline nanocomposite based gas sensor's response was 16.57%. Whereas, the gas sensors based on polyaniline nanofibers and graphene had the responses of 9.38% and 0.83% towards H_2 gas with the concentration of 1% respectively. This large response was attributed to the growth of polyaniline nanofibers on the surface of graphene nanosheets leading to a high surface area for the graphene/polyaniline nanocomposite compared to that of polyaniline nanofibers. Therefore, a larger number of adsorption sites for H_2 gas was available in the graphene/polyaniline nanocomposite compared to the polyaniline nanofibers and graphene.

- The response time of the graphene/polyaniline nanocomposite based gas sensor to the exposure to H₂ gas with the concentration of 1% was 68 s.

8.1.3 Electrical Characterization of Layered SAW Gas Sensors

Polythiophene Nanofibers/ZnO/36° YX LiTaO₃ SAW Gas Sensor

During the exposure of the polythiophene nanofibers/ZnO/36° YX LiTaO₃ SAW gas sensor to H₂ gas with the concentration of 1%, a 16.92 kHz shift in its operational frequency was observed by the author of this thesis. The response time was 36 s. The sensor's responses towards five concentrations of H₂ gas were repeatable.

Polypyrrole Nanofibers/ZnO/36° YX LiTaO₃ SAW Gas Sensor

The author of this PhD dissertation showed that the polypyrrole nanofibers/ZnO/36° YX LiTaO₃ SAW gas sensor produced a deviation in its operational frequency of 20.194 kHz and 4.5 kHz towards H₂ gas with the concentration of 1% and towards NO₂ gas with the concentration of 2.1 ppm at room temperature, respectively. The response time of the sensor during the exposure to these concentrations of H₂ and NO₂ gases was 39 s and 133 s, respectively. The observed responses were reproducible.

Nanoporous Polyaniline/ZnO/36° YX LiTaO₃ SAW Gas Sensor

The response of the nanoporous polyaniline/ZnO/36° YX LiTaO₃ SAW gas sensor to H₂ gas with the concentration of 1% was 48.86 kHz. The response time was 46 s. The layered SAW gas sensor based on nanoporous polyaniline outperformed a similar sensor based on polyaniline nanofibers reported in literature due to the high porosity and surface area of the nanoporous polyaniline.

Polyaniline Nanofibers/ZnO/36° YX LiTaO₃ SAW Gas Sensor

The polyaniline nanofibers/ZnO/36° YX LiTaO₃ SAW gas sensor produced a large response to H₂ gas at room temperature (294 kHz towards H₂ gas with the concentration of 1%). The response time was 72 s. Analysis of the SEM results of the deposited polyaniline nanofibers based film by the author of this thesis revealed that the nanofibers were not densely packed, which allows deep penetration of target gas molecules into the sensitive film and makes gas sensing possible over the entire lengths of the nanofibers.

Polyethylaniline Nanofibers/ZnO/36° YX LiTaO₃ SAW Gas Sensor

It was found that the polyethylaniline nanofibers/ZnO/36° YX LiTaO₃ SAW gas sensor had a stable baseline. During the exposure to H₂ gas with the concentration of 1%, the sensor's response was 31 kHz. The response time was 54 s. Reproducible responses of the gas sensor towards five concentrations of H₂ gas balanced in synthetic air were observed.

8.2 Future Work

Synthesis, characterization and applications of nanostructured conducting polymers and their nanocomposites with organic or inorganic inclusions is an active research area with an increasing number of publications every year. This is evident from the large number of citations to the work published by the author of this dissertation as indicated previously. Therefore, there are limitless possibilities for future research work in this area and the field of gas sensing is just one of them. Some suggestions for further research work are provided below:

- According to the findings of this thesis, the type of the incorporated counterion into the polymer matrix during synthesis affected the physical and chemical properties of the conductive polymer. Each of the perchlorate (ClO_4^-) and chloride (Cl^-) counterions was used to dope the nanostructured polythiophene and polypyrrole films that were investigated for their hydrogen gas sensing characteristics in this PhD dissertation. Other counterions can also be utilized during synthesis such as: tetrafluoroborate (BF_4^-), hexafluoroarsenate (AsF_6^-), hydrogen sulfate (HSO_4^-), or hexafluorophosphate (PF_6^-) etc. Therefore, the morphology and the chemical properties of a conductive polymer's film can be tailored in order to obtain the highest sensitivity of the resultant gas sensor to a particular gas or vapor.
- In this dissertation, nanostructured polythiophene films consisting of nanofibers ~10–40 nm in diameter were successfully electropolymerized on conductometric transducers without any template. Selective electrodeposition and mobilization of the nanostructures described in this thesis is possible through Electrochemical Dip-Pen Nanolithography (E-DPN). With this technique, conducting polymers' nanostructures can be deposited on miniature areas for the development of electronic devices such as organic thin-film transistors (OTFT) that can be used in electronic nose application.

-
- Homogeneously dispersed graphene nanofiller into a polymer's matrix can produce a nanocomposite with improved mechanical, electrical, thermal and other properties compared the original polymer due to the high aspect ratio and surface-to-volume ratio of the filler. In this dissertation, the graphene/polyaniline nanocomposite based gas sensor outperformed those based on polyaniline nanofibers and graphene in terms of its response towards hydrogen gas. Further research on nanocomposites of graphene with pure or alkyl-substituted conductive polymers for gas sensing or biosensing applications can be very promising.
 - Theoretical studies of the adsorption of a particular gaseous species into pure conjugated polymers and their nanocomposites such as the Density Functional Theory (DFT) analysis through the Vienna *Ab-initio* Simulation Package (VASP) can provide a valuable insight into the material's charge transport during the interaction with the target gas.

Bibliography

- [1] C. L. Yaws, S. S. Naphad, and J. D. Sameth, "Hydrogen", in *Matheson Gas Data Book*: McGraw-Hill, 7th ed., Chapter 79, 2001.
- [2] J. Hord, "Is hydrogen a safe fuel?", *International Journal of Hydrogen Energy*, vol. 3, pp. 157-176, 1978.
- [3] K. Pant and R. B. Gupta, "Fundamentals and use of hydrogen as a fuel", in *Hydrogen Fuel: Production, Transport, and Storage*, Boca Raton: CRC Press, Chapter 1, 2009.
- [4] L. W. Jones, "Liquid hydrogen as a fuel for the future", *Science*, vol. 174, pp. 367-370, 1971.
- [5] A. Midilli, M. Ay, I. Dincer, and M. A. Rosen, "On hydrogen and hydrogen energy strategies: I: current status and needs", *Renewable and Sustainable Energy Reviews*, vol. 9, pp. 255-271, 2005.
- [6] M. F. Hordeski, *Alternative Fuels: the Future of Hydrogen*, Lilburn: The Fairmont Press, 2008.
- [7] C. M. White, R. R. Steeper, and A. E. Lutz, "The hydrogen-fueled internal combustion engine: a technical review", *International Journal of Hydrogen Energy*, vol. 31, pp. 1292-1305, 2006.
- [8] B. R. Eggins, *Chemical Sensors and Biosensors*, West Sussex: John Wiley & Sons, 2002.
- [9] K. Kalantar-zadeh and B. Fry, *Nanotechnology-Enabled Sensors*, New York: Springer-Verlag, 2008.
- [10] J. RaviPrakash, A. H. McDaniel, M. Horn, L. Pilione, P. Sunal, R. Messier, R. T. McGrath, and F. K. Schweighardt, "Hydrogen sensors: Role of palladium thin film morphology", *Sensors and Actuators B: Chemical*, vol. 120, pp. 439-446, 2007.

- [11] T. Hübert, L. Boon-Brett, G. Black, and U. Banach, "Hydrogen sensors – A review", *Sensors and Actuators B: Chemical*, vol. 157, pp. 329-352, 2011.
- [12] R. C. Hughes and W. K. Schubert, "Thin films of Pd/Ni alloys for detection of high hydrogen concentrations", *Journal of Applied Physics*, vol. 71, pp. 542-544, 1992.
- [13] Y. T. Cheng, Y. Li, D. Lisi, and W. M. Wang, "Preparation and characterization of Pd/Ni thin films for hydrogen sensing", *Sensors and Actuators B: Chemical*, vol. 30, pp. 11-16, 1996.
- [14] L. Huang, H. Gong, D. Peng, and G. Meng, "Pd–Ni thin films grown on porous Al₂O₃ substrates by metalorganic chemical vapor deposition for hydrogen sensing", *Thin Solid Films*, vol. 345, pp. 217-221, 1999.
- [15] M. Wang and Y. Feng, "Palladium-silver thin film for hydrogen sensing", *Sensors and Actuators B: Chemical*, vol. 123, pp. 101-106, 2007.
- [16] K. Yoshimura, S. Nakano, S. Uchinashi, S. Yamaura, H. Kimura, and A. Inoue, "A hydrogen sensor based on Mg–Pd alloy thin film", *Measurement Science and Technology*, vol. 18, pp. 3335, 2007.
- [17] P. Soundarrajan and F. Schweighardt, "Hydrogen sensing and detection", in *Hydrogen Fuel*: CRC Press, 495-534, 2008.
- [18] W. J. Buttner, M. B. Post, R. Burgess, and C. Rivkin, "An overview of hydrogen safety sensors and requirements", *International Journal of Hydrogen Energy*, vol. 36, pp. 2462-2470, 2011.
- [19] D. K. Aswal and S. K. Gupta, *Science and Technology of Chemiresistor Gas Sensors*, New York: Nova Science Publishers, Inc., 2007.
- [20] M. B. Rahmani, S. H. Keshmiri, J. Yu, A. Z. Sadek, L. Al-Mashat, A. Moafi, K. Latham, Y. X. Li, W. Wlodarski, and K. Kalantar-zadeh, "Gas sensing properties of thermally evaporated lamellar MoO₃", *Sensors and Actuators B: Chemical*, vol. 145, pp. 13-19, 2010.
- [21] V. E. Henrich and P. A. Cox, *The Surface Science of Metal Oxides*, Cambridge; New York: Cambridge University Press, 1994.
- [22] M. Hübner, R. G. Pavelko, N. Barsan, and U. Weimar, "Influence of oxygen backgrounds on hydrogen sensing with SnO₂ nanomaterials", *Sensors and Actuators B: Chemical*, vol. 154, pp. 264-269, 2011.
- [23] N. Barsan and U. Weimar, "Conduction model of metal oxide gas sensors", *Journal of Electroceramics*, vol. 7, pp. 143-167, 2001.

- [24] A. Z. Sadek, S. Choopun, W. Wlodarski, S. J. Ippolito, and K. Kalantar-zadeh, "Characterization of ZnO nanobelt-based gas sensor for H₂, NO₂, and hydrocarbon sensing", *IEEE Sensors Journal*, vol. 7, pp. 919-924, 2007.
- [25] G. Sberveglieri, *Gas Sensors*, Dordrecht: Kluwer Academic Publishers, 1992.
- [26] S. Iijima, "Helical microtubules of graphitic carbon", *Nature*, vol. 354, pp. 56-58, 1991.
- [27] J. Li, "Carbon nanotube applications: Chemical and physical sensors", in *Carbon Nanotubes: Science and Applications*: CRC Press, 213-235, 2005.
- [28] A. Vaseashta, "Carbon nanotubes based devices and sensors", *Materials and Manufacturing Processes*, vol. 21, pp. 710-716, 2006.
- [29] T. Zhang, S. Mubeen, N. V. Myung, and M. A. Deshusses, "Recent progress in carbon nanotube-based gas sensors", *Nanotechnology*, vol. 19, pp. 332001, 2008.
- [30] K. Shin, L. Al-Mashat, J. S. Song, S. H. Han, D. S. Ahn, B. Y. Yoo, K. Kalantar-zadeh, and W. Wlodarski, "Polyaniline/MWCNT nanocomposite based hydrogen sensor operating at room temperature", *Sensor Letters*, vol. 9, pp. 69-72, 2011.
- [31] D. Li and R. B. Kaner, "Graphene-based materials", *Science*, vol. 320, pp. 1170-1171, 2008.
- [32] R. Arsat, M. Breedon, M. Shafiei, P. G. Spizziri, S. Gilje, R. B. Kaner, K. Kalantar-zadeh, and W. Wlodarski, "Graphene-like nano-sheets for surface acoustic wave gas sensor applications", *Chemical Physics Letters*, vol. 467, pp. 344-347, 2009.
- [33] J. D. Fowler, M. J. Allen, V. C. Tung, Y. Yang, R. B. Kaner, and B. H. Weiller, "Practical chemical sensors from chemically derived graphene", *ACS Nano*, vol. 3, pp. 301-306, 2009.
- [34] J. S. Arellano, L. M. Molina, A. Rubio, and J. A. Alonso, "Density functional study of adsorption of molecular hydrogen on graphene layers", *The Journal of Chemical Physics*, vol. 112, pp. 8114-8119, 2000.
- [35] P. Novák, K. Müller, K. S. V. Santhanam, and O. Haas, "Electrochemically active polymers for rechargeable batteries", *Chemical Reviews*, vol. 97, pp. 207-282, 1997.
- [36] A. Kaur, M. J. Cazeca, K. G. Chittibabu, J. Kumar, and S. K. Tripathy, "Mechanism of electroluminescence in dye doped thiophene based conjugated polymer", *Journal of Applied Physics*, vol. 89, pp. 3250-3255, 2001.

- [37] J. J. Miasik, A. Hooper, and B. C. Tofield, "Conducting polymer gas sensors", *Journal of the Chemical Society, Faraday Transactions 1*, vol. 82, pp. 1117-1126, 1986.
- [38] D. T. McQuade, A. E. Pullen, and T. M. Swager, "Conjugated polymer-based chemical sensors", *Chemical Reviews*, vol. 100, pp. 2537-2574, 2000.
- [39] H. Bai and G. Shi, "Gas sensors based on conducting polymers", *Sensors*, vol. 7, pp. 267-307, 2007.
- [40] U. Lange, N. V. Roznyatovskaya, and V. M. Mirsky, "Conducting polymers in chemical sensors and arrays", *Analytica Chimica Acta*, vol. 614, pp. 1-26, 2008.
- [41] A. G. Macdiarmid, "Synthetic metals: A novel role for organic polymers", *Synthetic Metals*, vol. 125, pp. 11-22, 2002.
- [42] J. C. Chiang and A. G. MacDiarmid, "'Polyaniline': Protonic acid doping of the emeraldine form to the metallic regime", *Synthetic Metals*, vol. 13, pp. 193-205, 1986.
- [43] Y. Osada and D. DeRossi, *Polymer Sensors and Actuators*, Berlin; Heidelberg: Springer-Verlag, 2000.
- [44] J. Janata and M. Josowicz, "Conducting polymers in electronic chemical sensors", *Nature Materials*, vol. 2, pp. 19-24, 2003.
- [45] A. J. Killard, "Nanostructured conducting polymers for (electro)chemical sensors", in *Nanostructured Conductive Polymers*, West Sussex: John Wiley & Sons, Chapter 14, 2010.
- [46] J. H. Burroughes, D. D. C. Bradley, A. R. Brown, R. N. Marks, K. Mackay, R. H. Friend, P. L. Burns, and A. B. Holmes, "Light-emitting diodes based on conjugated polymers", *Nature*, vol. 347, pp. 539-541, 1990.
- [47] G. Gustafsson, Y. Cao, G. M. Treacy, F. Klavetter, N. Colaneri, and A. J. Heeger, "Flexible light-emitting diodes made from soluble conducting polymers", *Nature*, vol. 357, pp. 477-479, 1992.
- [48] A. Tsumura, H. Koezuka, and T. Ando, "Macromolecular electronic device: Field-effect transistor with a polythiophene thin film", *Applied Physics Letters*, vol. 49, pp. 1210-1212, 1986.
- [49] J. Liu, T. Tanaka, K. Sivula, A. P. Alivisatos, and J. M. J. Fréchet, "Employing end-functional polythiophene to control the morphology of nanocrystal-polymer composites in hybrid solar cells", *Journal of the American Chemical Society*, vol. 126, pp. 6550-6551, 2004.

- [50] D. D. C. Bradley, "Electroluminescence: A bright future for conjugated polymers?", *Advanced Materials*, vol. 4, pp. 756-758, 1992.
- [51] L. Dai, *Intelligent Macromolecules for Smart Devices*, London: Springer-Verlag, 2004.
- [52] W. A. Harrison, *Solid State Theory*, New York: Dover Publications, Inc. , 1979.
- [53] P. Chandrasekhar, *Conducting Polymers, Fundamentals and Applications*, London: Kluwer Academic Publishers, 1999.
- [54] Y. W. Park, A. J. Heeger, M. A. Drury, and A. G. MacDiarmid, "Electrical transport in doped polyacetylene", *The Journal of Chemical Physics*, vol. 73, pp. 946-957, 1980.
- [55] J. M. Pochan, H. W. Gibson, and F. C. Bailey, "Oxygen doping of polyacetylene", *Journal of Polymer Science: Polymer Letters Edition*, vol. 18, pp. 447-451, 1980.
- [56] J. C. W. Chien, "Creation and annihilation of solitons, radicals, and ions in polyacetylene as related to the mechanisms of isomerization, doping, and conduction", *Journal of Polymer Science: Polymer Letters Edition*, vol. 19, pp. 249-260, 1981.
- [57] J. M. Pochan, D. F. Pochan, H. Rommelmann, and H. W. Gibson, "Kinetics of doping and degradation of polyacetylene by oxygen", *Macromolecules*, vol. 14, pp. 110-114, 1981.
- [58] J. M. Pochan, H. W. Gibson, and J. Harbour, "Effects of oxidation on I₂ doping of trans-polyacetylene as studied via e.s.r. and conductivity measurements", *Polymer*, vol. 23, pp. 439-444, 1982.
- [59] G. G. Wallace, G. M. Spinks, and P. R. Teasdale, *Conductive Electroactive Polymers: Intelligent Materials Systems*, Pennsylvania: Technomic, 1997.
- [60] A. Malinauskas, "Chemical deposition of conducting polymers", *Polymer*, vol. 42, pp. 3957-3972, 2001.
- [61] J. Reemts, J. Parisi, and D. Schlettwein, "Electrochemical growth of gas-sensitive polyaniline thin films across an insulating gap", *Thin Solid Films*, vol. 466, pp. 320-325, 2004.
- [62] G. Cao, *Nanostructures & Nanomaterials: Synthesis, Properties & Applications*, London: Imperial College Press, 2004.
- [63] J. Huang, S. Virji, B. H. Weiller, and R. B. Kaner, "Nanostructured polyaniline sensors", *Chemistry - A European Journal*, vol. 10, pp. 1314-1319, 2004.

- [64] S. Virji, R. B. Kaner, and B. H. Weiller, "Hydrogen sensors based on conductivity changes in polyaniline nanofibers", *Journal of Physical Chemistry B*, vol. 110, pp. 22266-22270, 2006.
- [65] A. Malinauskas, J. Malinauskiene, and A. Ramanavicius, "Conducting polymer-based nanostructured materials: electrochemical aspects", *Nanotechnology*, vol. 16, pp. R51, 2005.
- [66] J. Jang, "Conducting polymer nanomaterials and their applications", *Advances in Polymer Science*, vol. 199, pp. 189-260, 2006.
- [67] J. Huang and R. B. Kaner, "Polyaniline nanofibers: Syntheses, properties and application", in *Conjugated Polymers: Theory, Synthesis, Properties and Characterization*, Boca Raton: CRC Press, Chapter 7, 2007.
- [68] H. D. Tran, D. Li, and R. B. Kaner, "One-dimensional conducting polymer nanostructures: bulk synthesis and applications", *Advanced Materials*, vol. 21, pp. 1487-1499, 2009.
- [69] H. X. He, C. Z. Li, and N. J. Tao, "Conductance of polymer nanowires fabricated by a combined electrodeposition and mechanical break junction method", *Applied Physics Letters*, vol. 78, pp. 811-813, 2001.
- [70] A. G. MacDiarmid, W. E. Jones Jr, I. D. Norris, J. Gao, A. T. Johnson Jr, N. J. Pinto, J. Hone, B. Han, F. K. Ko, H. Okuzaki, and M. Llaguno, "Electrostatically-generated nanofibers of electronic polymers", *Synthetic Metals*, vol. 119, pp. 27-30, 2001.
- [71] C. R. Martin, "Template synthesis of electronically conductive polymer nanostructures", *Accounts of Chemical Research*, vol. 28, pp. 61-68, 1995.
- [72] K. Jackowska, A. T. Bieguński, and M. Tagowska, "Hard template synthesis of conducting polymers: a route to achieve nanostructures", *Journal of Solid State Electrochemistry*, vol. 12, pp. 437-443, 2008.
- [73] L. Pan, H. Qiu, C. Dou, Y. Li, L. Pu, J. Xu, and Y. Shi, "Conducting polymer nanostructures: Template synthesis and applications in energy storage", *International Journal of Molecular Sciences*, vol. 11, pp. 2636-2657, 2010.
- [74] K. Landfester, N. Bechthold, F. Tiarks, and M. Antonietti, "Formulation and stability mechanisms of polymerizable miniemulsions", *Macromolecules*, vol. 32, pp. 5222-5228, 1999.
- [75] K. Landfester, "The generation of nanoparticles in miniemulsions", *Advanced Materials*, vol. 13, pp. 765-768, 2001.

- [76] S. C. Hernandez, D. Chaudhuri, W. Chen, N. V. Myung, and A. Mulchandani, "Single polypyrrole nanowire ammonia gas sensor", *Electroanalysis*, vol. 19, pp. 2125-2130, 2007.
- [77] J. Duchet, R. Legras, and S. Demoustier-Champagne, "Chemical synthesis of polypyrrole: structure-properties relationship", *Synthetic Metals*, vol. 98, pp. 113-122, 1998.
- [78] M. Fu, Y. Zhu, R. Tan, and G. Shi, "Aligned polythiophene micro- and nanotubules", *Advanced Materials*, vol. 13, pp. 1874-1877, 2001.
- [79] G. Lu, W. Hong, L. Tong, H. Bai, Y. Wei, and G. Shi, "Drying enhanced adhesion of polythiophene nanotubule arrays on smooth surfaces", *ACS Nano*, vol. 2, pp. 2342-2348, 2008.
- [80] M. A. del Valle, M. Gacitúa, F. R. Díaz, F. Armijo, and R. d. Río, "Electrosynthesis of polythiophene nanowires via mesoporous silica thin film templates", *Electrochemistry Communications*, vol. 11, pp. 2117-2120, 2009.
- [81] V. Aboutanos, J. N. Barisci, P. C. Innis, and G. G. Wallace, "Factors affecting the electrochemical formation of polypyrrole-nitrate colloids", *Colloids and Surfaces A: Physicochemical and Engineering Aspects*, vol. 137, pp. 295-300, 1998.
- [82] Z. Tang, S. Liu, Z. Wang, S. Dong, and E. Wang, "Electrochemical synthesis of polyaniline nanoparticles", *Electrochemistry Communications*, vol. 2, pp. 32-35, 2000.
- [83] J. Liu, Y. Lin, L. Liang, J. A. Voigt, D. L. Huber, Z. R. Tian, E. Coker, B. McKenzie, and M. J. McDermott, "Templateless assembly of molecularly aligned conductive polymer nanowires: A new approach for oriented nanostructures", *Chemistry – A European Journal*, vol. 9, pp. 604-611, 2003.
- [84] R. Arsat, X. F. Yu, Y. X. Li, W. Wlodarski, and K. Kalantar-zadeh, "Hydrogen gas sensor based on highly ordered polyaniline nanofibers", *Sensors and Actuators B: Chemical*, vol. 137, pp. 529-532, 2009.
- [85] C. Debiemme-Chouvy, "Template-free one-step electrochemical formation of polypyrrole nanowire array", *Electrochemistry Communications*, vol. 11, pp. 298-301, 2009.
- [86] C. Debiemme-Chouvy, "One-step electrochemical synthesis of a very thin overoxidized polypyrrole film", *Electrochemical and Solid-State Letters*, vol. 10, pp. E24-E26, 2007.
- [87] J. Huang and R. B. Kaner, "A general chemical route to polyaniline nanofibers", *Journal of the American Chemical Society*, vol. 126, pp. 851-855, 2004.

- [88] J. Huang, "Syntheses and applications of conducting polymer polyaniline nanofibers", *Pure and Applied Chemistry*, vol. 78, pp. 15-27, 2006.
- [89] D. Li, J. Huang, and R. B. Kaner, "Polyaniline nanofibers: A unique polymer nanostructure for versatile applications", *Accounts of Chemical Research*, vol. 42, pp. 135-145, 2009.
- [90] D. Li and R. B. Kaner, "Shape and aggregation control of nanoparticles: Not shaken, not stirred", *Journal of the American Chemical Society*, vol. 128, pp. 968-975, 2006.
- [91] J. Huang and R. B. Kaner, "Nanofiber formation in the chemical polymerization of aniline: A mechanistic study", *Angewandte Chemie International Edition*, vol. 43, pp. 5817-5821, 2004.
- [92] H. D. Tran and R. B. Kaner, "A general synthetic route to nanofibers of polyaniline derivatives", *Chemical Communications*, pp. 3915-3917, 2006.
- [93] H. D. Tran, K. Shin, W. G. Hong, J. M. D'Arcy, R. W. Kojima, B. H. Weiller, and R. B. Kaner, "A template-free route to polypyrrole nanofibers", *Macromolecular Rapid Communications*, vol. 28, pp. 2289-2293, 2007.
- [94] H. D. Tran, I. Norris, J. M. D'Arcy, H. Tsang, Y. Wang, B. R. Mattes, and R. B. Kaner, "Substituted polyaniline nanofibers produced via rapid initiated polymerization", *Macromolecules*, vol. 41, pp. 7405-7410, 2008.
- [95] M. Jeffries-El and R. D. McCullough, "Regioregular polythiophenes", in *Conjugated Polymers: Theory, Synthesis, Properties and Characterization*, Boca Raton: CRC Press, Chapter 9, 2007.
- [96] L. Torsi, A. Tafuri, N. Cioffi, M. C. Gallazzi, A. Sassella, L. Sabbatini, and P. G. Zambonin, "Regioregular polythiophene field-effect transistors employed as chemical sensors", *Sensors and Actuators B: Chemical*, vol. 93, pp. 257-262, 2003.
- [97] M. R. Andersson, O. Thomas, W. Mammo, M. Svensson, M. Theander, and O. Inganäs, "Substituted polythiophenes designed for optoelectronic devices and conductors", *Journal of Materials Chemistry*, vol. 9, pp. 1933-1940, 1999.
- [98] X. Ma, G. Li, H. Xu, M. Wang, and H. Chen, "Preparation of polythiophene composite film by in situ polymerization at room temperature and its gas response studies", *Thin Solid Films*, vol. 515, pp. 2700-2704, 2006.
- [99] T. Hanawa, S. Kuwabata, H. Hashimoto, and H. Yoneyama, "Gas sensitivities of electropolymerized polythiophene films", *Synthetic Metals*, vol. 30, pp. 173-181, 1989.

- [100] S. R. Kim, S. A. Choi, J. D. Kim, K. J. Kim, C. Lee, and S. B. Rhee, "Preparation of polythiophene LB films and their gas sensitivities by the quartz crystal microbalance", *Synthetic Metals*, vol. 71, pp. 2027-2028, 1995.
- [101] B. Li, G. Sauv e, M. C. Iovu, M. Jeffries-El, R. Zhang, J. Cooper, S. Santhanam, L. Schultz, J. C. Revelli, A. G. Kusne, T. Kowalewski, J. L. Snyder, L. E. Weiss, G. K. Fedder, R. D. McCullough, and D. N. Lambeth, "Volatile organic compound detection using nanostructured copolymers", *Nano Letters*, vol. 6, pp. 1598-1602, 2006.
- [102] M. C. Lonergan, E. J. Severin, B. J. Doleman, S. A. Beaber, R. H. Grubbs, and N. S. Lewis, "Array-based vapor sensing using chemically sensitive, carbon black-polymer resistors", *Chemistry of Materials*, vol. 8, pp. 2298-2312, 1996.
- [103] S. Hamilton, M. J. Hefner, and J. Sommerville, "Polypyrrole materials for detection and discrimination of volatile organic compounds", *Sensors and Actuators B: Chemical*, vol. 107, pp. 424-432, 2005.
- [104] E. Johansson and S. Larsson, "Electronic structure and mechanism for conductivity in thiophene oligomers and regioregular polymer", *Synthetic Metals*, vol. 144, pp. 183-191, 2004.
- [105] B. Li and D. N. Lambeth, "Chemical sensing using nanostructured polythiophene transistors", *Nano Letters*, vol. 8, pp. 3563-3567, 2008.
- [106] J. B. Chang, V. Liu, V. Subramanian, K. Sivula, C. Luscombe, A. Murphy, J. S. Liu, and J. M. J. Frechet, "Printable polythiophene gas sensor array for low-cost electronic noses", *Journal of Applied Physics*, vol. 100, 2006.
- [107] V. Dua, S. P. Surwade, S. Ammu, X. Zhang, S. Jain, and S. K. Manohar, "Chemical vapor detection using parent polythiophene nanofibers", *Macromolecules*, vol. 42, pp. 5414-5415, 2009.
- [108] F. Liao, M. F. Toney, and V. Subramanian, "Thickness changes in polythiophene gas sensors exposed to vapor", *Sensors and Actuators B: Chemical*, vol. 148, pp. 74-80, 2010.
- [109] L. Al-Mashat, H. D. Tran, R. B. Kaner, R. Arsat, K. Kalantar-Zadeh, and W. Wlodarski, "A hydrogen gas sensor fabricated from polythiophene nanofibers deposited on a 36° YX LiTaO₃ layered surface acoustic wave transducer", in *Smart Structures, Devices, and Systems IV*, USA: SPIE - The International Society for Optical Engineering, pp. 72680M-8, 2008.

- [110] S. H. Cho, K. T. Song, and J. Y. Lee, "Recent advances in polypyrrole", in *Conjugated Polymers: Theory, Synthesis, Properties and Characterization*, Boca Raton: CRC Press, Chapter 8, 2007.
- [111] G. Inzelt, *Conducting Polymers: A New Era in Electrochemistry*, Heidelberg: Springer-Verlag, 2008.
- [112] D. Schmeisser, A. Bartl, L. Dunsch, H. Naarmann, and W. Göpel, "Electronic and magnetic properties of polypyrrole films depending on their one-dimensional and two-dimensional microstructures", *Synthetic Metals*, vol. 93, pp. 43-58, 1998.
- [113] A. F. Diaz, K. K. Kanazawa, and G. P. Gardini, "Electrochemical polymerization of pyrrole", *Journal of the Chemical Society, Chemical Communications*, pp. 635-636, 1979.
- [114] K. K. Kanazawa, A. F. Diaz, R. H. Geiss, W. D. Gill, J. F. Kwak, J. A. Logan, J. F. Rabolt, and G. B. Street, "'Organic metals': polypyrrole, a stable synthetic 'metallic' polymer", *Journal of the Chemical Society, Chemical Communications*, pp. 854-855, 1979.
- [115] C. Nylander, M. Armgarth, and I. Lundström, "An ammonia detector based on a conducting polymer", *Proceedings of the International Meeting on Chemical Sensors*, vol. 17, pp. 203-207, 1983.
- [116] G. Gustafsson, I. Lundström, B. Liedberg, C. R. Wu, O. Inganäs, and O. Wennerström, "The interaction between ammonia and poly(pyrrole)", *Synthetic Metals*, vol. 31, pp. 163-179, 1989.
- [117] J. P. Blanc, N. Derouiche, A. El Hadri, J. P. Germain, C. Maleysson, and H. Robert, "Study of the action of gases on a polypyrrole film", *Sensors and Actuators: B. Chemical*, vol. 1, pp. 130-133, 1990.
- [118] O. S. Kwon, J.-Y. Hong, S. J. Park, Y. Jang, and J. Jang, "Resistive gas sensors based on precisely size-controlled polypyrrole nanoparticles: Effects of particle size and deposition method", *Journal of Physical Chemistry C*, vol. 114, pp. 18874-18879, 2010.
- [119] M. A. Chougule, S. G. Pawar, S. L. Patil, B. T. Raut, P. R. Godse, S. Sen, and V. B. Patil, "Polypyrrole thin film: Room temperature ammonia gas sensor", *IEEE Sensors Journal*, vol. 11, pp. 2137-2141, 2011.
- [120] J. M. Slater and E. J. Watt, "Examination of ammonia-poly(pyrrole) interactions by piezoelectric and conductivity measurements", *Analyst*, vol. 116, pp. 1125-1130, 1991.

- [121] M. Penza, E. Milella, and V. I. Anisimkin, "Monitoring of NH₃ gas by LB polypyrrole-based SAW sensor", *Sensors and Actuators B: Chemical*, vol. 47, pp. 218-224, 1998.
- [122] P. N. Bartlett and S. K. Ling-Chung, "Conducting polymer gas sensors Part III: Results for four different polymers and five different vapours", *Sensors and Actuators*, vol. 20, pp. 287-292, 1989.
- [123] J. M. Slater, E. J. Watt, N. J. Freeman, I. P. May, and D. J. Weir, "Gas and vapour detection with poly(pyrrole) gas sensors", *Analyst*, vol. 117, pp. 1265-1270, 1992.
- [124] J. W. Gardner, M. Vidic, P. Ingleby, A. C. Pike, J. E. Brignell, P. Scivier, P. N. Bartlett, A. J. Duke, and J. M. Elliott, "Response of a poly(pyrrole) resistive micro-bridge to ethanol vapour", *Sensors and Actuators B: Chemical*, vol. 48, pp. 289-295, 1998.
- [125] P. Ingleby, J. W. Gardner, and P. N. Bartlett, "Effect of micro-electrode geometry on response of thin-film poly(pyrrole) and poly(aniline) chemoresistive sensors", *Sensors and Actuators, B: Chemical*, vol. 57, pp. 17-27, 1999.
- [126] J. E. G. de Souza, F. L. dos Santos, B. B. Neto, C. G. dos Santos, M. V. B. dos Santos, and C. P. de Melo, "Free-grown polypyrrole thin films as aroma sensors", *Sensors and Actuators B: Chemical*, vol. 88, pp. 246-259, 2003.
- [127] T. Hanawa, S. Kuwabata, and H. Yoneyama, "Gas sensitivity of polypyrrole films to NO₂", *Journal of the Chemical Society, Faraday Transactions 1*, vol. 84, pp. 1587-1592, 1988.
- [128] T. Hanawa and H. Yoneyama, "Gas sensitiveness of polypyrrole films doped chemically in the gas phase", *Synthetic Metals*, vol. 30, pp. 341-350, 1989.
- [129] T. Hanawa and H. Yoneyama, "Gas sensitivities of polypyrrole films to electron acceptor gases", *Bulletin of the Chemical Society of Japan*, vol. 62, pp. 1710-1714, 1989.
- [130] D. M. Liu, J. Aguilar-Hernandez, K. Potje-Kamloth, and H. D. Liess, "A new carbon monoxide sensor using a polypyrrole film grown on an interdigital-capacitor substrate", *Sensors and Actuators, B: Chemical*, vol. 41, pp. 203-206, 1997.
- [131] L. Torsi, M. Pezzuto, P. Siciliano, R. Rella, L. Sabbatini, L. Valli, and P. G. Zambonin, "Conducting polymers doped with metallic inclusions: New materials for gas sensors", *Sensors and Actuators B: Chemical*, vol. 48, pp. 362-367, 1998.

- [132] B. J. V. Tongol, C. A. Binag, and F. B. Sevilla III, "Surface and electrochemical studies of a carbon dioxide probe based on conducting polypyrrole", *Sensors and Actuators B: Chemical*, vol. 93, pp. 187-196, 2003.
- [133] S. A. Waghuley, S. M. Yenorkar, S. S. Yawale, and S. P. Yawale, "Application of chemically synthesized conducting polymer-polypyrrole as a carbon dioxide gas sensor", *Sensors and Actuators B: Chemical*, vol. 128, pp. 366-373, 2008.
- [134] P. G. Su and C. C. Shiu, "Flexible H₂ sensor fabricated by layer-by-layer self-assembly of thin films of polypyrrole and modified in situ with Pt nanoparticles", *Sensors and Actuators B: Chemical*, vol. 157, pp. 275-281, 2011.
- [135] Y.-C. Liu, B.-J. Hwang, and W.-C. Hsu, "Improvement in anti-aging of metallized Nafion® hydrogen sensors modified by chemical vapor deposition of polypyrrole", *Sensors and Actuators B: Chemical*, vol. 87, pp. 304-308, 2002.
- [136] L. Al-Mashat, H. D. Tran, W. Wlodarski, R. B. Kaner, and K. Kalantar-Zadeh, "Conductometric hydrogen gas sensor based on polypyrrole nanofibers", *IEEE Sensors Journal*, vol. 8, pp. 365-370, 2008.
- [137] L. Al-Mashat, H. D. Tran, W. Wlodarski, R. B. Kaner, and K. Kalantar-zadeh, "Polypyrrole nanofiber surface acoustic wave gas sensors", *Sensors and Actuators B: Chemical*, vol. 134, pp. 826-831, 2008.
- [138] J. Desilvestro, W. Scheifele, and O. Haas, "In situ determination of gravimetric and volumetric charge densities of battery electrodes", *Journal of the Electrochemical Society*, vol. 139, pp. 2727-2736, 1992.
- [139] D. C. Trivedi and S. K. Dhawan, "Shielding of electromagnetic interference using polyaniline", *Synthetic Metals*, vol. 59, pp. 267-272, 1993.
- [140] J. Joo and A. J. Epstein, "Electromagnetic radiation shielding by intrinsically conducting polymers", *Applied Physics Letters*, vol. 65, pp. 2278-2280, 1994.
- [141] W. K. Lu, R. L. Elsenbaumer, and B. Wessling, "Corrosion protection of mild steel by coatings containing polyaniline", *Synthetic Metals*, vol. 71, pp. 2163-2166, 1995.
- [142] M. Fahlman, S. Jasty, and A. J. Epstein, "Corrosion protection of iron/steel by emeraldine base polyaniline: an X-ray photoelectron spectroscopy study", *Synthetic Metals*, vol. 85, pp. 1323-1326, 1997.
- [143] Z. Jin, Y. Su, and Y. Duan, "Development of a polyaniline-based optical ammonia sensor", *Sensors and Actuators B: Chemical*, vol. 72, pp. 75-79, 2001.

- [144] S. Virji, J. Huang, R. B. Kaner, and B. H. Weiller, "Polyaniline nanofiber gas sensors: Examination of response mechanisms", *Nano Letters*, vol. 4, pp. 491-496, 2004.
- [145] A. L. Kukla, Y. M. Shirshov, and S. A. Piletsky, "Ammonia sensors based on sensitive polyaniline films", *Sensors and Actuators B: Chemical*, vol. 37, pp. 135-140, 1996.
- [146] S. K. Dhawan, D. Kumar, M. K. Ram, S. Chandra, and D. C. Trivedi, "Application of conducting polyaniline as sensor material for ammonia", *Sensors and Actuators B: Chemical*, vol. 40, pp. 99-103, 1997.
- [147] V. V. Chabukswar, S. Pethkar, and A. A. Athawale, "Acrylic acid doped polyaniline as an ammonia sensor", *Sensors and Actuators B: Chemical*, vol. 77, pp. 657-663, 2001.
- [148] N. E. Agbor, M. C. Petty, and A. P. Monkman, "Polyaniline thin films for gas sensing", *Sensors and Actuators B: Chemical*, vol. 28, pp. 173-179, 1995.
- [149] A. A. Athawale and M. V. Kulkarni, "Polyaniline and its substituted derivatives as sensor for aliphatic alcohols", *Sensors and Actuators B: Chemical*, vol. 67, pp. 173-177, 2000.
- [150] J. Huang, S. Virji, B. H. Weiller, and R. B. Kaner, "Polyaniline nanofibers: Facile synthesis and chemical sensors", *Journal of the American Chemical Society*, vol. 125, pp. 314-315, 2003.
- [151] S. Virji, J. D. Fowler, C. O. Baker, J. Huang, R. B. Kaner, and B. H. Weiller, "Polyaniline nanofiber composites with metal salts: Chemical sensors for hydrogen sulfide", *Small*, vol. 1, pp. 624-627, 2005.
- [152] S. Virji, R. B. Kaner, and B. H. Weiller, "Hydrazine detection by polyaniline using fluorinated alcohol additives", *Chemistry of Materials*, vol. 17, pp. 1256-1260, 2005.
- [153] H. Liu, J. Kameoka, D. A. Czaplewski, and H. G. Craighead, "Polymeric nanowire chemical sensor", *Nano Letters*, vol. 4, pp. 671-675, 2004.
- [154] A. Z. Sadek, C. O. Baker, D. A. Powell, W. Wlodarski, R. B. Kaner, and K. Kalantar-zadeh, "Polyaniline nanofiber based surface acoustic wave gas sensors-effect of nanofiber diameter on H₂ response", *IEEE Sensors Journal*, vol. 7, pp. 213-218, 2007.
- [155] X. Yu, Y. Li, and K. Kalantar-zadeh, "Synthesis and electrochemical properties of template-based polyaniline nanowires and template-free nanofibril arrays: Two

- potential nanostructures for gas sensors", *Sensors and Actuators B: Chemical*, vol. 136, pp. 1-7, 2009.
- [156] J. M. Slater and E. J. Watt, "Piezoelectric and conductivity measurements of poly(pyrrole) gas interactions", *Analytical Proceedings*, vol. 29, pp. 53-56, 1992.
- [157] L. Al-Mashat, D. S. Ahn, S. H. Han, W. G. Hong, K. Shin, C. S. Yoon, K. Kalantar-zadeh, and W. Wlodarski, "Layered surface acoustic wave hydrogen sensor with nanoporous polyaniline as the active layer", *Sensor Letters*, vol. 9, pp. 73-76, 2011.
- [158] L. Al-Mashat, H. D. Tran, W. Wlodarski, R. B. Kaner, and K. Kalantar-zadeh, "Hydrogen gas sensor fabricated from polyanisidine nanofibers deposited on 36°YX LiTaO₃ layered surface acoustic wave transducer", in *BioMEMS and Nanotechnology III, SPIE*, pp. 67991B-8, 2007.
- [159] L. Al-Mashat, R. B. Kaner, H. D. Tran, K. Kalantar-zadeh, and W. Wlodarski, "Layered surface acoustic wave hydrogen sensor based on polyethylaniline nanofibers", *Procedia Chemistry*, vol. 1, pp. 220-223, 2009.
- [160] K. Ogura and H. Shiigi, "A CO₂ sensing composite film consisting of base-type polyaniline and poly(vinyl alcohol)", *Electrochemical and Solid-State Letters*, vol. 2, pp. 478-480, 1999.
- [161] S. H. Hosseini and A. A. Entezami, "Conducting polymer blends of polypyrrole with polyvinyl acetate, polystyrene, and polyvinyl chloride based toxic gas sensors", *Journal of Applied Polymer Science*, vol. 90, pp. 49-62, 2003.
- [162] V. Bavastrello, E. Stura, S. Carrara, V. Erokhin, and C. Nicolini, "Poly(2,5-dimethylaniline)-MWNTs nanocomposite: a new material for conductometric acid vapours sensor", *Sensors and Actuators B: Chemical*, vol. 98, pp. 247-253, 2004.
- [163] M. K. Ram, O. Yavuz, and M. Aldissi, "NO₂ gas sensing based on ordered ultrathin films of conducting polymer and its nanocomposite", *Synthetic Metals*, vol. 151, pp. 77-84, 2005.
- [164] M. K. Ram, Ö. Yavuz, V. Lahsangah, and M. Aldissi, "CO gas sensing from ultrathin nano-composite conducting polymer film", *Sensors and Actuators B: Chemical*, vol. 106, pp. 750-757, 2005.
- [165] L. Geng, X. Huang, Y. Zhao, P. Li, S. Wang, S. Zhang, and S. Wu, "H₂S sensitivity study of polypyrrole/WO₃ materials", *Solid-State Electronics*, vol. 50, pp. 723-726, 2006.

- [166] R. P. Tandon, M. R. Tripathy, A. K. Arora, and S. Hotchandani, "Gas and humidity response of iron oxide-polypyrrole nanocomposites", *Sensors and Actuators B: Chemical*, vol. 114, pp. 768-773, 2006.
- [167] H. Bai, C. Li, F. e. Chen, and G. Shi, "Aligned three-dimensional microstructures of conducting polymer composites", *Polymer*, vol. 48, pp. 5259-5267, 2007.
- [168] Y. Chen, Y. Li, H. Wang, and M. Yang, "Gas sensitivity of a composite of multi-walled carbon nanotubes and polypyrrole prepared by vapor phase polymerization", *Carbon*, vol. 45, pp. 357-363, 2007.
- [169] V. Saxena, D. K. Aswal, M. Kaur, S. P. Koiry, S. K. Gupta, J. V. Yakhmi, R. J. Kshirsagar, and S. K. Deshpande, "Enhanced NO₂ selectivity of hybrid poly(3-hexylthiophene): ZnO-nanowire thin films", *Appl. Phys. Lett.*, vol. 90, pp. 043516, 2007.
- [170] H. Tai, Y. Jiang, G. Xie, J. Yu, and X. Chen, "Fabrication and gas sensitivity of polyaniline-titanium dioxide nanocomposite thin film", *Sensors and Actuators B: Chemical*, vol. 125, pp. 644-650, 2007.
- [171] Z. Ting, M. Syed, B. Elena, Y. Bong Young, C. H. Robert, V. M. Nosang, and A. D. Marc, "Poly(m-aminobenzene sulfonic acid) functionalized single-walled carbon nanotubes based gas sensor", *Nanotechnology*, vol. 18, pp. 165504, 2007.
- [172] L. Geng, Y. Zhao, X. Huang, S. Wang, S. Zhang, and S. Wu, "Characterization and gas sensitivity study of polyaniline/SnO₂ hybrid material prepared by hydrothermal route", *Sensors and Actuators B: Chemical*, vol. 120, pp. 568-572, 2007.
- [173] H. Tai, Y. Jiang, G. Xie, J. Yu, X. Chen, and Z. Ying, "Influence of polymerization temperature on NH₃ response of PANI/TiO₂ thin film gas sensor", *Sensors and Actuators B: Chemical*, vol. 129, pp. 319-326, 2008.
- [174] A. Z. Sadek, W. Wlodarski, K. Shin, R. B. Kaner, and K. Kalantar-zadeh, "A layered surface acoustic wave gas sensor based on a polyaniline/In₂O₃ nanofibre composite", *Nanotechnology*, vol. 17, pp. 4488-4492, 2006.
- [175] A. Z. Sadek, W. Wlodarski, K. Shin, R. B. Kaner, and K. Kalantar-zadeh, "A polyaniline/WO₃ nanofiber composite-based ZnO/64° YX LiNbO₃ SAW hydrogen gas sensor", *Synthetic Metals*, vol. 158, pp. 29-32, 2008.
- [176] K. Shin, L. Al-Mashat, D. Ahn, S. Han, and W. Wlodarski, "A room temperature conductometric hydrogen sensor with polyaniline/WO₃ nanocomposite", *Sensor Letters*, vol. 9, pp. 77-81, 2011.

- [177] Y. Li, J. Gong, G. He, and Y. Deng, "Fabrication of polyaniline/titanium dioxide composite nanofibers for gas sensing application", *Materials Chemistry and Physics*, vol. 129, pp. 477-482, 2011.
- [178] L. Dai, *Carbon Nanotechnology: Recent Development in Chemistry, Physics, Materials Science and Device Applications*, Amsterdam, Oxford: Elsevier, 2006.
- [179] M. R. Karim, C. J. Lee, and M. S. Lee, "Synthesis and characterization of conducting polythiophene/carbon nanotubes composites", *Journal of Polymer Science Part A: Polymer Chemistry*, vol. 44, pp. 5283-5290, 2006.
- [180] Y. Wanna, S. Pratontep, A. Wisitsoraat, and A. Tuantranont, "Development of nanofibers composite polyaniline/CNT fabricated by electro spinning technique for CO gas sensor", in *IEEE Sensors Conference*, pp. 342-345, 2006.
- [181] S. Srivastava, S. S. Sharma, S. Agrawal, S. Kumar, M. Singh, and Y. K. Vijay, "Study of chemiresistor type CNT doped polyaniline gas sensor", *Synthetic Metals*, vol. 160, pp. 529-534, 2010.
- [182] L. Al-Mashat, K. Shin, K. Kalantar-zadeh, J. D. Plessis, S. H. Han, R. W. Kojima, R. B. Kaner, D. Li, X. Gou, S. J. Ippolito, and W. Wlodarski, "Graphene/Polyaniline nanocomposite for hydrogen sensing", *The Journal of Physical Chemistry C*, vol. 114, pp. 16168-16173, 2010.
- [183] C. Lee, X. Wei, J. W. Kysar, and J. Hone, "Measurement of the elastic properties and intrinsic strength of monolayer graphene", *Science*, vol. 321, pp. 385-388, 2008.
- [184] A. A. Balandin, S. Ghosh, W. Bao, I. Calizo, D. Teweldebrhan, F. Miao, and C. N. Lau, "Superior thermal conductivity of single-layer graphene", *Nano Letters*, vol. 8, pp. 902-907, 2008.
- [185] K. I. Bolotin, K. J. Sikes, Z. Jiang, M. Kilma, G. Fudenberg, J. Hone, P. Kim, and H. L. Stormer, "Ultrahigh electron mobility in suspended graphene", *Solid State Communications*, vol. 146, pp. 351-355, 2008.
- [186] M. D. Stoller, S. Park, Y. Zhu, J. An, and R. S. Ruoff, "Graphene based ultracapacitors", *Nano Letters*, vol. 8, pp. 3498-3502, 2008.
- [187] Y. Zhang, Y. W. Tan, H. L. Stormer, and P. Kim, "Experimental observation of the quantum hall effect and Berry's phase in graphene", *Nature*, vol. 438, pp. 201-204, 2005.
- [188] K. S. Novoselov, A. K. Geim, S. V. Morozov, D. Jiang, Y. Zhang, S. V. Dubonos, I. V. Grigorieva, and A. A. Firsov, "Electric field effect in atomically thin carbon films", *Science*, vol. 306, pp. 666-669, 2004.

- [189] C. Berger, Z. Song, X. Li, X. Wu, N. Brown, C. Naud, D. Mayou, T. Li, J. Hass, A. N. Marchenkov, E. H. Conrad, P. N. First, and W. A. De Heer, "Electronic confinement and coherence in patterned epitaxial graphene", *Science*, vol. 312, pp. 1191-1196, 2006.
- [190] X. Li, W. Cai, J. An, S. Kim, J. Nah, D. Yang, R. Piner, A. Velamakanni, I. Jung, E. Tutuc, S. K. Banerjee, L. Colombo, and R. S. Ruoff, "Large-area synthesis of high quality and uniform graphene films on copper foils", *Science*, vol. 324, pp. 1312-1314, 2009.
- [191] A. Reina, X. Jia, J. Ho, D. Nezich, H. Son, V. Bulovic, M. S. Dresselhaus, and J. Kong, "Large area, few-layer graphene films on arbitrary substrates by chemical vapor deposition", *Nano Letters*, vol. 9, pp. 30-35, 2009.
- [192] R. Ruoff, "Graphene calling all chemists", *Nature Nanotechnology*, vol. 3, pp. 10-11, 2008.
- [193] S. Park and R. S. Ruoff, "Chemical methods for the production of graphenes", *Nature Nanotechnology*, vol. 4, pp. 217-224, 2009.
- [194] D. Li, M. B. Muller, S. Gilje, R. B. Kaner, and G. G. Wallace, "Processable aqueous dispersions of graphene nanosheets", *Nature Nanotechnology*, vol. 3, pp. 101-105, 2008.
- [195] A. K. Geim and K. S. Novoselov, "The rise of graphene", *Nature Materials*, vol. 6, pp. 183-191, 2007.
- [196] F. Schedin, A. K. Geim, S. V. Morozov, E. W. Hill, P. Blake, M. I. Katsnelson, and K. S. Novoselov, "Detection of individual gas molecules adsorbed on graphene", *Nature Materials*, vol. 6, pp. 652-655, 2007.
- [197] G. Lu, L. E. Ocola, and J. Chen, "Reduced graphene oxide for room-temperature gas sensors", *Nanotechnology*, vol. 20, pp. 445502, 2009.
- [198] S. Stankovich, D. A. Dikin, G. H. B. Dommett, K. M. Kohlhaas, E. J. Zimney, E. A. Stach, R. D. Piner, S. T. Nguyen, and R. S. Ruoff, "Graphene-based composite materials", *Nature*, vol. 442, pp. 282-286, 2006.
- [199] J. Yan, T. Wei, B. Shao, Z. Fan, W. Qian, M. Zhang, and F. Wei, "Preparation of a graphene nanosheet/polyaniline composite with high specific capacitance", *Carbon*, vol. 48, pp. 487-493, 2010.
- [200] N. F. Mott, "Conduction in glasses containing transition metal ions", *Journal of Non-Crystalline Solids*, vol. 1, pp. 1-17, 1968.
- [201] N. F. Mott, "Polarons", *Materials Research Bulletin*, vol. 13, pp. 1389-1394, 1978.

- [202] R. Österbacka, C. P. An, X. M. Jiang, and Z. V. Vardeny, "Two-dimensional electronic excitations in self-assembled conjugated polymer nanocrystals", *Science*, vol. 287, pp. 839-842, 2000.
- [203] X. Liu, K. Gao, Y. Li, J. Fu, J. Wei, and S. Xie, "Polaron formation dynamics in conducting polymers", *Synthetic Metals*, vol. 157, pp. 380-385, 2007.
- [204] V. N. Prigodin, A. N. Samukhin, and A. J. Epstein, "Variable range hopping in low-dimensional polymer structures", *Synthetic Metals*, vol. 141, pp. 155-164, 2004.
- [205] J. W. Gardner and P. N. Bartlett, "Design of conducting polymer gas sensors: Modelling and experiment", *Synthetic Metals*, vol. 57, pp. 3665-3670, 1993.
- [206] J. W. Gardner, P. N. Bartlett, and K. F. E. Pratt, "Modelling of gas-sensitive conducting polymer devices", *Circuits, Devices and Systems, IEE Proceedings -*, vol. 142, pp. 321-333, 1995.
- [207] P. N. Bartlett and J. W. Gardner, "Diffusion and binding of molecules to sites within homogeneous thin films", *Philosophical Transactions of the Royal Society London A*, vol. 354, pp. 35-57, 1996.
- [208] J. Crank, *The Mathematics of Diffusion*, 2nd ed, Oxford: Oxford University Press, 1975.
- [209] B. Bianco and A. Bonfiglio, "An electrical model for two-dimensional layers of conductive polymers", *Thin Solid Films*, vol. 284-285, pp. 520-522, 1996.
- [210] A. Sabadra, "Parameter identification and simulation of conducting polymer micro-sensors using global spectral projection methods", M.S. thesis, University of Maryland, Collage Park, 2001.
- [211] J. W. Gardner, "Electrical conduction in solid-state gas sensors", *Sensors and Actuators*, vol. 18, pp. 373-387, 1989.
- [212] M. Z. Y. Iskandarani, "An analogue organic neural processor", M. S. thesis, University of Warwick, U.K., 1991.
- [213] E. Milella and M. Penza, "SAW gas detection using Langmuir-Blodgett polypyrrole films", *Thin Solid Films*, vol. 327-329, pp. 694-697, 1998.
- [214] A. J. Ricco, S. J. Martin, and T. E. Zipperian, "Surface acoustic wave gas sensor based on film conductivity changes", *Sensors and Actuators*, vol. 8, pp. 319-333, 1985.
- [215] A. J. Ricco and S. J. Martin, "Thin metal film characterization and chemical sensors: monitoring electronic conductivity, mass loading and mechanical

- properties with surface acoustic wave devices", *Thin Solid Films*, vol. 206, pp. 94-101, 1991.
- [216] H. Wohltjen, "Mechanism of operation and design considerations for surface acoustic wave device vapour sensors", *Sensors and Actuators*, vol. 5, pp. 307-325, 1984.
- [217] J. D. N. Cheeke, *Fundamentals and Applications of Ultrasonic Waves*, Florida: CRC Press, 2002.
- [218] D. S. Ballantine, Jr., R. M. White, S. J. Martin, A. J. Ricco, G. C. Frye, E. T. Zellars, and H. Wohltjen, *Acoustic Wave Sensors - Theory, Design, and Physico-Chemical Applications*, San Diego: Academic Press, 1997.
- [219] S. J. Martin, G. C. Frye, and S. D. Senturia, "Dynamics and response of polymer-coated surface acoustic wave devices: Effect of viscoelastic properties and film resonance", *Analytical Chemistry*, vol. 66, pp. 2201-2219, 1994.
- [220] S. J. Martin and A. J. Ricco, "Effective utilization of acoustic wave sensor responses: simultaneous measurement of velocity and attenuation", in *Ultrasonics Symposium, 1989. Proceedings., IEEE 1989*, pp. 621-625 vol.1, 1989.
- [221] T. Shoji, K. Nakamura, and D. Yamazaki, "Propagation characteristics of the SH-SAW on (110) ZnO/ (012) LiTaO₃", in *IEEE Ultrasonics Symposium*, pp. 215-219 2001.
- [222] C. K. Campbell, *Surface Acoustic Wave Devices for Mobile and Wireless Communications*, San Diego: Academic Press, 1998.
- [223] M. J. Madou, *Fundamentals of Microfabrication : The Science of Miniaturization*, 2nd ed, Florida: CRC Press, 2002.
- [224] S. J. Ippolito, "Investigation of multilayered surface acoustic wave devices for gas sensing applications employing piezoelectric intermediate and nanocrystalline metal oxide sensitive layers", PhD thesis, RMIT University, Melbourne, 2006.
- [225] W. Plieth, *Electrochemistry for Materials Science*, Amsterdam; Oxford: Elsevier, 2008.
- [226] T. Bjornholm, T. Hassenkam, D. R. Greve, R. D. McCullough, M. Jayaraman, S. M. Savoy, C. E. Jones, and J. T. McDevitt, "Polythiophene nanowires", *Advanced Materials*, vol. 11, pp. 1218-1221, 1999.
- [227] J. Liu, E. Sheina, T. Kowalewski, and R. D. McCullough, "Tuning the electrical conductivity and self-assembly of regioregular polythiophene by block copolymerization: nanowire morphologies in new di- and triblock copolymers", *Angewandte Chemie International Edition*, vol. 41, pp. 329-332, 2002.

- [228] B. W. Maynor, S. F. Filocamo, M. W. Grinstaff, and J. Liu, "Direct-writing of polymer nanostructures: poly(thiophene) nanowires on semiconducting and insulating surfaces", *Journal of the American Chemical Society*, vol. 124, pp. 522-523, 2002.
- [229] M. R. Karim, K. T. Lim, C. J. Lee, and M. S. Lee, "A facile synthesis of polythiophene nanowires", *Synthetic Metals*, vol. 157, pp. 1008-1012, 2007.
- [230] Z. Wang, Y. Wang, D. Xu, E. S.-W. Kong, and Y. Zhang, "Facile synthesis of dispersible spherical polythiophene nanoparticles by copper(II) catalyzed oxidative polymerization in aqueous medium", *Synthetic Metals*, vol. 160, pp. 921-926, 2010.
- [231] V. P. Menon, J. Lei, and C. R. Martin, "Investigation of molecular and supermolecular structure in template-synthesized polypyrrole tubules and fibrils", *Chemistry of Materials*, vol. 8, pp. 2382-2390, 1996.
- [232] M. Ikegame, K. Tajima, and T. Aida, "Template synthesis of polypyrrole nanofibers insulated within one-dimensional silicate channels: hexagonal versus lamellar for recombination of polarons into bipolarons", *Angewandte Chemie - International Edition*, vol. 42, pp. 2154-2157, 2003.
- [233] X. Zhang and S. K. Manohar, "Bulk synthesis of polypyrrole nanofibers by a seeding approach", *Journal of the American Chemical Society*, vol. 126, pp. 12714-12715, 2004.
- [234] Y. Yang, J. Liu, and M. Wan, "Self-assembled conducting polypyrrole micro/nanotubes", *Nanotechnology*, vol. 13, pp. 771-773, 2002.
- [235] C. Saravanan, S. Palaniappan, and F. Chandezon, "Synthesis of nanoporous conducting polyaniline using ternary surfactant", *Materials Letters*, vol. 62, pp. 882-885, 2008.
- [236] S.-M. Yang and J.-H. Chiang, "Morphological study of alkylsubstituted polyaniline", *Synthetic Metals*, vol. 41, pp. 761-764, 1991.
- [237] A. Gruger, A. Novak, A. Régis, and P. Colombari, "Infrared and Raman study of polyaniline Part II: Influence of ortho substituents on hydrogen bonding and UV/Vis—near-IR electron charge transfer", *Journal of Molecular Structure*, vol. 328, pp. 153-167, 1994.
- [238] A. H. Kwon, J. A. Conklin, M. Makhinson, and R. B. Kaner, "Chemical synthesis and characterization of fluoro-substituted polyanilines", *Synthetic Metals*, vol. 84, pp. 95-96, 1997.

- [239] A. Cihaner and A. M. Önal, "Synthesis and characterization of fluorine-substituted polyanilines", *European Polymer Journal*, vol. 37, pp. 1767-1772, 2001.
- [240] A. Z. Sadek, W. Wlodarski, K. Kalantar-zadeh, C. O. Baker, and R. B. Kaner, "Doped and dedoped polyaniline nanofiber based conductometric hydrogen gas sensors", *Sensors and Actuators A: Physical*, vol. 139, pp. 53-57, 2007.
- [241] Y. Xia, J. M. Wiesinger, A. G. MacDiarmid, and A. J. Epstein, "Camphorsulfonic acid fully doped polyaniline emeraldine salt: conformations in different solvents studied by an ultraviolet/visible/near-infrared spectroscopic method", *Chemistry of Materials*, vol. 7, pp. 443-445, 1995.
- [242] O. Ngamna, "Synthesis, characterization and application of inherently conducting polymer nanoparticles", PhD thesis, University of Wollongong, Wollongong, 2006.
- [243] B. H. Stuart, *Infrared spectroscopy: fundamentals and applications*, West Sussex: John Wiley & Sons, 2004.
- [244] A. C. Ferrari and J. Robertson, "Interpretation of Raman spectra of disordered and amorphous carbon", *Physical Review B*, vol. 61, pp. 14095-14107, 2000.
- [245] P. J. Larkin, *Infrared and raman spectroscopy: principles and spectral interpretation*, Waltham, San Diego, Oxford, Amsterdam: Elsevier, 2011.
- [246] J. Roncali, "Conjugated poly(thiophenes): synthesis, functionalization, and applications", *Chemical Reviews*, vol. 92, pp. 711-738, 1992.
- [247] S. S. Jeon, S. J. Yang, K.-J. Lee, and S. S. Im, "A facile and rapid synthesis of unsubstituted polythiophene with high electrical conductivity using binary organic solvents", *Polymer*, vol. 51, pp. 4069-4076, 2010.
- [248] W. Yu, T. Yao, X. Li, T. Wang, H. Gao, J. Zhang, and B. Yang, "Electropolymerization of highly hydrophobic polythiophene films with high adhesion force", *Journal of Applied Polymer Science*, vol. 119, pp. 1052-1059, 2011.
- [249] B. Senthilkumar, P. Thenamirtham, and R. Kalai Selvan, "Structural and electrochemical properties of polythiophene", *Applied Surface Science*, vol. 257, pp. 9063-9067, 2011.
- [250] A. O. Patil, A. J. Heeger, and F. Wudl, "Optical properties of conducting polymers", *Chemical Reviews*, vol. 88, pp. 183-200, 1988.
- [251] L. E. Lyons, "Energy gaps in organic semiconductors derived from electrochemical data", *Australian Journal of Chemistry*, vol. 33, pp. 1717-1725, 1980.

- [252] S. Yang, P. Olishevski, and M. Kertesz, "Bandgap calculations for conjugated polymers", *Synthetic Metals*, vol. 141, pp. 171-177, 2004.
- [253] F. Alakhras and R. Holze, "In situ UV-vis- and FT-IR-spectroscopy of electrochemically synthesized furan-thiophene copolymers", *Synthetic Metals*, vol. 157, pp. 109-119, 2007.
- [254] E. T. Kang, K. G. Neoh, and K. L. Tan, "X-ray photoelectron spectroscopic studies of poly(2,2'-bithiophene) and its complexes", *Physical Review B*, vol. 44, pp. 10461-10469, 1991.
- [255] S. C. Ng, J. M. Xu, and H. S. O. Chan, "Synthesis and characterization of regioregular polymers containing substituted thienylene/bithienylene and phenylene repeating units", *Macromolecules*, vol. 33, pp. 7349-7358, 2000.
- [256] J. M. Xu, H. S. O. Chan, S. C. Ng, and T. S. Chung, "Polymers synthesized from (3-alkylthio)thiophenes by the FeCl₃ oxidation method", *Synthetic Metals*, vol. 132, pp. 63-69, 2002.
- [257] M. Kobayashi, J. Chen, T. C. Chung, F. Moraes, A. J. Heeger, and F. Wudl, "Synthesis and properties of chemically coupled poly(thiophene)", *Synthetic Metals*, vol. 9, pp. 77-86, 1984.
- [258] L. Al-Mashat, C. Debiemme-Chouvy, S. Borensztajn, and W. Wlodarski, "Electropolymerized polypyrrole nanowires for hydrogen gas sensing", *The Journal of Physical Chemistry C*, vol. 116, pp. 13388-13394, 2012.
- [259] H. D. Tran, Y. Wang, J. M. D'Arcy, and R. B. Kaner, "Toward an understanding of the formation of conducting polymer nanofibers", *ACS Nano*, vol. 2, pp. 1841-1848, 2008.
- [260] S. Carquigny, J. B. Sanchez, F. Berger, B. Lakard, and F. Lallemand, "Ammonia gas sensor based on electrosynthesized polypyrrole films", *Talanta*, vol. 78, pp. 199-206, 2009.
- [261] A. Yfantis, G. Appel, D. Schmeißer, and D. Yfantis, "Polypyrrole doped with fluoro-metal complexes: thermal stability and structural properties", *Synthetic Metals*, vol. 106, pp. 187-195, 1999.
- [262] S. Stafström, J. L. Brédas, A. J. Epstein, H. S. Woo, D. B. Tanner, W. S. Huang, and A. G. MacDiarmid, "Polaron lattice in highly conducting polyaniline: Theoretical and optical studies", *Physical Review Letters*, vol. 59, pp. 1464-1467, 1987.

- [263] R. P. McCall, J. M. Ginder, J. M. Leng, H. J. Ye, S. K. Manohar, J. G. Masters, G. E. Asturias, A. G. MacDiarmid, and A. J. Epstein, "Spectroscopy and defect states in polyaniline", *Physical Review B*, vol. 41, pp. 5202-5213, 1990.
- [264] M. Pumera, "Electrochemistry of graphene: New horizons for sensing and energy storage", *The Chemical Record*, vol. 9, pp. 211-223, 2009.
- [265] Y. Sun, S. R. Wilson, and D. I. Schuster, "High dissolution and strong light emission of carbon nanotubes in aromatic amine solvents", *Journal of the American Chemical Society*, vol. 123, pp. 5348-5349, 2001.
- [266] M. Cochet, G. Louarn, S. Quillard, J. P. Buisson, and S. Lefrant, "Theoretical and experimental vibrational study of emeraldine in salt form. Part II", *Journal of Raman Spectroscopy*, vol. 31, pp. 1041-1049, 2000.
- [267] I. Calizo, A. A. Balandin, W. Bao, F. Miao, and C. N. Lau, "Temperature dependence of the raman spectra of graphene and graphene multilayers", *Nano Letters*, vol. 7, pp. 2645-2649, 2007.
- [268] K. S. Kim, Y. Zho, H. Jang, S. Y. Lee, J. M. Kim, J. H. Ahn, P. Kim, J. Y. Choi, and B. H. Hong, "Large-scale pattern growth of graphene films for stretchable transparent electrodes ", *Nature*, vol. 457, pp. 706-710, 2009.
- [269] A. Gupta, G. Chen, P. Joshi, S. Tadigadapa, and Eklund, "Raman scattering from high-frequency phonons in supported n-graphene layer films", *Nano Letters*, vol. 6, pp. 2667-2673, 2006.
- [270] D. Graf, F. Molitor, K. Ensslin, C. Stampfer, A. Jungen, C. Hierold, and L. Wirtz, "Spatially resolved Raman spectroscopy of single- and few-layer graphene", *Nano Letters*, vol. 7, pp. 238-242, 2007.
- [271] A. C. Ferrari, "Raman spectroscopy of graphene and graphite: Disorder, electron-phonon coupling, doping and nonadiabatic effects", *Solid State Communications*, vol. 143, pp. 47-57, 2007.
- [272] G. Williams, B. Seger, and P. V. Kamat, "TiO₂-Graphene nanocomposites. UV-assisted photocatalytic reduction of graphene oxide", *ACS Nano*, vol. 2, pp. 1487-1491, 2008.
- [273] O. Akhavan and E. Ghaderi, "Photocatalytic reduction of graphene oxide nanosheets on TiO₂ thin film for photoinactivation of bacteria in solar light irradiation", *The Journal of Physical Chemistry C*, vol. 113, pp. 20214-20220, 2009.
- [274] D. Yang, A. Velamakanni, G. Bozoklu, S. Park, M. Stoller, R. D. Piner, S. Stankovich, I. Jung, D. A. Field, C. A. Ventrice Jr, and R. S. Ruoff, "Chemical

- analysis of graphene oxide films after heat and chemical treatments by X-ray photoelectron and Micro-Raman spectroscopy", *Carbon*, vol. 47, pp. 145-152, 2009.
- [275] O. Akhavan, "The effect of heat treatment on formation of graphene thin films from graphene oxide nanosheets", *Carbon*, vol. 48, pp. 509-519, 2010.
- [276] K. Zhang, L. L. Zhang, X. S. Zhao, and J. Wu, "Graphene/Polyaniline nanofiber composites as supercapacitor electrodes", *Chemistry of Materials*, vol. 22, pp. 1392-1401, 2010.
- [277] J. Crabb, M. F. Lewis, and J. D. Maines, "Surface-acoustic-wave oscillators: mode selection and frequency modulation", *Electronics Letters*, vol. 9, pp. 195-197, 1973.
- [278] S. J. Ippolito, S. Kandasamy, K. Kalantar-Zadeh, W. Wlodarski, and A. Holland, "Comparison between conductometric and layered surface acoustic wave hydrogen gas sensors", *Smart Materials and Structures*, vol. 15, pp. S131-S136, 2006.
- [279] T. C. Chung, J. H. Kaufman, A. J. Heeger, and F. Wudl, "Charge storage in doped poly(thiophene): Optical and electrochemical studies", *Physical Review B*, vol. 30, pp. 702-710, 1984.
- [280] B. Rasch, P. Novák, and W. Vielstich, "Electrochemical and in situ FTIR investigations on polythiophene in propylene carbonate", *Synthetic Metals*, vol. 43, pp. 2963-2966, 1991.
- [281] E. A. Bazzaoui, J. P. Marsault, S. Aeiyaich, and P. C. Lacaze, "Resonance Raman study of polythiophene films in the doped and undoped states. Relations between spectral data and physicochemical properties", *Synthetic Metals*, vol. 66, pp. 217-224, 1994.
- [282] B. Rasch and W. Vielstich, "Polythiophenes via thiophene, bithiophene and terthiophene in propylene carbonate: an electrochemical and in-situ FTIR study", *Journal of Electroanalytical Chemistry*, vol. 370, pp. 109-117, 1994.
- [283] A. D'Amico and C. Di Natale, "A contribution on some basic definitions of sensors properties", *IEEE Sensors Journal*, vol. 1, pp. 183-190, 2001.
- [284] G. R. Hutchison, M. A. Ratner, and T. J. Marks, "Hopping transport in conductive heterocyclic oligomers: Reorganization energies and substituent effects", *Journal of the American Chemical Society*, vol. 127, pp. 2339-2350, 2005.

- [285] M. Fu, G. Shi, F. Chen, and X. Hong, "Doping level change of polythiophene film during its electrochemical growth process", *Physical Chemistry Chemical Physics*, vol. 4, pp. 2685-2690, 2002.
- [286] K. Thuwachaowsoan, D. Chotpattananont, A. Sirivat, R. Rujiravanit, and J. W. Schwank, "Electrical conductivity responses and interactions of poly(3-thiopheneacetic acid)/zeolites L, mordenite, beta and H₂", *Materials Science and Engineering: B*, vol. 140, pp. 23-30, 2007.
- [287] S. Radhakrishnan and S. Paul, "Conducting polypyrrole modified with ferrocene for applications in carbon monoxide sensors", *Sensors and Actuators B: Chemical*, vol. 125, pp. 60-65, 2007.
- [288] D. J. Walton, C. E. Hall, and A. Chyla, "Characterization of poly(pyrroles) by cyclic voltammetry", *Analyst*, vol. 117, pp. 1305-1311, 1992.
- [289] J. W. Gardner and P. N. Bartlett, *Sensors and Sensory Systems for an Electronic Nose*, Reykjavik: Kluwer Academic Press, 1991.
- [290] A. Kaynak, "Electrical conductivity of polypyrrole films at a temperature range of 70 K to 350 K", *Materials Research Bulletin*, vol. 33, pp. 81-88, 1998.
- [291] X. Han and L. P. Naeher, "A review of traffic-related air pollution exposure assessment studies in the developing world", *Environment International*, vol. 32, pp. 106-120, 2006.
- [292] J. Janata, "Chemical modulation of the electron work function", *Analytical Chemistry*, vol. 63, pp. 2546-2550, 1991.
- [293] S. S. Srinivasan, R. Ratnadurai, M. U. Niemann, A. R. Phani, D. Y. Goswami, and E. K. Stefanakos, "Reversible hydrogen storage in electrospun polyaniline fibers", *International Journal of Hydrogen Energy*, vol. 35, pp. 225-230, 2010.
- [294] J. D. Fowler, S. Virji, R. B. Kaner, and B. H. Weiller, "Hydrogen detection by polyaniline nanofibers on gold and platinum electrodes", *The Journal of Physical Chemistry C*, vol. 113, pp. 6444-6449, 2009.
- [295] O. V. Prezhdo, P. V. Kamat, and G. C. Schatz, "Virtual issue: Graphene and functionalized graphene", *The Journal of Physical Chemistry C*, vol. 115, pp. 3195-3197, 2011.
- [296] J. Z. Zhang, "Improved sensing with nanostructures", *The Journal of Physical Chemistry Letters*, vol. 3, pp. 1806-1807, 2012.